The enzymology of *Streptococcus pneumoniae* peptidoglycan polymerisation

Katherine Anne Abrahams BSc (Hons)

A thesis submitted in partial fulfilment
of the requirements for the degree of

Doctor of Philosophy

School of Life Sciences
University of Warwick

June 2011

Contents

Table of contents

List of Tables

List of Figures

Acknowledgements

I would like to thank my supervisor Dr. David Roper for his guidance and support during this research. Many thanks to Dr. Adrian Lloyd for his expertise and inspirational advice throughout this project. I would also like to thank the members of the Structural Biology Group, past and present, especially the Chair of my Committee Professor Vilmos Fülöp, as well as Anita Catherwood and Ian Portman for their technical support.

Special thanks go to my family and friends, especially Jo, Darren, Vicky, Mike and John for their invaluable friendship and entertainment over the last three years and more.

Declaration

I hereby declare that I personally have carried out the work submitted in this thesis under the supervision of Dr. David Roper at the School of Life Sciences, University of Warwick.

No part of this work has previously been submitted to be considered for a degree or qualification. All sources of information have been specifically acknowledged in the form of references.

Abstract

Bacterial cell survival depends on intact peptidoglycan, an extensive cell wall polymer of alternating *N*-acetylglucosamine and *N*-acetylmuramic acid residues, cross-linked by short peptides. Peptidoglycan biosynthesis is a viable and validated antimicrobial target; the intracellular, membrane-bound and extracellular synthetic stages provide a multitude of enzymes for interception with inhibitors. The ultimate phase of peptidoglycan biosynthesis occurs on the extracellular face of the cytoplasmic membrane and involves the polymerisation of Lipid II (the monomeric peptidoglycan precursor) by the transglycosylase and transpeptidase activities of the Penicillin-Binding Proteins (PBPs).

The work presented in this thesis primarily focused on the biochemical characterisation of the integral membrane proteins *Streptococcus pneumoniae* PBP1a, PBP2b and PBP2x. These enzymes are clinically relevant; they are essential targets of β-lactam antibiotics and also mediate resistance against this important antimicrobial class. Full-length and truncated forms of the PBPs were cloned, expressed and purified to high levels. Two novel spectrophotometric assays were designed and developed to study the enzymology of the individual transglycosylase and transpeptidase activities of the PBPs with their natural substrate, Lipid II. Preliminary kinetic characterisations of the bifunctional PBP1a transglycosylase activity were performed and assay conditions were optimised to recreate an *in vivo* environment. PBP1a active site mutants revealed that transglycosylase activity was elevated in the absence of a functional transpeptidase domain. PBP1a and PBP2x exhibited transpeptidase activity with an apparent substrate preference for glycan polymers over Lipid II. PBP2x transpeptidase activity was not detected. The recorded rates of PBP activity were insufficient to support bacterial cell integrity, highlighting a gap in the understanding of PBP requirements. Finally, the PBPs were subjected to crystallisation trials for structural characterisations.

This work provides an excellent foundation for the analysis and elucidation of PBP specificities. Future information attained could contribute to the design of novel inhibitors, alleviating the global threat of antibiotic resistance.

Abbreviations

[^{14}C]-Lys-Lipid II	[^{14}C]-Glc*N*Ac-labelled Lipid II (L-Lys third position of stem)
3D	three-dimensional
Å	angstrom
A_{280nm}	Absorbance at 280 nm
A_{340nm}	Absorbance at 340 nm
A_{360nm}	Absorbance at 360 nm
A_{555nm}	Absorbance at 555 nm
A_{595nm}	Absorbance at 595 nm
A_{600nm}	Absorbance at 600 nm
A. aeolicus	*Aquifex aeolicus*
ADP	Adenosine 5'-diphosphate
APS	Ammonium persulfate
ASPRE	Active site Serine Penicillin Recognising Enzymes
atm	atmospheric pressure
ATP	Adenosine 5'-triphosphate
AU	Absorbance Unit
BCA	Bicinchoninic acid
bp	base pair
CAZY	Carbohydrate-Active enZYmes
CHAPS	3-[(3-cholamidopropyl)dimethylammonio]-1-propanesulfonate
CMC	Critical Micellar Concentration
cpm	counts per minute
C-terminus	Carboxy terminus
D-Ala	D-Alanine
D-Ala-D-Ala	D-Alanyl-D-Alanine
D-Ala-D-Lac	D-Alanyl-D-Lactate
D-Asn	D-Asparagine
D-Asp	D-Aspartate
Da	Dalton
DAAO	D-amino acid oxidase

DDM	n-Dodecyl-β-D-maltopyranoside
DEAE	Diethyl-aminoethyl
Decyl-PEG	Octaethylene glycol monodecyl ether
D-Glu	D-Glutamate
D-Lac	D-Lactate
DMSO	Dimethyl sulfoxide
DNA	Deoxyribonucleic acid
DNAse	Deoxyribonuclease I, from bovine pancreas
dpm	disintegrations per minute
D-Ser	D-Serine
DTT	Dithiothreitol
E. coli	*Escherichia coli*
EDTA	Ethylenediaminetetraacetic acid
EM	Electron Microscopy
E. faecalis	*Enterococcus faecalis*
E. faecium	*Enterococcus faecium*
ESI-MS	Electrospray Ionisation Mass Spectrometry
et al.	*et alia*, and others
FSEC	Fluorescence Size Exclusion Chromatography
g	gram
GFP	Green Fluorescent Protein
Glc*N*Ac	*N*-acetylglucosamine
Glycyl-L-α-amino-ε-pimelyl-D-Ala-D-Ala:	Glycyl-L-α-amino-ε-pimelyl-D-Alanyl-D-Alanine
Gly-Gly-Gly-Gly-Gly:	Glycyl-Glycyl-Glycyl-Glycyl-Glycine
GT	Glycosyl transfer
HCl	Hydrochloric acid
HEPES	*N-(*2-hydroxyethyl*)*piperazine-*N*'-(3-ethanesulfonic acid)
HMW	High molecular weight
HPLC	High Performance Liquid Chromatography
HPTLC	High Performance Thin Layer Chromatography
h	hour
HRP	Horseradish peroxidase

IMAC	Immobilised Metal Affinity Chromatography
IPP	Inorganic pyrophosphatase
IPTG	Isopropyl-β-D-thiogalactopyranoside
iso-Gln	*iso*-Glutamine
K	Kelvin
kb	kilobase
k_{cat}	turnover number
KCl	Potassium chloride
kDa	kiloDalton
K_m	Michaelis constant
K_{m1}	Michaelis constant at the first subsite of the enzyme
K_{m2}	Michaelis constant at the second subsite of the enzyme
kpsi	kilopound per square inch
K_s	Substrate inhibition constant
L	Litre
L-Ala	L-Alanine
L-Ala-L-Ala	L-Alanyl-L-Alanine
L-Ala-L-Ala-L-Ala-L-Thr:	L-Alanyl-L-Alanyl-L-Alanyl-L-Threonine
L-Ala-γ-D-Glu-L-Lys-D-Ala-D-Ala:	L-Alanyl-γ-D-Glutamyl-L-Lysyl-D-Alanyl-D-Alanine
LB	Lysogeny broth (Luria-Bertani bacteria growth media)
LDAO	Lauryldimethylamine oxide
L-Glu	L-Glutamate
LIC	Ligation Independent Cloning
Lipid I	Undecaprenyl pyrophosphoryl-*N*-acetylmuramyl-L-Alanyl-γ-D-Glutamyl-L-Lysyl-D-Alanyl-D-Alanine
Lipid II	Undecaprenyl pyrophosphoryl-*N*-acetylmurmayl-(*N*-acetylglucosaminyl)-L-Alanyl-γ-D-Glutamyl-X-D-Alanyl-D-Alanine (X is the amino acid at position 3 as stated by the prefix)
Lipid IV	Undecaprenyl pyrophosphoryl-(*N*-acetylmurmayl-(*N*-acetylglucosaminyl)-L-Alanyl-γ-D-Glutamyl-L-Lysyl-D-Alanyl-D-Alanine)$_2$

L-Lys	L-Lysine
LMW	Low molecular weight
L-Ser-L-Ala	L-Seryl-L-Alanine
M	Molar (grams per litre)
mA	milliamperes
mAU	milli absorbance unit
mCi	millicurie
MES	2-morpholinoethane sulphonic acid
MESG	7-methyl-6-thioguanosine
meso-DAP	*meso*-diaminopimelic acid
M. flavus	*Micrococcus flavus*
mg	milligram
MGT	monofunctional glycosyltransferase
MIC	Minimal Inhibitory Concentration
min	minute
mL	millilitre
mm	millimetre
mM	millimolar
MOPS	3-(N-morpholino)propanesulfonic acid
M_r	molecular weight
mRNA	messenger ribonucleic acid
MRSA	Methicillin-resistant *Staphylococcus aureus*
mS	milliSiemen
Mur*N*Ac	*N*-acetylmuramic acid
NAD^+	Nicotinamide adenine dinucleotide (oxidised)
NADH	Nicotinamide adenine dinucleotide (reduced)
$NADP^+$	Nicotinamide adenine dinucleotide phosphate (oxidised)
NADPH	Nicotinamide adenine dinucleotide phosphate (reduced)
ng	nanogram
NHS	National Health Service
nm	nanometre
nM	nanomolar
nmol	nanomole
NMR	Nuclear Magnetic Resonance spectroscopy

°C	degrees Celsius
OD_{600nm}	optical density at 600 nm
P. aeruginosa	*Pseudomonas aeruginosa*
PAGE	Polyacrylamide Gel Electrophoresis
PBP	Penicillin-Binding Protein
PBS	Phosphate Buffered Saline
PCR	Polymerase Chain Reaction
PDB	Protein Data Bank
PEG	Polyethylene glycol
Pentapeptide	L-Alanyl-γ-D-Glutamyl-X-D-Alanyl-D-Alanine (where X is L-Lys or *meso*-DAP as stated)
PEP	Phosphoenol pyruvate
pH	$\log_{10}[H^+]$
P_i	Inorganic phosphate
pI	Isoelectric point
PNP	Purine Nucleoside Phosphorylase
RNA	Ribonucleic acid
RTF	Resistance Transfer Factor
rpm	rotations per minute
SOC	Super Optimal broth with Catabolite repression
S. pneumoniae	*Streptococcus pneumoniae*
S. aureus	*Staphylococcus aureus*
SDS	Sodium Dodecyl Sulfate
SDS-PAGE	Sodium Dodecyl Sulfate Polyacrylamide Gel Electrophoresis
sec	second
SMALP	Styrene Maleic Acid copolymer Lipid Polymer
sp.	species
TAE	Tris Acetate Ethylenediaminetetraacetic acid
Tris	Tris (hydroxymethyl) aminomethane
TEMED	*N,N,N′,N′*-tetramethylethylenediamine
TM	Transmembrane domain
TMHMM	TransMembrane Hidden Markov Model
TNBS	Trinitrobenzene sulphonic acid

tRNA	transfer ribonucleic acid
UDP	Uridine 5'-diphosphate
UDP-Glc*N*Ac	Uridine 5'-diphospho-*N*-acetylglucosamine
UDP-Mur*N*Ac	Uridine 5'-diphospho-*N*-acetylmuramic acid
UDP-Mur*N*Ac-monopeptide:	Uridine 5'-diphospho-*N*-acetylmuramyl-L-Alanine
UDP-Mur*N*Ac-dipeptide:	Uridine 5'-diphospho-*N*-acetylmuramyl-L-Alanyl-D-Glutamate
UDP-Mur*N*Ac-tripeptide:	Uridine 5'-diphospho-*N*-acetylmuramyl-L-Alanyl-D-Glutamyl-L-Lysine
UDP-Mur*N*Ac pentapeptide:	Uridine 5'-diphospho-*N*-acetylmuramyl-L-Alanyl-D-Glutamyl-L-Lys-D-Ala-D-Ala
µCi	microcurie
µg	microgram
µL	microlitre
µm	micrometer
µM	micromolar
µmol	micromole
VanFL	BODIPY FL conjugate of vancomycin
V_{max}	maximal velocity
VRE	Vancomycin Resistant Enterococci
WHO	World Health Organisation
w/v	weight to volume ratio
V	Volts
v/v	volume to volume ratio
× g	centrifugal force

Other abbreviations are explained in the text where appropriate.

Standard three and one amino acid abbreviations are used throughout.

Amino acid	Three letter code	One letter code
Alanine	Ala	A
Arginine	Arg	R
Asparagine	Asn	N
Aspartic acid	Asp	D
Cysteine	Cys	C
Glutamic acid	Glu	E
Glutamine	Gln	Q
Glycine	Gly	G
Histidine	His	H
Isoleucine	Ile	I
Leucine	Leu	L
Lysine	Lys	K
Methionine	Met	M
Phenylalanine	Phe	F
Proline	Pro	P
Serine	Ser	S
Threonine	Thr	T
Tryptophan	Trp	W
Tyrosine	Tyr	Y
Valine	Val	V

Dedicated to:

Jon and Flic Abrahams

Ben and Pam George

Jack and Cynthia Abrahams

Chapter 1. Introduction

1.1. The impact of antimicrobial agents and bacterial resistance

Over the past half century, the introduction and development of antimicrobial agents to treat bacterial infectious diseases has been of great medical significance. The landmark discovery of penicillin by Fleming in 1928 and sulphonamides by Domagk in 1935 (Wainwright and Kristiansen, 2011) initiated a rapid global response in the search for novel antimicrobial structures. This led to the identification of a plethora of new antibiotic classes across two decades, 1940-1960, in what has been coined the 'Golden age' of antimicrobial drug discovery (Walsh and Wright, 2005). Control over infectious diseases triumphed and the availability of antibiotics was regarded as sufficient to maintain infection rates at low levels (von Nussbaum *et al.*, 2006). Consequently, drug development was focussed towards more profitable treatments and away from infectious disease. During this era, innovative antimicrobial compounds were not established to counteract the emerging global threat of antimicrobial resistance. This has resulted in a renewed interest in the study of targets for antimicrobial agents from a perspective of understanding resistance mechanisms and also in the search for new targets and strategies.

1.2. Antimicrobial agents

1.2.1. Targets of antimicrobial agents

Antimicrobial targets are constituents of a bacterial cell that are fundamental for viability and can be distinguished from homologous or equivalent eukaryotic cellular components; the selective toxicity of inhibitors allows bacterial cellular processes or structures to be impeded without compromising the eukaryotic host. The advances in bioinformatics, molecular biology and microbiological techniques over the past decade have enabled the detection of ~200-400 essential bacterial genes that could be *a priori* antimicrobial targets (Walsh, 2003). There are three classical metabolic pathways that consist of enzymes validated as successful targets: protein biosynthesis; DNA replication, repair and transcription; bacterial cell wall biosynthesis.

1.2.1.1. Protein biosynthesis

Protein biosynthesis is a complex process making it an attractive multifaceted target for antimicrobial agents. The bacterial biosynthetic machinery is sufficiently distinct from the analogous counterparts in eukaryotes. The central feature of protein synthesis is the bacterial ribosome, a ribonucleoprotein consisting of two subunits (30S and 50S) that associate to form a 70S ribosomal assembly (Lodish *et al*., 2004; Steitz, 2010). The initiation, elongation and termination of protein synthesis provide numerous potential binding sites and catalytic stages that could be disrupted by the introduction of different classes of antibiotics. Examples are illustrated in Table 1.1.

1.2.1.2. DNA replication, repair and transcriptional events

In order to access the information contained in DNA sequences, the complementary duplex strands of circular bacterial DNA have to be unwound temporarily or permanently for bacterial transcription and replication events respectively. Organisms possess topoisomerases, which are responsible for controlling DNA topology and relieving torsional stress by introducing transient single or double-strand breaks in the DNA. DNA gyrase is a topoisomerase unique to prokaryotes and is capable of performing the crucial events of both positive and negative DNA supercoiling (Champoux, 2001). Transcriptional events are performed by RNA polymerase, which involves the production of mRNA from information encoded within the DNA sequence (Cramer, 2002). The functions of the bacterial DNA gyrase and bacterial RNA polymerase are essential for viability, making them suitable antimicrobial targets (Table 1.1).

1.2.1.3. Cell wall biosynthesis

The bacterial cell wall is located on the extracellular face of the plasma membrane and is essential for viability. The central component, peptidoglycan, is an extensive glycan polymer of repeating disaccharide units with short peptide cross-links. It acts as an exoskeleton, conferring mechanical strength, enabling the cell to endure high internal osmotic pressures. Although peptidoglycan composition can vary greatly between different bacterial species, the enzymology of the biosynthetic pathway is

highly conserved, permitting a single class of antimicrobial to inhibit homologous targets (Lazar and Walker, 2002). The biosynthesis of peptidoglycan is a primary focus of this thesis and therefore Sections 1.5 and 1.6 provide a comprehensive overview of its role, chemical structure and biosynthetic pathway.

1.2.2. Major classes of antibiotics and their mode of action

The term antibiotic was initially denoted by Waksman (1944) to describe natural growth inhibitors; it is now broadly used to describe natural, semi-synthetic and synthetic antimicrobials. Antibiotics are classed according to common structural features. Table 1.1 illustrates the diverse structures of several different classes of antibiotics and the targets they inhibit.

Year	Class of Antibiotic	Example	Mode of Action
1935	Sulphonamide	Sulfadimethoxine 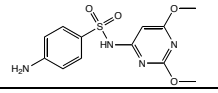	Corrupts the pathway of folate synthesis.
1940	β-lactam	Benzylpenicillin 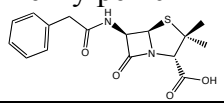	Inhibits transpeptidation, the final step in peptidoglycan synthesis.
1945	Tetracycline	Tetracycline 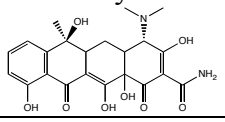	Binds to the 16S rRNA of the 30S ribosomal subunit, preventing the binding of the aminoacyl-tRNA, inhibiting protein synthesis.
1952	Macrolide	Erythromycin 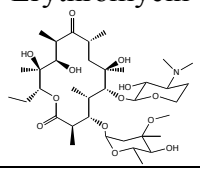	Binds to the 50S ribosomal subunit and prevents the translocation of peptidyl tRNA, inhibiting the elongation of the peptide chain during protein synthesis.
1958	Glycopeptide	Vancomycin 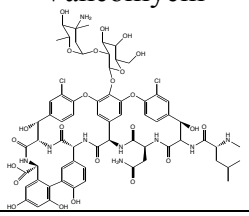	Binds to the D-Ala-D-Ala terminal of the pentapeptide side chain of the glycan chains, inhibiting the final steps of peptidoglycan synthesis.
1962	Quinolone	Ciprofloxacin 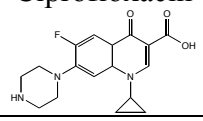	Inhibits bacterial DNA gyrase and topoisomerase IV, preventing DNA replication and transcription.
2000	Oxazolidinone	Linezolid 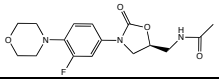	Inhibits the initiation complex formation during bacterial protein translation.

Table 1.1: Classes of antimicrobial agents. The first year of the commercial availability of each antibiotic class is shown. A member of each class is displayed as a structure, highlighting extensive structural disparities. The mode of action of the antibiotic class is briefly described. The examples are not intended to be an exhausted list of antibiotic classes. Adapted from von Nussbaum *et al.* (2006).

1.3. Antibiotic resistance

The ability of bacteria to survive in the presence of an antimicrobial compound is not a new phenomenon; it is a natural progression of evolution and classical Darwinian selection (Normark and Normark, 2002). Bacterial resistance to many antibiotics is often reported prior to the commercial exposure of the drug in a human population. As discussed by Harwell and Brown (2000), resistance to optochin, one of the first

antibiotics administrated to target pneumococcal infections, was reported in laboratory animals in 1912 ahead of its generalised release into the community. Optochin-resistant clinical isolates were later identified, providing one of the primary indications that antibiotic efficacy could be compromised. The time frame for antibiotic resistance development is highly varied. In the case of vancomycin, resistance was not detected until almost 30 years after its clinical introduction (Johnson *et al.*, 1990). As it stands, bacterial resistance to the majority of clinically used antibiotics has been documented (Levy and Marshall, 2004); this only becomes a problem when the efficacy of the drug therapy is affected.

Bacterial resistance to antimicrobial compounds is not restricted to pathogenic strains. An antibiotic will be active against susceptible, non-pathogenic bacteria, whilst selecting for resistant strains. Thus, non-pathogenic bacteria are able to harbour resistance elements within the environment, which can lead to the rapid dissemination of resistance genes through different taxonomic and ecological bacterial populations (Levy and Marshall, 2004).

1.3.1. Emergence or acquisition of resistance

A bacterial population can be resistant to an antimicrobial prior to its introduction into the environment (inherently resistant or containing previously acquired resistance elements) or develop or acquire resistance elements following antibiotic exposure. A biological fitness defect is often incurred upon attaining antibiotic resistance, which can generally be alleviated by a series of compensatory mutations (Andersson and Hughes, 2010). There are three main routes that enable bacteria to acquire resistance: inherent resistance, mutations and gene transfer (described below).

1.3.1.1. Inherent resistance

An entire bacterial species that exhibits a characteristic rendering it resistant to a specific antibiotic (or class) without further genetic modification is said to be inherently resistant (Normark and Normark, 2002). An unambiguous example is exemplified by the resistance to the β-lactam class of antibiotics by *Mycoplasma*, a

species that lack the peptidoglycan constituent of the cell wall (Bebear and Pereyre, 2005). A second example is the high level of intrinsic resistance displayed by *Pseudomonas aeruginosa*; a restricted outer-membrane permeability to hydrophobic antibiotics and the presence of multidrug efflux pumps impede the entry of antibiotics, such as macrolides, into the cell (Lambert, 2002; Normark and Normark, 2002).

1.3.1.2. Mutation

Under a persistent selection pressure exerted by an antibiotic, resistance can develop through spontaneously occurring mutations within the bacterial genome in the form of point mutations, deletions, inversions and insertions. Mutation frequencies conferring resistance vary between different bacterial strains depending on the efficacy of the DNA repair system and the desired resistance mechanism. Certain bacterial species, such as *Mycobacterium tuberculosis*, have a limited capability of genetic exchange, and solely rely on genetic alterations for resistance to antibiotics (Normark and Normark, 2002). For example, resistance to fluoroquinolones by this organism occurs by a series of successive mutations in the 'quinolone-resistance determining regions' of the targets *gyrA* and *gyrB* encoding the DNA gyrase (Takiff *et al.*, 1994). The stepwise development of mutations causing antibiotic resistance makes the identification of organisms with low-level resistance paramount; they provide the genetic platform for future generations of mutations, which can direct higher levels of resistance (Normark and Normark, 2002).

1.3.1.3. Genetic exchange

Sequencing of bacterial genomes has identified that proportions of their DNA originate from various sources (Normark and Normark, 2002). This is made possible through a process known as horizontal gene transfer, which is common among bacteria of the same genus, and has also been observed between evolutionary distant organisms (Alekshun and Levy, 2007). Resistance genes are collected on a mobile genetic element, propagated in the local environment and disseminated to other hosts and geographical locations (Levy and Marshall, 2004).

The major mechanisms that enable the genetic transfer of antibiotic resistance are transduction, transformation and conjugation. Transduction is the transfer of genetic material via bacteriophages. Transformation is the uptake of environmental naked DNA by naturally competent bacteria. Conjugation is the direct transfer of DNA between bacterial cells, which involves cell-cell contact via a sex pilus, linking their cytoplasms for genetic exchange.

The mobile genetic elements can be of various forms including plasmids, transposons and integrons, discussed briefly below.

1.3.1.3.1. Plasmids

Plasmids, previously referred to as resistance transfer factors (RTFs), were described as the vehicle that drove the spread of antibiotic resistance between bacteria. They are complex genetic elements, varying in size from 1-<100 kb. Plasmids contain several genes conferring resistance against different antibiotic classes, and they also encode transmissible functions, enabling self-replication and dissemination amongst the bacterial population (Alekshun and Levy, 2007).

1.3.1.3.2. Transposons

Transposons are mobile genetic elements that can exist in plasmids, other transposons or integrate into the chromosome of the host. They encode a site-specific transposase, which facilitates their own site-specific insertions and excisions (Alekshun and Levy, 2007). The antibiotic resistances encoded are specific to the transposon. For example, Tn5 encodes resistance to kanamycin, bleomycin and streptomycin (Mazodier *et al.*, 1985).

1.3.1.3.3. Integrons

Integrons are DNA elements that are able to acquire exogenous gene cassettes (that often encode antibiotic resistance) and convert them into functional genes. Integrons are unable to promote self-transposition and are stably incorporated into genetic elements as either mobile integrons (associating with transposons or plasmids) or super integrons (associating with immobile DNA i.e. chromosomes). They are

composed of an integrase (*intI*, a site-specific recombinase), a primary integration site (*attI*) and a promoter, directing the capture and transcriptional regulation of gene cassettes (Mazel, 2006). The physical association of integrons with stable genetic material allows the preservation of integrated gene cassettes in the absence of selection pressures (Fluit and Schmitz, 2004).

1.3.2. Biological mechanisms of antibiotic resistance

Bacteria have established and evolved a myriad of physiological mechanisms to evade the action of antimicrobial agents. The three major types are described below. A resistant bacterium can accommodate one or more of these mechanisms, thus they are not mutually exclusive.

1.3.2.1. Reduced antimicrobial uptake and accumulation

In order to be effective, antibiotics must accumulate to a bacteriocidal, or at least a bacteriostatic, level. Bacteria have developed strategies to prevent this occurrence. Gram-negative bacteria contain an outer-membrane (not possessed by Gram-positive bacteria), which restricts the permeability of small hydrophilic molecules and excludes larger ones, providing a barrier to the penetration of antibiotics (Lambert, 2002). The outer membrane contains porins, aqueous channels, which allow the acquisition of nutrients and other compounds including β-lactam and quinolone antibiotics from the surrounding environment (Lambert, 2002). *P. aeruginosa* exhibits a reduced absorption efficiency of these molecules through porins, accounting for low levels of antibiotic resistance (Lambert, 2002).

Efflux pumps provide an alternative means of preventing antibiotics from reaching inhibitory concentrations within the bacterial cell. They are found in all bacteria, where they are situated in the cytoplasmic or outer membrane and function to actively extrude toxic substances such as antibiotics, detergents and organic solvents from within the cell, driven by an energy source. Antibiotic resistance develops as a result of mutational hyper-expression of the efflux pumps, where transcriptional repressors are abolished (Normark and Normark, 2002). The genes encoding these systems can be located on the chromosome or on mobile genetic elements. Efflux

pumps exhibit a range of specificity; they may export a single substrate or a range of dissimilar compounds (Webber and Piddock, 2003). *P. aeruginosa* produces efflux pumps with a broad substrate specificity, allowing for a multidrug resistant phenotype (Lambert, 2002).

1.3.2.2. Antibiotic structural alterations

Resistance to antibiotics can arise through an enzymatic structural modification of the drug, rendering it ineffective. A prime example of this resistance mechanism involves the β-lactamases. These enzymes inactivate β-lactam-based antibiotics by hydrolysing the chemically functional β-lactam ring (Figure 1.1). This results in a structure that can no longer act as a suicide substrate for the inhibition of the penicillin-binding proteins (PBPs). β-lactamases can hydrolyse 10^3 penicillin molecules/sec, allowing the rapid destruction of the drug before it reaches the target enzymes (Walsh, 2000).

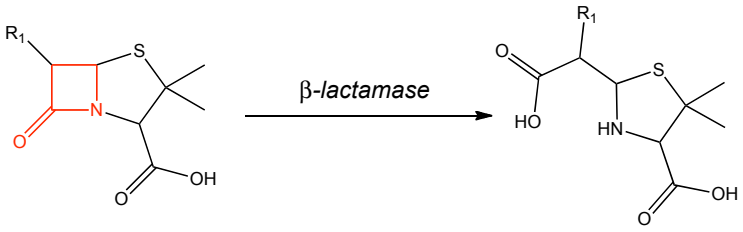

Figure 1.1: β-lactamase hydrolysis of the β-lactam ring. Common to all β-lactam antibiotics is the β-lactam ring (red). Hydrolysis of this moiety renders the antibiotic inactive.

A second example is the irreversible chemical modification of ribosomally targeted agents such as chloramphenicol and the aminoglycoside antibiotics. Functional groups are added to the periphery of the antibiotic by *N*-acetylation, *O*-phosphorylation or *O*-adenylation performed by acetyl transferases, phosphoryl transferases and adenyltransferases respectively (Walsh, 2000). These alterations to the antibiotic structure confer resistance by interfering with the affinity of these antimicrobials for their 50S (chloramphenicol) or 30S (aminoglycoside) ribosomal targets, thus preventing the inhibition of protein synthesis (Walsh, 2000).

1.3.2.3. Structural modification of the antibiotic target

Modifications to the antibiotic target can prevent drug recognition and can lead to high levels of antibiotic resistance. A classic example of the target alteration strategy is employed by vancomycin resistant enterococci (VRE). Vancomycin binds to the major component of the cell wall, peptidoglycan, and more specifically the D-Ala-D-Ala terminal of the pentapeptide chain constituent (Nieto and Perkins, 1971), obstructing the transpeptidation activity of the PBPs. This leads to a weakening of the cell wall and ultimately cell rupture. In high-level vancomycin resistant strains, the cell wall is reprogrammed by a structural set of genes *vanHAX* in conjunction with the regulatory genes, *vanSR*. The products of these genes replace the peptide stem terminal D-Ala-D-Ala with D-Ala-D-Lac (Walsh *et al.*, 1996). The binding of vancomycin to the termini of the pentapeptide stem from vancomycin-sensitive and resistant strains is depicted in Figure 1.2. The affinity of vancomycin for the altered terminal residues of the pentapeptide stem is decreased by 1000-fold, attributed to the loss of a single hydrogen bond and the introduction of a destabilising lone pair of electrons on the ester oxygen of D-Lac (McComas *et al.*, 2003).

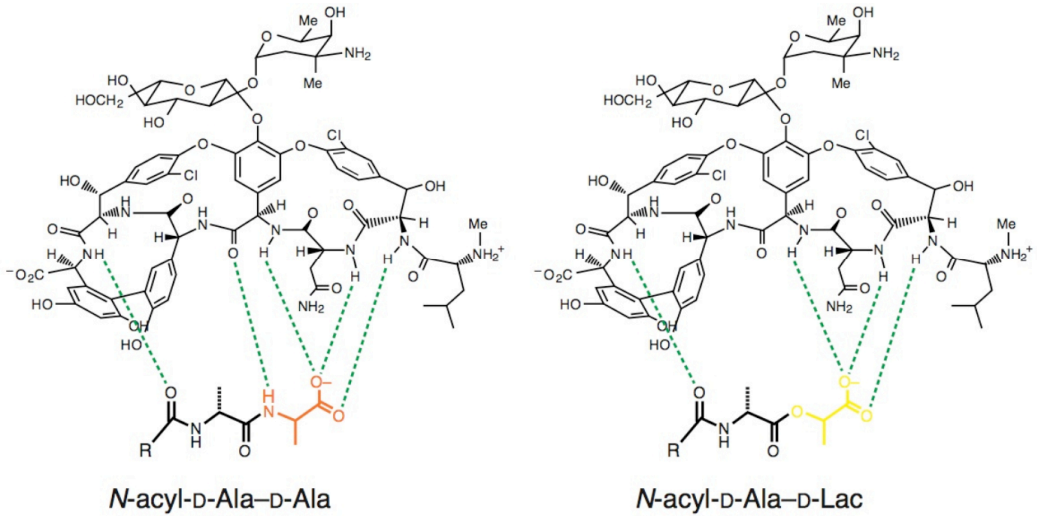

Figure 1.2: The interaction of vancomycin with the terminal of the pentapeptide stem. (a) D-Ala-D-Ala terminal. (b) D-Ala-D-Lac terminal. The terminal D-Ala and D-Lac residues are shown in orange and yellow respectively. The hydrogen bonds are displayed as green dashed lines. The presence of D-Lac confers resistance to vancomycin by causing the loss of a single hydrogen bond, which significantly reduces the affinity of antibiotic binding. Figure from Healy *et al.* (2000).

Another elegant example is the modification of the β-lactam targets, the PBPs. Mutations in the active site of *S. pneumoniae* PBPs cause a reduction in affinity for the antibiotic whilst maintaining enzyme functionality. This will be discussed in later sections in relation to the work of this thesis.

1.3.3. Strategies to combat antimicrobial resistance

A concerted effort by society to intervene with the emergence and spread of antibiotic resistance is paramount; failure to do so could cause a reversion back to the pre-World War II era when life-threatening diseases were untreatable. Emphasis should be targeted towards methods to conserve the efficacy and prolong the lifespan of existing antibiotics (relying on the response by healthcare organisations) and providing new tactics for combating resistance mechanisms (identifying novel targets and classes of antibiotics). With the decline of investment in antimicrobial design by the pharmaceutical industry and the prevalence of resistance mechanisms, antimicrobial agents are and should be considered a precious and finite source.

1.3.3.1. Healthcare policy

Healthcare organisations represent a key area for the control of antibiotic resistance development and dissemination. The prudent use of current drugs, prevention of unnecessary prescriptions and complete dismissal of antimicrobials from treatment programs could decrease the occurrence of resistance. Frequent surveillance of administrated drugs can correlate usage with the incidence of resistance. Thus, knowledge of local antibiotic susceptibilities is vital to ensure the appropriate therapy is prescribed (Masterton, 2008).

Healthcare environments provide a reservoir for antibiotic resistant bacteria. Various strategies have been implemented to tackle the spread of resistance. Statistics provided by the National Audit Office (2009) have shown that over a four year period (2004-2008), a predicted £57 million was spent on national initiatives to deal with healthcare associated infections.

A new campaign, supported by the Department of Health, has been promoted across Europe: the European Antibiotic Awareness Day (EAAD). This is a single day aiming to build on the public awareness of the antibiotic resistance threat, alerting the need for prudent and responsible use of antibiotics.

1.3.3.2. Development of new antibiotics and strategies

1.3.3.2.1. Traditional approaches to identify novel antibiotics

Over the past 60 years, natural products have been the focal point in the discovery and development of new antimicrobial agents. Early methods of identifying antibiotics from natural sources, such as soil bacteria, were hindered by the high volume screening strategies and the rediscovery of established classes of antibiotics: 22 % of soil actinomycetes produce streptothricin (Taylor and Wright, 2008). However, modern detection methods, including mass spectrometry, allow for high-resolution separation and analysis of small molecules from the environment (Davies, 2011). It has been predicted that merely 1-10 % of the metagenome has been sampled, thus a plethora of undiscovered molecules remain to be identified (Walsh, 2003).

Optimisation of established antibiotic structures is a common approach to derive new antimicrobial active compounds. Using existing scaffolds, modifications including attachment, removal or substitution of functional groups can provide many alternatives to a common structure with desirable pharmacological properties (von Nussbaum *et al.*, 2006). These alterations are often used to replace and consequently enhance the efficacy of natural products and represent the semisynthetic group of antibiotics. Between 1983 and 1994, 75 % of compounds were variants of natural products (Newman *et al.*, 2003), thus filling the void generated by the absence of new structural classes of antibiotics.

1.3.3.2.2. Bioinformatics and genomics

Following the first report of the complete bacterial genome of *Haemophilus influenzae* in 1995 (Fleischmann *et al.*, 1995), bioinformatics and genomics have been valuable tools in antibacterial drug discovery. Genome sequencing has allowed the identification of gene clusters involved in the biosynthesis of small compounds. From this analysis, it has been revealed that individual species of actinomycetes are capable of producing more than 20 secondary metabolites, some of which may have antibacterial activity (Baltz, 2008).

Genomics can also be exploited to discover new antimicrobial targets (McDevitt and Rosenberg, 2001). Various studies, such as gene disruption, deletion and over-expression, have identified essential genes for bacterial viability within a genome. In *E. coli*, it has been established that there are approximately 300 essential genes, which represent approximately 7 % of the genome (Gong *et al.*, 2008; Taylor and Wright, 2008). Comparisons with eukaryotic genomes can identify bacterial genes that do not share substantial homology, and consequently could present novel antimicrobial targets (Taylor and Wright, 2008).

1.3.3.2.3. High throughput screening

High-throughput screening involves a library of thousands of potential inhibitors, which are screened against a drug target. The efficacy of this process at identifying antimicrobials is illustrated with the following example. GlaxoSmithKline utilised the high-throughput technique to screen 67 antibiotic targets with ~530,000 small molecules. The structure of only five candidates were pursued, none of which passed through clinical trials (Payne *et al.*, 2007).

Conventional high-throughput screening methods use libraries containing natural products, often large complex molecules, which are less likely to successfully interact with a specified target. These libraries are now being replaced by molecules of 250 Da or less. These smaller and structurally simpler ‘fragments’ are more accessible for target binding (Waldrop, 2009).

1.3.3.2.4. Virtual screening

Virtual screening is a computational technique used to identify compounds of interest from chemical databases using two different approaches. The ligand-based method uses the structures of active ligands to retrieve similar compounds, which could interact with a target in an analogous manner. The receptor-based approach employs the 3D structure of a target to screen for compounds that bind in an equivalent or dissimilar way to known ligands. The increasing availability of 3D structures of drug targets makes virtual screening a valid technique to rapidly identify lead compounds (Agarwal and Fishwick, 2010).

1.3.3.2.5. Rational and *de novo* drug design

Rational drug design is a targeted approach based on significant functional and structural information of the drug target. The structural insights of protein-ligand interactions provided by NMR and X-ray crystallography enable structures (often substrate derivatives) to be generated and optimised rationally.

De novo computational drug design utilises the known 3D structural features of an antimicrobial target to iteratively generate specific inhibitors. Compounds are computationally constructed based on the steric and chemical properties of the target site. SPROUT is an example of such computational software that can be employed in *de novo* drug design (Gillet *et al.*, 1993). The application of SPROUT to the 3D-structures of *E. coli* DdlB (Besong *et al.*, 2005), *E. faecium* VanA (Sova *et al.*, 2009) and *E. coli* MurD (Horton *et al.*, 2003) has yielded specific inhibitor molecules to these important enzymes involved in peptidoglycan biosynthesis. Although this demonstrates the utility of *de novo* drug design in generation of inhibitory ligands against essential bacterial targets, it does not circumvent the problems of penetration of the inhibitor to its target. This is exemplified by the fact that none of these molecules possessed antimicrobial properties.

1.3.3.2.6. Inhibition of the resistance mechanisms

Following the characterisation of a resistance mechanism (such as those described in Section 1.3.2), a viable strategy is to design drugs for its inhibition. Although not antibiotics themselves, these drugs can be used in combination with an active antimicrobial. This approach can potentially restore and preserve the efficacy of therapies against which resistance has developed.

A prime example of this is the secondary metabolite clavulanic acid, a potent β-lactamase inhibitor, isolated from *Streptomyces clavuligerus* in 1977 (Reading and Cole, 1977). It has weak intrinsic antibacterial activity, but can be co-administered with β-lactam antibiotics such as amoxicillin (augmentin). Clavulanic acid has a higher affinity for the β-lactamase than amoxicillin and can irreversibly bind to the active site serine of the β-lactamase catalytic site, forming a stable acylated intermediate (Yang *et al.*, 1999). This combination therapy allows the antibiotic to exert its effect without the detrimental interference of a resistance mechanism.

1.3.4. Economic cost of antibiotic resistance

Additional to the importance of combating resistance socially, it is necessary to regard the issue from an economic perspective. Numerous considerations must be addressed when establishing the financial cost of antibiotic resistant infections including the duration of hospital stay, sick leave payments, treatments (often multi-faceted), morbidity and mortality. The cost of antibiotic resistant infections is hard to predict. However, it has been estimated that healthcare associated infections alone cost the NHS £4,300 for every avoidable healthcare inflicted infection, amounting to £1 billion a year (National Audit Office, 2009). The burden of antibiotic resistance on socio-economic costs justifies the necessity for its eradication.

1.4. Does the biosynthesis of peptidoglycan remain a viable antibiotic target?

The biosynthesis of the peptidoglycan layer of the bacterial cell wall is an established antibiotic target, validated by the action several clinically significant drugs including the β-lactam and glycopeptide classes of antimicrobials (Bugg, 1999). The essential nature and complexity of peptidoglycan biosynthesis, containing intracellular, membrane bound and extracellular enzymatic steps for interception with inhibitors, makes it an attractive target for antimicrobial therapy. Targeting the extracellular catalytic phase alleviates the structural difficulties associated with the design of drugs that must penetrate the cytoplasmic membrane, which can hinder antimicrobial development. To date, the peptidoglycan biosynthetic enzymes have been underexploited as antibiotic targets, although their appeal remains. The recent advances in molecular and structural biology will aid the future biochemical characterisations of the enzymes involved in peptidoglycan biosynthesis with the ultimate goal of developing antimicrobials for clinical practice and concomitantly conquering antibiotic resistance.

1.5. Peptidoglycan as an antimicrobial target

The work in this thesis focuses on the enzymes involved in the ultimate extracellular step of peptidoglycan synthesis, the penicillin-binding proteins (PBPs), with the aim of providing a valuable insight into their kinetic and structural characteristics. PBPs are the target of the most extensively used class of antimicrobials: the β-lactam based antibiotics. To demonstrate the role and significance of these enzymes, peptidoglycan must be understood in terms of its structural and biochemical properties and its biosynthesis; these aspects are summarised in the following sections.

1.5.1. The peptidoglycan layer of the bacterial cell wall

Peptidoglycan represents a vital dynamic constituent of the cell wall, present in nearly all eubacteria (with few exceptions including *Chlamidiae* sp. (although many of the biosynthetic genes have been identified in this species (McCoy and Maurelli, 2006)) and *Mycoplasma*) and is found exclusively in these organisms. Bacteria are crudely classified into two major groups, either Gram-positive or Gram-negative based on their reaction with the Gram stain (a dye-iodine complex) (Gram, 1884). In Gram-positive bacteria, the Gram reagent becomes trapped in the peptidoglycan layer surrounding the cytoplasmic membrane, which ranges from 20-80 nm in thickness (Bugg, 1999) and comprises 30-70 % of the cell wall (Schleifer and Kandler, 1972). In Gram-negative bacteria, the stain is not retained in the thin 2-3 nm peptidoglycan layer (Beveridge and Davies, 1983; Bugg, 1999; Gram, 1884). The composition of Gram-positive cell walls exhibits extensive variation between species in terms of amino acid composition and cross-linking. This contrasts the relatively constant architecture of Gram-negative cell walls (Schleifer and Kandler, 1972), which have an additional complex layer of phospholipids, lipoproteins, lipopolysaccharides and porins, known as the outer membrane (Bugg, 1999). Figure 1.3 highlights the key features of the Gram-negative and Gram-positive bacterial cell wall architecture.

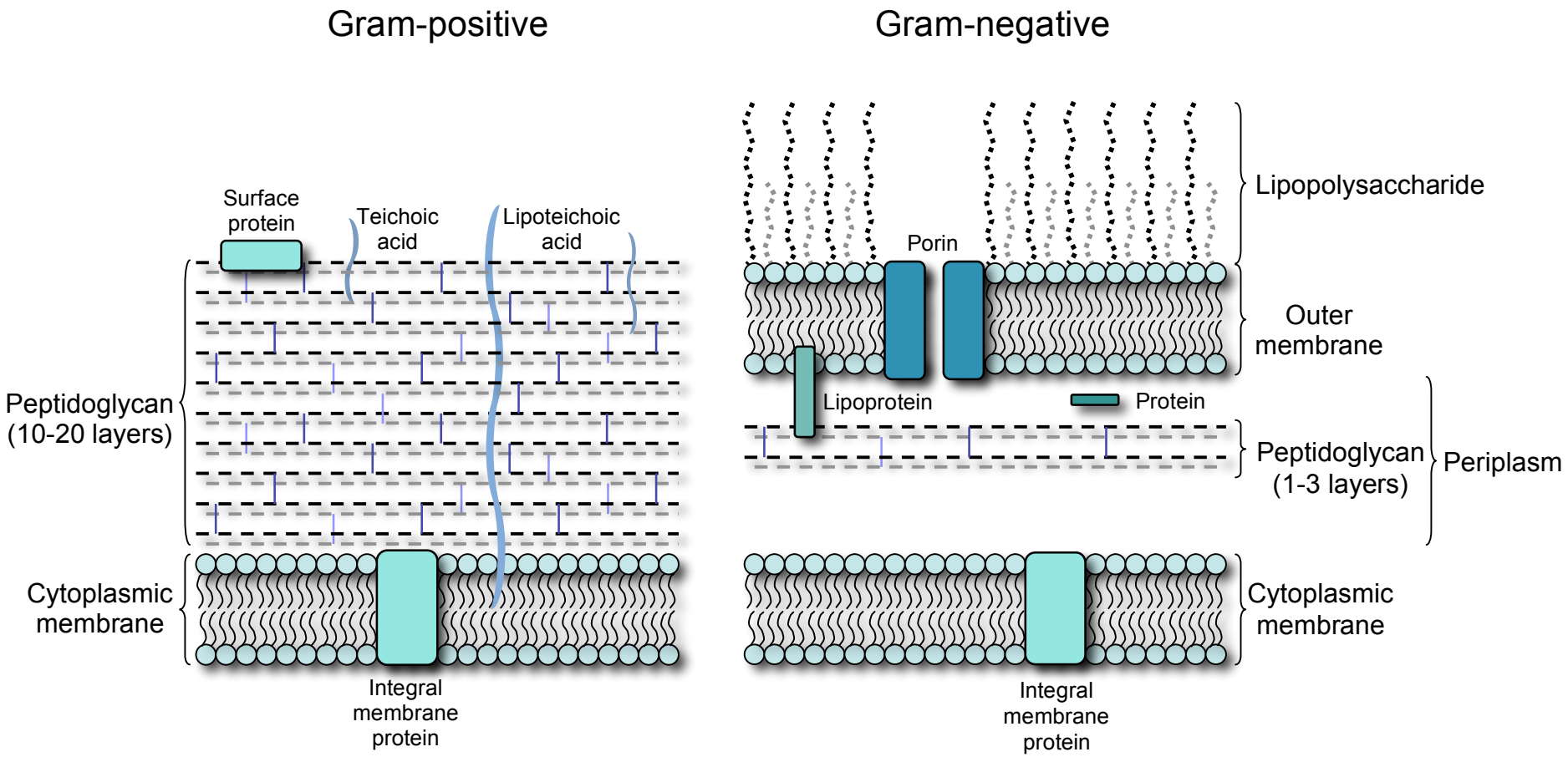

Figure 1.3: Schematic representation of the major structural components of Gram-positive and Gram-negative cell walls. Both cell walls have a peptidoglycan layer situated outside of the cytoplasmic membrane. Gram-negative bacteria have an additional lipid bilayer, the outer membrane, which is in close proximity to the peptidoglycan layer (Matias *et al*., 2003). Figure adapted from Cabeen and Jacobs-Wagner, (2005).

1.5.2. The role of peptidoglycan

Peptidoglycan performs the primary function of the cell wall: to endure the high internal pressures that can develop within a cell (up to 30 atm for some Gram-positive bacteria) (Bugg, 1999). Consequently, peptidoglycan must be mechanically strong and flexible, allowing reversible expansion under pressure. Globular, uncharged proteins are able to diffuse through the porous architecture of peptidoglycan. As reviewed by Vollmer *et al.* (2008a), the pore radii are of similar average sizes between Gram-positive and Gram-negative species; when relaxed or tort, proteins with molecular weights of 22-24 kDa and greater than 50 kDa respectively are able to penetrate the peptidoglycan layer in a non-selective manner. Peptidoglycan also serves as a scaffold to anchor external structures including proteins and teichoic acids of Gram-positive species and lipoproteins associated with the outer membrane of Gram-negative species (Bugg, 1999). The surface proteins of Gram-positive bacteria (covalently anchored to the peptide constituent of the peptidoglycan layer by the action of sortases (Mazmanian *et al.*, 1999; Ton-That *et al.*, 1999)) often have a part in the pathogenicity of the organism, promoting bacterial adhesion to specific tissues, invasion of host cells or resistance to phagocytic killing. The secondary role of peptidoglycan is to maintain a defined cell shape, a trait that is stable and heritable (Young, 2003), thus peptidoglycan is intimately involved in cell growth and division (Vollmer *et al.*, 2008a).

1.5.3. The chemical composition and architecture of peptidoglycan

Peptidoglycan is a continuous covalent macromolecule, consisting of extensive polymerised linear glycan strands, cross-linked via short peptide side chains. It can be modified during or after its biosynthesis, concurrent with aging or adaptation to environmental conditions, eliciting a great potential for interspecies variation. The basic structure of peptidoglycan, described in the monumental work of Schleifer and Kandler (1972), is discussed in the following sections.

1.5.3.1. The glycan strand backbone

The glycan chains are composed of alternating *N*-acetylglucosamine (Glc*N*Ac) and *N*-acetylmuramic acid (Mur*N*Ac) units, integrated as a disaccharide into the

elongating strand, linked by β-1,4 glycosidic bonds. A sequence of up to five amino acids (referred to as the pentapeptide) is appended by a peptide bond to the lactoyl carbonyl group of the Mur*N*Ac sugar ring (Vollmer *et al.*, 2008a). In Gram-positive bacteria, the reducing ends of glycan chains contain either a Glc*N*Ac or Mur*N*Ac residue. In all Gram-negative and some Gram-positive bacteria, the glycan chains terminate with a 1,6-anhydro-*N*-acetylmuramic acid residue by the action of lytic transglycosylases. Secondary modifications are frequent in glycan chains including *N*-deacylation, *O*-acetylation, *N*-glycolylation and attachment of surface polymers (Vollmer, 2008).

1.5.3.2. The pentapeptide side chain or stem

The common residues of the pentapeptide side stem are of the sequence L-Ala-γ-D-Glu-X-D-Ala-D-Ala, where X is a diamino acid generally L-Lys (Gram-positive) or *meso*-diaminopimelic acid (*meso*-DAP) (Schleifer and Kandler, 1972). D-amino acids are unique to bacteria, formed from the racemisation of L-amino acids, providing protection against proteases present in the external medium of the cell (Bugg, 1999). A significant degree of variation can occur at the level of each amino acid residue in the pentapeptide stem. The greatest discrepancies occur at the third position of the pentapeptide chain, which is involved in cross-linking in mature peptidoglycan; in a few strains, L-Lys, L,L-DAP or *meso*-DAP can be replaced by diverse residues including L-ornithine, 2,4-diaminobutyric acid, L-homoserine or *meso*-lanthionine (Vollmer *et al.*, 2008a). Notably, it was originally considered that position 5 of the stem was invariantly D-Ala. However, as a result of vancomycin resistance, this residue can be substituted by D-Lac or D-Ser in high and low level resistant strains respectively (Bugg, 1999). As the pentapeptide chain is truncated typically to four or sometimes three residues in the mature peptidoglycan, it is generically referred to as the stem peptide.

1.5.3.3. Stem peptide cross-links

Cross-linking of the peptide side chains provide peptidoglycan with the aforementioned tensile strength and introduce further structural and chemical

variation that can be used for taxonomic purposes (Schleifer and Kandler, 1972). Interstrand cross-links occur between peptide chains situated on adjacent glycan chains. Cross-links formed between the ε-amino group belonging to either L-Lys or *meso*-DAP at position 3 and the α-carbonyl group of D-Ala at position 4 of individual stem peptides are termed direct 4→3 cross-links (employed by Gram-negative and Gram-positive bacteria). Indirect cross-links (used by only Gram-positive species) are mediated by a chain of amino acids ranging from 1 to 7 amino acid residues in length, referred to as an interpeptide bridge. The amino acid residues constituting the interpeptide bridge are assembled via peptide bond formation onto the ε-amino group of the third position *meso*-DAP or L-Lys by intracellular enzymes (Vollmer *et al.*, 2008a). In this instance, cross-linking is now between the α-amino group of the N-terminal amino acid of the interpeptide bridge and the α-carbonyl group of D-Ala at position 4 of an adjacent stem peptide. Interpeptide bridges are species specific; examples are demonstrated in Table 1.2.

Bacterial species	**Interpeptide bridge**
Streptococcus pneumoniae	L-Ser-L-Ala, L-Ala-L-Ala
Staphylococcus aureus	Gly-Gly-Gly-Gly-Gly
Enterococcus faecalis	L-Ala-L-Ala
Lactobacillus viridescens	L-Ala-L-Ser
Enterococcus faecium	D-Asp, D-Asn
Micrococcus roseus	L-Ala-L-Ala-L-Ala-L-Thr

Table 1.2: Interpeptide bridges attached to the third position amino acid residue of the peptidoglycan stem peptide (Schleifer and Kandler, 1972). The sequence order is carboxyl to amino terminal (left to right).

Cross-linking reactions are performed by PBPs (detailed in later Sections). Although 4→3 cross-links are the most common, other transpeptide linkages exist in peptidoglycan. PBP-dependent 4→2 indirect cross-links are found in corynebacteria (Vollmer *et al*., 2008a). PBP-independent 3→3 cross-links constitute a minor proportion of the linkages in *E. coli* (Glauner *et al*., 1988), but have been found to predominate the peptidoglycan layer of non-replicating *M. tuberculosis* (Lavollay *et al*., 2008) and are found exclusively in the peptidoglycan of a β-lactam resistant mutant of *E. faecium* (Mainardi *et al*., 2000). The formation of 3→3 cross-links is

catalysed by L,D-transpeptidases, which are unrelated to the PBPs, and consequently provide a cross-linking reaction that is insensitive to all β-lactam antibiotics (with the exception of carbapenems (Lavollay *et al*., 2008; Triboulet *et al*., 2011)).

The degree of cross-linking is species dependent: 25-50 % and 70-90 % of peptides are cross-linked in Gram-negative and Gram-positive species respectively, accounting for the differences in peptidoglycan rigidity observed between the two groups of organisms (Bugg, 1999).

1.5.3.4. Summary of the basic constituents of peptidoglycan

The key features of peptidoglycan architecture, as described in the above sections, are represented diagrammatically in Figure 1.4.

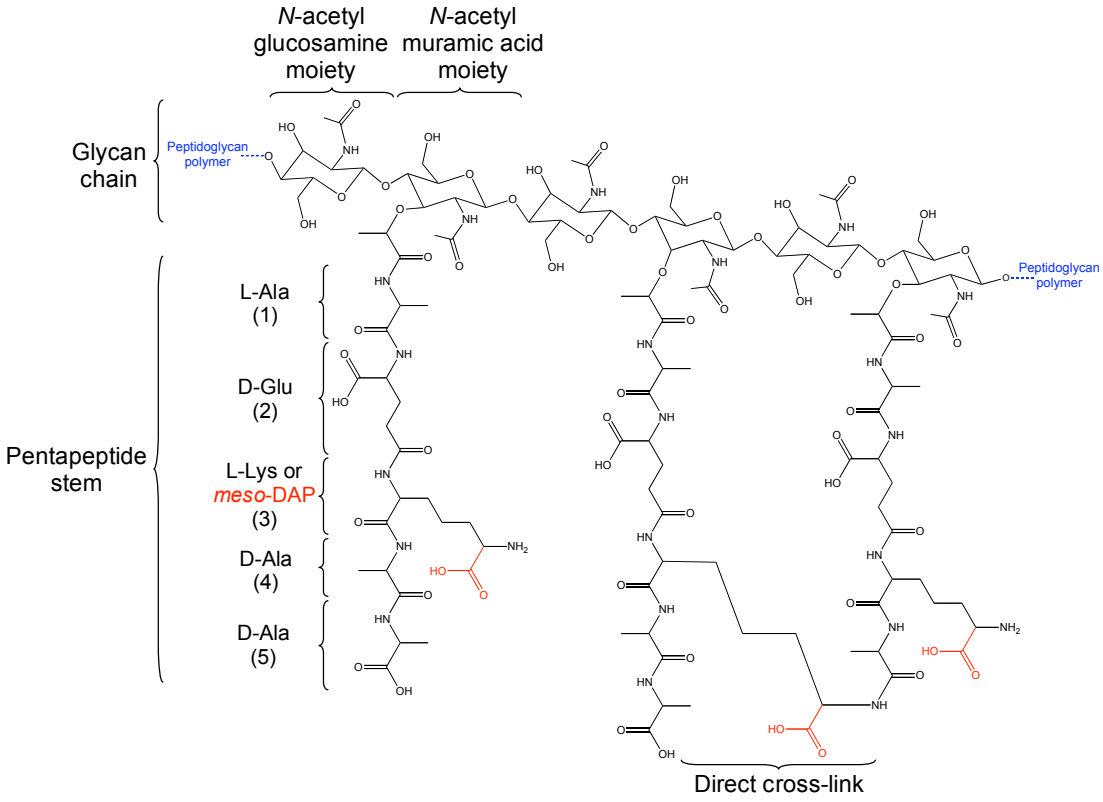

Figure 1.4: Key structural components of peptidoglycan. Gram-positive bacteria generally contain L-Lys at position 3 of the pentapeptide stem, whereas Gram-negative bacteria usually contain *meso*-DAP (additional carboxyl group (red) on the ε-carbon of L-Lys).

1.6. Peptidoglycan biosynthesis

Peptidoglycan biosynthesis occurs in three distinct phases, defined by the cellular location of each stage in the pathway: the cytoplasmic steps, the intracellular membrane bound steps and the extracellular membrane bound steps. The temporal and spatial control of the enzymes involved in the biosynthesis is essential to ensure that the integrity of peptidoglycan is not compromised. The following sections provide an overview of the peptidoglycan biosynthetic pathway.

1.6.1. Cytoplasmic steps of peptidoglycan biosynthesis

The cytoplasmic phase of peptidoglycan synthesis encompasses a series of enzymatic steps that culminate in the production of uridine-5'-disphospho (UDP)-Mur*N*Ac pentapeptide from UDP-Glc*N*Ac via a succession of nucleotide precursors.

The first committed stage of peptidoglycan synthesis is constituted by six enzymes: MurA-F. The majority of these enzymes were known by the mid-1970s, and since then their catalytic mechanisms have been characterised (Lazar and Walker, 2002). Table 1.3 summarises the role of MurA-F.

Enzyme	Substrates and cofactors	Enzyme role
MurA	UDP-Glc*N*Ac, PEP	Transfer of enolpyruvate to the hydroxyl group at position 3 of UDP-Glc*N*Ac
MurB	UDP-Glc*N*Ac-enolpyruvate, NADPH	Reduction of the enol group (forming UDP-Mur*N*Ac)
MurC	UDP-Mur*N*Ac, ATP, amino acid (usually L-Ala)	Addition of the first amino acid of the peptide stem to the lactoyl ether group of UDP-Mur*N*Ac
MurD	UDP-Mur*N*Ac-monopeptide, ATP, amino acid (usually D-Glu)	Addition of the second amino acid to the peptide stem of UDP-Mur*N*Ac
MurE	UDP-Mur*N*Ac-dipeptide, ATP, amino acid (usually *meso*-DAP or L-Lys)	Addition of the third amino acid to the γ-carboxyl group of the previous residue in the peptide stem of UDP-Mur*N*Ac
MurF	UDP-Mur*N*Ac-tripeptide, ATP, dipeptide (usually D-Ala-D-Ala)	Addition of the final two residues forming the pentapeptide stem of UDP-Mur*N*Ac

Table 1.3: An overview of the catalytic functions of MurA-F (Barreteau *et al.*, 2008).

MurC-F are referred to as the Mur ligases, which sequentially assemble amino acids to form the pentapeptide side chain using equivalent catalytic mechanisms. These enzymes share 10-20 % sequence identity (Bugg and Walsh, 1992), with most variation locating to the N-terminal domain, allowing specificity for their substrate amino acid (Barreteau *et al.*, 2008). The formation of the peptide stem proceeds as follows: the carboxyl group of the terminal amino acid residue of the nucleotide substrate is activated by ATP-dependent phosphorylation. This undergoes nucleophilic attack by the amino group of an amino acid or dipeptide, with the concomitant release of inorganic phosphate and peptide bond formation (Bouhss *et al.*, 1999).

The cytoplasmic phase is completed upon the formation of UDP-Mur*N*Ac-pentapeptide. Figure 1.5 shows the components involved in this stage of peptidoglycan biosynthesis.

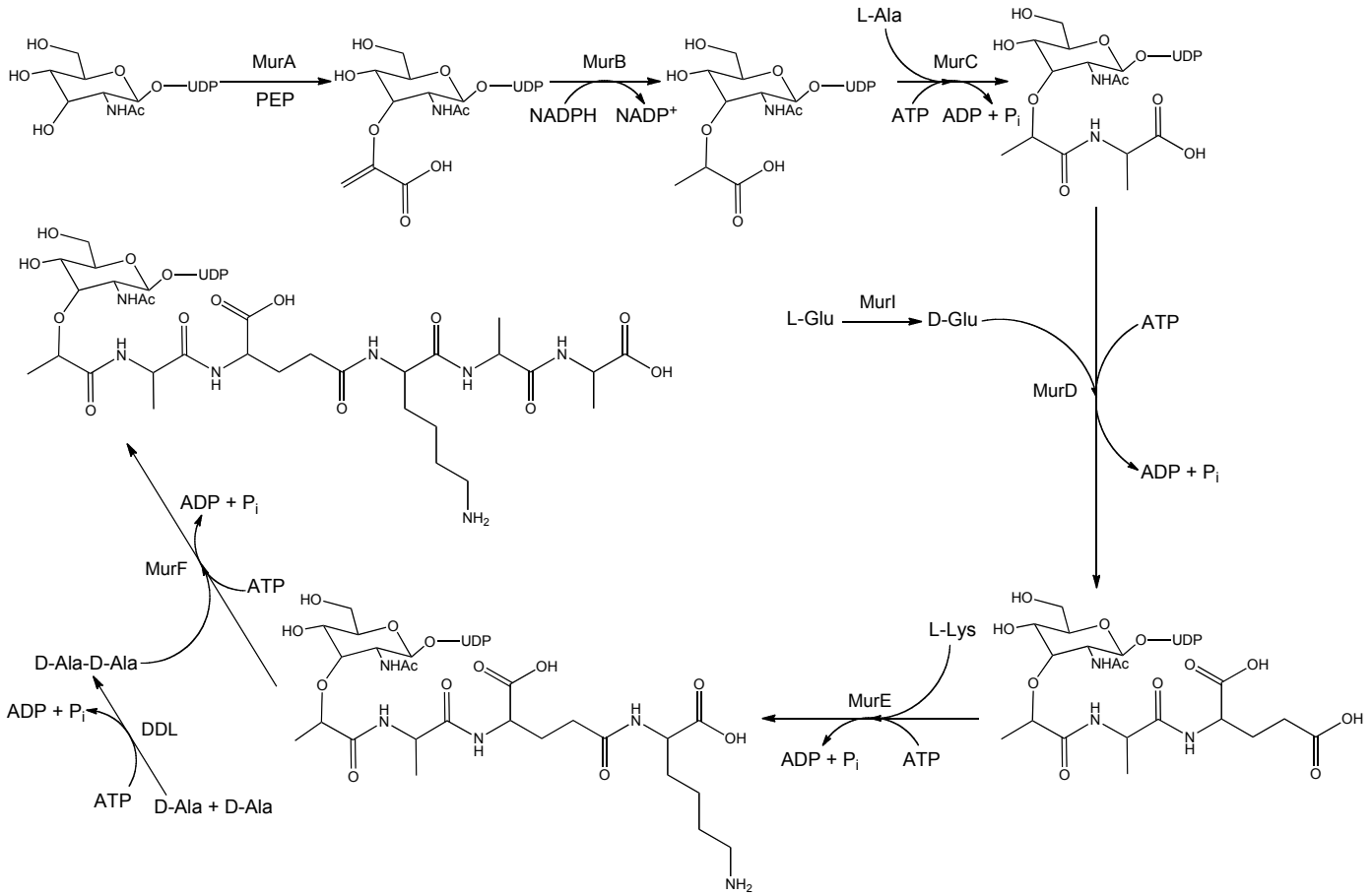

Figure 1.5: The cytoplasmic steps in peptidoglycan biosynthesis. UDP-Glc*N*Ac is converted into UDP-Mur*N*Ac by MurA and MurB. The amino ligases, MurC-MurF, sequentially add L-Ala, D-Glu, L-Lys (or *meso*-DAP, not shown) and D-Ala-D-Ala dipeptide to the lactoyl group of UDP-Mur*N*Ac, completing the cytoplasmic phase of peptidoglycan biosynthesis with the formation of UDP-Mur*N*Ac-pentapeptide. The D-Ala-D-Ala dipeptide substrate of MurF is synthesised by the condensation of two D-Ala by D-Ala:D-Ala ligase (DDL). This enzyme is not a member of the Mur ligase family but is specific to peptidoglycan biosynthesis (Barreteau *et al.*, 2008).

1.6.2. Intracellular membrane bound steps of peptidoglycan biosynthesis

The first membrane bound step of peptidoglycan synthesis occurs on the cytoplasmic face of the membrane, linking the product of the cytoplasmic phase to undecaprenyl phosphate, C_{55}. This classical lipid carrier can be synthesised in two ways: direct phosphorylation of undecaprenol by a kinase or recycling of undecaprenyl pyrophosphate by dephosphorylation (Hartley *et al.*, 2008). MraY, a translocase, catalyses the transfer of the hydrophilic phospho-Mur*N*Ac-pentapeptide moiety of UDP-Mur*N*Ac-pentapeptide onto undecaprenyl phosphate, yielding undecaprenyl pyrophosphoryl-Mur*N*Ac-pentapeptide (Lipid I) and UMP (Bouhss *et al.*, 2004; Lloyd *et al.*, 2004; Ikeda *et al.*, 1991). The reaction is reversible, but *in vivo* it is drawn in one direction by coupling it to the enzyme involved in the final intracellular membrane stage, MurG (Bouhss *et al.*, 2004), which catalyses the transfer of Glc*N*Ac from UDP to the hydroxyl group on the carbon at position 4 of the muramyl sugar ring of lipid-linked Mur*N*Ac-pentapeptide (Ha *et al.*, 1999). The production of undecaprenyl pyrophosphoryl-Mur*N*Ac-(Glc*N*Ac)-pentapeptide (Lipid II) completes the second phase of peptidoglycan synthesis. Variations in mature peptidoglycan composition are often incorporated onto Lipid II prior to the remaining extracellular reactions of the biosynthetic pathway. Examples include amidation, hydroxylation, acetylation and integration of amino acid branches involved in indirect peptide cross-links (Vollmer *et al.*, 2008a).

1.6.3. Linking the intracellular and extracellular membrane bound steps of peptidoglycan biosynthesis

In order for peptidoglycan to be assembled in the extracellular region of the cell, Lipid II must be translocated across the cytoplasmic membrane at a rate of 5000 molecules per sec to match the rate of peptidoglycan synthesis (Sanyal and Menon, 2009). Until very recently, the so-called putative flippase responsible this role has remained highly elusive. The potential flippases had to fulfil various requirements; they have to be inner membrane proteins, and essential and conserved in peptidoglycan producing eubacteria (Ruiz, 2008). Candidates have been speculated for over 30 years, the most plausible being MurJ, FtsW, RodA and SpoVE. The

latter three enzymes belong to the SEDS (shape, elongation, division and sporulation) family and are present in complexes involved in elongation, division and sporulation respectively. Mohammadi *et al*. (2011) have validated that FtsW (and not MurJ) is capable of transporting Lipid II across a membrane vesicle or proteoliposome. The identification of the flippase as FtsW will further the understanding of peptidoglycan synthesis and cellular growth, as well as presenting a new antimicrobial target.

1.6.4. Extracellular membrane bound steps of peptidoglycan biosynthesis

The final stage of peptidoglycan synthesis occurs on the extracellular face of the cytoplasmic membrane and involves the continuous and tightly coupled transglycosylation and transpeptidation activities of the integral membrane proteins, the PBPs. These enzymes are subject to this thesis and will be discussed in detail in the following sections. Briefly, transglycosylation reactions incorporate the hydrophilic disaccharide pentapeptide moiety of Lipid II into a pre-existing, elongating glycan chain. The C4 hydroxyl group of the Glc*N*Ac component belonging to the attacking Lipid II displaces the undecaprenyl pyrophosphate anchor at the terminal Mur*N*Ac C1 of a glycan chain, forming a β-1,4-glycosidic bond (Bugg, 1999). The glycan chains of peptidoglycan have varying lengths, specific to the PBP catalysing the transglycosylation reaction and its cellular location (Wang *et al.*, 2008). The undecaprenyl pyrophosphate is flipped back across the membrane and dephosphorylated, which can occur before or after translocation depending on the phosphatase (Tatar *et al*., 2007), regenerating undecaprenyl phosphate.

The transglycosylation of Lipid II forms a soluble glycan polymer (Ward, 1984). It is not until PBP-mediated transpeptidation occurs perpendicular to the glycan chains that the peptidoglycan forms an insoluble matrix, thereby fulfilling its role of maintaining structural integrity of the cell (Ward, 1984). As described in Section 1.5.3.3 the transpeptidation reactions occur via peptide bond formation between peptide stems in close proximity; the amino group side chain of the third position amino acid (or an amino acid branch) of one stem (acceptor) forms a peptide bond with the carbonyl group of the fourth position D-Ala of an adjacent stem (donor),

displacing the terminal D-Ala (Sauvage *et al*., 2008a). The resulting 4→3 transpeptide cross-link contains a tetrapeptide, the terminal of which is no longer recognised by the PBPs and thus it can only serve as an acceptor for future transpeptidation reactions (Goffin and Ghuysen, 2002).

The intracellular and extracellular membrane-bound stages of peptidoglycan biosynthesis are summarised in Figure 1.6.

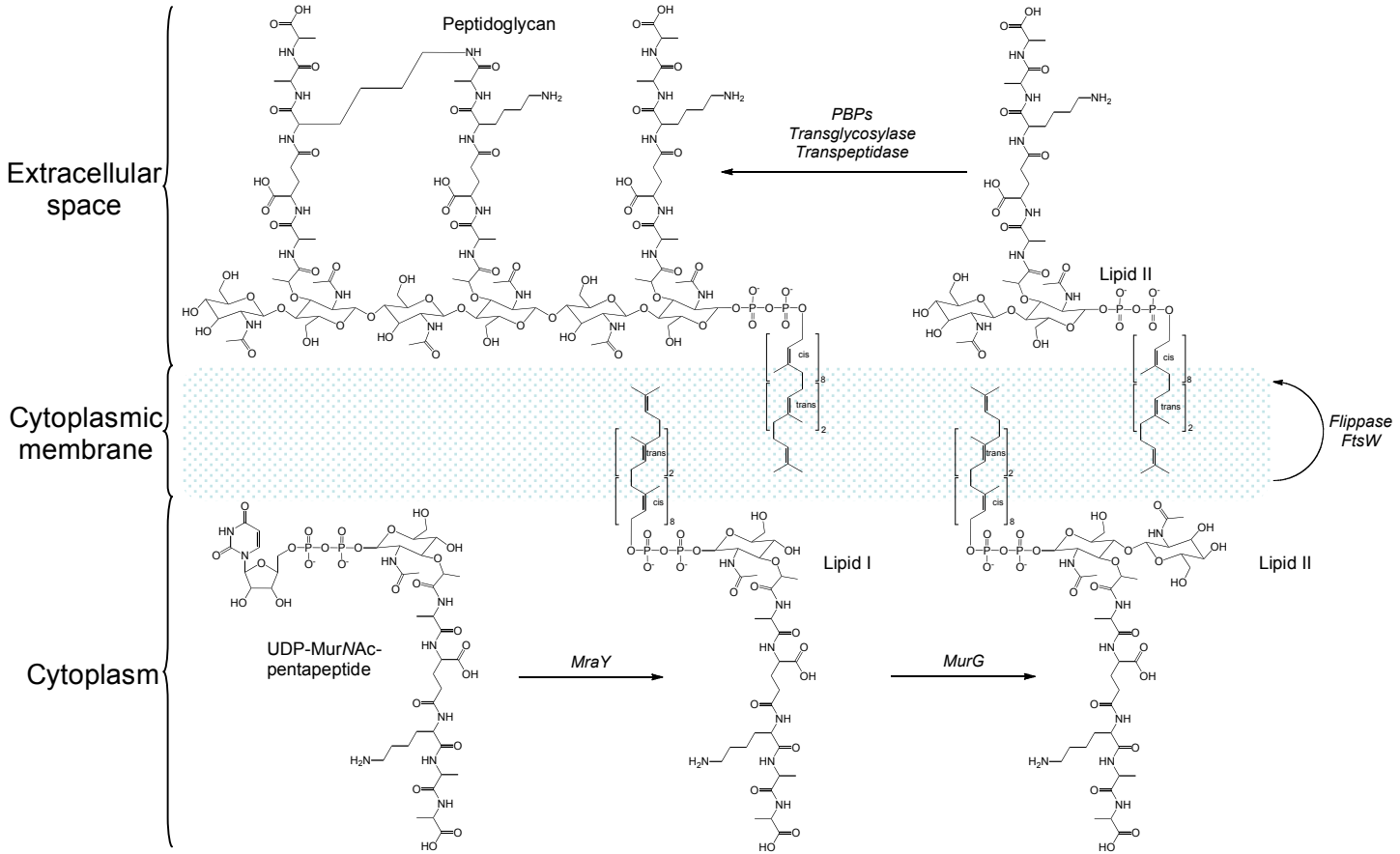

Figure 1.6: The membrane bound steps of peptidoglycan biosynthesis. The product from the cytoplasmic phase of peptidoglycan biosynthesis, UDP-Mur*N*Ac-pentapeptide, is the substrate for the membrane bound steps. MraY and MurG substitute UMP for undecaprenyl phosphate and add a Glc*N*Ac moiety respectively, generating Lipid II. Lipid II is translocated across the membrane where it is polymerised by the transglycosylation and transpeptidation activities of the PBPs. The pathway is exemplified with an unmodified L-Lys at position 3 within the stem peptides. This template applies equally to pathways where the L-Lys is modified by aminoacylation or is replaced by *meso*-DAP.

1.6.5. Peptidoglycan remodelling

During different phases of the cell cycle, peptidoglycan undergoes extensive remodelling and rebuilding. The enzymes responsible for the structural adjustments and chemical alterations are peptidoglycan hydrolases, a vast group of enzymes with diverse activities. The hydrolases have numerous roles: peptidoglycan maturation; regulation of cell wall growth, peptidoglycan expansion and elongation; separation of daughter cells during cell division; enlargement of pore size; release of signalling molecules from products of peptidoglycan turnover; peptidoglycan cleavage during sporulation or spore germination; autolysis, removing damaged cells from a population (Vollmer *et al.*, 2008b). Many hydrolases have been identified and characterised in *E. coli*, examples are given in Figure 1.7.

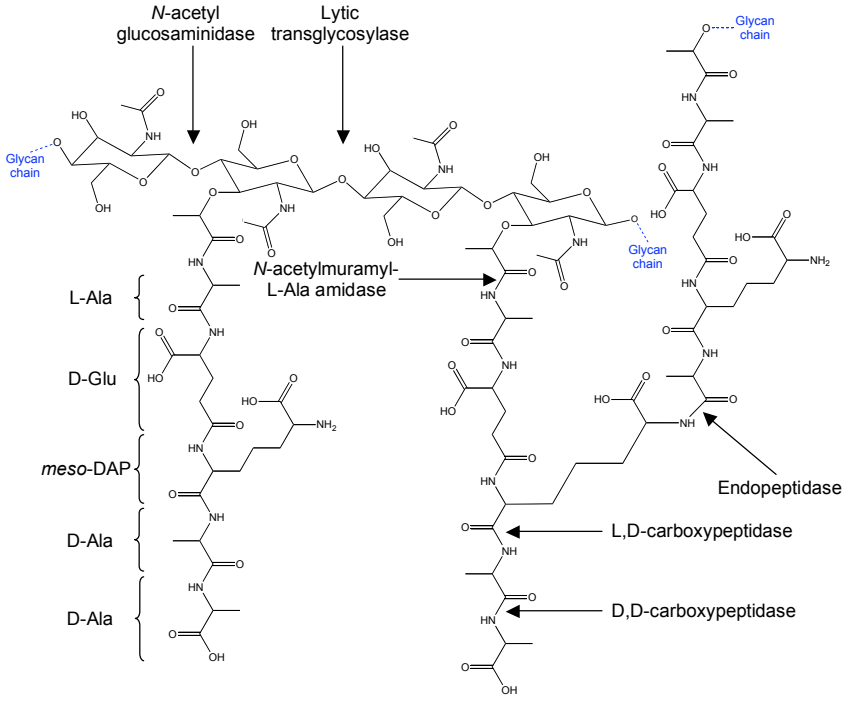

Figure 1.7: *E. coli* peptidoglycan hydrolases. The basic structure of *E. coli* peptidoglycan is shown. The arrows mark the point of cleavage by the stated hydrolase. Adapted from Bugg (1999).

Temporal and spatial regulation of hydrolase activity is essential to prevent excessive peptidoglycan degradation, which would be detrimental to the cell. This can be achieved by various factors (as reviewed by Vollmer *et al.* (2008b)) including transcriptional and translational control, chemical alteration of the substrate and targeting the enzyme to specific cellular locations.

1.6.6. Peptidoglycan recycling

In 1985, Goodell and Schwarz discovered the important phenomenon of peptidoglycan recycling in Gram-negative bacteria, where turnover products from the activity of the hydrolases are retained and utilised by the cell. Peptidoglycan recycling has largely been studied in *E. coli*, identifying the involvement of nine cytoplasmic enzymes, an inner membrane permease and a periplasmic peptide binding protein (Park and Uehara, 2008). Recycling plays an important role in peptidoglycan metabolism; it has been estimated that *E. coli* only lose 6-8 % of its peptidoglycan per generation (Goodell and Schwarz, 1985); up to 50 % of the peptidoglycan is degraded and recycled (Goodell, 1985), which is either used in the resynthesis of peptidoglycan or as an energy source (Park and Uehara, 2008).

Peptidoglycan recycling has not been documented in Gram-positive bacteria. New peptidoglycan is incorporated at the inner cell surface, moving and expanding the peptidoglycan in an outwards fashion, until it is shed as large fragments into the surrounding medium by the action of the hydrolases. 25-50 % of peptidoglycan is lost in this way per generation (Goodell, 1985; Park and Uehara, 2008).

1.6.7. Models of peptidoglycan expansion

Peptidoglycan is classically depicted as a static layer, which is far from reality. It is constantly subject to morphological changes to support different stages of the cell cycle including elongation and division. Different models have been proposed to explain the controlled turnover of peptidoglycan during the cell cycle. An 'inside-to-outside' model has been proposed for growth of Gram-positive bacteria (Koch and Doyle, 1985). Nascent peptidoglycan is synthesised directly adjacent to the cytoplasmic membrane, causing the layers to move outwards, becoming tort. The conformationally stretched layers then become the target of hydrolase activity. In this model, new covalent layers of peptidoglycan are formed before older ones are eliminated, thus the integrity of the cell wall is never compromised (Koch and Doyle, 1985).

A 'three-for-one' growth model has been suggested for *E. coli* (Höltje, 1998). In this model, three newly synthesised cross-linked glycan chains form peptide cross-links with glycan chains on either side of a single so-called docking strand. Specific hydrolysis of the covalent links of the pre-existing docking strand leads to its release from the peptidoglycan layer (Scheffers and Pinho, 2005). This model conforms with the 'make-before-break' strategy proposed by (Koch and Doyle, 1985) where three new glycan chains are inserted into the peptidoglycan layer before the removal of the old docking strand, avoiding the risk of autolysis (Scheffers and Pinho, 2005).

1.6.8. Antimicrobial inhibitors of peptidoglycan biosynthesis

Peptidoglycan is a validated target for inhibition by antimicrobial agents. Table 1.4 summarises the known inhibitors of various committed enzymatic steps of peptidoglycan synthesis.

Target	Inhibitor
MurA	Fosfomycin
MurB	Structural derivatives of 3,5-dioxopyrazolidines (Yang *et al.*, 2006)
Mur ligases	Phosphinate compounds (Strancar *et al.*, 2007)
Ddl	D-cycloserine
MraY	Tunicamycin
MurG	Ramoplanin
PBP: transglycosylase activity	Moenomycin
PBP: transpeptidase activity	β-lactams

Table 1.4: Antibiotics and inhibitors available against various essential steps of peptidoglycan synthesis.

1.7. Thesis direction

The work of this thesis focuses on the ultimate stages of peptidoglycan biosynthesis, the polymerisation of Lipid II by the action of the PBPs. The following section details the existing knowledge of the PBPs in terms of their classification, structure and their inhibition by antibiotics.

1.8. The penicillin-binding proteins

In the 1960s, intensive studies on bacterial cell wall biosynthesis identified that penicillin irreversibly bound to multiple undefined components locating outside of the cell membrane. Later studies revealed that these 'penicillin-binding components' (Tipper and Strominger, 1965) represented a group of enzymes sensitive to penicillin and β-lactam derivatives, which are now termed the penicillin-binding proteins (PBPs). These enzymes are essential for cell viability, responsible for the tensile strength of peptidoglycan, and encompass a family of validated antimicrobial targets (Bugg, 1999).

PBPs have been the subject of biochemical investigations for almost half a century (Tipper and Strominger, 1965). In spite of this, these enzymes remain poorly characterised in comparison to other members of the peptidoglycan biosynthetic pathway. This can be attributed to the difficulties associated with the study of PBPs, the majority of which are integral membrane proteins that require structurally complex substrates, such as Lipid II or its polymerised counterpart. However, the recent advances in the field of membrane protein biology and the ability to synthesise significant quantities of peptidoglycan precursors have propelled progress in this area of research.

1.8.1. Establishing the nomenclature of penicillin-binding proteins

In general, bacteria contain between 1,000 to 10,000 PBP molecules per cell, which constitutes approximately 1 % of the entire membrane protein population (Waxman and Strominger, 1983). The number of different PBPs expressed by individual bacterial species has been resolved through genome sequencing. Each bacterial cell contains typically three to eight distinct PBPs (with sixteen identified in *Bacillus subtilis* (Sauvage *et al.*, 2008a)) that vary in their relative abundance (Waxman and Strominger, 1983). Historically, once the number of PBPs within an organism had been determined, they would be numbered according to their migration through SDS-PAGE with decreasing molecular size. This can lead to confusion, as PBPs from different species with comparable properties and molecular weights are often

not denoted with the same number; *S. aureus* PBP1 is equivalent to *E. coli* PBP3 (Sauvage *et al.*, 2008a). Additional PBPs discovered thereafter are designated a letter following the appropriate number. For example, a novel 78 kDa PBP was revealed in methicillin-resistant *Staphylococcus aureus* (MRSA) strains in addition to the four native *S. aureus* PBPs (PBP1, PBP2, PBP3 and PBP4) and so was termed PBP2a. This system avoids renumbering, which could introduce comparative issues with older literature (Georgopapadakou, 1993).

1.8.2. Classification and basic topology of the penicillin-binding proteins

From analyses of over 200 unique peptidoglycan-producing eubacterial genomes, it has been determined that PBPs have multimodular structures, and although they share homologous domains, they also exhibit variations (Macheboeuf *et al.*, 2006). PBPs are grossly categorised on the basis of their molecular size, amino acid sequence similarities and catalytic activity of their N-terminal domain. Primarily, PBPs are segregated into two main groups depending on their size: low molecular weight (LMW) (40-50 kDa) and high molecular weight (HMW) (60-140 kDa) (Waxman and Strominger, 1983).

The LMW-PBPs (also referred to as Class C PBPs) are either soluble enzymes or are associated with the extracellular face of the cytoplasmic membrane by a transmembrane or amphiphatic helix (Macheboeuf *et al.*, 2006). They can be further subdivided into classes A, B and C (Ghuysen, 1991). These enzymes have a single catalytic domain that exhibits D,D-carboxypeptidase or endopeptidase activity, responsible for controlling the degree of transpeptidation or structural modifications of peptidoglycan and are not essential for cell viability (Denome *et al.*, 1999).

The HMW-PBPs are integral membrane proteins and have a basic topology consisting of a short N-terminal cytoplasmic tail, an α-helical transmembrane anchor and two extracellular domains connected by an inert linker region. They are divided into Classes A and B depending on the activity of the extracellular N-terminal domain and further subdivided based on sequence alignments (Goffin and Ghuysen, 1998; Sauvage *et al.*, 2008a). Class A HMW-PBPs are bifunctional enzymes with

extracellular N-terminal and C-terminal domains exhibiting transglycosylase and transpeptidase activity respectively. Class B HMW-PBPs have only one catalytic domain, which is located at the C-terminus and displays transpeptidase activity. An N-terminal domain exists but has unassigned activity; it has been suggested that this domain could be involved in cell morphogenesis, protein dimerisation, or function in the positioning of the transpeptidase domain of Class B PBPs at an equal distance from the membrane as the equivalent domain of Class A PBPs (Macheboeuf *et al.*, 2006; Sauvage *et al.*, 2008a).

A further group of monofunctional integral membrane proteins of importance are the monofunctional glycosyl transferases (MGT) (Di Berardino *et al*., 1996; Spratt *et al*., 1996). These enzymes are not PBPs as they lack a penicillin-binding domain, but they have a complementary role to the transglycosylase activity of HMW Class A PBPs and so are highly relevant in peptidoglycan chain polymerisation (Macheboeuf *et al.*, 2006).

The classification and domain topology of the PBPs and MGTs are summarised in Figure 1.8.

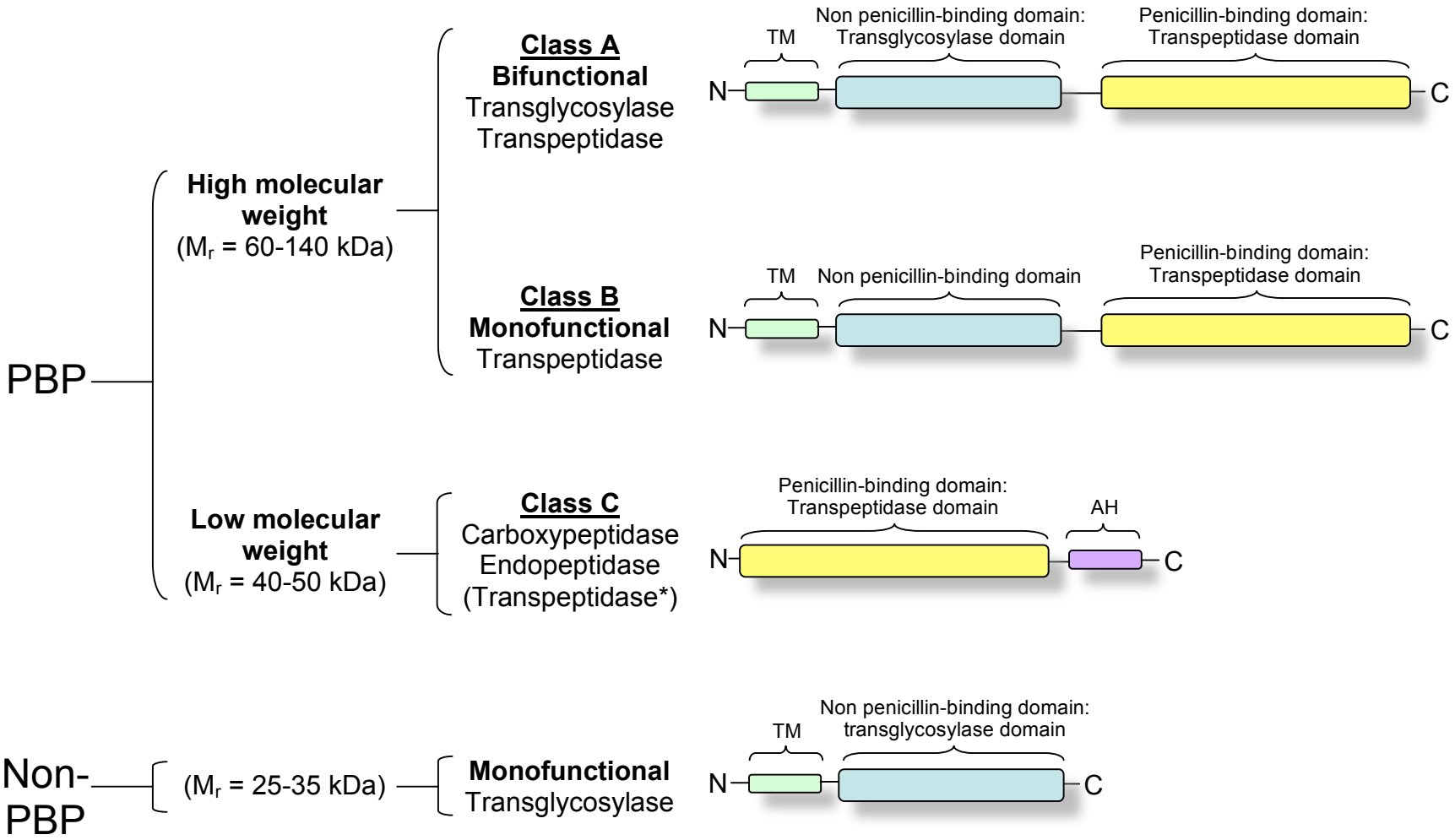

Figure 1.8: Classification, enzymatic activities and topology of the Penicillin-Binding Proteins. Broad classification (left) and the generalised domain topology (right) of the enzymes are shown. TM, transmembrane domain; AH, amphiphatic helix. *LMW-PBP transpeptidation has been demonstrated *in vitro* (Kumar and Pratt, 2005).

1.8.3. Localisation of PBPs at different stages of the cell cycle

PBPs function at specific points during the cell cycle; some have redundant activities, whereas others are unique and essential, causing a loss of viability when deletions are incurred. During the cell cycle, cell wall metabolism can essentially be divided into two stages: elongation and division; both processes require precise temporal and spatial control of numerous essential proteins, which are conserved in all cell wall synthesising bacteria (Morlot *et al.*, 2003). The localisation of *S. pneumoniae* PBPs will be discussed, as these enzymes are the primary focus of work in this thesis. *S. pneumoniae* contains one LMW-PBP (PBP3), and five HMW-PBPs (class A PBP1a, PBP1b and PBP2a; class B PBP2b and PBP2x) (discussed in Section 1.10).

S. pneumoniae are lancet-shaped and are surrounded by an equatorial ring, which is signified by an outgrowth of the cell wall. As the cell grows, the equatorial ring is duplicated and the resulting two rings progressively separate, marking the position of future division sites of the daughter cells (Higgins and Shockman, 1970). Nascent peptidoglycan is inserted between the duplicated rings, and septal cell wall growth occurs perpendicular to the long cell axis at the original position of the equatorial ring (before duplication). FtsZ coordinates division at the septum by initiating the interdependent assembly of various proteins. The polymerisation of FtsZ into a ring-like structure and its subsequent constriction is believed to drive the division process (Morlot *et al.*, 2003).

Elegant localisation studies of *S. pneumoniae* PBPs have been performed by Morlot *et al.* (2003) and (2004) using immunofluorescence. In non-dividing cells, HMW-PBPs are located equatorially with FtsZ. Immunolabelling revealed that during the division process, PBP1a and PBP2x remain at the midcell where the septum forms, and PBP2a and PBP2b follow the localisation of the duplicated equatorial rings (Figure 1.9). Interestingly, it was apparent that following recruitment to the septum by possible interactions with cell-division proteins, PBP1a and PBP2x persist independently of division complex. PBP1b locates exclusively septally or equatorially, but simultaneous localisation never occurs (Morlot *et al.*, 2003). The LMW *S. pneumoniae* PBP3 is evenly distributed across the hemispheres where

mature peptidoglycan exists but is absent from the division site. The D,D-carboxypeptidase activity of PBP3 removes the substrate for HMW-PBP transpeptidation, thus HMW-PBP localisation is also mediated by substrate availability (Morlot *et al.*, 2004).

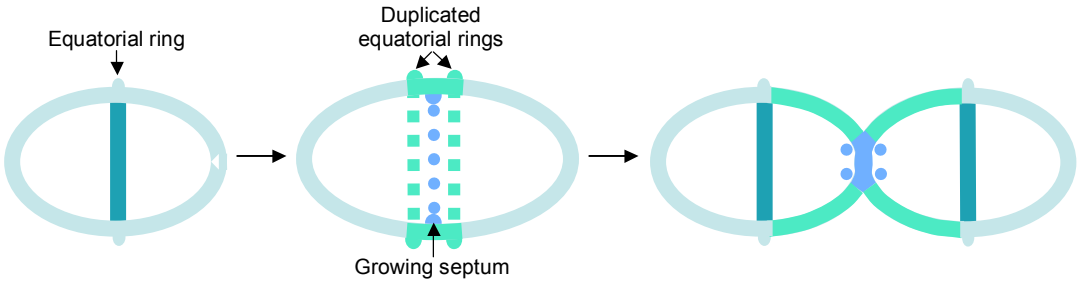

Figure 1.9: Organisation of the HMW-PBPs during *S. pneumoniae* growth and division. HMW-PBPs are located equatorially (turquoise band) in non-dividing cells. As the cell grows, the equatorial rings are duplicated and peripheral peptidoglycan (green) is biosynthesised by PBP2b and PBP2a (green squares). Septal peptidoglycan synthesis (blue) proceeds by the action of PBP2x and PBP1a (blue circles). Following division, the PBPs locate equatorially once again.

1.9. The functional domains of PBPs

The catalytic domains of HMW-PBPs are of great interest from a mechanistic and therapeutic perspective. The present knowledge regarding the transglycosylase and transpeptidase activities is described below and in subsequent Chapters.

1.9.1. The transglycosylase domain of HMW-PBPs

1.9.1.1. Structure of the transglycosylase domain

The sole purpose of the transglycosylase domain of PBPs and MGTs is to catalyse the polymerisation of Lipid II monomers, which is the initial step in the assembly of peptidoglycan. Proteins that degrade, modify or generate glycosidic bonds can be organised by sequence, structural or functional homology into families according to the Carbohydrate-Active enZYmes (CAZY) classification scheme (www.cazy.org). Peptidoglycan transglycosylases are categorised into the glycosyltransfer family 51

(GT51). This family exhibits a novel structural fold. The GT51 domains are always membrane-bound and use undecaprenyl-based substrates.

Structural insight into the GT51 domain has only become available within the last 5 years. To date, X-ray crystal structures exist for three bifunctional PBPs (*Aquifex aeolicus* PBP1a (Yuan *et al.*, 2007), *S. aureus* PBP2 (Lovering *et al.*, 2007) and *E. coli* PBP1b (Sung *et al.*, 2009)) and one MGT (*S. aureus* MGT (Heaslet *et al.*, 2009)). Of these structures, only *E. coli* PBP1b is based on the full-length protein sequence (devoid only of the short N-terminal cytoplasmic tail); the remaining structures are soluble counterparts of the membrane proteins (with the absence of the transmembrane anchor).

The elucidated transglycosylase domain structures are in general accordance with each other and exhibit a common topological fold. The GT fold is predominantly α-helical and is organised into two lobes: a large globular 'head' region and a smaller 'jaw' region (Lovering *et al.*, 2007) (Figure 1.10). The 'jaw' is comprised of a significant number of hydrophobic residues and is closely associated, if not embedded into the extracellular face of the cytoplasmic membrane, and is postulated to mediate the interaction with the membrane and the Lipid II substrate (Lovering *et al.*, 2007; Yuan *et al.*, 2007). The two lobes are separated by an extended cleft, which contains many conserved residues and constitutes the active site (Yuan *et al.*, 2007). There are no direct interactions between the transpeptidase and transglycosylase domains of *S. aureus* PBP2 or *A. aeolicus* PBP1a. However, in *E. coli* PBP1b, the transpeptidase and transglycosylase domains are linked by an extra domain of five anti-parallel β-sheets and a single α-helix. This so-called UB2H domain has been shown to interact with the outer membrane protein LpoB, which directly stimulates the transpeptidase activity of *E. coli* PBP1b (Paradis-Bleau *et al*., 2010; Typas *et al.*, 2010).

1.9.1.2. Conserved residues of the transglycosylase domain

Peptidoglycan transglycosylases are defined by five conserved sequence motifs revealed through sequence alignments: EDX_2FX_2H, $GXSTXTQQX_2K$, RKX_2E, KX_2IX_3YXN and RX_3VL (motifs 1-5 respectively) (Lovering *et al.*, 2008b). The first three motifs are located in the catalytic cleft, whereas motif 4 lines the back wall of the cleft and motif 5 is situated further away from the active site in the 'head' domain (Sauvage *et al.*, 2008a).

Various studies have probed the role of the conserved residues in transglycosylation reactions. Di Guilmi *et al.* (2003a) generated truncated constructs of *S. pneumoniae* PBP1b and analysed their capability of binding Lipid II. In the absence of the first motif, PBP1b was able to bind Lipid II, indicating that motif 1 had little or no role in substrate recognition. Deletion of both motif 1 and motif 2 from the protein sequence eliminated the association with Lipid II, thus indicating that motif 2 is essential for substrate binding. Mutational analysis of the conserved residues, such as those performed by Terrak *et al.* (1999) on *E. coli* PBP1b, have demonstrated the importance of the glutamate residue belonging to the first motif; mutation to glutamine caused a reduction in glycan chain polymerisation to 0.2 % of the wild-type enzyme. This residue has since been referred to as the catalytic residue. Further studies by Terrak *et al.* (2008) have postulated that the remaining conserved residues of motif 1 are important for the positioning of the putative catalytic residue. The positively charged lysine and arginine residues of motifs 2 and 3 are proposed to position the negatively charged pyrophosphate moiety of the substrate (Lovering *et al.*, 2007; Terrak *et al.*, 2008). The roles of motifs 4 and 5 are believed to be regulatory, maintaining the transglycosylase domain structure and active site cleft, and stabilising the charges on the catalytic residues (Lovering *et al.*, 2007; Lovering *et al.*, 2008b; Terrak *et al.*, 2008). Figure 1.10 shows a comparison of the transglycosylase domain architecture and the location of the conserved motifs of *A. aeolicus* PBP1a, *E. coli* PBP1b, *S. aureus* MGT and *S. aureus* PBP2.

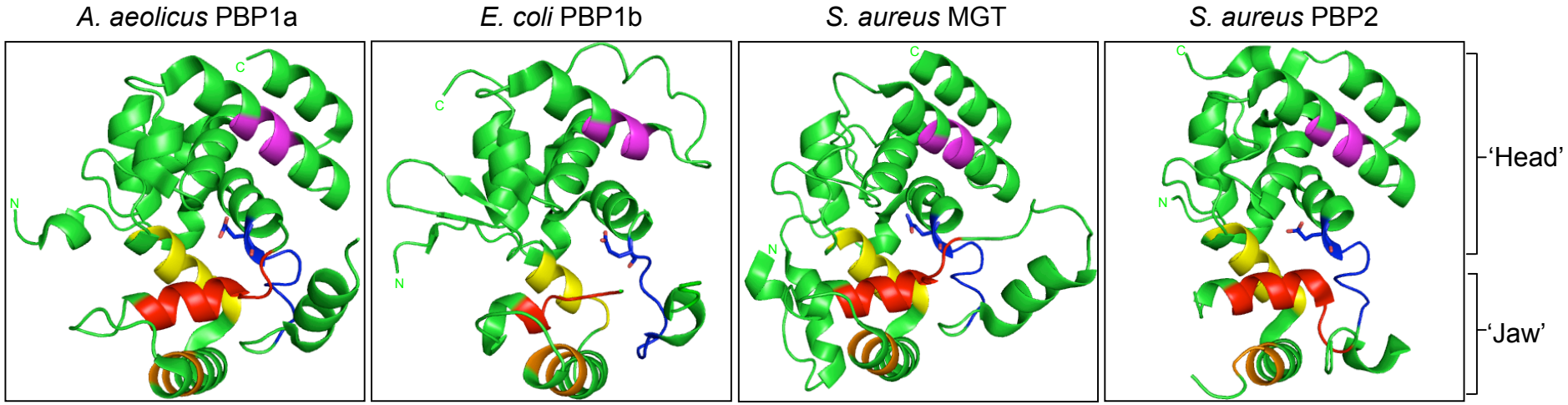

Figure 1.10: Structural comparison of the transglycosylase domains from *A. aeolicus* PBP1a, *E. coli* PBP1b, *S. aureus* MGT *and S. aureus* PBP2. The overall domain is shown in green. The conserved motifs 1-5 are displayed in blue, red, orange, yellow and magenta respectively. The putative catalytic Glu of motif 1 is shown in stick form.

1.9.1.3. Structural similarities of the transglycosylases to lysozyme

Terrak *et al.* (1999) first proposed that peptidoglycan transglycosylases are reminiscent of lysozyme; the enzymes use similar substrates, where lysozyme cleaves the β-1,4-glycosidic bond between the Mur*N*Ac and Glc*N*Ac units of peptidoglycan, which are generated by the transglycosylases. Significant secondary structural homology exists between the GT51 domains of *S. aureus* PBP2 and *A. aeolicus* PBP1a with bacteriophage λ lysozyme despite low sequence homology (Lovering *et al.*, 2007; Yuan *et al.*, 2007). Both domains are composed of a large 'head' region and a small 'jaw' region separated by a cleft. When superimposed, the 'head' regions have a similar overall topology, but the 'jaw' regions differ. In lysozyme, this subdomain is comprised of soluble β-sheets, which contrasts the α-helical structure of the GT51 domain (Yuan *et al.*, 2007). The substrate specificity could account for these differences (Lovering *et al.*, 2007). The essential glutamic acid residue of bacteriophage λ lysozyme overlays the putative catalytic glutamate residue of the GT51 domain. The relationship between the GT51 domain and bacteriophage λ lysozyme suggests that the bacteriophage could have acquired the GT51 domain at a distant point in evolution (Lovering *et al.*, 2007). The established lysozyme catalytic mechanism could provide valuable information to elucidate the transglycosylase mechanism (refer to Section 4.1).

1.9.1.4. Moenomycin, an inhibitor of the transglycosylase domain

Moenomycin is a secondary metabolite produced by *Streptomyces ghanaensis*. It is a complex structure consisting of an oligosaccharide chain attached to a lipid alcohol via a phosphoric acid diester and a glycerol acid (Di Guilmi *et al.*, 2002). Soon after its isolation, the highly potent antibiotic properties of moenomycin were revealed. It is more effective at inhibiting Gram-positive bacteria compared to Gram-negative species; the minimum inhibitory concentrations (MICs) for the Gram-negative *E. coli* and Gram-positive *S. aureus* and *S. pneumoniae* are 80 μM, 0.075 μM and 0.625 μM respectively (Cheng *et al.*, 2008). The discrepancies between the MICs are owed to the inability of moenomycin to penetrate the outer membrane of Gram-negative bacteria (Di Guilmi *et al.*, 2002). Moenomycin exhibits encouraging

antimicrobial properties but cannot be used in clinical practice due to its adverse pharmacological effects (poor absorption, long half life). It has been extensively used in agriculture as a growth promoter without the development of antibiotic resistance as documented with other antimicrobials; significantly resistant isolates from humans and animals have not been detected and no plasmid-bourne moenomycin resistance has been described (Ostash and Walker, 2010).

Huber and Nesemann (1968) identified that moenomycin interfered with peptidoglycan synthesis. Subsequently, van Heijenoort *et al.* (1978) established that the inhibitor targeted the transglycosylases and it was later speculated by Welzel *et al.* (1987) that moenomycin was a competitive inhibitor of the transglycosylase reaction. The structure of moenomycin, a glycolipid, is reminiscent of Lipid IV (the product of a single transglycosylation reaction). A structural comparison is displayed in Figure 1.11.

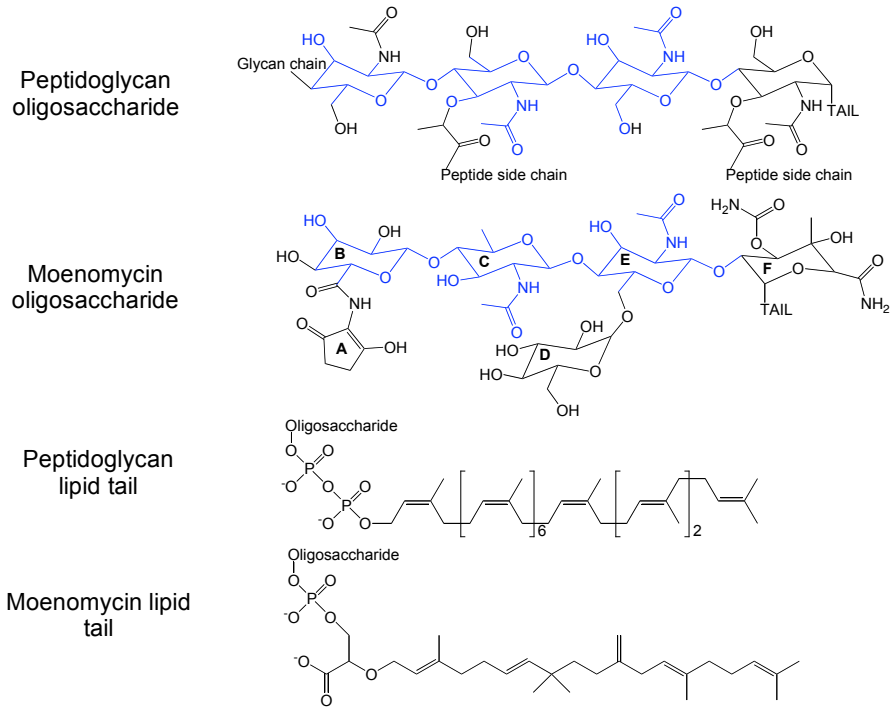

Figure 1.11: Structural comparisons of moenomycin and peptidoglycan components. The head group of Lipid IV (two disaccharide units) is shown, representing a fragment of the peptidoglycan oligosaccharide. The glycan components of Lipid IV and moenomycin are extremely similar (regions in blue highlight regions of structural identity). The lipid moieties of the peptidoglycan lipid anchor and the moenomycin lipid tail are also comparable. The ring units of the moenomycin oligosaccharide are labelled A-F. TAIL and oligosaccharide (specific to peptidoglycan or moenomycin) refer to the phosphorylated lipid component and glycan head group respectively. Figure adapted from Lovering *et al.* (2008a).

Upon the binding of moenomycin, the transglycosylase domain is proposed to undergo a conformational change. Binding of moenomycin to *S. pneumoniae* PBP1b caused the enzyme to be more sensitive to chymotrypsin, suggesting that a conformational change led to the exposure of regions that are normally concealed in the apoenzyme (Di Guilmi *et al.*, 2003a). Crystal structures of *S. aureus* PBP2 in the apo and ligand-bound form revealed that binding of moenomycin induced a conformational change in the 'jaw' subdomain (Lovering *et al.*, 2007).

The *E. coli* PBP1b crystal structure in complex with moenomycin revealed that there were no direct interactions between the transmembrane domain and the antibiotic (Sung *et al.*, 2009). This contradicts previous findings that demonstrated the dependence of the transmembrane domain on the binding affinity for moenomycin (Cheng *et al.*, 2008). The transglycosylase domain of *E. coli* PBP1b and *S. aureus* PBP2 (devoid of the transmembrane anchor) exhibit many similarities in topology and binding interactions with moenomycin, suggesting that the removal of the transmembrane domain does not affect the transglycosylase binding site. From these observations, Sung and coworkers have proposed that the transmembrane domain stabilises the protein within the membrane environment, and appropriately orientates the protein for interaction with Lipid II or moenomycin (Sung *et al.*, 2009).

Based on the interactions identified in transglycosylase structures complexed with moenomycin and the structural similarities between Lipid IV and moenomycin, Lovering *et al*. (2008a) have developed an elegant model for substrate binding and transglycosylation. In this model, the elongating glycan chain of Lipid IV superimposes the sugar units B, C, E and F and a portion of the undecaprenyl lipid tail overlays the moenomycin C_{25} isoprenoid chain. Moenomycin is proposed to locate to the donor site of the transglycosylase domain, which conforms to a processive model for glycan chain polymerisation (Section 4.1). Figure 1.12 shows the crystal structure of *S. aureus* PBP2 with the substrate analogue bound.

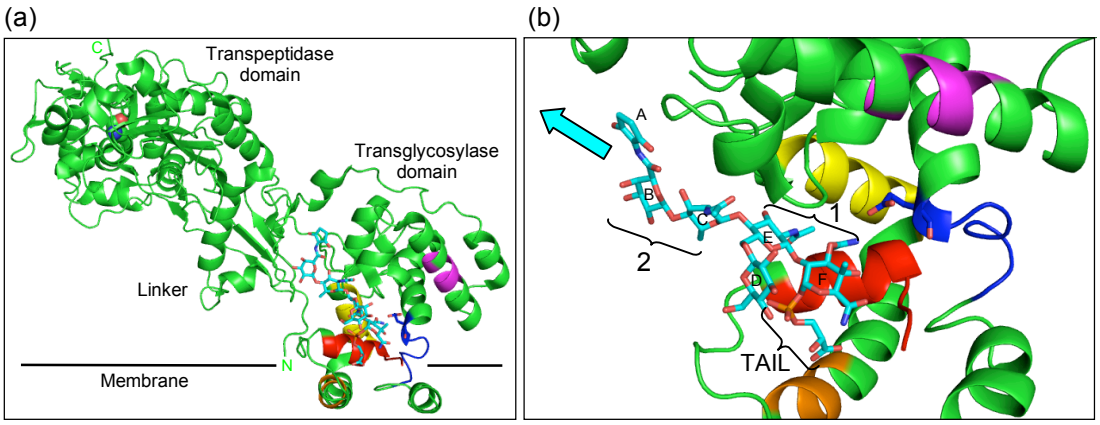

Figure 1.12: The binding of a moenomycin analogue to *S. aureus* PBP2. The conserved transglycosylase motifs 1-5 are blue, red, orange, yellow and magenta respectively. The putative transglycosylase catalytic Glu of motif 1 is displayed in a stick format. The moenomycin analogue is shown in cyan. (a) Domain architecture of *S. aureus* PBP2. The transpeptidase catalytic serine is shown in spheres. Adapted from Lovering *et al.* (2008b). (b) Close-up of the transglycosylase active site. The disaccharide constituents of Lipid IV superimpose the rings grouped 1 (F and E) and 2 (C and B). The arrow marks the direction of the elongating transglycosylase product. The lipid tail of moenomycin is likely to be in an equivalent position to the undecaprenyl lipid chain of transglycosylase substrates.

Conclusively, studies with the substrate analogue moenomycin have provided a valuable insight into the potential mechanism of transglycosylation and inhibition, information from which can be exploited in the future development of new transglycosylase antibiotics.

1.9.2. The penicillin-binding domain of HMW and LMW-PBPs

1.9.2.1. Discovery of the penicillin-binding proteins mediated by β-lactam inhibition

Since 1928, when the antimicrobial effects of penicillin were first identified, the mechanism by which the β-lactam antibiotics exert their inhibition has been of immense interest. Gardner (1940) demonstrated that low concentrations of penicillin induced morphological changes in *E. coli* and later Martin (1964) proposed that penicillin blocked the formation of peptide cross-links in the linear glycopeptide (peptidoglycan). This was supported by the accumulation of uncross-linked peptides, which retained the D-Ala-D-Ala terminal (Tipper and Strominger, 1965).

This lead to the theory by Tipper and Strominger (1965), that a transpeptidase catalysed the cleavage of the D-Ala-D-Ala terminal of the peptide chain, mediated by a covalent enzyme intermediate, which would be resolved by the formation of a cross-link. Further more, it was postulated that penicillin (6-aminopenicillanic acid) acted as a structural, cyclic analogue of the D-Ala-D-Ala terminal of the pentapeptide side chain (Figure 1.13.), exerting its inhibition by obstructing the transpeptidase active site by the formation of a stable, covalent penicilloyl enzyme with an active site residue (Tipper and Strominger, 1965). These transpeptidases were denoted Penicillin-Binding Proteins.

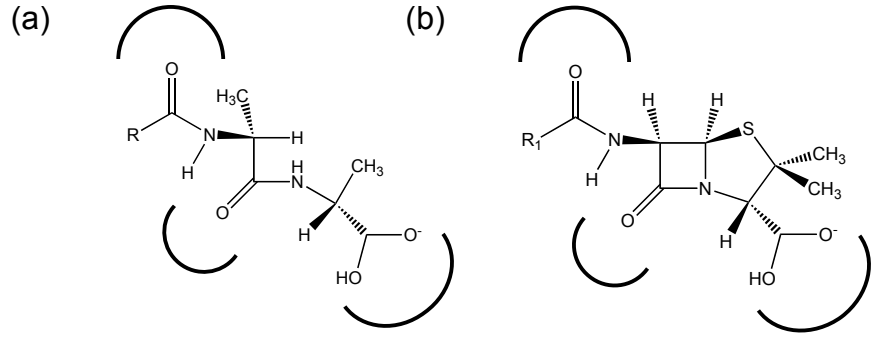

Figure 1.13: Structural comparison between β-lactams and the natural substrate of the PBPs. (a) D-Ala-D-Ala terminus of the peptidoglycan pentapeptide stem. (b) Penicillin backbone. The distribution of negative charge is similar in both structures (shown by curves). Figure from Zapun *et al.* (2008).

It was found that the penicilloyl enzyme was susceptible to an enzymatically catalysed release, supporting the hypothesis that both natural substrate and penicillin bind to the same residue in the transpeptidase active site. Through the binding of [^{14}C]-benzylpenicillin and protease digestion, the active site residue was identified as Serine (Frère *et al.*, 1976), to which the substrate also binds (Yocum *et al.*, 1979). The mechanism of β-lactam inhibition is illustrated in Figure 1.14.

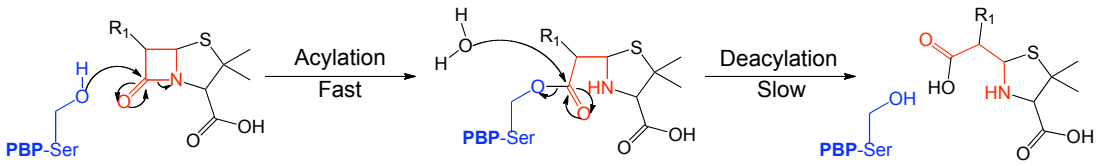

Figure 1.14: Schematic representation of PBP inhibition by β-lactam antibiotics. The active site nucleophilic serine (blue) attacks the carbonyl carbon atom of the β-lactam ring (red), forming a covalent ester linkage. This bond is hydrolysable, but the rate at which this occurs is insignificant in comparison to the rate of bacterial division. β-lactam antibiotics are classed as 'suicide substrates'; opening of the β-lactam ring leads to a biologically inactive compound.

The penicillin-binding domain is not restricted to transpeptidases; it is also present in the D,D-carboxypeptidases and endopeptidases, making these enzymes liable to β-lactam inhibition. PBPs differ in their susceptibilities to β-lactam antibiotics. For example, LMW-PBPs are less sensitive to penicillin and cephalosporin, whereas HMW-PBPs are more sensitive by comparison (Waxman and Strominger, 1983). Inactivation of the HMW-PBPs is significant as this group generally include enzymes essential for viability. Following the inhibition of the transpeptidases, there is an equilibrium shift towards the augmented activity of the hydrolases (Höltje, 1998). These enzymes continue to hydrolyse peptidoglycan to allow the insertion of new material into the cell wall. In the absence of transpeptidation, the peptidoglycan becomes fragile threatening the prospect of cell lysis.

Before the introduction of penicillin as a chemotherapeutic agent, resistance had already been established in bacteria. This was primarily noted by Abraham and Chain in 1940, where an enzyme capable of neutralising the antibiotic, now known as the β-lactamase (detailed in Section 1.3.2.2), had been identified in *E. coli* (Abraham and Chain, 1988). Over the years, other mechanisms of β-lactam resistance also emerged; mutations to the penicillin-binding domain of PBPs can distort the active site, restricting the entry of the β-lactam (as employed by *S. aureus* PBP2a in methicillin resistant strains) or mutation can result in the alteration of the active site polarity, reducing the affinity of the β-lactam (as achieved by *S. pneumoniae* PBPs) (reviewed by Zapun *et al.* (2008)). This latter mechanism of acquisition of resistance in pneumococci is discussed in detail in Chapter 3.

1.9.2.2. Structure and conserved residues of the penicillin-binding domain

Crystal structures of D,D-carboxypeptidases, endopeptidases and transpeptidases have been solved in apo and liganded forms to shed light on the signature fold topology and the molecular interactions of the penicillin-binding domain. The overall architecture consists of two subdomains. One subdomain consists of a central five-stranded β-sheet flanked by α-helices on both faces (generally α1 and α11 are in front of the sheet and α8 behind), and the second subdomain is all α-helical (Fonzé *et al.*, 1999; Gordon *et al.*, 2000; Macheboeuf *et al.*, 2005; Morlot *et al.*, 2005; Sauvage *et al.*, 2008a). The active site is positioned at the interface of the subdomains, at the bottom of an elongated cleft (Fonzé *et al.*, 1999; Contreras-Martel *et al*., 2006). A degree of flexibility between the subdomains enables PBPs to have varying affinities for different ligands (Sauvage *et al.*, 2008a).

The penicillin-binding domain is defined by three conserved motifs that encompass the active site. The first, SXXK, contains the catalytic serine (Frère *et al.*, 1976; Yocum *et al.*, 1979), which is invariably positioned at the N-terminus of α2, occupying the centre of the catalytic cleft. The second, SXN, is located in a loop between helices α4 and α5. The third, KT/SG lines the innermost β3 of the β-sheet. The latter two motifs lie on opposite sides of the catalytic cavity (Fonzé *et al.*, 1999; Macheboeuf *et al.*, 2005). A conserved glycine is situated on an extended loop at the rear of the active site (Morlot *et al.*, 2005). The positions of these conserved motifs in *S. pneumoniae* PBP1a, PBP2b and PBP2x are demonstrated in Figure 1.15.

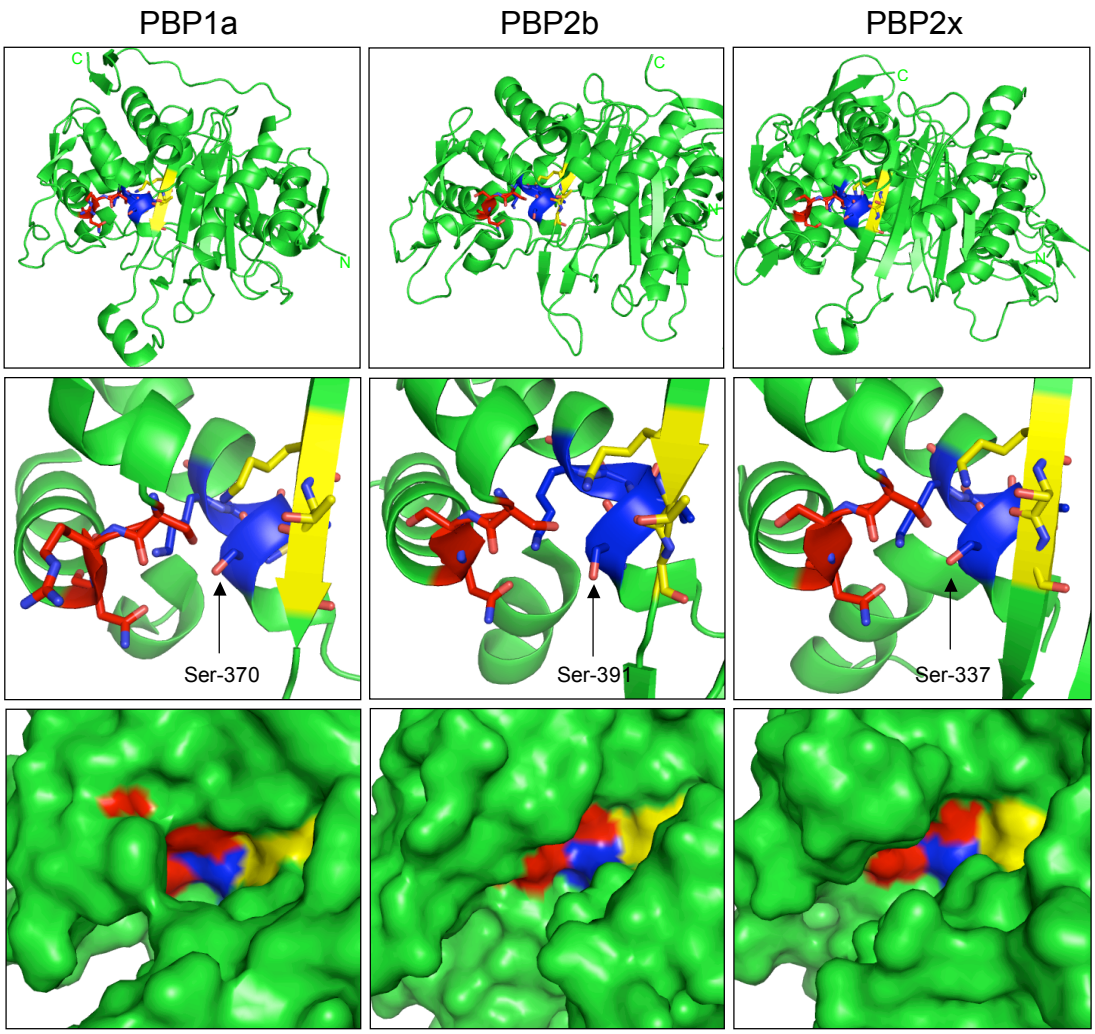

Figure 1.15: Comparison of the transpeptidase domains of *S. pneumoniae* PBP1a, PBP2b and PBP2x. Ribbon diagram representation of an overview of the transpeptidase domain and a close up of the transpeptidase active site (the catalytic serine is labelled) (upper and middle sections respectively). Surface representation of the transpeptidase active site (lower section). In all sections, the conserved motifs 1-3 are blue, red and yellow respectively.

The binding of substrate analogues to the penicillin-binding domain has identified specific features of the active site and the roles of conserved residues. An oxyanion hole is formed by the amide groups of the catalytic serine and the residue immediately following the third motif (Morlot *et al.*, 2005); the backbone carbonyl oxygen of the penultimate D-Ala (or β-lactam ring) hydrogen bonds with the oxyanion hole (McDonough *et al.*, 2002). The methyl group of the same D-Ala inserts into a hydrophobic pocket, which contains the conserved glycine and is important for binding specificity of the penultimate D-Ala (McDonough *et al.*, 2002; Morlot *et al.*, 2005). This explains the stringency of D-Ala at position 4 of the

pentapeptide chain in comparison to the terminal (McDonough *et al.*, 2002). The hydroxyl residues of the third motif that comprise β3 orientate the incoming substrate as if they were antiparallel extensions of the enzyme β-sheet (Kelly *et al.*, 1998). The glycine in this motif is essential in avoiding steric hindrance that could prevent substrate entry into the active site. The Lys of the first motif is essential for catalysis. It is proposed that this residue acts as a base, abstracting a proton from the catalytic serine, activating it as a nucleophile for an acylation event (Lee *et al.*, 2001; Rhazi *et al.*, 2003). These interactions position the substrate ready for catalysis and stabilise any intermediate species. Figure 1.16 illustrates the binding of a substrate analogue in the active site of *Streptomyces* R61 D,D-peptidase.

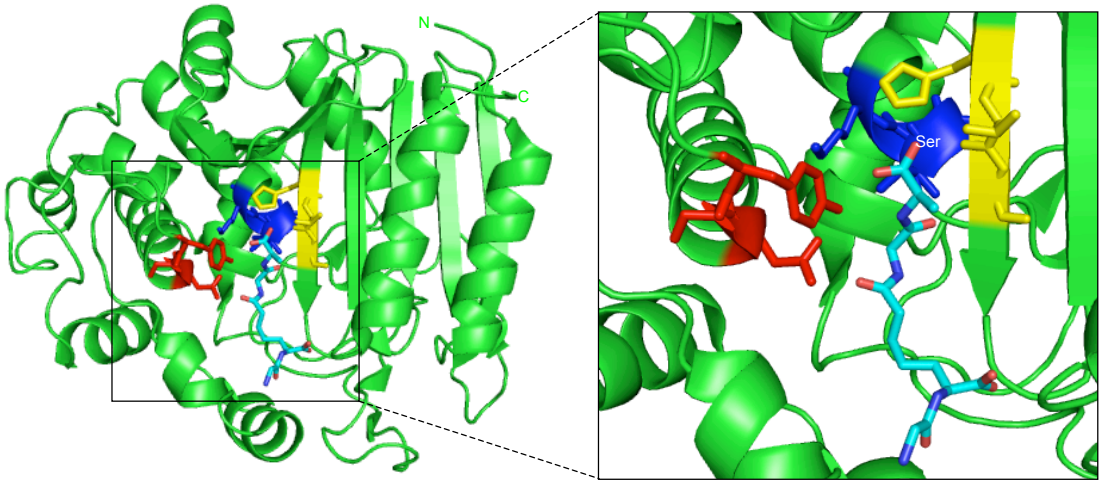

Figure 1.16: Structural representation of *Streptomyces* R61 D,D-peptidase with a bound substrate analogue. The conserved motifs 1-3 (blue, red and yellow respectively) are shown in stick form. The peptide side stem substrate analogue glycyl-L-α-amino-ε-pimelyl-D-Ala-D-Ala (cyan) is oriented as an anti-parallel extension of the β-sheet comprising the third conserved motif. The terminal D-Ala is positioned for nucleophilic attack by the Ser-Oγ. Following carboxypeptidation, the residues lining the active site adjust their interactions with the products glycyl-L-α-amino-ε-pimelyl-D-Ala and D-Ala, which may facilitate product ejection. Adapted from McDonough *et al.* (2002).

Recent structures of *S. pneumoniae* PBP1b have revealed that substrate binding induces a conformational change in the active site (Macheboeuf *et al.*, 2005). In the apo form, the active site cavity is closed whereby movement in an intervening loop disrupts the antiparallel interaction of β3 with β4, allowing β3 to contact the left hand side of the cleft. In liganded structures, β3 and β4 are perfectly parallel, thus the active site is 'open'. This change in conformation could regulate the activity of

the PBP, where until their catalytic activity is required, the enzyme remains in a 'closed', inactive state. Activation could be brought about by interaction with protein complexes or the availability of substrate (Macheboeuf *et al.*, 2005).

A further conformational change has been shown in the active site of *Streptomyces* R61 D,D-peptidase upon binding a tetrapeptide and D-Ala (representative of D,D-carboxypeptidase products) (McDonough *et al.*, 2002). In this structure, a water molecule binds in the oxyanion hole, causing Thr of the third motif to take up an alternative conformation. As a result, the peptide product loses a hydrogen bond and initiates further movements in the active site. This is believed to facilitate the expulsion of the product from the active site (McDonough *et al.*, 2002).

1.9.2.3. The three-stage model of PBP activity

The PBPs (transpeptidases, D,D-carboxypeptidases and endopeptidases) react with substrates and inhibitors according to a common three-step mechanism (substrate binding, acylation, deacylation) as described in Scheme 1 (E, enzyme; S, substrate; ES and ES*; intermediate complexes; P, product).

Scheme 1 $$[E]+[S]\underset{k_{-1}}{\overset{k_1}{\rightleftharpoons}}[ES]\xrightarrow{k_2}[ES^*]\xrightarrow{k_3}[E]+[P]$$

The reaction proceeds by the rapid, reversible formation of a non-covalent Henri-Michaelis complex between the D,D-peptidase and the peptidoglycan pentapeptide stem (the donor strand). The nucleophilic serine attacks the carbonyl carbon atom of the fourth position D-Ala peptide bond, leading to the formation of tetrahedral intermediate and subsequently an acyl enzyme intermediate, with the concomitant release of the terminal D-Ala (transpeptidation and D,D-carboxypeptidation) or cross-linking peptide stem (endopeptidation). Depending on the enzyme, deacylation occurs either by hydrolysis of the covalent intermediate, or by cross-link formation via a second peptide stem (acceptor strand) (Sauvage *et al.*, 2008a). Product release enables the enzyme to resume its initial conformation. The catalytic mechanism for transpeptidation and D,D-carboxypeptidation is illustrated in Chapter 5.

1.9.2.4. The structural and functional relationship between PBPs and β-lactamases

The PBPs and many β-lactamases are penicilloyl serine transferases (or Active site Serine Penicillin Recognising Enzymes, ASPREs). They share similar structural and active site sequence motifs, bind penicillin in the same orientation and have a common catalytic mechanism leading to the formation of a stable, covalent acyl-enzyme intermediate (Ghuysen, 1994). It was initially proposed by Tipper and Strominger (1965) that the β-lactamase was a modified form of the transpeptidase and it is now believed that the enzymes are derived from a common ancestor (Ghuysen, 1991). It is in general agreement that the genes from an ancient PBP gave rise to a β-lactamase (not *vice versa*) (Ghuysen, 1991), allowing peptidoglycan to become an established component of the bacterial cell wall (Koch, 2000).

The β-lactamases significantly contribute to β-lactam resistance. They are secretory proteins that inactivate β-lactam antibiotics. Structural analysis of these enzymes has revealed that they do not contain peptidoglycan binding sites, abolishing the recognition of PBP substrates (Meroueh *et al.*, 2003). Their reaction with penicillin (and β-lactam antibiotics) proceeds in an analogous mechanism to the transpeptidases. However, whereas the transpeptidases are inactivated by the formation of a penicilloyl acyl-linked enzyme, the β-lactamases are capable of efficiently hydrolysing this moiety, recovering the enzyme with the release of penicilloate (a biologically inert compound) (Ghuysen, 1991). This can be attributed to the uninhibited access of a water molecule into the active site of β-lactamases, which must be excluded from that of the transpeptidases (allowing the integrity of the cross-linking reaction to be maintained) (Ghuysen, 1991). Class A β-lactamases contain a glutamate residue that is essential for deacylation of the active site serine (Adachi *et al.*, 1991). This residue is absent in an equivalent position in the active site of PBPs, providing an explanation as to why these enzymes are unable to hydrolyse the acyl intermediate at an appreciable rate (Gordon *et al.*, 2000; Macheboeuf *et al.*, 2006). Figure 1.17 summarises the chemistry underpinning the turnover of β-lactam antibiotics by the β-lactamases and PBPs.

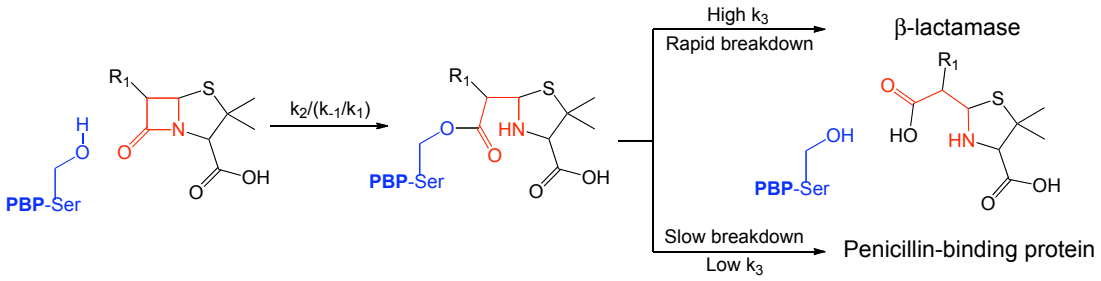

Figure 1.17: Reactions of penicilloyl serine transferases with β-lactam carbonyl donors. The kinetic constants for acylation ($k_2/(k_{-1}/k_1)$) and deacylation (k_3) refer to those of Scheme 1. The rate of k_3 determines the efficiency of β-lactam inhibition. Figure adapted from Ghuysen (1991).

1.10. *Streptococcus pneumoniae*

The PBPs from *S. pneumoniae* are the primary focus of this thesis. The following sections describe *S. pneumoniae* in terms of its clinical significance and its PBP-mediated resistance to β-lactam antibiotics (additional detail in Section 3.1).

1.10.1. *S. pneumoniae* and disease

S. pneumoniae is a clinically relevant organism, being one of the leading causes of disease globally (Alpuche *et al.*, 2007). It is a Gram-positive, commensal bacterium, which has a carrier state, colonising the nasopharynx of adults (up to 4 % of the population) and children (greater than 50 %) (Regev-Yochay *et al.*, 2004). *S. pneumoniae* is responsible for infections including pneumonia, otitis media, meningitis and bacteraemia and is a primary cause of mortality amongst children, the elderly and vulnerable patients (Centres for Disease Control and Prevention, 1997).

1.10.2. *S. pneumoniae* and β-lactam resistance

Despite the availability of antimicrobial agents, mortality rates remain high; in 2005, WHO estimated that pneumococcal infections resulted in 1.6 million deaths worldwide (World Health Organisation, 2007). This can be attributed to the development of bacterial resistance to β-lactam antibiotics, which are ubiquitously employed inhibitors against pneumococcal infections. *S. pneumoniae* resistance to β-lactam antibiotics is not imparted by the common resistance mechanism of the production of β-lactamases; a β-lactamase expressing strain has not been

documented. Instead, *S. pneumoniae* have evolved a sophisticated resistance mechanism that is mediated by the intricate restructuring of the antibiotic target (Hakenbeck *et al.*, 1999) (detailed in Section 3.1). PBPs of resistant strains have a reduced affinity for β-lactam antibiotics but vitally retain their natural physiological activity (Job *et al.*, 2008). Thus, *S. pneumoniae* PBPs are fascinating antimicrobial targets.

1.10.3. *S. pneumoniae* PBPs and the resistance determinants

S. pneumoniae has six penicillin-binding proteins: a single LMW-PBP (PBP3, 41.4 kDa) and five HMW-PBPs, three of which belong to Class A (PBP1a, 79.7 kDa; PBP1b, 89.4 kDa; PBP2a, 80.7 kDa) and the remaining two belong to Class B (PBP2b, 74.4 kDa; PBP2x, 82.2 kDa). Of these enzymes, PBP2b and PBP2x are crucial for viability (Kell *et al.*, 1993), PBP3 (Severin *et al.*, 1992) and PBP1b are not essential and either PBP1a or PBP2a must be functional (Hoskins *et al.*, 1999). PBP2b and PBP2x are classified as primary resistance determinants; mutations in these enzymes, selected by β-lactam antibiotics, confer low resistance (Grebe and Hakenbeck, 1996). Low affinity PBP2b and PBP2x are a prerequisite for high resistance levels, which are mediated by mutations present in PBP1a (Smith and Klugman, 1998). The remaining PBPs obtain fewer mutations in comparison to PBP1a, PBP2b and PBP2x and are generally not responsible for elevated resistance in clinical isolates (Sanbongi *et al.*, 2004). Thus, PBP1a, PBP2b and PBP2x are the major β-lactam resistance determinants of *S. pneumoniae* (further discussed in Section 3.1) and, accordingly, the biochemical characteristics of these enzymes were investigated in this thesis.

1.11. Aims of the thesis

The growing threat of bacterial resistance to clinically prescribed antibiotics presents a global health problem. The discovery or design of new antimicrobial classes is a key strategy to evade antimicrobial resistance. Towards this primary goal, it is a necessity to characterise drug targets and resistance mechanisms at a molecular level. Information obtained from these studies could provide insight into the structural and biochemical substrate specificity of the target enzymes and ultimately contribute to the rational development of novel inhibitors.

S. pneumoniae PBPs, more explicitly the enzymes essential for mediating β-lactam resistance, are the focus of this thesis. These enzymes represent the drug target as well as providing the basis of resistance. Whilst the recent advances in biochemical and structural characterisation techniques of membrane proteins has led to an improved understanding of the transglycosylase activity of HMW-PBPs and MGTs, the transpeptidase activity of HMW-PBPs has remained somewhat of a mystery. The main aim of this thesis is to develop spectrophotometric assays to enable the rapid, kinetic characterisation of the PBP transglycosylase and transpeptidase activities, whilst concomitantly establishing conditions in which these activities can be detected (including an investigation into substrate specificity of the *S. pneumoniae* β-lactam resistance determinants). This is a prerequisite for further exploration into the enzymology of catalysis and β-lactam resistance mechanisms of these enzymes. It is anticipated that conversion of the assays into a high throughput system will allow libraries of potential inhibitors to be screened against β-lactam sensitive and resistant enzymes. A secondary aim is to obtain structural information of the integral membrane proteins, in the presence or absence of ligands, which together with biochemical data, could enhance the understanding of catalytic mechanisms and resistance-determining features of *S. pneumoniae* PBPs.

Chapter 2. Materials and Methods

2.1. Buffers and solutions

The buffers and solutions were prepared with Purite Prestige purified water (double deionised). Buffers for use in chromatography, crystallography and spectrophotometric measurements were filtered using a 0.2 μm filter (Millipore, UK). The solution pH was determined by inoLAB WTW pH meter using pH 4.01, pH 7.01 and pH 10.01 buffer standards (Hanna Instruments) for calibration purposes.

2.2. Growth and maintenance of *E. coli* strains

2.2.1. Bacterial growth media

2.2.1.1. Super Optimal broth with Catabolite repression (SOC) media

2 % (w/v) peptone, 0.5 % (w/v) yeast extract, 10 mM NaCl, 2.5 mM KCl, 10 mM $MgCl_2$, 10 mM $MgSO_4$, 20 mM glucose.

2.2.1.2. Luria Bertani (LB) broth (Bertani, 1951)

1 % (w/v) tryptone, 0.5 % (w/v) NaCl, 0.5 % (w/v) yeast extract.

2.2.1.3. 2xYT media

1.6 % (w/v) tryptone, 1 % (w/v) yeast extract, 0.5 % (w/v) NaCl, adjusted to pH 7.0.

2.2.1.4. ZY media (Studier, 2005)

1 % (w/v) N-Z amine, 0.5 % (w/v) yeast extract.

2.2.1.5. Autoinduction media (Studier, 2005)

ZY media, 1 mM $MgSO_4$, 1 × NPS (final concentrations of 25 mM ammonium sulphate, 50 mM potassium dihydrogen phosphate, 50 mM disodium hydrogen phosphate) and 1 × 5052 (final concentrations of 0.5 % (v/v) glycerol, 0.05 % (w/v) glucose, 0.2 % (w/v) α-lactose) with appropriate antibiotics.

All growth media were prepared to one litre and autoclaved.

2.2.1.6. Preparation of LB-agar plates

LB-agar plates were composed of LB media with 1.5 % (w/v) bacto-agar and sterilised by autoclaving. The media was cooled to 50°C and appropriate antibiotics were added before pouring 25 mL into sterile Petri dishes. Plates were stored at 4°C.

2.2.2. Bacterial strains

***E. coli* strain**	**Genotype**	**Reference**
TOP10	F^- *mcrA* Δ(*mrr-hsdRMS-mcrBC*) ϕ80*lacZ*ΔM15 Δ*lacX*74 *deoR recA*1 *araD*139 Δ (*ara-leu*)7697 *galU galK rpsL* (Str^R) *endA1 nupG*	Grant *et al.* (1990)
NovaBlue	*endA1 hsdR17*(r_{K12}^- m_{K12}^+) *supE44 thi-1 recA1 gyrA96 relA1 lac* F'[$proA^+B^+$ $lacI^qZ\Delta M15$::Tn*10* (Tc^R)]	Merck-Chemicals
BL21 (DE3)	F^- *ompT hsd*SB(rB–, mB–) *gal dcm* (DE3)	Studier and Moffatt (1986)
BL21 Star (DE3)	F^- *ompT hsdS*$_B$ (r_B^- m_B^-) *gal dcm rne*131 (DE3)	Lopez *et al.* (1999)
C41 (DE3)	Derivative of *E. coli* BL21 (DE3): F^- *ompT hsdS*$_B$ (r_B^- m_B^-) *gal dcm* (DE3)) and contains at least one uncharacterised mutation. Prevents cell death associated with expression of toxic recombinant proteins.	Miroux and Walker (1996)
C43 (DE3)	Derivative of C41 (DE3) obtained using F-ATPase subunit gene, contains no plasmid.	Miroux and Walker (1996)

Table 2.1: Bacterial strains used for DNA cloning and protein over-expression.

2.2.3. Preparation of chemically competent cells for DNA transformation

E. coli cells were used to inoculate 5 mL sterile LB broth containing the appropriate antibiotic. The cells were grown at 37°C, with shaking at 180 rpm overnight. 250 mL sterile LB containing 20 mM $MgSO_4$ and antibiotics (in a 1 L conical flask to allow optimum aeration) was inoculated with 2.5 mL of the overnight culture and incubated at 37°C with shaking at 180 rpm until the optical density at A_{600nm} (OD_{600nm}) reached between 0.4 and 0.6. The cells were pelleted by centrifugation at 4,500 × g (Beckman JA-14 rotor) for 5 min. From this point forward, cells and buffers were cooled to 4°C. The cell pellet was gently resuspended in 100 mL TFB1 buffer (30 mM potassium acetate, 10 mM calcium chloride, 50 mM manganese chloride, 100 mM rubidium chloride, 15% (v/v) glycerol, pH 5.8), incubated on ice for 5 min, centrifuged at 4,500 × g for 5 min, resuspended in 10 mL TFB2 buffer (10 mM MOPS, pH 6.5, 75 mM calcium chloride, 10 mM rubidium chloride, 15 % (v/v) glycerol) and incubated on ice for 1 h. The competent cells were immediately frozen in 50 µL aliquots using liquid nitrogen and stored at -80°C.

2.2.4. DNA transformation of *E. coli*

A 50 µL aliquot of competent cells was thawed on ice and incubated with 1 µL DNA (25-100 ng) for 30 min on ice. The cells were then incubated at 42°C for 30 sec and incubated on ice for a further 2 min. 250 µL of LB was added to the cells, which were then incubated at 37°C for 30-60 min with shaking. 100 µL of the transformed cells were plated onto LB-agar plates containing the appropriate antibiotic for selection. The plates were incubated at 37°C overnight.

2.2.5. Preparation of Glycerol Stocks

An *E. coli* colony from a fresh transformation was used to inoculate 5 mL LB media containing the appropriate antibiotic and cultured at 37°C with shaking at 180 rpm

overnight. 1 mL of the culture was aseptically mixed with 1 mL sterile 100 % (v/v) glycerol in a Corning cryo-vial, frozen in liquid nitrogen and stored at -80°C.

2.3. DNA manipulation and cloning techniques

2.3.1. Oligonucleotides

DNA oligonucleotides were designed according to the specified DNA manipulation technique against a target gene and ordered from Integrated DNA Technologies (UK).

2.3.2. DNA concentration determination

DNA quantification was determined using a NanoDrop ND-1000 spectrophotometer (Thermo Scientific) using 1.5 µL samples.

2.3.3. Polymerase Chain Reaction (PCR)

DNA amplification was achieved using AccuPrime *Taq* DNA Polymerase High Fidelity or *Taq* Polymerase following the manufacturer's (Invitrogen) instructions. Unless otherwise stated, a 100 µL master mix of reagents was prepared and divided into five 20 µL aliquots. The PCR was carried out in an Eppendorf Mastercycler Gradient thermocycler over an annealing temperature gradient of (45-65°C). A negative control was used in each PCR where the template DNA was replaced with an equal volume of water.

2.3.4. Restriction enzyme digestion of DNA

Single, double and triple restriction enzyme digests were performed using restriction enzymes and buffer system according to the manufacturer's (NEB) instructions. 500 ng of plasmid DNA was used and the reactions were incubated at 37°C overnight. In the event of star activity, the reaction was repeated with an incubation time of 2 h to limit this activity.

2.3.5. Purification of DNA from PCR and restriction digests

DNA was purified following PCR and restriction digests to remove polymerases and endonucleases using the Wizard PCR Extraction kit (Promega) according to the manufacturer's instructions.

2.3.6. Preparation of Plasmid DNA

Following a transformation and overnight culture, plasmid DNA was extracted from *E. coli* TOP10 cells using a miniprep extraction kit (Qiagen or Fermentas) according to the manufacturer's instructions.

2.3.7. Agarose Gel Electrophoresis

A 0.8 % (w/v) solution of high-melting point agarose was prepared by adding 2 g of agarose to 250 mL of 1 × Tris-acetate-EDTA (TAE, 40 mM Tris acetate, 1 mM EDTA) buffer and heating in a microwave oven until complete dissolution. The solution was cooled to hand-heat and 25 µL of a 10,000 × solution of SYBR Safe (Invitrogen) DNA gel stain was added. The solution was poured into a gel cast and allowed to set. The gel was submerged in a gel tank (Geneflow) containing 1 × TAE. The DNA samples were loaded into the wells with a 1 in 6 dilution of 6 × DNA loading dye solution (0.25 % (w/v) bromophenol blue, 0.25 % (w/v) xylene cyanol FF and 15 % (v/v) Ficoll 400) (Fermentas). 5 µL of DNA standard 1 Kb ladder (pre-mixed with loading buffer) (Fermentas) was loaded to allow size determination of the DNA samples. Electrophoresis was performed at 100 V for 40 min and the gel was visualised under ultraviolet light using a Syngene GeneSnap G:Box gel illuminator and analysis system.

2.3.8. Ligation independent cloning

In this work, each target gene was cloned into the pET46 Ek/LIC vector (Figure 2.1) (Merck Chemicals).

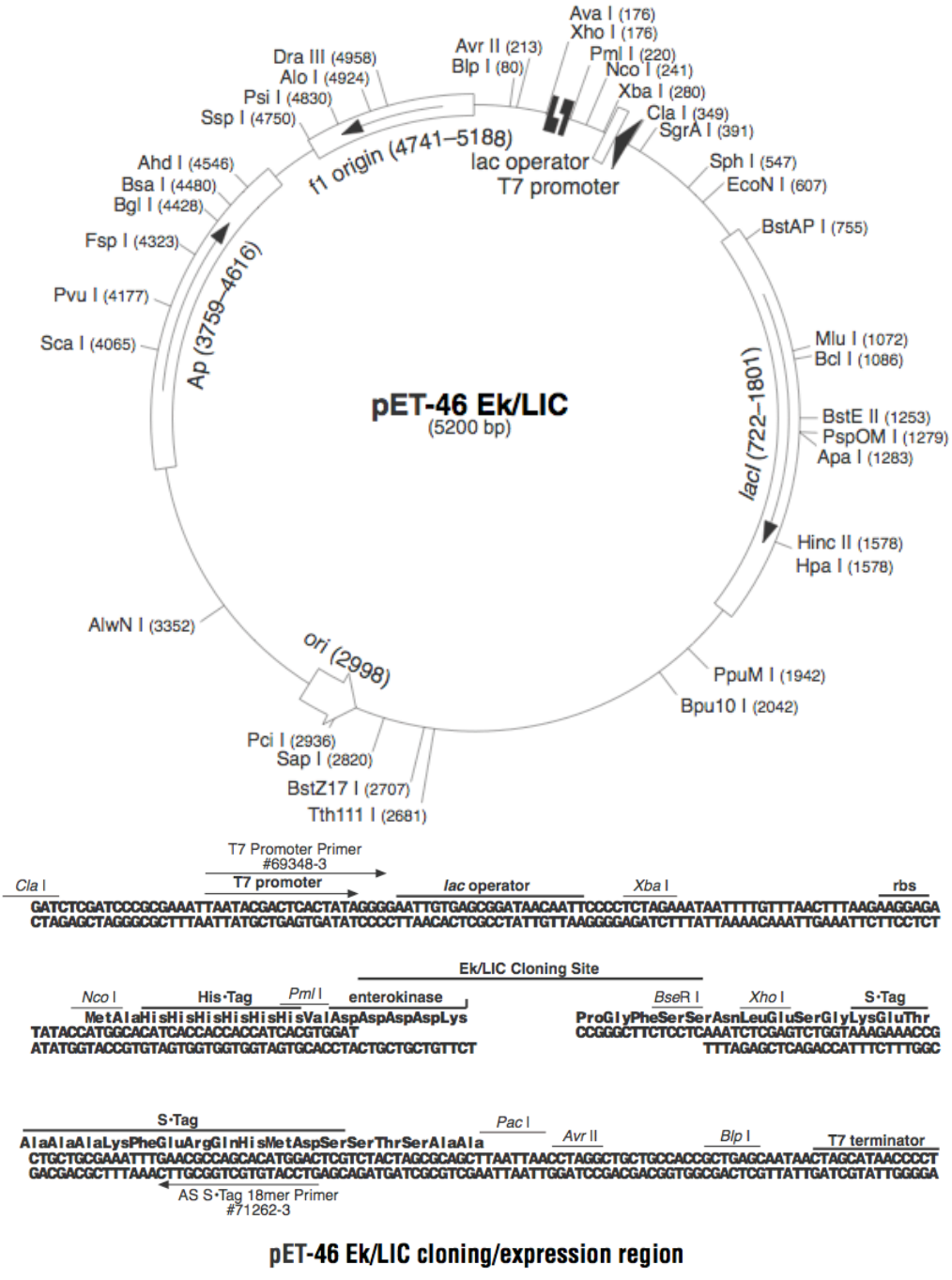

Figure 2.1:Vector map of pET-46 Ek/LIC. The vector map was obtained from Novagen, Merck Chemicals. The cloning site, situated 3' to the vector encoded hexa-histidine fusion tag and the enterokinase cleavage site, is indicated.

This vector system employs ligation independent cloning (LIC), outlined in Figure 2.2, eliminating the need of restriction digests and ligation reactions of traditional cloning methods (Aslanidis and de Jong, 1990).

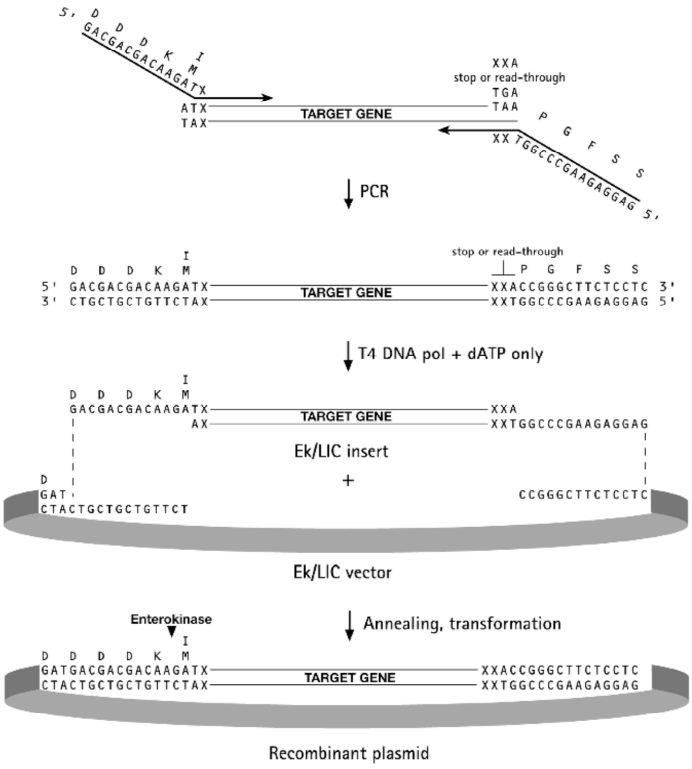

Figure 2.2: Ligation independent cloning. The Figure was taken from Novagen Ek/LIC cloning kit protocol (Merck Chemicals). Specific bases are engineered onto the 5' and 3' terminals of the insert by PCR. LIC uses the 3'-5' exonuclease activity of T4 DNA polymerase to create specific 13- or 14-base single-stranded overhangs on the Ek/LIC vector and insert. T4 DNA polymerase treatment of the insert occurs in the presence of a single dNTP (in this case dATP), where the exonuclease activity excises nucleotides until the first adenine (corresponding to the single dNTP) is encountered. The 5'-3' polymerase activity then becomes dominant, opposing the exonuclease activity, preventing further excision. Plasmid sequences adjacent to the linearization site are non-complementary, preventing re-annealing of the vector. The 5' extensions of the insert are compatible with the vector, allowing cohesion of the insert in the desired orientation.

The cloning of the PCR-amplified gene into the pET46 Ek/LIC vector (Merck Chemicals) was performed according to the manufacturer's instructions. A positive control ligation was performed using a β-galactosidase PCR product provided with the kit.

2.3.9. DNA Sequencing of plasmid constructs

DNA constructs were sequenced to ensure the cloned gene had been inserted into the plasmid vector in the desired orientation in the correct reading frame and no mutations were introduced by PCR errors. 250-400 ng of plasmid DNA and 10 pmol primer (specific to the promoter and terminator regions of the pET vectors (Table 2.2)) were used per sequencing reaction in a total reaction volume of 10 µL. The reactions were submitted to the Molecular Biology Sequencing Service (University of Warwick). The sequences were blasted against a database (www.ncbi.nih.gov/BLAST; Altschul *et al.* (1990)) and aligned using *ClustalW* (Larkin *et al.*, 2007) to check for point mutations. The start and stop codons were identified manually.

Primer	Primer sequence (5'-3' orientation)
T7 promoter	TAA TAC GAC TCA CTA TAG GG
pET-46 Ek/LIC terminator	AGG GGT TAT GCT AGT TAT TGC TCC G

Table 2.2: Sequences of the T7 promoter and pET-46 Ek/LIC terminator primers for use in DNA sequencing.

2.3.10. Site-directed mutagenesis of DNA constructs

Single point mutations were created in various gene constructs using the Stratagene Site-Directed Mutagenesis QuikChange II kit, according to the manufacturer's instructions. Oligonucleotides containing the desired mutations were designed (see tables in relevant text) to replace parental DNA. This was achieved through PCR using *PfuUlta* DNA polymerase. Parental DNA was denatured at 95°C for 30 sec, followed by eighteen cycles of 95°C for 30 sec (to denature double stranded DNA), 55°C for 1 min (to anneal primers), 68°C for 1 min/kb of plasmid length (to extend mutagenic primers in a 5'-3' direction). Finally, a 68°C step for 5 min ensured complete primer extension.

Parental DNA was digested using the endonuclease *Dpn* I, leaving the mutated plasmid, which was used to transform *E. coli* TOP10 cells (Section 2.2.4). The plasmid DNA was extracted from overnight cultures of positive clones (Section

2.3.6) and submitted for sequencing (Section 2.3.9). The sequence was aligned and compared to the wild-type sequence to identify clones containing the desired mutation.

2.3.11. Plasmid vectors used in this project

Vector	Purpose	Antibiotic selection	Supplier
pET28d	Cloning	Kanamycin	Novagen
pET46 Ek/LIC	Cloning	Ampicillin	Novagen
pTrcHis60	Cloning	Ampicillin	Amersham Pharmacia Biotech
pET3a	Cloning	Ampicillin	Novagen
pLysS	Reduction of basal expression of recombinant genes	Chloramphenicol	Novagen
pRosetta	Rare codon over-expression	Chloramphenicol	Novagen
pRIL	Rare codon over-expression	Chloramphenicol	Novagen
pRARE	Rare codon over-expression	Chloramphenicol	Novagen

Table 2.3: Commercial vectors used in this project for cloning and to aid protein over-expression.

2.3.12. Gene constructs used in this project

Construct	Selection	Description
pET46::*pbp1a*	Ampicillin	pET46 vector containing *S. pneumoniae* D39 *pbp1a*
pET46::*pbp1a-Δ30*	Ampicillin	pET46 vector containing *S. pneumoniae* D39 *pbp1a-Δ30*
pET46::*pbp1a-S370A*	Ampicillin	pET46 vector containing *S. pneumoniae* D39 *pbp1a,* Ser-370 replaced with Ala
pET46::*pbp1a-E91Q*	Ampicillin	pET46 vector containing *S. pneumoniae* D39 *pbp1a,* Glu-91 replaced with Gln
pET46::*pbp1a-5204*	Ampicillin	pET46 vector containing *S. pneumoniae* 5204 *pbp1a*
pET46::*pbp2b*	Ampicillin	pET46 vector containing *S. pneumoniae* D39 *pbp2b*
pET46::*pbp2b-Δ39*	Ampicillin	pET46 vector containing *S. pneumoniae* D39 *pbp2b-Δ39*
pET46::*pbp2b-S391A*	Ampicillin	pET46 vector containing *S. pneumoniae* D39 *pbp2b,* Ser-391 replaced with Ala
pET46::*pbp2b-5204*	Ampicillin	pET46 vector containing *S. pneumoniae* 5204 *pbp2b*
pET46::*pbp2x*	Ampicillin	pET46 vector containing *S. pneumoniae* D39 *pbp2x*
pET46::*pbp2x-Δ48*	Ampicillin	pET46 vector containing *S. pneumoniae* D39 *pbp2x-Δ48*
pET46::*pbp2x-S337A*	Ampicillin	pET46 vector containing *S. pneumoniae* D39 *pbp2x,* Ser-337 replaced with Ala
pET46::*pbp2x-5204*	Ampicillin	pET46 vector containing *S. pneumoniae* 5204 *pbp2x*
pET46::*mgt**	Ampicillin	pET46 vector containing *S. aureus* MGT (Δ67)
pET46::*mgt-E100Q*	Ampicillin	pET46 vector containing *S. aureus* MGT (Δ67), Glu-100 replaced with Gln
pTrcHis60::*pgpB**	Ampicillin	pTrcHis60 vector containing *E. coli* PgpB
pET28d::*vanA**	Kanamycin	pET28d vector containing *E. faecalis* VanA
pET3a::*murG**	Ampicillin	pET3a vector containing *E. coli* MurG

Table 2.4: Gene constructs generated and provided (*) for use in this project.

2.4. Cytoplasmic protein expression and purification

2.4.1. Protein over-expression in *E. coli*

Recombinant proteins were over-expressed in a number of *E. coli* strains suitable for protein expression (Table 2.1). Strains were made competent (Section 2.2.3) and transformed (Section 2.2.4) with an expression plasmid containing the recombinant gene and plated onto the appropriate selective media. The cell colonies were treated differently depending on the induction method specified.

2.4.1.1. Isopropyl-β-D-thiogalactopyranoside (IPTG) induction

A single colony from a fresh transformation was used to inoculate a small-scale culture of 10 mL LB containing 0.2 % (v/v) glucose and the appropriate antibiotic. Cells were cultured at 37°C, with shaking at 180 rpm overnight. The whole overnight culture was used to inoculate 1 L LB with antibiotic selection and grown at 37°C with shaking at 180 rpm. At OD_{600nm} of 0.5, the cultures were induced with 0.5 mM IPTG and incubated at 25°C for 18 h (unless otherwise stated). Cells were harvested at 10,000 × g using a Beckman JLA-8.100 rotor. The cell pellet was resuspended in 3 mL/g wet cell weight of phosphate buffered saline (PBS: 8.1 mM Na_2HPO_4, 137 mM NaCl, 2.7 mM KCl, 1.5 mM KH_2PO_4, pH 7.4) unless otherwise stated and stored at -20°C.

2.4.1.2. Autoinduction

The method used in this work was adapted from the Studier Autoinduction System (Studier, 2005). A freshly transformed colony from an LB-Agar plate supplemented with 1 % (w/v) glucose was used to inoculate 2 mL ZYP-0.8G medium (ZY, 1 mM $MgSO_4$, 0.8 % (w/v) glucose, NPS) with appropriate antibiotic selection and grown overnight at 25°C with 225 rpm shaking. 1 mL of overnight culture was used to inoculate 1 L of ZYP-5052 rich medium (ZY, 1 mM $MgSO_4$, 5052, NPS) for autoinduction with the appropriate antibiotic selection. The cells were cultured at 25°C for 22 h with agitation at 225 rpm. Cells were harvested at 10,000 × g using a

Beckman JLA-8.100 rotor at 4°C. The cell pellet was resuspended in 3 mL/g wet cell weight of PBS and subsequently stored at -20°C.

2.4.2. Preparation of crude cell lysates

Cell lysates were prepared from previously frozen cells (Section 2.4.1). Following thawing on ice, the cell suspension was supplemented with 2.5 mg/mL chicken egg white lysozyme (Calbiochem) and incubated at 4°C with agitation for 30 min. The lysozyme-treated cells were sonicated on ice for four bursts of 30 sec at 70 % power using a Bandelin Sonoplus sonicator. The cell debris was pelleted at 20,000 × g for 20 min using a Beckman JA-25.50 rotor at 4°C. The location of the target protein, either in the supernatant or the pellet, directed the following stages of the protocol.

2.4.2.1. Soluble protein

Following the 20,000 × g centrifugation step (Section 2.4.2), the supernatant (containing soluble and membrane-bound proteins) was centrifuged at 50,000 × g for 20 min at 4°C using a Beckman JA-25.50 rotor to pellet the membranes, producing clear cell lysates. The clarified cell lysates were ready for the purification of the target protein.

2.4.2.2. Insoluble proteins

Following the 20,000 × g centrifugation step (Section 2.4.2), the pellet (containing the target protein expressed in the insoluble fraction of the cells) was resuspended in 25 mL 50 mM sodium phosphate, 500 mM NaCl, 20 % (v/v) glycerol, 1 % (w/v) n-Dodecyl-β-D-Maltopyranoside (DDM) pH 7.6, frozen at -20°C and then thawed to promote the solubilisation process. A centrifugation step of 50,000 × g for 20 min (using a Beckman JA-25.50 rotor) pelleted the remaining insoluble material. The supernatant contained detergent-solubilised proteins and was ready for the purification of the target protein.

2.4.3. Protein purification

2.4.3.1. Affinity chromatography

Purification of proteins with hexa- or dodeca-histidine affinity tags was carried out using immobilised metal affinity chromatography (IMAC) unless otherwise stated. Columns were prepared with TALON Metal Affinity Resin (Cobalt metal ions, Clontech) and developed using gravity-flow.

Columns were prepared using a 10 mL syringe barrel. A final volume of 5 mL resin was used to form the column bed, with glass wool acting as a frit to retain the resin in the barrel. The column was washed with 10 column volumes sterile water and equilibrated with the required buffer (typically PBS, with additional 150 mM NaCl (287mM final [NaCl], unless otherwise stated). The soluble proteins from Section 2.4.2 were loaded directly onto the column and the flow-through was collected. The column was washed with 10 column volumes of buffer to remove unbound proteins. Columns were developed by washing with 100 mL buffer containing 15 mM imidazole and the target protein was eluted with 60 mL buffer containing 300 mM imidazole, collected in 10 mL fractions (unless otherwise stated). After use, columns were washed with 10 column volumes of buffer containing 1 M imidazole, 10 column volumes of sterile water and 10 column volumes of 20 % (v/v) ethanol, in which the column was stored at 4°C.

2.4.3.2. Size exclusion chromatography

Proteins were separated on the basis of size using Superdex 75 or 200 resin (GE Healthcare) (separation of proteins with a mass range of 3-75 kDa or 10-600 kDa respectively) on a 26/60 column attached to either AKTA Prime or AKTA 10/100 purifier systems (GE Healthcare) unless otherwise stated. The resolution of Superdex resin is dependent on the dextran components, which are covalently bound to highly cross-linked porous agarose beads. Columns were equilibrated with 1.5 column volumes of the stated buffer. Samples were loaded onto the column via an injection loop in volumes of 5 mL or less to prevent loss of resolution due to sample smearing. Buffer was passed through the column at a rate of 1 mL/min for one

column volume and 10 mL fractions were collected. Protein elution was monitored by an increase in absorbance at 280 nm.

2.4.3.3. Anion exchange chromatography

Anion exchange was carried out using a MonoQ HR 5/5 column (10 μm beads) attached to an AKTA purifier system (GE Healthcare). MonoQ resin (Q Sepharose) contains a quaternary amine group, providing a strong positive charge over the stationary phase surface between pH 2 and 12. The positively charged functional groups were neutralised by a negatively charged ion (Cl^-) by washing the column with 10 column volumes of 20 mM Tris, pH 7.5 containing 1 M NaCl, followed by a wash with 20 mM Tris, pH 7.5 to remove any non-bound Cl^- ions. The protein was loaded onto the column via an injection loop in a low salt buffer with a pH of 7.5, which is at least 1 pH unit above the protein isoelectric point to ensure a net negative charge, allowing the protein to bind strongly to the positively charged resin. A salt gradient was applied to the column from 0-1 M (in 20 mM Tris, pH 7.5) over 10 column volumes with a flow-rate of 0.5 mL/min. The Cl^- ions displaced the proteins with differing net surface charges, allowing protein separation. 1 mL fractions were collected throughout the gradient and the eluting protein was monitored by an increase at A_{280nm}.

2.4.4. Buffer exchange and protein concentration

Protein solutions were buffer exchanged using Vivaspin centrifugal concentrator membranes with a molecular weight cut-off of either 10,000 or 30,000 Da (as stated). Protein solution was placed in the top chamber of the concentrator, and centrifuged at 3,000 × g at 4°C in a bench-top centrifuge (Eppendorf Centrifuge 5810R) for a specified time period. The top chamber containing the protein was refilled with the exchange buffer and the flow-through in the bottom chamber was discarded. The process was repeated a number of times depending on the dilution factors calculated for acceptable buffer exchange. The protein was concentrated and monitored intermittently until the desired volume of protein solution was reached.

2.5. Membrane protein expression and purification

2.5.1. Protein over-expression in *E. coli*

The over-expression of membrane proteins was carried out in an analogous manner to that of cytoplasmic proteins, described in Section 2.4. However, treatment of the resulting cell pellet varied as detailed in the following sections. The PBP variants were all expressed in *E. coli* BL21 Star (DE3) harbouring the pRosetta plasmid.

2.5.2. Small-scale production of membrane protein lysates

For a small-scale production, membrane protein lysates were prepared as described in Ward *et al*. (2000), with few modifications. Cells from a 100 mL overnight expression of a target membrane protein (Section 2.4) were harvested at 10,000 × g in a Beckman JA-25.50 rotor (rotor used throughout this protocol) at 4°C for 10 min. The cell pellet was resuspended in 5 mL 0.2 M Tris pH 8.0 and incubated at 25°C with shaking at 180 rpm for 20 min. 9.7 mL sucrose buffer (1 M sucrose, 1 mM EDTA, 0.2 M Tris pH 8.0) was added, followed by 1.3 mg/mL lysozyme and 20 ml deionised water before incubation at 25°C for 1 h with shaking at 180 rpm. The spheroplasts formed were pelleted at 20,000 × g at 4°C for 20 min and resuspended in 30 mL deionised water using a hand-held homogeniser and allowed to stand for 30 min at 25°C. Membranes were sedimented at 30,000 × g at 4°C for 20 min and the supernatant containing the cytoplasmic fraction of the cells was retained. The membranes were washed three times in 15 mL of membrane resuspension buffer (0.1 M sodium phosphate pH 7.2, 1 mM β-mercaptoethanol) using a hand-held homogeniser to resuspend the pellet each time. After the final wash, membranes were resuspended in 0.5 mL membrane resuspension buffer with 1 mM $MgCl_2$ and 20 μg/ml DNAse. Preparations were incubated at 37°C for 30 min before the addition of 1 mM EDTA. The cytoplasmic and membrane fractions were analysed by SDS-PAGE (Section 2.6.2), frozen in liquid nitrogen and stored at -80°C.

This protocol was also used to evaluate protein expression in large-scale cultures by analysing a fraction of the cells.

2.5.3. Preparation of *E. coli* membranes

The frozen cell pellet containing the over-expressed target membrane protein (Section 2.5.1) was thawed on ice before the addition of 20 μg/mL DNAse, 1 mM $MgCl_2$, 2.5 mg/mL lysozyme, and submitted to rotatory shaking at 4°C for 1 h. Cells were lysed by passing twice through a continuous cell disruptor (Constant Cell Disruption Systems) (pre-equilibrated in ice-cold PBS) at 28 kpsi at 4°C. The lysates were centrifuged for 12 min at 24,000 × g (Beckman JA-25.50 rotor) at 4°C. The resulting pellet was discarded and the centrifugation step was repeated with the supernatant to remove cellular debris. The supernatant was transferred to ultracentrifuge tubes and centrifuged at 150,000 × g for 1 h at 4°C using a Beckman Ti45 rotor in an ultracentrifuge (Beckman Coulter Optima L-90K) to pellet the membrane fraction. The membranes were resuspended in PBS (10 mL/original 1 L cell culture), frozen in liquid nitrogen and stored at -80°C.

2.5.4. Detergent solubilisation screen

1 mL prepared membranes (from Section 2.5.3) was incubated with 1 % (w/v) detergent (assuming this percentage was at least 2-3 × greater than the critical micellar concentration (CMC)) for 1 h with rotatory shaking at 4°C. The insoluble material was pelleted at 150,000 × g for 30 min at 4°C using a Beckman Ti45 rotor in an ultracentrifuge. The soluble and insoluble fractions were analysed by SDS-PAGE and Western blot.

2.5.5. Membrane protein solubilisation and purification

2.5.5.1. Membrane protein solubilisation

Prepared membranes (in PBS) were thawed on ice and 1 % (w/v) sodium deoxycholate (CMC, 0.08-0.25 % (w/v); micellar molecular weight, ~1.2-5 kDa, Sigma-Aldrich) (employed based on the solubilisation screen, Section 2.5.4) was added before membranes were incubated at 4°C with rotatory shaking for 3 h. The

solubilised preparation was transferred to ultracentrifuge tubes, which were filled to the maximum volume by the general purification buffer PBS, 0.1 % (w/v) DDM (Sigma-Aldrich) (CMC, 0.01 % (w/v), micellar molecular weight, ~40-75 kDa, Anatrace, Affymetrix) with additional 150 mM NaCl, unless otherwise stated. Addition of DDM in the buffer gradually began detergent exchange to minimise protein aggregation and precipitation that could occur if this process were rapid. The solubilised membranes were centrifuged at 150,000 × g for 30 min at 4°C using the Beckman Ti45 rotor and ultracentrifuge (Beckman Coulter Optima L-90K) to pellet any remaining insoluble membranes. The supernatant containing solubilised membrane proteins was ready for target protein purification.

2.5.5.2. Affinity chromatography

Purification of membrane proteins with hexa- or dodeca-histidine affinity tags was carried out using TALON Metal Affinity Resin (Cobalt ions) via immobilised metal affinity chromatography (IMAC) under gravity. 5 mL resin was pelleted at 800 × g for 5 min, washed twice in sterile water, and washed twice in the buffer used for purification (PBS, 150 mM NaCl, 0.1 % (w/v) DDM) to equilibrate the resin. Following the final centrifugation, the buffer was discarded from the resin pellet and the solubilised membranes (Section 2.5.5.1) were incubated with the resin with stirring at 4°C for 3 h. The protein-resin mix was poured into a column (length 9 cm, diameter 2 cm) and the resin bed allowed to settle. Flow-through was collected and retained for analysis before the column was resolved with a step gradient of imidazole: 100 mL buffer with 15 mM imidazole (collected as 10 mL fractions), 50 mL buffer with 50 mM imidazole (collected as 5 mL fractions) and 50 mL buffer with 250 mM imidazole (collected as 5 mL fractions), unless otherwise stated. Samples at different stages of the purification were analysed by SDS-PAGE (Section 2.6.2).

2.5.5.3. Size exclusion chromatography

Size exclusion chromatography was used to further purify the protein in addition to detergent and buffer exchange. Size exclusion chromatography was performed using

the analytical Superose 6 (cross-linked agarose-based medium, separating capability of 5-5000 kDa) 10/300 GL column (GE Healthcare) attached to an AKTA purifier 100 system (GE Healthcare). The smaller column size reduces the volume of buffer required, which often contains expensive detergent, but can successfully resolve membrane proteins given their substantially lower yield compared to cytoplasmic proteins. The column was equilibrated in 1.5 column volumes of 20 mM Tris pH 7.5, 150 mM NaCl, 0.03 % (w/v) DDM. 500 µL protein was loaded onto the column via an injection loop. Buffer was passed through the column with a flow rate of 0.4 mL/min and 0.5 mL fractions were collected in a 96-well plate. The elution of the protein was monitored by a change in absorbance at 280 nm. The column was washed in 5 column volumes sterile water and stored in 20 % (v/v) ethanol. Following size exclusion chromatography, the fractions containing protein of the highest level of purity (as determined by SDS-PAGE, Section 2.6.2) were combined, concentrated and stored at -20°C in 50 % (v/v) glycerol.

2.6. Protein analysis and detection

2.6.1. Protein Quantification

2.6.1.1. Soluble proteins

The concentration of soluble proteins was determined using a colourimetric assay at 595 nm (BioRad) (Bradford, 1976). For the BioRad reagent method, 10 µL of protein solution was added to 200 µL of BioRad reagent and 790 µL water in a cuvette, mixed and allowed to stand for 5 minutes. The absorbance was measured at 595 nm using a Jenway 6305 UV-visible spectrophotometer. The procedure was repeated to get an average reading. If the reading was outside the linear range of the assay (above 0.6 at 595 nm), the protein solutions were diluted and reanalysed. The protein concentration (µg/mL) was calculated using the following formula according to the manufacturer's instructions:

$$[\text{Protein}]\ (\mu g/mL) = (A_{595nm}/0.1) \times 1.95 \times \text{dilution factor} \times (1000/\text{volumed assayed})$$

2.6.1.2. Membrane proteins

The concentration of membrane proteins was established using the bicinchoninic acid (BCA) assay (Pierce) (Smith *et al.*, 1985), where unlike other methods, the presence of detergent does not interfere with the protein quantification. The BCA assay was carried out according to the manufacturer's instructions. Reagents A and B were mixed in a 50:1 ratio and 2 mL of this working reagent was added to 100 µL of each sample. Reagents were incubated at 37°C before cooling to room temperature. The absorbance of the samples was measured at 562 nm using a Jenway 6305 UV-visible spectrophotometer. Protein concentrations were calculated based on a bovine serum albumin standard curve. The assay has a working range of 20-2000 µg/mL.

2.6.2. SDS-Polyacrylamide Gel Electrophoresis

SDS-Polyacrylamide Gel Electrophoresis (SDS-PAGE) Tris-glycine buffer system (Laemmli, 1970) was used to separate and visualise polypeptides under denaturing conditions on a discontinuous gel system: resolving gel, pH 8.8; stacking gel, pH 6.8. 5 mL resolving gel (375 mM Tris pH 8.8, 0.4 % (w/v) SDS, 12 % acrylamide:bis-acrylamide (29:1) was prepared, allowing the resolution of proteins between 25 and 75 kDa. Gels were cast using the Hoeffer Mighty Small gel kit and polymerised by the addition of 100 µL 10 % (w/v) APS (ammonium persulfate) and 10 µL *N,N,N′,N′*-Tetramethylethylenediamine (TEMED), then overlaid with 100 % (v/v) ethanol to remove the gel meniscus. 2 mL stacking gel (125 mM Tris pH 6.8, 0.4 % (w/v) SDS, 4 % acrylamide:bis-acrylamide (29:1)) was prepared, polymerised with 50 µL 10 % (w/v) APS and 10 µL TEMED, and pipetted on top of the polymerised resolving gel (removing the ethanol first). A plastic comb was added to form the wells.

25 µg protein samples (or a maximum volume of 20 µL if the [protein] was too dilute) were prepared for analysis in 1 × loading buffer (6 ×; 63.5 mM Tris pH 6.8, 0.4 % (w/v) SDS, 5 % (v/v) β-mercaptoethanol, 20 % (v/v) glycerol, 2.5 % (w/v) bromophenol blue. The samples were heat-denatured at 95°C for 10 min and cooled

to 4°C for 2 min using an Eppendorf Mastercycler Gradient thermocycler. The gel comb was removed, wells were washed with SDS-PAGE running buffer (25 mM Tris pH 8.3, 0.19 M glycine, 0.1 % (w/v) SDS) and the samples were pipetted into the wells. The gels were run in SDS-PAGE running buffer at 180 V or until the gel front reached the base of the gel, typically 55 min.

2.6.2.1. Development of SDS-PAGE gels

Proteins separated by SDS-PAGE were detected using Colloidal-Coomassie stain (8 % (w/v) ammonium sulphate, 0.08 % (w/v) Coomassie G-250, 1.6 % (v/v) phosphoric acid, 20 % (v/v) ethanol). Following SDS-PAGE, gels were rinsed in water for 5 min before staining overnight. Gels were destained in water and imaged using Syngene GeneSnap G:Box Gel Doc and analysis system.

2.6.3. Western blotting for probing with antibodies

SDS-PAGE gels destined for a Western blot analysis were run with a BenchMark His-tagged Protein Standard (molecular weight markers, Invitrogen). Polypeptides that had been resolved by SDS-PAGE (Section 2.6.2) were transferred from the gel to a polyvinylidene difluoride (PVDF) membrane (Hybond-P, Amersham Biosciences) (pre-treated with a 5 minute wash in methanol and a 5 minute wash in the Western Transfer buffer (50 mM Tris, 40 mM Glycine, 0.04 % (w/v) SDS, 20 % (v/v) methanol)). The transfer took place in Western Transfer buffer at 90 mA overnight using an Electrophoretic Protein Blotting Tank (BioRad) at 4°C.

The PVDF membrane was placed in 50 mL blocking solution (comprised of PBS containing 10 % (w/v) skimmed milk powder) for 1 h to prevent non-specific antibody binding to the membrane. The membranes were then washed 3 times for 15 min in 50 mL PBS containing 0.1 % polyoxyethylene (20) sorbitan monolaurate (Tween 20) (PBS-Tween). The blot was then incubated for 1 h with 50 mL PBS-Tween and 50 µL of mouse monoclonal antibody raised against a C-terminal 6-histidine tag (Roche). Three 50 mL PBS-Tween wash steps followed. The blot was incubated in 50 mL PBS-Tween containing 30 µL of the secondary rabbit antibody

raised against mouse IgG (whole molecule) conjugated to horseradish peroxidase (Sigma) for 1 h. After a further 3 washes in PBS-Tween, the blot was reacted with 5 mL of enhanced chemiluminescence (ECL) detection reagents 1 and 2 (Amersham Biosciences) for 5 min. The blot was wrapped in cling film and placed in a cassette containing KODAK BioMax MR film. The exposure time ranged from 5 min to 30 min depending on the antibody concentration applied and intensity of bands required. The film was developed using an AGFA Curix 60 developing machine.

2.7. Lipid I and II synthesis

2.7.1. UDP-Mur*N*Ac-pentapeptide preparation (Adapted from Lloyd *et al.* (2008))

2.7.1.1. Biosynthesis

Typically, biosynthesis of UDP-Mur*N*Ac-pentapeptide occurred in a 2 mL total volume and contained the following components: 50 mM 4-(2-hydroxyethyl)-1-piperazinethanesulphonic acid (HEPES) pH 7.5, 10 mM $MgCl_2$, 200 mM phosphoenol pyruvate (PEP), 50 mM KCl, 1 mM dithiolthreitol (DTT), 10mM UDP-*N*-acetyl glucosamine (UDP-Glc*N*Ac), 30 mM L-Ala, 30 mM D-Glu, 30 mM L-Lys, 30 mM D-Ala-D-Ala, 200 µM NADPH, 6 mM ATP, 25 mM isocitrate, 8 units of isocitrate dehydrogenase (Sigma-Aldrich), 500 units of pyruvate kinase (Sigma-Aldrich), 400 µg of MurA, 2000 µg of MurB, 300 µg of MurC, 350 µg of MurD, 750 µg of MurE and 350 µg of MurF (Mur enzymes provided by A. Catherwood). The reaction components were incubated overnight at 37°C, after which 5 mL sterile water was added and the enzymes were removed by ultrafiltration with a Vivaspin centrifugal concentrator (cut-off of 10,000 Da). The filtrate was ready to be purified.

2.7.1.2. Purification

The UDP-Mur*N*Ac-pentapeptide was purified by anion exchange chromatography using a Source 30Q column (26 × 120 mm) attached to the AKTA purifier 100 system (Amersham Biosciences). The column was sequentially equilibrated with 6

column volumes each of 10 mM ammonium acetate pH 7.6, 1 M ammonium acetate pH 7.6 and 10 mM ammonium acetate pH 7.6 to ensure that the resin was charged with the appropriate ion and no excess salt was present. 10 mM ammonium acetate pH 7.6 was added to the filtrate (from Section 2.7.1.1) to a final volume of 200 mL and loaded onto the column via an injection loop at a rate of 15 mL/min. The column was washed with three column volumes of 10 mM ammonium acetate pH 7.6. An ammonium acetate gradient was set up from 10 mM to 1 M over 18 column volumes (15 mL/min for 60 min). Fractions of 10 mL were collected throughout the gradient and the presence of the eluted UDP-Mur*N*Ac-pentapeptide was judged by an increase in absorbance at 254 nm. The fractions comprising the peak of the UDP-Mur*N*Ac-pentapeptide were freeze-dried to remove trace amounts of buffer, dissolved in 250 μL sterile water and stored at -20°C.

The concentration of UDP-Mur*N*Ac-pentapeptide synthesised was calculated by measuring the absorbance of the solution at 260 nm, where the uracil moiety of the pentapeptide has an extinction coefficient of 10,000 $M^{-1}cm^{-1}$.

2.7.2. *Micrococcus flavus* membrane preparation providing lipid-linked intermediates

2.7.2.1. Culturing *M. flavus*

M. flavus cells from a frozen glycerol stock were used to inoculate 100 mL of tryptone soya broth (TSB) and the cells were cultured overnight at 37°C with 180 rpm agitation. 10 mL of the overnight culture was used to inoculate 8 × 650 mL TSB and the liquid cultures were incubated at 37°C with agitation at 180 rpm until OD_{600nm} reached 4.0 (mid-exponential phase). The cells were harvested by centrifugation at 10,000 × g for 10 min using a Beckman JLA-8.100 rotor.

2.7.2.2. *M. flavus* membrane preparation

The *M. flavus* cell pellet (from Section 2.7.2.1) was washed once in the ice-cold membrane buffer (20 mM Tris, 1 mM $MgCl_2$ and 2 mM β-mercaptoethanol, pH 7.5)

and the final pellet was resuspended in 3 mL/g of cells of the membrane buffer supplemented with 2.5 mg/mL of chicken egg white lysozyme. After a 15 min incubation on ice, the *M. flavus* cells were disrupted by passage through a continuous cell disrupter at 30,000 psi. Unbroken cells and particulate debris were removed by centrifugation at 10,000 × g for 1 h at 4°C. The supernatant was centrifuged at 50,000 × g for 1 h at 4°C to pellet the membranes. The pellet was resuspended in membrane buffer at three times the volume of the pellet. The membranes were centrifuged at 50,000 × g for 1 h at 4°C and the final membrane pellet was resuspended in 3 mL of membrane buffer. The protein concentration of the membranes was calculated using the BioRad assay (Section 2.6.1.1). The membranes were stored at -80°C.

2.7.3. Lipid I and II preparation

2.7.3.1. Synthesis

Lipid I and Lipid II syntheses were performed in an adaptation of the method of Breukink *et al.* (2003). In a glass vial, with a final reaction volume of 3.5 mL, *M. flavus* membranes (3.5 mg/ml) were incubated together with 1.62 mM undecaprenyl phosphate (Larodan Fine Chemicals AB, Sweden), 2 mM UDP-Mur*N*Ac pentapeptide and 35 mM UDP-Glc*N*Ac (Sigma), in a buffer containing 100 mM Tris, pH 8.5, 5 mM $MgCl_2$, and 1 % (v/v) Triton X-100. The UDP-Glc*N*Ac was omitted during the synthesis of Lipid I. The reaction components were incubated at 37°C for 2.5 h. The lipids were then extracted by the sequential addition of 3.5 mL of 6 M pyridinium acetate pH 4.2 and 7 mL *n*-butanol. The top layer (*n*-butanol) was collected after centrifugation (3,000 × g, 10 min, 4°C) and washed with an equal volume of water to remove any water-soluble impurities from the lipid phase (mainly pyridine). The mixture was centrifuged (3,000 × g, 10 min, 4°C) and the top phase (containing lipid) was evaporated under reduced pressure and stored at -80°C prior to purification.

2.7.3.2. Purification

Lipid I and II were purified using anion exchange on a DEAE-Sephacel column. The column was run using organic solvents to retain the lipids in a soluble phase. The organic nature of the solvents dictated that glassware was used to avoid contamination with plasticizers, which can interfere with mass spectrometric analysis. The column was prepared by pouring a final volume of 3 mL DEAE-Sephacel into a sawn-off 20 mL glass burette with glass wool acting as a fret to prevent the resin escaping from the column base. The column was washed consecutively with 40 mL 1 M ammonium acetate (to charge the Sephacel resin with acetate groups), 60 mL water and 40 mL chloroform/methanol/water 2:3:1 (v/v) (solvent A). The dried lipid was resuspended in 6 mL solvent A and pipetted onto the solvent bed and the flow-through was collected. The column was developed with a step-wise gradient using four column volumes of various percentages of chloroform/methanol/1 M ammonium bicarbonate 2:3:1 (v/v) (solvent B) (0 %, 5 %, 10 %, 15 %, 20 %, 25 %, 30 %, 50 % and 100 %) in solvent A. The fractions were collected accordingly and analysed by thin-layer chromatography (TLC) (Section 2.7.4). Fractions containing the desired lipid were evaporated under reduced pressure, resuspended in 10 mL/fraction of sterile water and freeze-dried to remove the ammonium bicarbonate. The lipid was ultimately resuspended in 1.5 mL solvent A and stored in a glass vial at -80°C.

2.7.4. Analysis by thin layer chromatography

High performance silica thin layer chromatography (HPTLC) was performed to separate the lipid components. Initially, 0.5 mL of each fraction from the purification step (Section 2.7.3.2) was dried under reduced pressure and the samples were resuspended in 25 µL of chloroform/methanol/water 2:3:1 (v/v). The samples were loaded onto the HPTLC plate at marked positions: 2 cm apart and 1.5 cm from the base of the plate. Samples were loaded in 5 µL aliquots with air drying to prevent the spot size from getting too large. The sheet was placed evenly in a tank containing a 1 cm depth of chloroform/methanol/water/0.88 ammonia 88:48:10:1 (v/v) (Breukink *et al.*, 2003). Chromatography was carried out for 3.5 h at room

temperature. The HPTLC plate was removed and the solvent front marked with pencil and allowed to dry before placing in a sealed tank, containing solid iodine to stain the sample components using iodine vapour. The HPTLC plate was removed from the tank after 30 min and because iodine staining is not permanent, the image was recorded immediately using a flat-bed scanner attached to a computer (Appendix A).

2.7.5. Concentration determination

Two 50 µL lipid samples and 50 µL chloroform/methanol/water 2:3:1 (v/v) (acting as a blank) were dried down and resuspended in 50 µL 50 mM HEPES, 10 mM $MgCl_2$, 30 mM KCl, 1.5 % (w/v) CHAPS, pH 7.6. One of the lipid samples and the blank were treated with: 50 µL 1 M HCl, boiled for 30 min, centrifuged at 3,000 × g for 5 min, and readjusted to pH 7.6.

The inorganic phosphate hydrolysed from the lipids was quantified using a P_i detection assay (Section 2.8.1). In a 200 µL spectrophotometric assay containing 50 mM HEPES, pH 7.6, 10 mM $MgCl_2$, 200 µM 7-methyl-6-thioguanosine (MESG) (Berry and Associates, USA), 1 unit purine nucleoside phosphorylase (PNP), 1 unit inorganic pyrophosphatase (IPP), a stable baseline was reached by measuring the absorbance at 360 nm before addition of 10 µL lipid sample. The concentration of the lipid was calculated based on the knowledge that there are two P_i per molecule Lipid I or Lipid II and the extinction coefficient of the change in absorbance at A_{360nm} by 1 M P_i is 10,000 $M^{-1}cm^{-1}$ (caused by the phosphorolysis of MESG).

2.7.6. Mass spectrometry

The lipid samples were analysed by Biological Mass Spectrometry and proteomics service (School of Life Sciences, University of Warwick). Mass estimates were obtained by negative ion electrospray ionisation mass spectrometry (ESI-MS).

2.7.7. Preparation of [^{14}C]-labelled Lipid II

2.7.7.1. [^{14}C]-labelled Lipid II synthesis

This method was designed based on the synthesis of non-radiolabelled Lipid II and a method described by Bertsche *et al.* (2005). The synthesis of radiolabelled Lipid II was performed as in Section 2.7.3.1 with minor adjustments. The components were assembled in 3.5 mL, replacing UDP-Glc*N*Ac with 100 µL 78.88 µM [^{14}C]-UDP-Glc*N*Ac (317 mCi/mmol, supplied in 200 µL, Amersham Biosciences) providing 5 µCi/15.78 nmol. 140 µg *E. coli* MurG (prepared as described by Ha *et al*. (1999); pET3a::*murG* construct kindly provided by S. Walker (Harvard University)) was used to supplement the MurG in the *M. flavus* membranes, enhancing the formation of Lipid II from Lipid I. The reaction was incubated in a water bath at 37°C for 1 h to allow optimum conditions for the incorporation of the radiolabelled Glc*N*Ac moiety. Non-radiolabelled UDP-Glc*N*Ac was added to provide a final concentration of 35 mM UDP-Glc*N*Ac (radiolabelled and non-radiolabelled) and the reaction was incubated for a further 2 h with intermittent agitation. The reaction was stopped and the lipid constituents were extracted as for non-radiolabelled Lipid II (Section 2.7.3.1).

2.7.7.2. [^{14}C]-Lipid II purification

Purification of [^{14}C]-Lipid II used an identical approach to the purification of non-radiolabelled Lipid II (Section 2.7.3.2). The only divergence to the protocol was the development of the column, where fewer steps of the solvent B gradient were applied to minimise the amount of radioactive waste. The solvent B gradient washes occurred using four column volumes as follows: 0 %, 10 %, 25 % ((v/v) of solvent B in solvent A). From the Lipid II synthesis, it was apparent that all lipid contaminants were removed with 25 % (v/v) solvent B, and at percentages higher than this, Lipid II eluted. [^{14}C]-Lipid II was eluted with eight column volumes of 100 % (v/v) solvent B to ensure no lipids were retained on the column and the overall yield of lipid was maximal. The fractions were analysed for radioactivity by scintillation counting using a Packard Liquid Scintillation Analyser Tri-Carb 2900TR. Radioactivity was

solely detected in the 100 % (v/v) solvent B fractions, which were dried under reduced pressure and the purified [^{14}C]-Lipid II was freeze dried to remove the ammonium bicarbonate. The [^{14}C]-Lipid II was resuspended in 1.5 mL solvent A and stored in a glass vial at -80°C. A sample was assessed by scintillation to determine the radioactivity of [^{14}C]-Lipid II in terms of counts per minute (cpm).

2.7.8. Concentration and purity determination by HPTLC

To avoid contaminating equipment with radioactivity, the concentration and purity of [^{14}C]-Lipid II were determined concomitantly using a different approach compared to non-radiolabelled Lipid II. HPTLC was performed as described in Section 2.7.4. Standards of non-radiolabelled Lipid II with known concentrations were loaded onto the silica TLC plate in addition to 15 µL of [^{14}C]-Lipid II. Chromatography was carried out as in Section 2.7.4. Following removal from the tank, the solvents were evaporated from the HPTLC plate for 1 h to ensure complete dryness. The plate was then exposed to a phosphoimaging plate for 48 h. The phosphoimaging plate was imaged using the Fujifilm FLA-5000 imaging system. The HPTLC plate was stained using iodine vapour and immediately imaged as described in Section 2.7.4.

Image Processing and Analysis in Java (ImageJ) software (Abràmoff *et al.*, 2004) was used to analyse the intensity of the iodine-stained Lipid II bands, which enabled the quantity of [^{14}C]-Lipid II to be estimated by comparing the mean grey values of the [^{14}C]-Lipid II sample with the standards containing known amounts of Lipid II.

2.8. Assays to analyse transglycosylase activity

2.8.1. Biochemical spectrophotometric assays

This assay is based on the release of P_i due to the dephosphorylation of undecaprenyl pyrophosphate (a product of transglycosylation) by the coupling enzyme, undecaprenyl pyrophosphate phosphatase. PNP depends on P_i to convert MESG (strong absorbance at 330 nm) to ribose-1-phosphate and 7-methyl-6-guanine (strong absorbance maximum at 360 nm), which can be measured spectrophotometrically (Webb, 1992). The assay principle is outlined in Figure 4.4 and discussed in the accompanying text.

2.8.1.1. Continuous spectrophotometric assay for the coupling enzyme activity

The activity of *E. coli* PgpB, the undecaprenyl pyrophosphate phosphatase (characterised by Touzé *et al.* (2008)) was analysed using the natural substrate, undecaprenyl pyrophosphate (a kind gift from E. Kula-Swiezewska, Institute of Biochemistry and Biophysics, Poland). The substrate was supplied in volatile solvents; the solvents were evaporated prior to use and the lipid was resuspended in 5 µL 0.1 % (w/v) DDM. The following reaction components were mixed together in a cuvette in a final volume of 200 µL: 20 mM Tris pH 7.5, 150 mM NaCl, 0.1 % (w/v) DDM (to maintain membrane proteins and lipids in a solubilised state), 1 unit PNP, 400 µM MESG, 0-817 µM undecaprenyl pyrophosphate and up to 10 µL PgpB to a final concentration of 1.78 µM. Enzyme or substrate initiated the reactions. Assays were performed using a Varian Cary 100 spectrophotometer equipped with a cell changer at 360 nm and 37°C. Controls of different potential lipid substrates were evaluated in an identical manner at final concentrations of 200 µM.

2.8.1.2. Discontinuous spectrophotometric assay for transglycosylation

The reaction of a transglycosylase with its substrate was performed in a discontinuous manner, and the products were analysed using the PgpB-coupled spectrophotometric assay.

2.8.1.2.1. Discontinous transglycosylase assays

The following text describes the basic reaction conditions for transglycosylase activity; optimisation of these conditions is described in Chapter 4. The transglycosylase reactions of *S. aureus* MGT and *S. pneumoniae* PBP1a variants occurred in a reaction volume of 15 µL and 18 µL respectively unless otherwise stated. The solvents of the Lipid II substrate were removed by evaporation and Lipid II (present at concentrations between 0 and 1.47 mM) was resuspended in the reaction buffer: 20 mM Tris pH 8.0, 10 mM $MgCl_2$, 0.1% (w/v) DDM by vigorous vortexing followed by a centrifugation, to ensure the maximum amount of Lipid II had solubilised. The addition of 155 µM MGT or 77 µM PBP1a variants (unless otherwise stated) initiated the reaction. The reactions of the PBP1a variants were immediately sonicated in a water bath at 20°C for 30 sec. The reactions were performed in duplicate at 20°C over a specified time frame before heat inactivating the protein at 60°C for 10 min. The reactions were centrifuged for 5 min at 10,000 × g to pellet the precipitated protein.

When transglycosylase activity was measured at time points, a master mix was prepared and 15 µL (MGT) or 18 µL (PBP1a) aliquots were sampled at given times.

2.8.1.2.2. Spectrophotometric assay

The components of the spectrophotometric assay are described in Section 2.8.1.1. 13 µL and 16 µL of the MGT and PBP1a transglycosylation reactions were sampled from the total discontinuous reaction volume (to avoid the protein pellet) and added to the cuvette. A baseline at 360 nm was obtained prior to the addition of 4.4 µM PgpB.

2.8.2. Analysis of transglycosylation products by SDS-PAGE

2.8.2.1. SDS-PAGE conditions

SDS-PAGE gels were prepared as described by Barrett *et al.* (2007) for the detection of glycan chains with few modifications to the protocol. Gels were cast using the Hoeffer Mighty Small gel kit with a 10 mL gel recipe of 0.5 M Tris pH 8.45, 0.1 % (w/v) SDS, 9 % T (total percentage concentration of both acrylamide and bis-acrylamide), 2.6 % C (percentage bis-acrylamide relative to T) and polymerised by the addition of 30 µL of 10 % (w/v) APS and 7.5 µL TEMED. The samples were loaded with a 25 % volume of sample buffer: 120 mM Tris pH 8.8, 2 % (w/v) SDS, 50 % (v/v) glycerol without heat denaturation. Bromophenol blue was omitted from the sample buffer, as the constituents can impede the detection of transglycosylation products. In a single lane, sample buffer with bromophenol blue was loaded to monitor migration. Gels were run in anode buffer (0.1 M Tris, pH 8.8) and cathode buffer (0.1 M Tris, 0.1 M Tricine, 0.1 % (w/v) SDS, pH 8.25) at 100 V for 1 h.

2.8.2.2. Detection of glycan chains separated by SDS-PAGE

2.8.2.2.1. [^{14}C]-Lipid II detection

Transglycosylase reactions were performed as described in Section 2.8.1.2.1 replacing non-radiolabelled Lipid II with its radioactive counterpart. A higher concentration of the [^{14}C]-Lipid II was used to ensure a signal could be detected (as stated in the corresponding text), dependent on the specific activity of [^{14}C]-Lipid II. The transglycosylation reactions were quenched by heat-denaturation and the precipitated protein was removed by centrifugation prior to sample preparation. Gels were prepared and run according to Section 2.8.2.1.

Gels were dried for 3 h using a BioRad Model 583 gel drier before being exposed to a phosphoimaging plate for 14 days. Phosphoimaging plates were imaged using the Fujifilm FLA-5000 imaging system.

2.8.2.2.2. VanFL detection

Transglycosylase reactions were performed as described in Section 2.8.1.2.1 using 2 mM Lipid II substrate. The reactions were stopped by heat denaturation and the precipitated material was removed by centrifugation. VanFL was added at a final concentration of 24 μM to the reactions, which were incubated in the dark (to reduce fluorescence quenching) for 5 min, prior to loading onto the gel. Gels were prepared and run according to Section 2.8.2.1 in the dark. VanFL fluorescence was detected using Syngene GeneSnap G:Box Gel Doc and analysis system with the blue light converter with appropriate filter for detecting VanFL-specific fluorescence (emission maximum, 512 nm).

2.9. Assays to analyse D-Ala release

2.9.1. Continuous spectrophotometric assay for D-Ala release

2.9.1.1. VanA-coupled assay

The basis of this assay is the VanA-dependent ligation of D-Lac and D-Ala (released from transpeptidation or D,D-carboxypeptidation reactions) with the concomitant hydrolysis of ATP producing ADP and P_i, both of which can be detected spectrophotometrically (outlined in Figure 5.5a and discussed in the accompanying text).

2.9.1.1.1. Detection of ADP

ADP is linked to NADH oxidation by the coupling enzyme pyruvate kinase and lactate dehydrogenase (as described by Wampler and Westhead (1968)). The following components were mixed together in a cuvette with a final volume of 200 μL: 50 mM HEPES pH 7.6, 10 mM $MgCl_2$, 20 μM VanA, 100 mM D-Lac, 1 mM ATP, 2 mM PEP, 100 μM NADH, 1.6 units pyruvate kinase, 2.4 units lactate dehydrogenase, 0-4 mM UDP-Mur*N*Ac-L-Ala-γ-D-Glu-L-Lys-D-Ala-D-Ala. The reaction was monitored at 340 nm at 37°C using the Varian Cary 100

spectrophotometer. A baseline was obtained before the addition of 35 nM *Actinomadura* R39 D,D-peptidase, which initiated the reactions.

2.9.1.1.2. Detection of P_i

P_i was monitored by the phosphorolysis of MESG as described in Section 2.8.1. The following components were mixed together in a cuvette with the final volume of 200 µL: 50 mM HEPES pH 7.6, 10 mM $MgCl_2$, 20 µM VanA, 100 mM D-Lac, 1 mM ATP, 1 unit PNP, 400 µM MESG, 0-320 µM UDP-Mur*N*Ac-L-Ala-γ-D-Glu-*meso*-DAP-D-Ala-D-Ala. The reaction was monitored at 360 nm at 37°C and initiated by the addition of 35 nM *Actinomadura* R39 D,D-peptidase.

2.9.2. Discontinuous spectrophotometric assay for D-Ala release

The VanA coupled assay was not sufficiently sensitive to detect D-Ala release from *S. pneumoniae* PBPs under investigation, thus the Amplex Red assay was employed (assay principle outlined in Figure 5.5b).

2.9.2.1. Discontinuous D-Ala release assay

The D-Ala release assays of *S. pneumoniae* PBP1a, PBP2b and PBP2x variants took place in 30 µL. The solvents were evaporated from Lipid II, which was thoroughly resuspended in 20 mM Tris pH 8.0, 1 mM $MgCl_2$, 0.1 % (w/v) DDM, 22 mM Decyl PEG, 20 % (v/v) DMSO, giving a final concentration of 0.33 mM Lipid II. In reactions requiring a polymerised form of Lipid II, 120 µM MGT or 45 µM PBP1a-S370A were incubated with Lipid II for 1 h at 20°C, and remained present during the D-Ala release reactions. 45 µM of each PBP was added to individual reactions and incubated for 18 h at 20°C. Proteins were inactivated by heat denaturation at 60°C for 10 min and the precipitated protein was removed by centrifugation at 10,000 × g for 10 min.

2.9.2.2. Spectrophotometric assay

The following components were mixed together in a cuvette with a final reaction volume of 200 µL: 50 mM HEPES pH 7.6, 10 mM $MgCl_2$, 0.1 % (w/v) DDM, 0.75 units D-amino acid oxidase (DAAO), 2.5 units horseradish peroxidase, 50 µM Amplex Red reagent. Addition of 20 µL of the 30 µL discontinued reaction initiated the detection of D-Ala, measured at 555 nm, 37°C. Assays were performed in a Varian Cary 100 spectrophotometer.

2.9.3. Analysis of transpeptidase or D,D-carboxypeptidase products by SDS-PAGE

Transpeptidation or D,D-carboxypeptidation reactions were performed in a similar manner as described in Section 2.9.2.1 (omitting Decyl PEG and DMSO) in a total volume of 18 µL with 2 mM Lipid II. In reactions requiring a glycan chain substrate, 155 µM MGT was initially incubated with Lipid II. 77 µM *S. pneumoniae* PBP variants were added to initiate the reactions with Lipid II, which were incubated at 20°C for 3 h. Enzymes were heat-inactivated and the precipitated protein was removed by centrifugation. The reaction products were incubated with 24 µM VanFL and separated by SDS-PAGE according to Section 2.8.2.1. VanFL fluorescence was detected as detailed in Section 2.8.2.2.2.

2.10. Protein crystallisation

2.10.1. Vapour diffusion crystallisation method

In order for a protein to crystallise, internal changes to a system are required to cause the protein to exceed its limit of solubility, resulting in a transition from a thermodynamically stable state to an unstable supersaturated state. This can be achieved by adjusting the parameters of a system including composition of the aqueous protein solution (precipitants or additives); pH; temperature. It is during supersaturation where the protein can form intermolecular contacts, spontaneously generating either crystal nuclei or amorphous precipitate. Following nucleation, crystal growth can proceed, sequestering protein from the surrounding solution.

Vapour diffusion is the conventional method for altering the precipitant concentration and bringing the protein into a supersaturated state. The sitting drop and hanging drop methods of vapour diffusion were used in this work and are explained diagrammatically with the corresponding phase diagram in Figure 2.3.

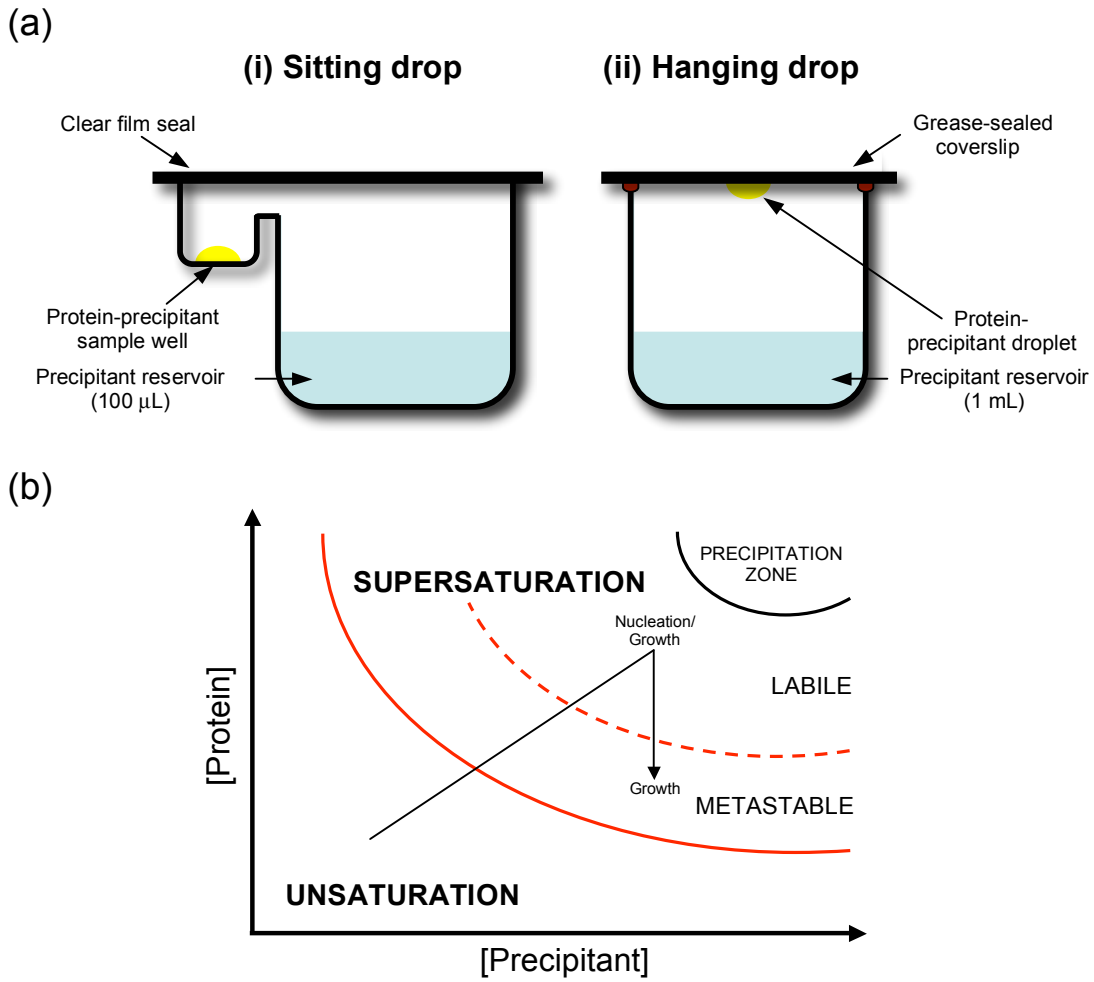

Figure 2.3: Crystallisation by vapour diffusion. (a) A cross-section of the experimental set-up of vapour diffusion methods. An unsaturated protein solution containing precipitant 'sitting' in a well ((i) sitting drop) or suspended over the precipitant reservoir ((ii) hanging drop). The [protein] increases as vapour equilibration between the droplet and reservoir occurs, bringing the protein into a supersaturated state. (b) Phase diagram of vapour diffusion. Vapour diffusion results in the trajectory of the protein solution from an unsaturated to a supersaturated state. Nucleation and crystal growth occur in the supersaturated zone but require distinct conditions: high (labile) and low (metastable) supersaturated states respectively. Nucleation does not occur if the supersaturated state is too low (metastable zone) or too high (precipitation zone, which leads to the formation of precipitate). Following nucleation in the labile zone, the protein will be sequestered as the crystal grows, returning the solution to the metastable zone. The black arrow indicates the ideal strategy for crystal growth.

2.10.2. Sparse matrix screens

Sparse matrix screens have been developed with a bias towards conditions that have successfully generated protein crystals with an emphasis on either soluble or transmembrane proteins. The screens are used as a starting point when studying a protein that has not been previously crystallised. Soluble protein sparse matrix screens utilised include: Wizard I screen (Emerald Biosciences); Newcastle I screen (University of Newcastle); Clear Strategy I screen (Molecular Dimensions); Index screen (Hampton Research); JCSG-*plus* (Molecular Dimensions) and PACT-premier (Molecular Dimensions). Transmembrane protein sparse matrix screens include: MemStart (Molecular Dimensions), MemSys (Molecular Dimensions) and MemGold (Molecular Dimensions). The Honeybee *963* crystallisation robot (Digilab) was used as an automated facility to set up the crystallisation screens in a sitting-drop format in 96-well Greiner plates or 96-well MRC plates, using a volume of 100 µL precipitant per reservoir. The sitting drops consisted of 200 nL protein mixed with 200 nL precipitant and the trials were carried out at 18°C unless otherwise stated.

2.10.3. Optimisation screening

2.10.3.1. In-house screen development

Following an indication of a successful crystal nucleation and growth in a sparse matrix condition, the reproducibility of the crystals and improvements in crystal quality were pursued by traversing the initial condition across buffer pH, precipitant concentrations, protein concentrations and protein to precipitant ratio. Crystal screens were set-up using the hanging drop method of vapour diffusion in a 24-well plate, with 1 mL precipitant solution in the reservoir and total droplet size of 2 µL (containing protein and precipitant). The trials were carried out at 18°C.

2.10.3.2. Additive screen

The Additive screen (Hampton Research) is a library of small molecules introduced into crystallisation screens to manipulate the conditions. The crystallisation trials

were performed according to the manufacturer's instructions in a 96-well plate using the sitting drop vapour diffusion method. The trials were carried out at 18°C.

2.10.3.3. Silver Bullet screen

The Silver Bullet screen (Hampton Research) contains small molecules that have been documented to promote crystal lattice formation. The crystallisation trials were performed according to the manufacturer's instructions using the sitting drop vapour diffusion method in a 96-well plate. The trials were carried out at 18°C.

2.10.4. Cryoprotection

The X-ray exposure to protein crystals can cause secondary radiation damage within the crystal lattice, where free radicals are generated at room temperature (Garman and Doublié, 2003). To minimise this effect and to preserve the life of the crystal, data collection was carried out at 100°K in a nitrogen vapour stream, allowing better quality data to be obtained at a higher resolution. Cryoprotectants were employed during the freezing of the crystal to allow the formation of vitreous ice as opposed to crystalline ice, by reducing the water molecules in contact with each other, thus avoiding disruption of the crystal lattice. In this work, 20-30 % (v/v) glycerol was used as a cryoprotectant. Crystals were mounted with rayon fibre tubes of 0.05-0.3 mm, held within the loop by surface tension. Crystals were transferred to 5 µL drop of mother liquor containing cryoprotectant (replacing the appropriate volume of water). In the cryoprotectant of 30 % (v/v) glycerol, crystals were soaked in a three-step gradient. The loop was plunged into liquid nitrogen to freeze the crystal. Frozen crystals were stored in a Taylor Wharton dewar.

2.10.5. Data collection

Preliminary diffraction data was obtained using the in-house X-ray facility. Complete data sets were collected at the Diamond Lightsource Radiation Facility (UK) on the I24 microfocus beamline using a Pilatus 6M solid state detector with an oscillation angle of 0.2° and a crystal to detector distance of 416 mm.

Chapter 3. Cloning, expression and purification of *Streptococcus pneumoniae* PBP1a, PBP2b and PBP2x

3.1. Introduction

The penicillin-binding proteins of *S. pneumoniae* have been subjected to intense investigation with regards to their role in β-lactam resistance. Of the six PBPs from *S. pneumoniae*, PBP1a, PBP2b and PBP2x are regarded as the major resistance determinants (as described in Section 1.10.3). In resistant clinical isolates (such as *S. pneumoniae* 5204), these enzymes are found to be genetically altered; certain mutations are integral to the resistance mechanism and confer a reduced affinity of the PBP for β-lactam antibiotics (Zapun *et al.*, 2008).

3.1.1. *S. pneumoniae* D39 and 5204 strains

The work in this Chapter focuses on PBPs from two different strains of *S. pneumoniae*: D39 and 5204. *S. pneumoniae* D39 is a penicillin-susceptible strain and is the progenitor of *S. pneumoniae* R6 (Williams *et al.*, 2007), which is a common standard used in comparative experiments of β-lactam sensitive and resistant strains (examples are included in Chesnel *et al.* (2005), Contreras-Martel *et al.* (2009) and Job *et al.* (2008)). There are no deviations at the nucleotide level of the *pbp* genes between the D39 and R6 strain as identified by sequence comparisons. *S. pneumoniae* 5204 was first isolated from sputum in 1999 in Grenoble, France (Chesnel *et al.*, 2003). It is highly resistant to β-lactam antibiotics: penicillin G MIC is 6.0 μg/ml; cefotaxime MIC is 12 μg/ml (Chesnel *et al.*, 2005). Given these high MICs, the 5204 strain can be used as a credible reference for low affinity PBPs.

3.1.2. Generation of PBPs with a low affinity for β-lactam antibiotics

The *S. pneumoniae pbp*s of penicillin-sensitive isolates are genetically uniform (Dowson, *et al.*, 1989). However, the *pbps* from penicillin-resistant isolates exhibit diverse genetic alterations, which develop either through a series of step-wise spontaneous point mutations (Grebe and Hakenbeck, 1996) or by recombination

events between homologous *pbp* genes of *S. pneumoniae* and related species (Dowson *et al*., 1989; 1990). The *pbp1a*, *pbp2b* and *pbp2x* genes from penicillin-resistant pneumococci contain sequence blocks that are identical in the homologous genes of at least two streptococcal species (Dowson *et al*., 1989; Laible *et al*., 1991; Martin *et al*., 1992). Thus, these processes can generate highly mosaic *pbp* genes. For example, the sequence of *pbp2b* from a penicillin-resistant strain of *S. pneumoniae* (DN87/557) was found to contain blocks of nucleotides that diverged from the *S. pneumoniae* R6 sequence by up to 21 % (Dowson *et al.*, 1990). Genes conferring low affinity for the antibiotic can be disseminated by horizontal gene transfer. Evidence for this process is provided by the >99.6 % nucleotide sequence identity of PBP2b between penicillin-resistant strains of *S. pneumoniae* and *S. oralis*, whereas sequences of PBP2b between penicillin-susceptible strains diverge by ~20 % (Coffey *et al*., 1993). The resulting amino acid substitutions have a higher occurrence in the transpeptidase domain (exemplified in Table 3.1), indicating that the antibiotic pressure promotes genetic rearrangement in the antimicrobial target region (Sanbongi *et al.*, 2004). Only a restricted set of the substitutions are important in the β-lactam resistance mechanism (Chesnel *et al.*, 2003).

Enzyme	Total number of amino acid substitutions	Number of amino acid substitutions specific to the transpeptidase domain	Reference
PBP1a	48	45	Job *et al.* (2008)
PBP2b	58	44	Contreras-Martel *et al.* (2009), Pagliero *et al.* (2004)
PBP2x	80	41	Chesnel *et al.* (2003)

Table 3.1: Amino acid substitutions in the major resistance determinants of *S. pneumoniae* 5204.

3.1.3. Mutations of the *S. pneumoniae* resistance determinants implicated in β-lactam resistance

The following section discusses important mutations that are relevant in the β-lactam resistance mechanism of *S. pneumoniae* PBP1a, PBP2b and PBP2x.

3.1.3.1. PBP2x

PBP2x is normally the first PBP to be modified under the selection pressure of β-lactam antibiotics (Grebe and Hakenbeck, 1996). The sequences of PBP2x from

clinical strains are normally categorised into three groups. The first includes sequences that are comparable to the β-lactam sensitive reference, *S. pneumoniae* R6. The other two groups represent PBP2x sequences from β-lactam resistant stains and are classified according to the presence of either T338A or Q552E mutation (Chesnel *et al.*, 2003). The different substitutions confer a reduced susceptibility of PBP2x for β-lactam antibiotics via two independent mechanisms, which are not necessarily mutually exclusive (Carapito *et al.*, 2006). *S. pneumoniae* 5204 PBP2x is a member of the T338A family of resistant protein sequences (Carapito *et al.*, 2006). Out of the numerous amino acid substitutions in *S. pneumoniae* 5204 PBP2x, only six have been shown to be essential for high levels of resistance (Carapito *et al.*, 2006). The individual roles of the mutations are described in Table 3.2.

Amino acid substitution	Role in the β-lactam resistance mechanism	Reference
Q552E	The substitution indroduces a negative charge at the entrance to the active site, disfavouring the binding of the negatively charged β-lactam.	Mouz *et al.* (1999)
T338A	Located in the first conserved motif, the substitution reduces the acylation efficiency of the catalytic serine. It has been implemented in the loss of a water molecule, which results in the destabilisation of the active site.	Mouz *et al.* (1998)
M339F	The substitution in conjunction with T338A, causes the distortion of the active site, causing the reorientation of the active site serine hydroxyl group.	Chesnel *et al.* (2003)
M400T	The substitution potentiates the effect of the M339F mutation.	Carapito *et al.* (2006)
I371T and R384G	Co-operation between the two mutations is believed to increase the flexibility of the loop in which they are situated, remodelling the active site and consequently weakening the non-covalent interactions with the antibiotic and potentially affecting the reactivity of the catalytic serine.	Carapito *et al.* (2006)
N605T	The substitution directly impacts the acylation efficiency of the catalytic serine by destabilising a hydrogen bond network. The loss of a hydrogen bond could participate in the disruption of a loop that borders the active site.	Carapito *et al.* (2006)

Table 3.2: The roles of the essential amino acid substitutions in *S. pneumoniae* 5204 PBP2x implemented in high levels of β-lactam resistance. Although it is not found in the sequence of *S. pneumoniae* 5204 PBP2x, the role of the Q552E substitution is described as it is an important mutation in other resistant sequences of PBP2x.

Carapito *et al.* (2006) found that reversion of the six amino acid substitutions in PBP2x (strain 5204) back to the original amino acids of the β-lactam sensitive sequence caused the acylation efficiency for the β-lactam to increase by 1000-fold. However, if the converse mutations were made to β-lactam sensitive sequence of PBP2x, the acylation efficiency decreases by only 100-fold, an order of magnitude lower. This discrepancy is believed to result from the cooperativity of additional uncharacterised mutations that collectively impact the level of resistance.

3.1.3.2. PBP2b

PBP2b has not been subjected to such a vigorous investigation unlike PBP2x. This is presumably due to the difficulties in obtaining X-ray crystal structural information of truncated forms of PBP2b (Zapun *et al.*, 2008). The T446A mutation is prominent in all identified β-lactam resistant sequences and lies downstream of the SSN conserved motif. It is believed to directly affect the affinity of antibiotics, although its effect is propagated by other uncharacterised substitutions (Pagliero *et al.*, 2004). Applying this mutation to the *S. pneumoniae* R6 sequence decreases the affinity of PBP2b for penicillin G by 60 %. Other substitutions including E476G and T489S/A are frequently found in the PBP2b sequences of highly resistant strains, although their roles have not been thoroughly investigated (Pagliero *et al.*, 2004).

3.1.3.3. PBP1a

PBP1a is clinically important due to its essential requirement for the development of high levels of β-lactam resistance. A common substitution found in sequences of resistant strains is T371A, which lies adjacent to the catalytic serine (Smith and Klugman, 1998). This mutation results in the loss of a hydrogen bond, which normally forms between T371 and W368, and causes the catalytic serine to change its orientation (Job *et al.*, 2008). Similar blocks of mutations have been identified in the PBP1a sequences from β-lactam resistant clinical isolates; in the majority of drug resistant strains, NTGY replaces the TSQF sequence at positions 574-577 (Job *et al.*, 2008; Smith and Klugman, 1998). This sequence is situated in a loop that borders the active site. The substituted residues are proposed to increase the local

hydrophilicity, which can interfere with the antibiotic recognition. Substituting NTGY into the PBP1a sequence from the R6 strain causes the acylation efficiency for penicillin G to decrease 49-fold (Job *et al.*, 2008).

3.1.4. PBPs to be investigated in this study

The major resistance determinants of *S. pneumoniae* strains D39 and 5204 are the focal point of this thesis. The key objective is to obtain a greater understanding of these PBPs in terms of their natural enzymology and the complex β-lactam resistance mechanisms they impart. This chapter discusses the cloning, expression and purification of PBP1a, PBP2b and PBP2x, which is a prerequisite for future biochemical and structural characterisations.

3.2. Experimental Aims

- To clone the major β-lactam resistance determinants of *S. pneumoniae*, *pbp1a*, *pbp2b* and *pbp2x*, from the penicillin-sensitive strain, D39, and the penicillin-resistant strain, 5204, into an appropriate vector for expression in *E. coli*

- To clone *S. pneumoniae* D39 *pbp1a*, *pbp2b* and *pbp2x*, devoid of the cytoplasmic and membrane domains, into an appropriate vector for expression in *E. coli*

- To create single desired mutations in the active site domains of the *S. pneumoniae* D39 Class A, PBP1a, and Class B, PBP2b and PBP2x, eliminating transglycosylase or transpeptidase activity

- To optimise the expression conditions of the *S. pneumoniae* PBP variants in *E. coli*, providing the highest level of protein expression with the lowest level of degradation

- To optimise the solubilisation and purification conditions of each *S. pneumoniae* PBP variant, obtaining suitable quantities for prospective kinetic and structural characterisations

3.3. The cloning of PBP1a, PBP2b and PBP2x variants from *S. pneumoniae* strains D39 and 5204 as N-terminal dodeca-histidine fusion proteins

There are many challenges associated with the study of integral membrane proteins; difficulties in obtaining adequate quantities of homogenous, monodisperse protein impedes biochemical and structural analysis. Consequently, two cloning strategies were adopted for *S. pneumoniae pbp1a*, *pbp2b* and *pbp2x*: cloning of the full-length genes and the corresponding genes devoid of the sequence encoding the membrane-spanning region. Thus, if the study of the full-length forms proved problematic, the more readily soluble counterpart could be analysed. Additionally, these constructs would allow the role of the membrane-spanning region to be investigated, which is proposed to be involved in protein stability, PBP association with proteins, lipids, or substrate or the localisation of the enzyme within a cell (Potluri *et al.*, 2010; Sung *et al.*, 2009).

3.3.1. Prediction of the transmembrane domain region

S. pneumoniae PBP1a, PBP2b and PBP2x are integral membrane proteins. The PBPs are translated with a short N-terminal cytoplasmic sequence that is connected by a hydrophobic segment to the bulk of the polypeptide (comprising the catalytic domains) residing on the extracellular face of the cytoplasmic membrane. This hydrophobic sequence functions as a non-cleavable secretion signal, enabling the translocation of the C-terminal of the protein across the cytoplasmic membrane. It also acts as a stop transfer sequence, forming a single α-helical membrane anchor (Ghuysen, 1991). It has been well documented that removal of the hydrophobic stretch can lead to a soluble protein (Di Guilmi *et al.*, 2003a; Di Guilmi *et al.*, 1998; Pagliero *et al.*, 2004).

The TransMembrane Hidden Markov Model (TMHMM) (Krogh *et al.*, 2001), a programme designed to predict the topology of membrane proteins, was used to locate the exact position of the N-terminal transmembrane domain of each PBP under investigation (Table 3.3). Using this specialised model, various factors

(including the length of transmembrane helices, location of helical caps (cytoplasmic or non-cytoplasmic), identification of regions close to the membrane, globular domains and cytoplasmic and non-cytoplasmic regions) can be estimated with 97-98 % accuracy, constraining the possible topologies and increasing the reliability of the transmembrane domain prediction (Krogh *et al.*, 2001).

To design the truncated PBP constructs, the N-terminal amino acid residues encompassing the predicted transmembrane domain and cytoplasmic sequences needed to be eliminated. The lengths of the desired amino acid truncations are documented in Table 3.3. The corresponding codons were eliminated from the gene sequence during the primer design (Section 3.3.2) to create the truncated constructs during the cloning procedure.

S. pneumoniae **PBP**	**Sequence length comprising each domain**			**Length of truncation**
	Cytoplasmic	**Transmembrane**	**Extracellular**	
PBP1a	0-12	13-30	31-719	Δ30
PBP2b	0-20	21-39	40-685	Δ39
PBP2x	0-28	29-48	49-750	Δ48

Table 3.3: *S. pneumoniae* PBP domain prediction and length of required truncation. The sequence length of each domain was predicted using TMHMM. The number of N-terminal amino acid residues required to eliminate the transmembrane region is denoted by 'Δ'. The truncated constructs were designed on this basis.

3.3.2. Primer design

The *S. pneumoniae pbps* were cloned into the expression vector pET46 Ek/LIC (vector map displayed in Figure 2.1). The vector encodes a hexa-histidine tag, which yields an N-terminal fusion upon protein translation, a desirable property for future protein purification considerations. The N-terminal fusion tag should not interfere with the enzyme activity, being located far from the catalytic sites.

3.3.2.1. Primer design with an engineered dodeca-histidine fusion tag

The primers for the PCR were designed according to the Ek/LIC cloning system, following the manufacturer's instructions (Section 2.3.8, Figure 2.2). A sequence of nucleotides specific to the cloning procedure was incorporated 5' and 3' to the insert specific sequences of the sense and antisense primers respectively. An *Nde* I site and codons for six histidine residues were additionally integrated into the sense primer directly 5' to the insert specific sequence (Table 3.4). Upon expression of the fusion protein, the vector and primer-encoded six histidine residues would be in close proximity (separated by a short sequence of amino acid residues), essentially creating a dodeca-histidine tag (proposed to aid protein purification) (Figure 3.1). The *Nde* I restriction site was incorporated as a precaution, in case an alternative cloning method was required. The start codon, ATG, was eliminated from the gene-specific sequence, due to its presence in the *Nde* I site. The stop codon, TAA, remained in the gene-specific sequence of the antisense primer to terminate translation.

3.3.2.2. Sequences of primers for the pET46 Ek/LIC cloning

The sense and antisense primers for the ligation independent cloning (LIC) of *S. pneumoniae* PBP variants into the pET46 vector are recorded in Table 3.4. It is noteworthy that the full-length *S. pneumoniae* 5204 *pbp2b* and *pbp2x* gene sequences are unknown; the sequences at the 5' ends (and thus N-termini of the proteins) were undefined. The 3' sequences of *S. pneumoniae* 5204 *pbp1a*, *pbp2b* and *pbp2x* are known, thus the insert specific sequences of the antisense primers were designed accordingly. The *S. pneumoniae* 5204 *pbp1a* gene sequence directly at the 5' end does not differ from that of the D39 strain, permitting identical sense primers to be employed. It was therefore assumed that *S. pneumoniae* 5204 *pbp2b* and *pbp2x* gene sequences at the 5' ends also do not differ from those of the D39 strain, allowing sense primers to be designed (identical to the sense primers of the strain D39 PBPs). The 5' ends of the gene sequences from the penicillin-resistant strain are unlikely to deviate from the penicillin-sensitive strain as they encode residues located distant to the transpeptidase domain, which is subject to antibiotic selection pressures. Any disregarded amino acid changes at the N-terminal would be unlikely to affect the resistance mechanism of the *S. pneumoniae* 5204 PBP or impede its activity.

***S. pneumoniae pbp* gene target**	**Description of primer**	**Primer sequence (5'-3' orientation)**
D39 *pbp1a*	Sense primer (FL)	**GAC GAC GAC AAG ATG CAT ATG CAC CAT CAC CAT CAC CAT** AAC AAA CCA ACG ATT CTG CGC C
	Sense primer (-TM, Δ30)	**GAC GAC GAC AAG ATG CAT ATG CAC CAT CAC CAT CAC CAT** GTT TTT TTC TAC TAC GTT AGC AAG
	Antisense primer	**GAG GAG AAG CCC GGT** TTA TGG TTG TGC TGG TTG AGG ATT C
5204 *pbp1a*	Sense primer (FL)	**GAC GAC GAC AAG ATG CAT ATG CAC CAT CAC CAT CAC CAT** AAC AAA CCA ACG ATT CTG CGC C
	Antisense primer	**GAG GAG AAG CCC GGT** TTA TGG TTG TGC TGG TTG AGG ATT C
D39 *pbp2b*	Sense primer (FL)	**GAC GAC GAC AAG ATG CAT ATG CAC CAT CAC CAT CAC CAT** AGA CTG ATT TGT ATG AGA AAA TTT AAC AGC
	Sense primer (-TM, Δ39)	**GAC GAC GAC AAG ATG CAT ATG CAC CAT CAC CAT CAC CAT** CAG GTT TTG AAC AAG GAT TTT TAC G
	Antisense primer	**GAG GAG AAG CCC GGT** CTA ATT CAT TGG ATG GTA TTT TTG ATA CAG
5204 *pbp2b*	Sense primer (FL)	**GAC GAC GAC AAG ATG CAT ATG CAC CAT CAC CAT CAC CAT** AGA CTG ATT TGT ATG AGA AAA TTT AAC AGC
	Antisense primer	**GAG GAG AAG CCC GGT** CTA ATT CAT TGG ATG GTG TTG G
D39 *pbp2x*	Sense primer (FL)	**GAC GAC GAC AAG ATG CAT ATG CAC CAT CAC CAT CAC CAT** AAG TGG ACA AAA AGA GTA ATC CG
	Sense primer (-TM, Δ48)	**GAC GAC GAC AAG ATG CAT ATG CAC CAT CAC CAT CAC CAT** GGG ACA GGC ACT CGC TTT GGA ACA G
	Antisense primer	**GAG GAG AAG CCC GGT** TTA GTC TCC TAA AGT TAA TGT AAT TTT TTT AAT G
5204 *pbp2x*	Sense primer (FL)	**GAC GAC GAC AAG ATG CAT ATG CAC CAT CAC CAT CAC CAT** AAG TGG ACA AAA AGA GTA ATC CG
	Antisense primer	**GAG GAG AAG CCC GGT** TTA GTC TCC TAA AGT TAA TTT AAT TTT TTT AAT G

Table 3.4: The primers required to amplify different variants of *pbp1a*, *pbp2b* and *pbp2x* for cloning into the pET46 vector. The regions in bold, black type indicate the nucleotides that are a cloning-specific requirement as dictated in the manufacturer's instructions. The sequence GAC GAC GAC AAG ATG encodes the enterokinase cleavage site that is incorporated at the 5' terminal of the gene sequence. The bold, red type represents the *Nde* I restriction enzyme cleavage site. The bold, blue type shows the engineered codons for the extra six histidine residues. The plain text shows the 5' or 3' gene specific sequences, essential for annealing during the PCR. FL, full-length sequence; -TM, sequence devoid of the transmembrane and cytoplasmic region, where the length of protein truncation is denoted.

The ATG codon, required for the functionality of the protein enterokinase restriction site, and the DNA *Nde* I site, were assumed not to act as start codons; a vector-specific ATG codon, locating 5' to the vector-encoded histidine tag, fulfilled this role, being in close proximity to the vector ribosomal binding site. Following protein expression, a recombinant protein would be produced as illustrated in Figure 3.1.

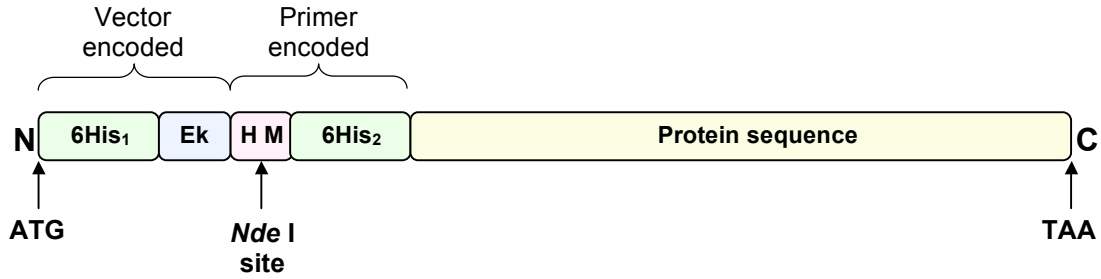

Figure 3.1: Domain organisation of the recombinant proteins. The recombinant protein contains an N-terminal vector-encoded cleavable six histidine tag ($6His_1$), separated from a primer-encoded non-cleavable six histidine tag ($6His_2$) (not anticipated to interfere with enzyme activity) by a short sequence of amino acids encompassing an enterokinase cleavage site (Ek) and the amino acids encoded by the *Nde* I site (histidine and methionine). The locations of the start (ATG) and stop (TAA) codons are indicated. N, amino-terminus; C, carboxy-terminus.

3.3.3. Polymerase chain reaction

The genes *pbp1a*, *pbp2b* and *pbp2x* (with and without transmembrane domains) were amplified by PCR from *S. pneumoniae* D39 genomic DNA using specific oligonucleotide primers (Table 3.4) and AccuPrime *Taq* High Fidelity polymerase, as described in Section 2.3.3. The annealing stage of the PCR was performed over a temperature gradient (45.1, 47.3, 54.4, 59.7 and 65.2°C). The PCR products were analysed on a 0.8 % (w/v) agarose gel (Section 2.3.7) to establish the occurrence of gene amplification.

The PCR-dependent amplification of *S. pneumoniae* 5204 *pbp1a*, *pbp2b* and *pbp2x* from genomic DNA was performed by A. Zapun (Institut de Biologie Structurale, Grenoble) using the primers in Table 3.4.

The PCR products corresponding to the correct gene size were combined and purified using the Wizard PCR purification system (Section 2.3.5) to remove remnants of the PCR that could interfere with the imminent cloning procedure.

3.3.4. Ligation independent cloning

Ligation independent cloning was performed as described in Section 2.3.8, allowing the directional insertion of the PCR product and eliminating the requirement of restriction enzyme digestions and ligation reactions. In brief, complimentary overhangs were generated in the vector and PCR product due to the 3'-5' exonuclease activity of T4 DNA polymerase (Aslanidis and de Jong, 1990). Annealing of the compatible overhangs enabled the PCR product to be integrated into the vector. Transformation into competent *E. coli* NovaBlue GigaSingles cells allowed the covalent bond formation at the vector-insert junction, creating a circularised plasmid. Following an overnight culture of positive transformants, plasmid DNA was extracted (Section 2.3.6) for future analytical procedures.

3.3.5. Verification of the construct

3.3.5.1. Diagnostic restriction digest

Plasmid constructs were analysed to ensure the correct insert sequence was integrated into the vector. Single, double and triple diagnostic DNA restriction digests were performed using various restriction enzymes, which were chosen based on the location of the restriction site within the gene sequence. The digested DNA fragments were analysed on a 0.8 % (w/v) agarose gel, displayed in Figure 3.2.

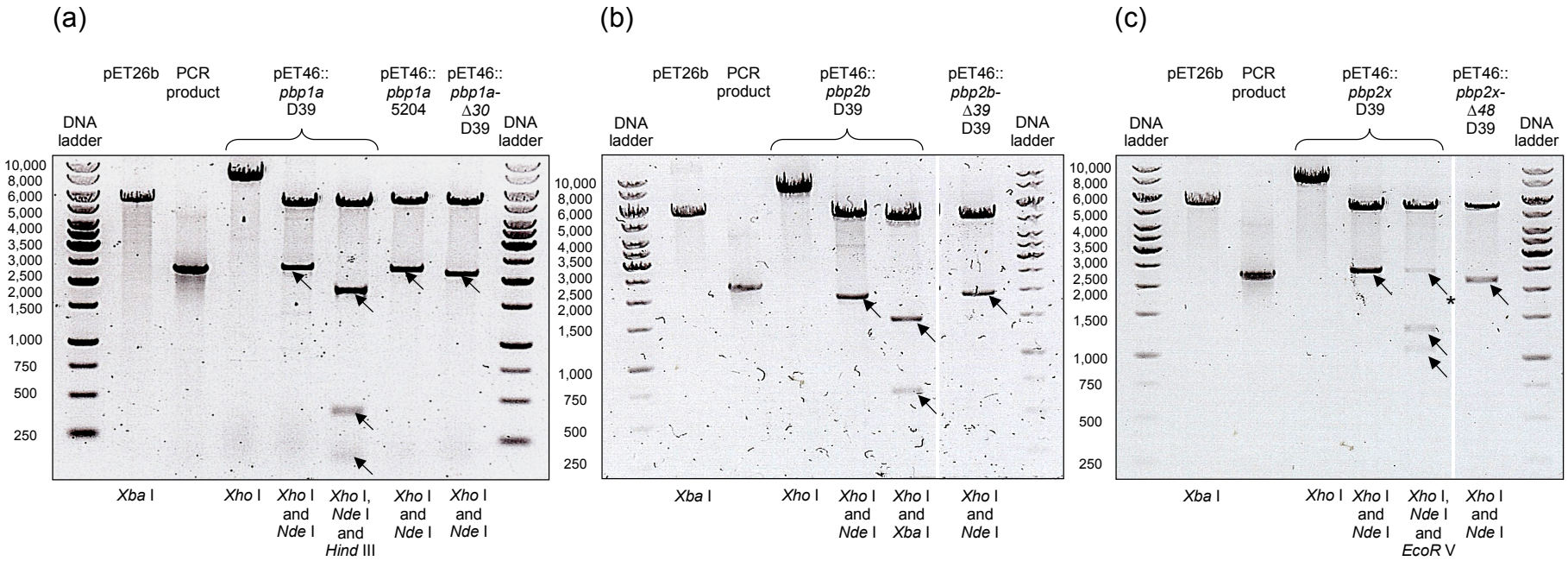

Figure 3.2: 0.8 % (w/v) agarose gel of the diagnostic restriction digests. (a) Restriction digests of *pbp1a* variants. Full length *S. pneumoniae* D39 *pbp1a* has a size of 2169 bp, containing two restriction sites for *Hind* III. (b) Restriction digests of *pbp2b* variants. Full length *S. pneumoniae* D39 *pbp2b* has a size of 2040 bp, containing one restriction site for *Xba* I. (c) Restriction digests of *pbp2x* variants. Full length *S. pneumoniae* D39 *pbp2x* has a size of 2253 bp, containing one restriction site for *EcoR* V. The constructs all contain a single *Nde* I site, integrated into the sequence through the primer design, and a single vector encoded *Xba* I and *Xho* I site located on opposite sides of the multiple cloning site. The DNA ladder (bp), constructs and restriction enzymes employed are displayed on the figure. Linearised pET26b vector (with *Xba* I), highly similar in size to pET46, was used as a vector size comparison. (*), incompletely digested DNA.

The expected size DNA fragments from the restriction digests provided evidence that the correct *pbp* gene inserts were present in the constructs. The restriction digest was not used to analyse the plasmid constructs containing *S. pneumoniae* 5204 *pbp2b* and *pbp2x* because the full gene sequences (and hence the number of restriction sites for a particular restriction enzyme) were unknown. Instead, a diagnostic PCR with *Taq* DNA polymerise was performed using the oligonucleotides specific to the 5' and 3' sites of the multiple cloning region of the pET46 vector (T7 promoter and pET46 terminator, Table 2.2). Analysis of the PCR products on an agarose gel showed the expected gene size had been amplified, and thus the correct gene had been inserted into the vector.

3.3.5.2. Sequencing

Constructs that contained the correct sized gene inserts (identified from the diagnostic restriction digests and PCR) were sequenced using the T7 promoter and pET46 terminator oligonucleotides (as described in Section 2.3.9) to ensure the sequences did not deviate from the original genomic sequence. Additional oligonucleotides were required to sequence the entire genes, shown in Table 3.5.

Name of primer	Region sequenced	Primer sequence (5'-3' orientation)
pbp1a 5' middle	The middle section of *pbp1a* towards the 5' end.	GGG GGA TTG ATA CCA TCC G
pbp1a 3' middle	The middle section of *pbp1a* towards the 3' end.	GCC CAA GAC CGC CGA AAC TTG G
pbp2b 5' middle	The middle section of *pbp2b* towards the 5' end.	GGC TTT CCA AGA TAG CGT GGA TGC
pbp2b 3' middle	The middle section of *pbp2b* towards the 3' end.	GGA AAC TTT GCG ACA GGA ACC ATT GC
pbp2x 5' middle	The middle section of *pbp2x* towards the 5' end.	GGA AGC TGC AGA GGT CAA GGG G
pbp2x 3' middle	The middle section of *pbp2x* towards the 3' end.	GAT GCC ACG ATT CGA GAT TGG GAC G

Table 3.5: Additional primers used to sequence the middle regions of the *pbp* genes. The region of the gene sequenced by using each oligo is specified along with the nucleotide sequence.

3.3.6. Site-directed mutagenesis

For future analytical purposes, it was desirable to create mutations within the active site of the PBP transglycosylase domain or transpeptidase domain, to essentially eliminate the activity. This can be achieved by replacing catalytic residues with amino acid residues that do not have complimentary properties for catalysis. It has been established that a glutamate residue, present in the first conserved motif of the transglycosylase domain, is essential for transglycosylation as documented for: *E. coli* PBP1b (Terrak *et al.*, 1999), *S. pneumoniae* PBP1b (Liu and Wong, 2006), *S. aureus* MGT (Terrak and Nguyen-Distèche, 2006) and *A. aeolicus* PBP1a (Barrett *et al.*, 2007). It was decided to substitute the conserved glutamate residue of the transglycosylase domain with glutamine, effectively replacing the carboxyl group proposed to deprotonate Lipid II with an amide, which is unable to perform the equivalent catalytic role. The catalytic serine residue, present in the first conserved motif of the transpeptidase domain, forms a covalent intermediate with the penultimate D-Ala residue of the Lipid II pentapeptide during transpeptidation or D,D-carboxypeptidation (Frère *et al.*, 1976; Yocum *et al.*, 1979). An inert residue, alanine, was chosen to replace the transpeptidase active site serine residue, having no side chains with charged residues that could affect the topology of the active site.

Site-directed mutagenesis was performed on pET46 constructs containing *S. pneumoniae* D39 *pbp1a*, *pbp2b* and *pbp2x* using the Stratagene QuikChange II kit, following the procedures recommended by the manufacturer (Section 2.3.10). Primers for the mutagenic PCR (Table 3.6) were designed to introduce a single, specified mutation, where the positions of the codons encoding the crucial catalytic residues were identified by locating the conserved sequences within the polypeptide chain and the gene sequence counterpart.

Target	Mutation	Primer sequence (5'-3' orientation)
PBP1a Ser370	Ser to Ala	**S:** CAAACCGCGACTGGGGA**G**C**A**ACTATGAAACCGATC
		AS: GATCGGTTTCATAGT**TG**CTCCCCAGTCGCGGTTTG
PBP1a Glu91	Glu to Gln	**S:** GTTAAGGCAATCGTTTCTATC**C**A**A**GACCATCGCTTCTTCGAC
		AS: GTCGAAGAAGCGATGGTC**TT**GGATAGAAACGATTGCCTTAAC
PBP2b Ser391	Ser to Ala	**S:** GTCTTTGTTCCAGGT**G**C**G**GTTGTCAAGGCG
		AS: CGCCTTGACAAC**CG**CACCTGGAACAAAGAC
PBP2x Ser337	Ser to Ala	**S:** GTAACTATGAGCCAGGT**G**C**C**ACTATGAAAGTGATG
		AS: CATCACTTTCATAGT**GG**CACCTGGCTCATAGTTAC

Table 3.6: Primer sequences for site-directed mutagenesis of the *S. pneumoniae pbps*. The oligonucleotide sequences for mutagenesis of the target amino acid residue are shown. The red type identifies the site-directed mutation, which is embedded within the bold type, highlighting the codon of the target amino acid residue to be mutated. S, sense primer; AS, antisense primer.

Following PCR, the parental non-mutated plasmid DNA was digested by *Dpn* I treatment (selective for methylated and hemimethylated DNA) and the products were analysed on a 0.8 % (w/v) agarose gel as shown in Figure 3.3.

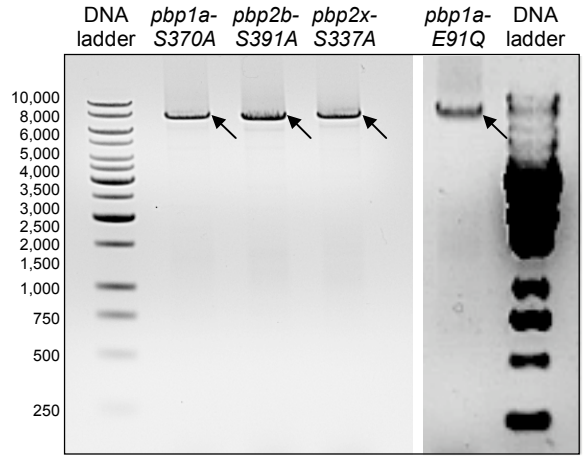

Figure 3.3: 0.8 % (w/v) agarose gel of amplified plasmid DNA following site-directed mutagenesis. Lanes contain pET46::*pbp* constructs amplified with mutagenic primers (shown by arrows) and are labelled according to the mutated gene insert. DNA ladder, 1 kb.

Given the small quantity of parental plasmid DNA used in the mutagenic PCR, the intense bands on the agarose gel were expected to be amplified DNA containing the desired mutation. The PCR products were transformed into competent *E. coli* Top10

cells (to circularise the nicked plasmid), and following an overnight culture, the plasmid was extracted and sequenced, confirming the presence of the designed mutation.

3.3.7. Final constructs generated

The nomenclature and domain architecture of the constructs generated from cloning and site-directed mutagenesis are depicted in Figure 3.4 and displayed in Table 2.4. From this point forward, PBPs derived from *S. pneumoniae* are assumed to be from strain D39 unless otherwise denoted (*S. pneumoniae* 5204, PBP-5204).

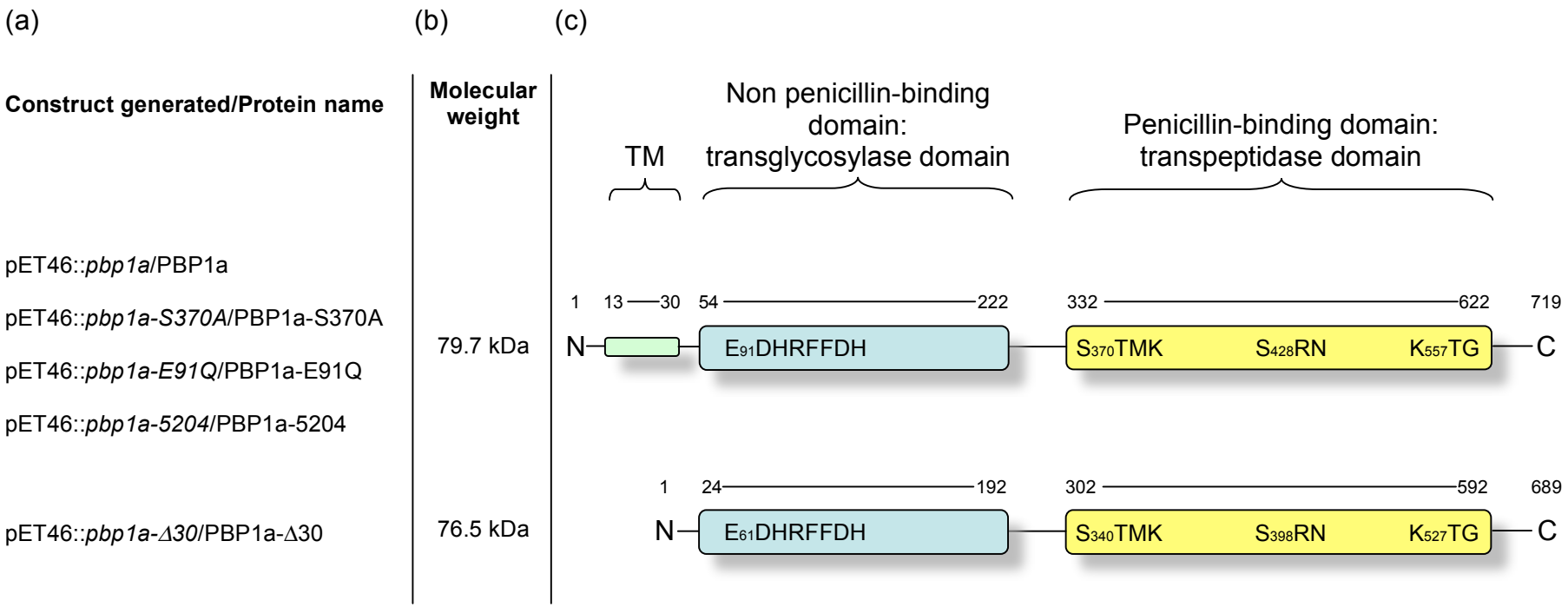

Figure 3.4 (continues on subsequent page): The constructs generated and domain architecture of *S. pneumoniae* PBP variants. (a) Nomenclature of constructs and equivalent proteins. (b) Molecular weight of the recombinant proteins. (c) Protein domain architecture corresponding to the proteins described in (a). The histidine tag is located on the N-terminal of each recombinant protein. Amino acid residues at the start and end of each domain are numbered accordingly and the residues of the first conserved transglycosylase motif (PBP1a only) and the three conserved transpeptidase motifs are highlighted.

(a) (b) (c)

Construct generated/Protein name	Molecular weight
pET46::*pbp2b*/PBP2b	
pET46::*pbp2b-S391A*/PBP2b-S391A	74.4 kDa
pET46::*pbp2b-5204*/PBP2b-5204	
pET46::*pbp2b-Δ39*/PBP2b-Δ39	69.8 kDa
pET46::*pbp2x*/PBP2x	
pET46::*pbp2x-S337A*/PBP2x-S337A	82.2 kDa
pET46::*pbp2x-5204*/PBP2x-5204	
pET46::*pbp2x-Δ48*/PBP2x-Δ48	76.7 kDa

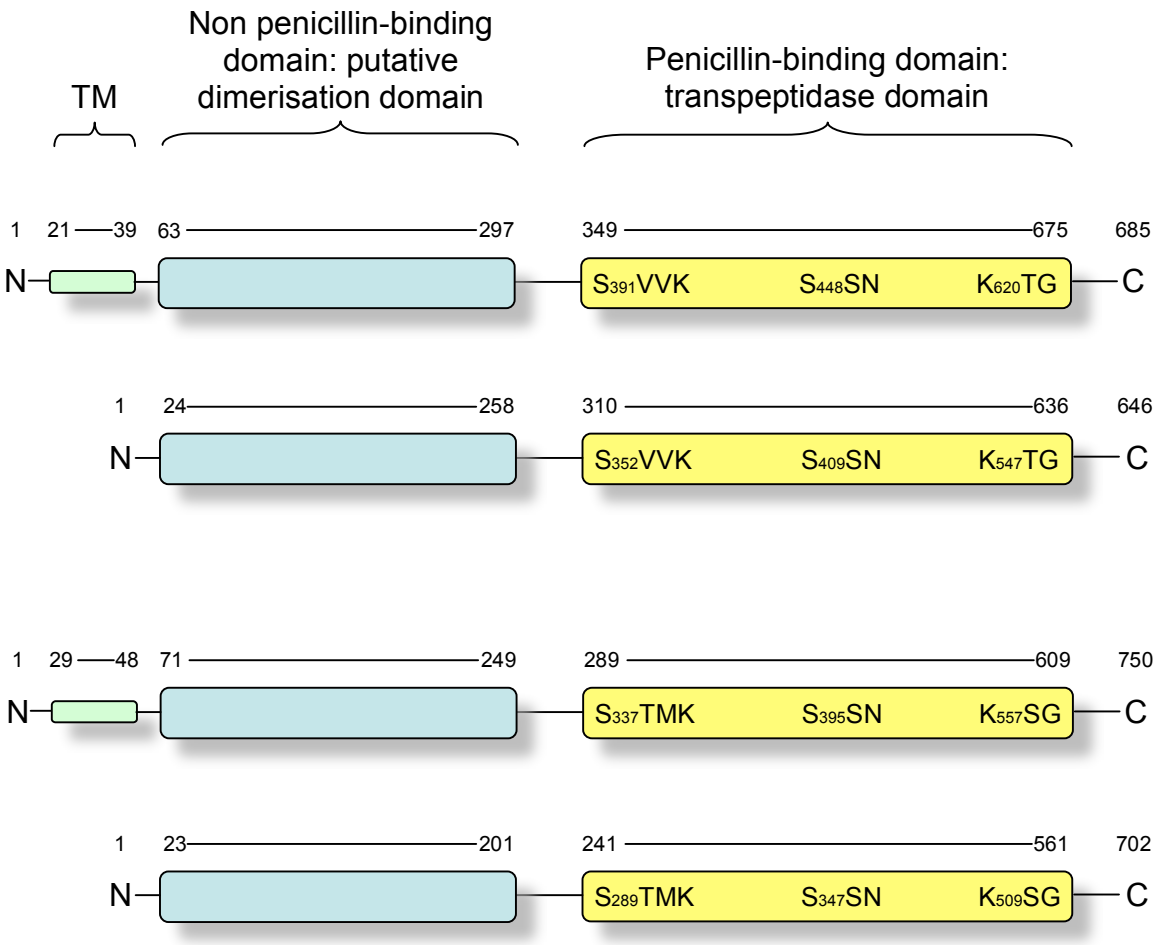

3.4. The expression of *S. pneumoniae* PBP1a, PBP2b and PBP2x variants as N-terminal dodeca-histidine fusion proteins

3.4.1. Establishing an optimal expression system for PBP1a, PBP2b and PBP2x

The expressions of PBP1a, PBP2b and PBP2x as full-length proteins were evaluated under a large number of conditions to establish a system that provided optimum levels of protein expression in the membrane fraction of cells with minimal aggregation and degradation. In brief, expression trials were performed in 100 mL cultures (containing the appropriate antibiotic selection) inoculated with 200 µL uninduced cells from an overnight culture and protein over-expression was induced by either IPTG or autoinduction (Section 2.4.1). A crude membrane preparation was prepared using water-lysis (described in Section 2.5.2) and proteins expressed in the cytoplasmic and membrane fractions of the cells were analysed by SDS-PAGE (Section 2.6.2) and Western blots (Section 2.6.3). Different *E. coli* expression cell lines, induction methods and induction temperatures were investigated and the results are summarised in Table 3.7.

E. coli expression system	Induction temperature (°C)	Induction method	Detectable protein expression		
			PBP1a	PBP2b	PBP2x
C41 (DE3)	12	0.5 mM IPTG			
		Autoinduction			
	25	0.5 mM IPTG			
		Autoinduction			
C41 (DE3) pRIL	12	0.5 mM IPTG			
		Autoinduction			
C41 (DE3) pRARE	12	0.5 mM IPTG			
		Autoinduction			
C43 (DE3)	12	0.5 mM IPTG			
		Autoinduction			
C43 (DE3) pRIL	12	0.5 mM IPTG			
		Autoinduction			
C43 (DE3) pRARE	12	0.5 mM IPTG			
		Autoinduction			
BL21 Star (DE3) pRosetta	12	Autoinduction			
	25				

Table 3.7: Expression levels of full-length PBP1a, PBP2b and PBP2x under different conditions. Detectable protein expression was classified as a band on a Western Blot of correct molecular weight size: ■, no detectable protein expression; ■, detectable expression at varying low levels (faint, thin bands on the blot); ■ substantial expression levels (large, intense bands on the blot). IPTG induction, cells were cultured at 37°C until OD_{600nm} reached 0.5, where they were transferred to and induced at the temperature stated; autoinduction, cells were cultured and induced at the stated temperature.

Substantial expression of the full-length membrane proteins was achieved in BL21 Star (DE3) pRosetta cells under autoinduction at 25°C, where the expression levels were great enough to distinguish target protein expression from *E. coli* host proteins on an SDS-PAGE gel.

3.4.2. Expression of *S. pneumoniae* 5204 PBPs and the active site mutants of *S. pneumoniae* D39

Given the high sequence similarity of *S. pneumoniae* D39 PBPs with the corresponding transpeptidase and transglycosylase active site mutant and the *S. pneumoniae* 5204 PBPs, it was anticipated that the established expression conditions for the former proteins could be used to yield similar levels of expression of the latter recombinant proteins. The different constructs were transformed into BL21 Star (DE3) pRosetta and ultimately the protein was expressed using autoinduction at 25°C. The membrane fraction was extracted from the *E. coli* host cells and expression levels were analysed by SDS-PAGE, Figure 3.5.

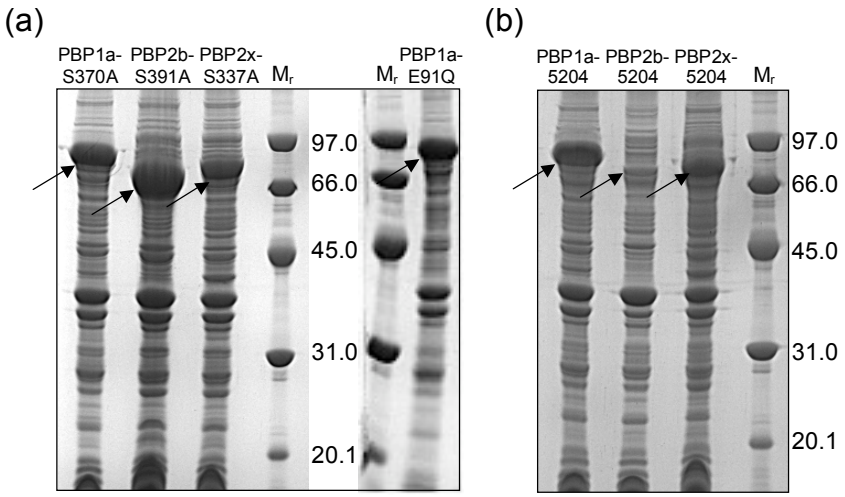

Figure 3.5: A 12 % SDS-PAGE Coomassie-stained gel of the membrane fractions of *E. coli* cells expressing *S. pneumoniae* D39 PBP active site mutants and *S. pneumoniae* 5204 PBPs. (a) *S. pneumoniae* D39 PBPs with a single point mutation in the catalytic sites of the transglycosylase or transpeptidase domains. (b) *S. pneumoniae* 5204 PBPs. M_r, molecular weight markers (kDa). The arrows signify the presence of the over-expressed recombinant proteins.

The expression levels of the membrane proteins are efficiently high, enabling the recombinant proteins to be distinguished from the *E. coli* host proteins by SDS-PAGE. Thus, the requirement of the highly sensitive Western blot to detect low levels of protein expression was eliminated.

3.4.3. Expression and cellular localisation of PBPs devoid of transmembrane domains

The expressions of PBP1a-Δ30, PBP2b-Δ39 and PBP2x-Δ48 were performed using the established optimum conditions for the full-length counterparts (Section 3.4.1) with a similar success. On the basis that PBPs have hydrophobic regions on the protein surface that associate or are in close proximity with the membrane, the sub-cellular localisations of the truncated proteins (devoid of the membrane anchor) were determined.

The membrane fractions of induced *E. coli* host cells were extracted following the protocol outlined in Section 2.5.3. The pellet following 24,000 × g centrifugation step represented the insoluble fraction of the cells, containing cellular debris, aggregated protein, inclusion bodies and large pieces of membranes that were not completely fragmented upon cell disruption. *E. coli* membranes were pelleted during the 150,000 × g centrifugation step, where the supernatant contained the soluble, cytoplasmic proteins. The protein content of the fractions was analysed by SDS-PAGE, Figure 3.6.

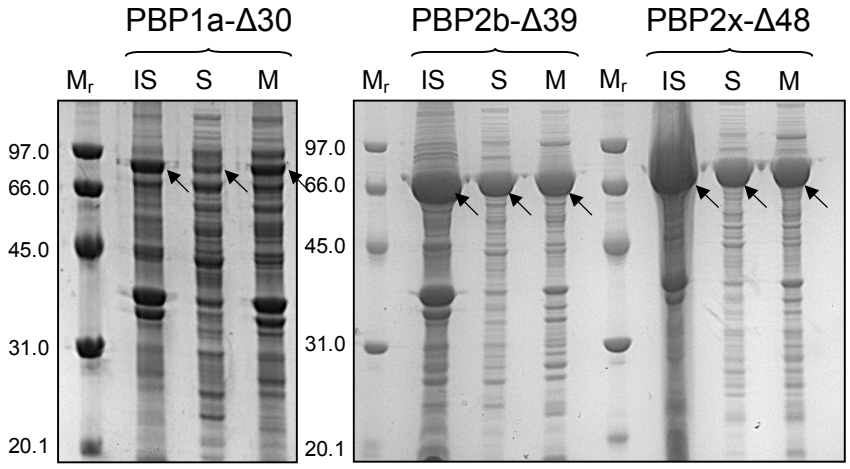

Figure 3.6: SDS-PAGE analysis of the cellular localisations of PBP1a-Δ30, PBP2b-Δ39 and PBP2x-Δ48. The lanes are labelled according to the cellular fraction: IS, insoluble fraction; S, soluble cytoplasmic fraction; M, membrane fraction. The protein was visualised by Coomassie staining. M_r, molecular weight markers (kDa). Arrows show the position of the over-expressed protein.

Expression of each PBP truncate was detected in the insoluble and membrane fractions of the cells, due to protein aggregation or inclusion body formation and association with the membrane (despite the absence of the membrane anchor) respectively. PBP1a-Δ30 was poorly expressed in the soluble fraction of the cells. Conversely, soluble forms of PBP2b-Δ39 and PBP2x-Δ48 expressed to high levels in the cytoplasmic fractions.

3.5. Purification of the PBP variants as integral membrane proteins

3.5.1. Detergent solubilisation of membrane proteins

A prerequisite to purification is the isolation of the integral membrane proteins from the membrane by the use of detergents. Detergents interact with proteins and surrounding lipid membranes as micelles. Micelles, formed by a process of micellisation (thermodynamically driven association of non-polar groups in an aqueous environment), are dynamic structures, exhibiting rapid exchange of detergent monomers within a micelle and solution (Wennerström and Lindman, 1979). Solubilisation of membrane proteins is initiated by the penetration of detergent monomers into a lipid bilayer. The bilayer becomes destabilised forming lipid-detergent mixed fragments. Further integration of detergent causes bilayer dissolution and the protein becomes surrounded by a lipid-detergent monolayer (le Maire *et al.*, 2000).

A solubilisation screen of the PBPs (full-length and devoid of the transmembrane domain) was performed (Section 2.5.4) using a variety of detergents (Table 3.8) with differing properties to establish the ideal conditions that provided the greatest solubilisation efficiency of the specific proteins.

Detergent	Type	CMC (% (w/v))
Triton X-100	Non-ionic	0.01-0.02 (v/v)
n-Dodecyl-β-D-maltopyranoside (DDM)	Non-ionic	0.01
N-lauroyl sarcosine	Ionic (anionic)	0.42*
Sodium deoxycholate	Ionic (anionic)	0.08-0.25
3-[(3-Cholamidopropyl)dimethylammonio]-1-propanesulfonate (CHAPS)	Zwitterionic	0.49
Lauryldimethylamine oxide (LDAO)	Zwitterionic	0.02

Table 3.8: Detergents used in the solubilisation trials. The percentage CMC of each detergent is shown (data taken from Anatrace-Affymetrix and (*) Sigma-Aldrich).

In short, membranes were solubilised in 1 % (w/v) detergent (given this percentage is significantly (at least 2-3 times) greater than the critical micellar concentration (CMC), enabling micelles to form) for 1 h, the insoluble material pelleted and the protein content in solution and the insoluble pellet was analysed by Western blot. The solubilisation trial of PBP1a is shown in Figure 3.7.

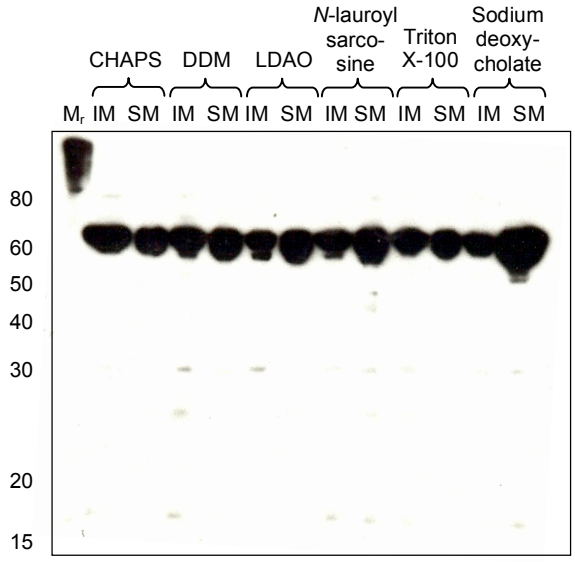

Figure 3.7: Western blot of PBP1a detergent solubilisation trial. The detergents used in the solubilisation of PBP1a are labelled above the corresponding lanes. The total solubilised PBP cannot be quantified. Equivalent amounts of protein were loaded into each lane of the SDS-PAGE gel prior to the Western blot, thus the size of the target protein bands are comparable. The protein was detected by probing with antibodies and ECL reagents. M_r, molecular weight markers (kDa). IM, insoluble membrane proteins; SM, solubilised membrane proteins.

Analogous to PBP1a, the detergent providing the greatest level of protein solubilisation for each PBP was sodium deoxycholate. It was therefore assumed that this detergent would have a similar successful solubilisation efficiency towards the active site mutants and PBPs-5204. This analysis does not give an indication of the stability of the proteins in the detergent micelle. However, sodium deoxycholate, a bile acid salt, is a mild ionic detergent having minimal deactivating properties in comparison to linear chain detergents (Seddon *et al.*, 2004). A large quantity of PBP remained insoluble after 1 h. Longer incubation periods could rectify this, but the stability of the protein could be jeopardised, where it has been found that long periods of solubilisation promote protein degradation and aggregation.

3.5.2. Affinity chromatography

The preliminary technique to purify the full-length PBPs was immobilised metal affinity chromatography (IMAC), which exploits the reversible high affinity of histidine tags of fusion proteins for specific divalent metal ions, most commonly cobalt or nickel ions.

3.5.2.1. Experimental design for the general IMAC purification of membrane proteins

The solubilisation and IMAC purification of the full-length PBPs is described in Section 2.5.5.2. Briefly, *E. coli* membranes in PBS containing over-expressed target proteins were solubilised in 1 % (w/v) sodium deoxycholate for 3 h (a compromise between optimum protein solubilisation and minimal protein aggregation). Sodium deoxycholate, although an effective emulsifier, exhibits unfavourable properties, causing buffer solutions to become highly viscous in the presence of high salt concentrations (from previous observations and also documented by Murata *et al.* (1982)). Therefore, following solubilisation, the insoluble membranes were pelleted by centrifugation at 150,000 × g for 30 min, concomitantly with gradual detergent exchange from sodium deoxycholate to 0.1 % (w/v) DDM (by addition of buffer containing the latter and not the former detergent). DDM, a universally used detergent in membrane protein purification, has mild, non-denaturing properties, maintaining proteins in a biologically active form (Privé, 2007). This detergent is

regularly used during the successful growth of membrane protein crystals, indicating that it does not disrupt protein structure (Privé, 2007). The supernatant, containing solubilised proteins, was incubated for 3 h with 5 mL cobalt-chelated sepharose resin pre-equilibrated in the purification buffer (PBS, 0.1 % (w/v) DDM with additional 150 mM NaCl) with stirring at 4°C. Earlier evaluations established that histidine-tagged protein affinity with the IMAC resin reached an equilibrium after an incubation of 2-3 h, where longer incubation periods promoted protein aggregation without an increase in resin binding. The protein-resin mix was poured to form a column and the column was developed. Fractions from the different stages of purification were collected and analysed by SDS-PAGE. An example of PBP1a purification by IMAC is displayed in Figure 3.8.

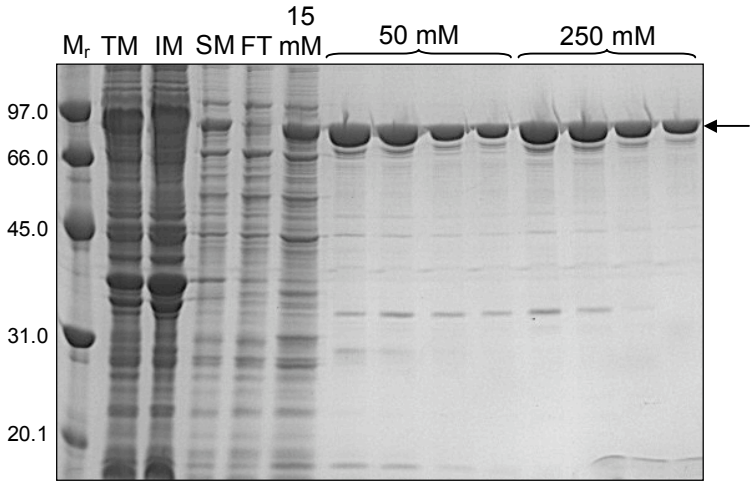

Figure 3.8: A 12 % SDS-PAGE Coomassie-stained gel of PBP1a purification by IMAC. M_r, molecular weight markers (kDa); TM, total membrane fraction; IM, insoluble membrane proteins following detergent treatment; SM, detergent-solubilised membrane proteins incubated with cobalt resin; FT, flow through; 15 mM, 100 mL buffer with 15 mM imidazole; 50 mM and 250 mM, consecutive fractions from 50 mL buffer with 50 mM and 250 mM imidazole. The arrow shows the position of the target protein.

Protein fractions containing the highest level of target protein purity were combined and concentrated for future purification techniques.

3.5.2.2. Optimisation of IMAC to improve the level of purity of PBP2b and PBP2x and *S. pneumoniae* 5204 PBPs

PBP1a and its active site mutant counterparts, purified to a high level following the generalised method of IMAC. However, the wild-type and transpeptidase active site mutants of PBP2b and PBP2x and the PBPs-5204 co-purified with a higher level of *E. coli* host protein contaminants. A variety of parameters were addressed to alleviate this problem: buffer constituents (salt concentration, non-specific ionic interactions; glycerol, hydrophobic interactions; pH, protein surface charge); concentration of imidazole wash steps; incubation period of protein with cobalt resin; micelle disruption (reducing the detergent concentration to below the CMC (0.003 % (w/v) DDM)) in the presence of 5 mM imidazole following protein binding to the column).

The greatest improvement of target protein purity was achieved by introducing an extensive column wash step of buffer containing 20 mM imidazole (replacing 15 mM imidazole), causing a higher degree of non-specifically bound contaminants to elute (final level of purity shown in Figure 3.11). The level of purity subsequently obtained was suitable for the next purification technique.

3.5.3. Size exclusion chromatography

Following IMAC purification, the full-length PBP variants were subjected to size exclusion chromatography to endeavour to purify the target protein further and to separate aggregated and non-aggregated protein. The protein was injected onto the analytical Superose 6 10/300 GL gel filtration column pre-equilibrated in 20 mM Tris pH 7.5, 150 mM NaCl, 0.03 % (w/v) DDM. The lower detergent concentration (just above the CMC) enabled the removal of excess micelles devoid of protein that could interfere with future structural analyses (Chapter 6). The chromatogram trace for the purification of PBP1a is displayed in Figure 3.9.

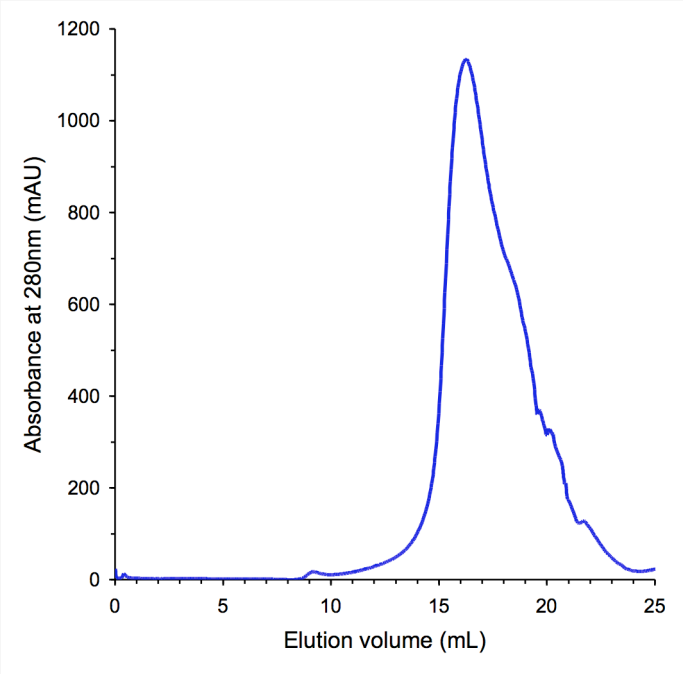

Figure 3.9: Chromatogram of PBP1a from size exclusion chromatography using a Superose 6 10/300 GL column.

3.5.4. Protein storage conditions and degradation analysis

The storage conditions of the proteins are essential to maintain the enzyme in a stable, functionally active state. Three conditions were trialled for the storage of PBP1a: gel filtration buffer (20 mM Tris pH 7.5, 150 mM NaCl, 0.03% (w/v) DDM) 4°C; gel filtration buffer with 50 % (v/v) glycerol, -20°C; gel filtration buffer with 50 % (v/v) glycerol, -80°C. After a five day storage, the protein samples were analysed for degradation by SDS-PAGE and a Western blot, shown in Figure 3.10.

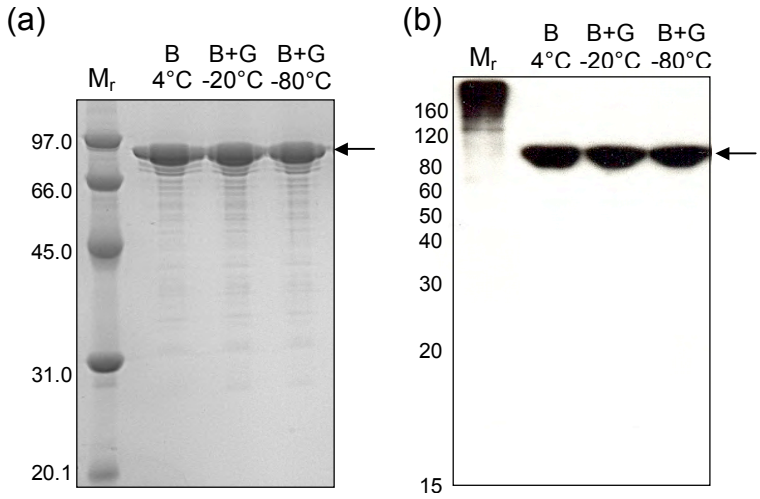

Figure 3.10: Degradation analysis of PBP1a in different storage conditions. (a) 12 % SDS-PAGE Coomassie-stained gel. (b) Western blot (protein probed with antibodies and ECL reagents). Equal amounts of protein were loaded into each lane (20 µg). Lanes are labelled with the storage conditions trialled. M_r, molecular weight markers (kDa); B, buffer: 20 mM Tris pH 7.5, 150 mM NaCl, 0.03% (w/v) DDM; G, 50 % (v/v) glycerol. Arrows indicate the position of PBP1a on the gel and blot.

The Western blot identifies that there was no observable degradation of PBP1a from the C-terminus in any of the storage conditions trialled. Exopeptidase degradation from the N-terminus could not be established using this method, where the antibodies employed were specific for the N-terminal histidine tag. Antibodies specific to the target protein would solve this dilemma.

Purified proteins were stored in 20 mM Tris pH 7.5, 150 mM NaCl, 0.03% (w/v) DDM, 50 % (v/v) glycerol, -20°C. Storage at -20°C minimises the loss of enzyme activity compared to higher (4°C) and lower (-80°C) temperatures (as observed from activity assays (Chapters 4 and 5). The inclusion of 50 % (v/v) glycerol enhances the stability of proteins by reducing conformational freedom and prevents the protein solution from freezing at the selected temperature, eliminating the production of ice crystals, which can disrupt the structural and functional integrity of the enzyme.

3.5.5. Final levels of purity of all full-length PBP variants

The integral membrane proteins were extracted from the membranes and purified by IMAC and size exclusion chromatography under near-identical procedures; specific proteins required minor adaptations from the generic protocol (as discussed). The final level of purity of each full-length PBP variant is exhibited in Figure 3.11.

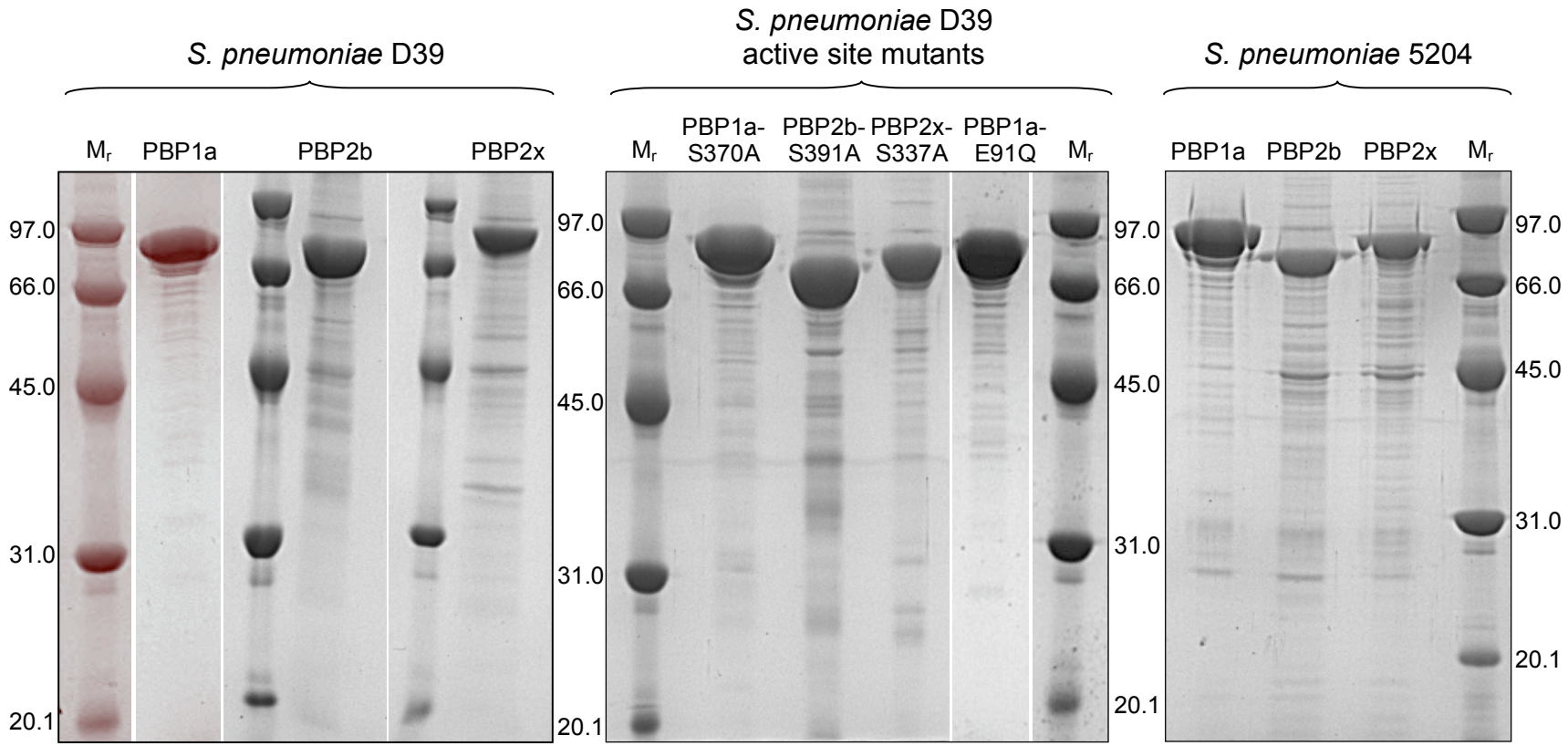

Figure 3.11: SDS-PAGE Coomassie-stained gels of the final level of purity and protein yield of each full-length PBP under investigation. Lanes are labelled with the corresponding PBP and are grouped according to the bacterial origin of the protein sequence. Protein yield refers to the total amount of purified target protein extracted from 1 L *E. coli* culture. M_r, molecular weight markers (kDa).

3.6. Purification of PBPs devoid of the membrane anchor

Due to the cellular localisation of PBP1a-Δ30, PBP2b-Δ39 and PBP2x-Δ48 over-expression (established in Section 3.4.3), two different purification strategies were required. PBP1a-Δ30, poorly expressed in the soluble fraction, was detected in the membrane fraction of the cells (though to a lesser extent compared to its full-length counterpart). Thus, PBP1a-Δ30 was treated analogously to the full-length membrane proteins throughout purification. PBP2b-Δ39 and PBP2x-Δ48 were substantially over-expressed in the soluble and membrane fractions of the cells. Proteins locating to the former cellular fraction were selected for purification, where it was advantageous to work in the absence of detergent.

3.6.1. Purification of PBP1a-Δ30

It was anticipated that PBP1a-Δ30 could require a detergent for solubilisation as documented for a number of PBPs devoid of the membrane anchor, including *S. pneumoniae* PBP2a (Di Guilmi *et al.*, 1999). It has been identified through structural studies that bifunctional PBPs have a membrane interaction site, distinct from the transmembrane anchor, enabling partial submersion of the transglycosylase domain into the lipid bilayer, which is believed to allow access to the Lipid II substrate (Lovering *et al*., 2007; Sung *et al*., 2009).

PBP1a-Δ30 was purified by IMAC and size exclusion chromatography in an identical approach to the purification of the full-length equivalent. The final level of purity is demonstrated on the SDS-PAGE gel in Figure 3.13. The overall yield of purified protein was significantly lower compared to the other full-length and truncated PBPs studied. This is a consequence of the initial low levels of expression (illustrated in Figure 3.6).

3.6.2. Purification of PBP2b-Δ39 and PBP2x-Δ48

High levels of PBP2b-Δ39 and PBP2x-Δ48 expression in the cytoplasmic fraction of the cells allowed the enzymes to be treated as stable, soluble proteins, alleviating the need for detergents. The soluble cellular fractions were prepared (Section 2.4.2.1) and the target proteins were purified by IMAC (Figure 3.12a) (Section 2.4.3.1), followed by size exclusion chromatography (Figure 3.12b) (Section 2.4.3.2) and anion exchange chromatography (Figure 3.12c) (Section 2.4.3.3). Fractions were analysed by SDS-PAGE and those containing the highest level of target protein purity were selected for future analyses.

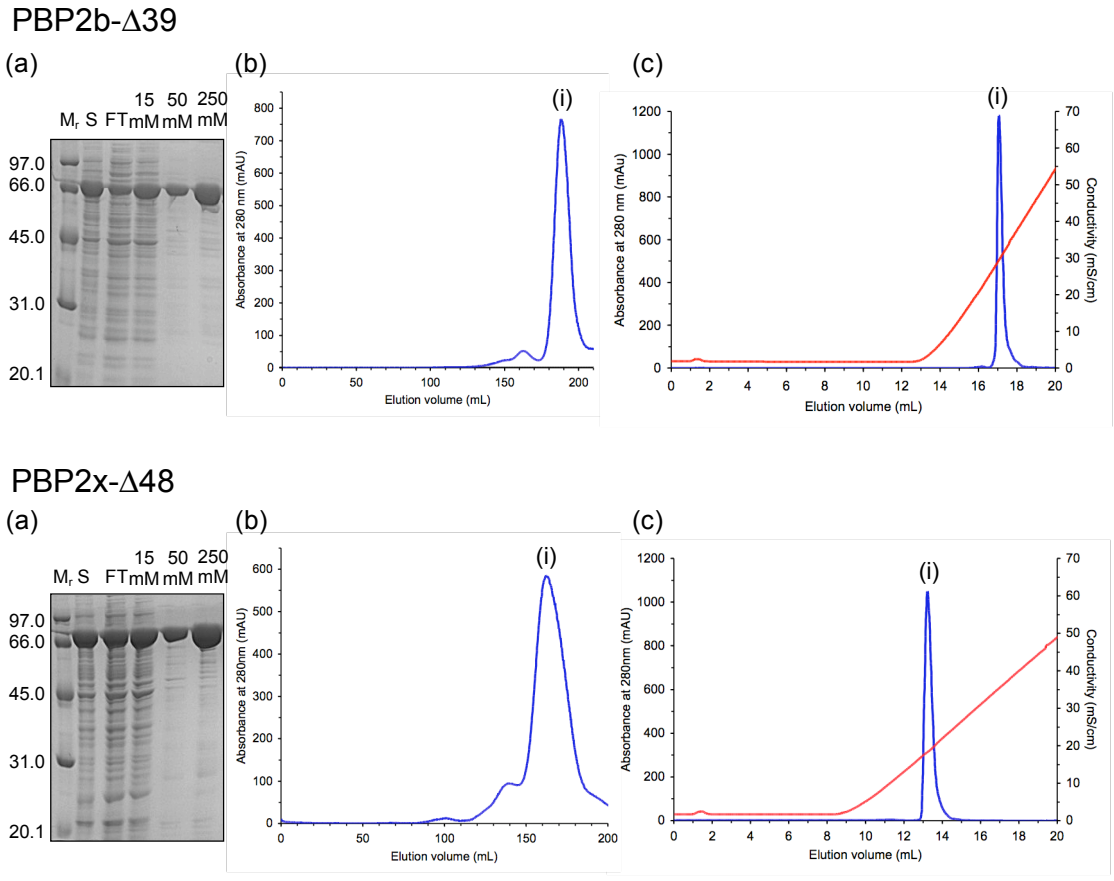

Figure 3.12: Summary of the techniques employed for the purification of PBP2b-Δ39 and PBP2x-Δ48. (a) 12 % SDS-PAGE Coomassie-stained gel following IMAC. M_r, molecular weight markers (kDa); S, soluble cell extract before loading onto the IMAC column; FT, flow through; 15 mM, 50 mM and 250 mM, buffer washes containing the corresponding concentrations of imidazole. (b) Chromatogram from size exclusion chromatography (Superdex 200 26/60 column; 20 mM Tris pH 7.5, 150 mM NaCl). (c) Chromatogram from anion exchange chromatography (MonoQ HR 5/5 column; 20 mM Tris pH 7.5). Absorbance at 280 nm (—); Conductivity (mS/cm) (—). (i) denotes PBP2b-Δ39 or PBP2x-Δ48 elution on Figures (b) and (c).

3.6.3. Final levels of purity of PBP1a-Δ30, PBP2b-Δ39 and PBP2x-Δ48

The final levels of purity of the PBPs devoid of the transmembrane (and cytoplasmic) domain are demonstrated in SDS-PAGE gels in Figure 3.13, achieved by the different purification techniques as described in the above sections.

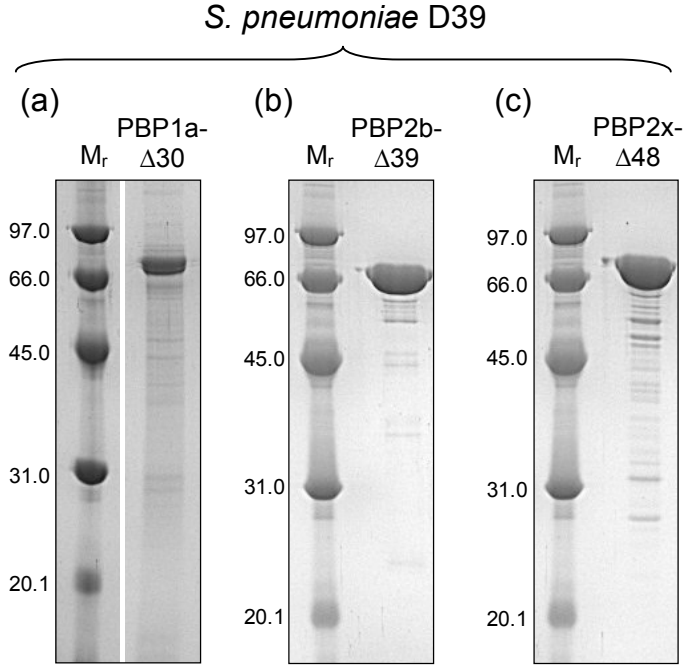

Figure 3.13: SDS-PAGE Coomassie-stained gels showing the purity and protein yield of the truncated PBPs after purification. (a) PBP1a-Δ30: expressed in the membrane fraction of cells; detergent-extracted from membranes; purified by IMAC and size exclusion chromatography in the presence of detergent. (b) PBP2b-Δ39 and (c) PBP2x-Δ48: expressed as soluble proteins in the cytoplasmic fraction of cells; purified by IMAC, size exclusion chromatography and anion exchange chromatography. Protein yield refers to the total amount of purified target protein extracted from 1 L *E. coli* culture. M_r, molecular weight markers (kDa).

3.7. Binding of fluorescent-labelled penicillin to PBPs

The commercially available BOCILLIN FL is a fluorescent-labelled penicillin. The penicillin moiety binds to the penicillin-binding domain of PBPs via a covalent bond with the catalytic serine residue, labelling PBPs with a fluorophore. This is an established sensitive technique to detect PBPs (Zhao *et al.*, 1999) and can be used to

assess the native conformation of the penicillin-binding domain. PBPs were incubated with BOCILLIN FL (3:1 molar ratio) at 37°C for 1 h (in the dark to preserve the integrity of the fluorescent label). The binding of BOCILLIN FL to the PBPs was analysed by SDS-PAGE. Figure 3.14 shows the Coomassie-stained SDS-PAGE gels and the BOCILLIN FL specific fluorescence. Fluorescence was detected prior to staining.

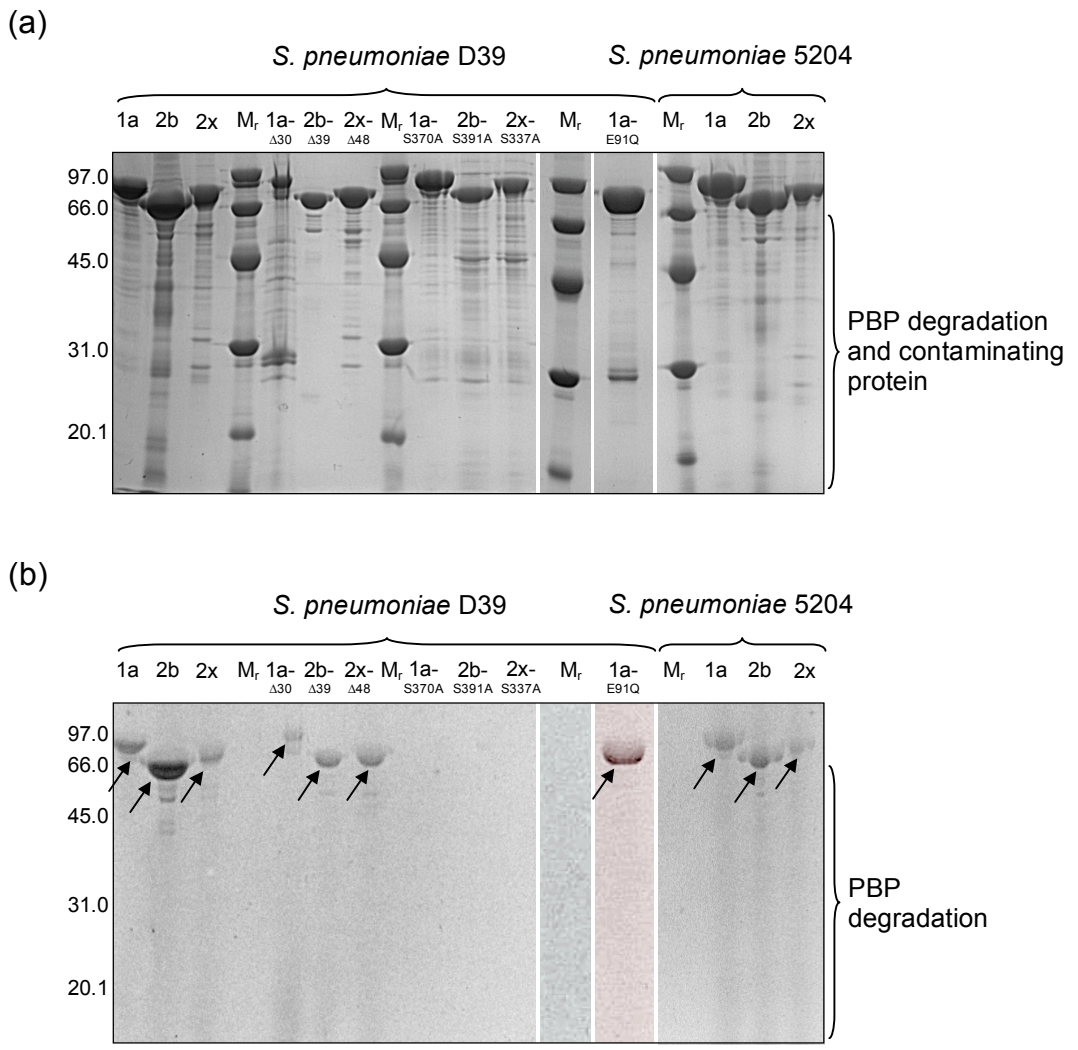

Figure 3.14: BOCILLIN FL, a labelling reagent for the detection of PBPs. (a) A 12 % SDS-PAGE Coomassie-stained gel of the PBP variants incubated with BOCILLIN FL. (b) BOCILLIN FL-specific fluorescence (identified by arrows) of the equivalent SDS-PAGE gel of (a). Lanes are labelled according to the PBP denominations, and are grouped depending on the protein origin (*S. pneumoniae* D39 or 5204). M_r, molecular weight markers (kDa). Fluorescence was detected using the Syngene GeneSnap G:Box Gel Doc with the blue light converter and filter for detecting BOCILLIN FL emission at 520 nm. (a) shows the non-specific protein staining by Colloidal-Coomassie, highlighting contaminating proteins, whereas (b) shows BOCILLIN FL fluorescence, specific to PBP binding, signifying protein degradation or the presence of contaminating host PBPs.

The BOCILLIN FL-specific fluorescent bands on the SDS-PAGE gel of Figure 3.14b are in corresponding positions to the Colloidal-Coomassie-stained protein, indicating the labelling of the PBPs with BOCILLIN FL. In order for this to occur, the transpeptidase active sites must be in at least a near-native conformation, enabling the correct positioning of the active site serine for attack of the β-lactam scissile bond. Information regarding the structural integrity of the bifunctional PBP transglycosylase domain cannot be established using this technique. The *S. pneumoniae* D39 PBPs, full-length and truncated, are able to bind BOCILLIN FL, indicating the truncation did not interfere with the conformation of the transpeptidase domain. The transpeptidase active site serine mutants were unable to bind BOCILLIN FL as expected, although the effect of the mutation on the penicillin-binding domain architecture cannot be analysed. *S. pneumoniae* PBPs from clinical resistant isolates can bind β-lactam antibiotics (example in Pagliero *et al.* (2004)) and Figure 3.14 demonstrates that the PBPs from the *S. pneumoniae* penicillin-resistant strain 5204 were capable of binding BOCILLIN FL. In principle, their affinity for BOCILLIN FL would be lower in comparison to the PBPs derived from the penicillin-sensitive strain, thus the intensity of the fluorescent signal would be lower. This is not evident on Figure 3.14b where the exposure conditions were adjusted to optimise the visualisation of the BOCILLIN FL-protein bands.

3.8. Discussion

The work presented in this Chapter details strategies to produce quantities of PBP variants for future biochemical characterisations. The following section discusses the results in terms of the successes, providing the rational behind the techniques employed. Areas for improvement are highlighted and strategies to solve problems encountered are described.

3.8.1. Cloning and expression of PBP variants

3.8.1.1. Constructs generated

Varying constructs of *S. pneumoniae pbp1a*, *pbp2b* and *pbp2x* were cloned into the pET46 vector and specified site-directed mutants were generated. Codons for six histidine residues were integrated onto the 5' terminal of the target gene sequence, additional to those encoded by the vector sequence. Upon expression, a recombinant protein with an N-terminal dodeca-histidine tag was produced. The additional histidine residues were proposed to allow the tag to clearly protrude from the detergent micelle and to augment the binding affinity to the affinity chromatography resin, enhancing the yield and level of purity of the low abundant membrane proteins. Construction of a cleavage site between the target protein and the engineered histidine residues is a future consideration; biochemical analyses could be impeded by the presence of the histidine tag, where only the vector-encoded sequence was removable via an enterokinase cleavage site.

3.8.1.2. Expression conditions

Optimal expression conditions were established for *S. pneumoniae* PBP1a, PBP2b and PBP2x. The enzymes were expressed substantially in *E. coli* BL21 Star (DE3) pRosetta cells under autoinduction at 25°C. These conditions were evaluated for the over-expression of the remaining PBP variants, yielding a similar degree of success (with the exception of PBP1a-Δ30). The over-expression of integral membrane proteins often results in toxicity due to the overloading of secretory machinery (which targets the protein to the membrane) in conjunction with the insertion of unnaturally large quantities of typically low abundant proteins into the membrane. Cells were cultured and induced at a low temperature, reducing basal levels of expression and maximising the efficiency of protein insertion into the membrane.

3.8.1.3. Protein stability estimations

Expression levels of PBP1a-Δ30 were lower than the full-length counterpart. This was unexpected and prompted an exploration into PBP1a-Δ30 stability. The PBP1a protein sequence was analysed using Regional Order Neural Network software (RONN, Yang *et al.* (2005)), which provides an image of predicted natively disordered regions in proteins (Figure 3.15). The position of truncation was not located in a region of disorder at the N-terminal (predicted disorder, residues 40-78).

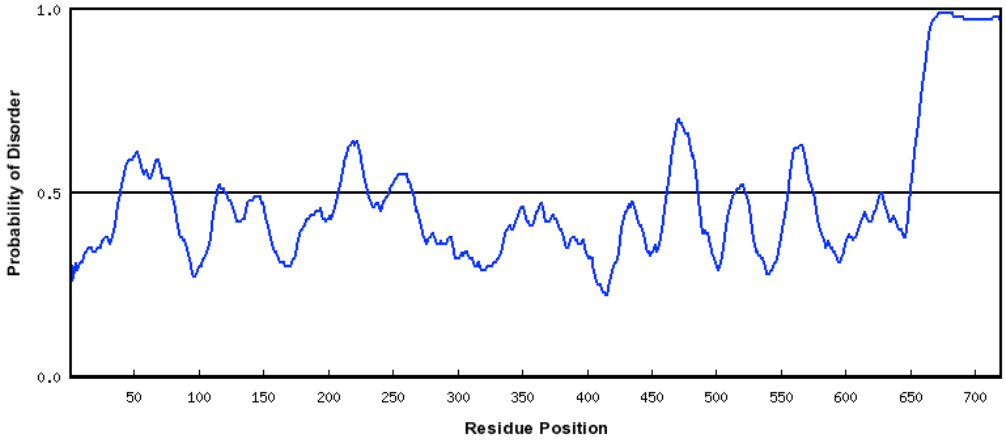

Figure 3.15: Probability of disorder for PBP1a. RONN software was used to predict regions of disorder in PBP1a. The first region of disorder is between amino acid residues 40-78.

Different lengths of sequence truncation from the N-terminal could provide a more stable protein devoid of the membrane anchor ensuring the transglycosylase domain is not impacted upon (residues 54-222). RONN analysis predicted a large region of disorder at the C-terminal of the protein; truncation of the terminal 69 residues could improve protein stability. Prior to future truncations, disorder of the protein sequence should be addressed by RONN analysis.

3.8.1.4. Molecular weight predictions of membrane proteins by SDS-PAGE

SDS-PAGE and Western blot analysis underestimated the molecular weight of the recombinant proteins. Due to the hydrophobic properties, membrane proteins bind a different ratio of SDS and travel through the gels at different rates during electrophoresis compared to soluble proteins. Thus, it has been documented that the

molecular masses of integral membrane proteins can be underestimated by 30-35 % (Henderson *et al.*, 2000) explaining the discrepancy between the true size of the protein and that predicted by SDS-PAGE.

3.8.2. Detergent solubilisation trials of membrane proteins

A solubilisation screen was performed to identify a detergent that isolated the target protein from the membranes with optimum efficiency. The screen was limited by the inability to detect detergent-imposed protein aggregation. Separation of a partially purified protein by size exclusion chromatography using a calibrated column would identify protein elution in the void volume (exceeding the exclusion limit), indicative of protein aggregation. This would allow the detergent to be selected on the basis of solubilisation efficiency and the ability to maintain protein integrity.

3.8.2.1. SMALPs: a novel technique for membrane protein solubilisation

Detergent solubilisation often renders the membrane protein in a functionally inactive state by: promoting protein aggregation and precipitation; removing essential natively-associating lipids; co-concentrating detergent micelles; affecting enzyme activity and native interactions. A novel technique provides a solution to many of these issues: Styrene Maleic Acid copolymer Lipid Polymer (SMALP) technology (structure shown in Figure 3.16).

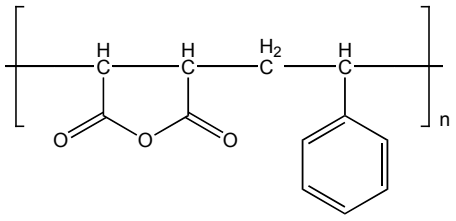

Figure 3.16: SMALP structure. SMALPs consist of a copolymer of styrene and maleic anhydride (hydrolysed to maleic acid), containing a pendant phenyl group and a weakly negatively charged pendant group (Tonge and Tighe, 2001).

At the appropriate pH (above its pKa), the copolymer enters a hypercoiled state (Tonge and Tighe, 2001). A uniformly sized disc forms, 11 nm in diameter, encapsulating a protein (with its surrounding lipids) from the membrane in a

monodisperse state, enabling access to both cytoplasmic and extracellular faces of the membrane protein (Knowles *et al.*, 2009).

This strategy could be investigated to solubilise the PBPs from the membranes if detergent extraction rendered the enzymes inactive.

3.8.3. Membrane protein purification

3.8.3.1. Detergent exchange

Following solubilisation of the membrane proteins, sodium deoxycholate was exchanged for DDM (a detergent frequently used in the study of membrane proteins). In addition to avoiding the adverse effects of sodium deoxycholate on buffer solutions, detergent exchange had a role in enhancing protein purification. The distribution of proteins within a detergent micelle is largely unknown; single or multiple natively associating or non-associating proteins could exist in the same micelle as the target protein. Disruption of the micelle during detergent exchange aims to isolate the target protein, thus eliminating contaminating proteins and improving protein purity.

3.8.3.2. Affinity chromatography and size exclusion

Two purification strategies were employed in the purification of the integral membrane proteins to minimise the loss of protein incurred. The preliminary purification step of affinity chromatography was developed to optimise target protein association with affinity resin, whilst minimising the aggregation potential.

Size exclusion chromatography was performed with three objectives: to purify proteins based on size, to remove aggregated material and to buffer exchange. The membrane proteins eluted from the column as a relatively broad peak (as demonstrated by PBP1a, Figure 3.9), which could indicate that the protein was not monodispersed, present in a range of conformations, associating with contaminants or degrading. Isolated membrane proteins are not single entities; they are in a detergent micelle complex. The detergent micelle of DDM varies in size (~40-75

kDa (Anatrace-Affymetrix)), which would also contribute to the broad elution peak of the protein. This issue could be solved by using a detergent with a smaller, uniform micelle size. CHAPS, with a micelle size of 6 kDa (Sigma-Aldrich), was trialled in the size exclusion chromatography of PBP1a, PBP2b and PBP2x but caused severe protein aggregation, which was evident from the elution of the protein in the column void volume. Many other small micellar weight detergents could be tested for suitability during the size exclusion chromatography of the membrane proteins such as N-lauroyl sarcosine (average micellar weight of 0.6 kDa, Sigma-Aldrich).

3.8.3.3. Final levels of protein purity

PBP1a purified to a marginally higher level compared to PBP2b and PBP2x and the counterparts from *S. pneumoniae* 5204. The expression levels of the *S. pneumoniae* 5204 PBPs were slightly lower compared to those from the penicillin-sensitive strain and thus during affinity chromatography, *E. coli* host proteins were more prominent as contaminants. Despite the similarity of PBP1a, PBP2b and PBP2x expression levels, PBP1a purified with fewer contaminants. It was anticipated that the PBPs would be expressed as active enzymes within the *E. coli* expression system. Therefore, these enzymes could interact with host proteins in an analogous manner to the native associations formed in *S. pneumoniae*, such as the localisation of PBPs to cell division machinery (Morlot *et al.*, 2003). If these interactions were not disrupted by detergent solubilisation, the contaminants could co-purify.

3.9. Conclusion

The major β-lactam resistance determinants of *S. pneumoniae* were successfully cloned as different length constructs from the penicillin-sensitive and penicillin-resistant strains, D39 and 5204. Mutations to active site residues of the full-length *S. pneumoniae* D39 PBPs were generated. Each variant was successfully expressed and purified to greater than 90 % homogeneity, providing sufficient quantities for future biochemical characterisations.

Chapter 4. Enzymology of transglycosylation: assay development and preliminary kinetic characterisations of *Staphylococcus aureus* MGT and *Streptococcus pneumoniae* PBP1a

4.1. Introduction

The peptidoglycan transglycosylases belong to the highly conserved GT51 family of carbohydrate active enzymes (www.cazy.org). These enzymes have a vital role in peptidoglycan synthesis: they catalyse the polymerisation of the disaccharide constituent of Lipid II, although the precise catalytic mechanism is yet to be fully resolved (Lovering *et al.*, 2007). The elucidation of this mechanism and the biochemical characterisation of the transglycosylases will guide the future design of antimicrobials against this desirable, underexploited antibiotic target.

4.1.1. Mechanistic features of transglycosylation

To begin to establish the catalytic mechanism, details of transglycosylation need to be defined including the direction of glycan chain elongation, the length of glycan chains and whether transglycosylation conforms to a processive or dispersive model of substrate polymerisation. These features are addressed in the following sections.

Perlstein *et al.* (2007) provided the first biochemical data determining the direction of glycan chain polymerisation. In the study, β-1,4-galactosyltransferase was used to transfer [^{14}C]-labelled-galactose to the C4 hydroxyl group of the terminal Glc*N*Ac (the non-reducing end) of Lipid II substrate analogues, preventing this end from serving as a glycosyl acceptor. These labelled substrates were incubated with four transglycosylases (*E. coli* PBP1a, *E. coli* PBP1b, *S. aureus* PBP2 and *A. aeolicus* PBP1a) and Lipid II. Despite obstruction at the non-reducing end, chain extension was observed, indicating that the transglycosylases polymerised Lipid II by integrating the disaccharide units onto the diphospholipid, reducing (although not a lactol) terminus (Perlstein *et al.*, 2007).

By general agreement, transglycosylases are processive rather than dispersive, where they catalyse multiple rounds of polymerisation without releasing the elongating glycan polymer (Yuan *et al.*, 2007). The processive model has been validated by the use of high-resolution gel electrophoresis, which allows the separation of glycan chains to a single disaccharide resolution, enabling the length of the glycan chains to be established (Barrett *et al.*, 2007; Yuan *et al.*, 2007). This technique was used to analyse the distribution of transglycosylase products following time-dependent incubations of *E. coli* PBP1a and *A. aeolicus* PBP1a with heptaprenyl-[^{14}C]-Lipid II. Long glycan chains appeared without the accumulation of short chains, concurrent with the processive model of transglycosylation (Barrett *et al.*, 2007). The crystal structure of *A. aeolicus* PBP1a is also consistent with the processive model of transglycosylation. A flap exists that folds over the active site cleft, which has been proposed to prevent the dissociation of the elongating polymer from the active site (Yuan *et al.*, 2007).

The gel electrophoresis technique was also used by Wang *et al.* (2008) to establish whether transglycosylases have a specific limiting chain length. It was discovered that *E. coli* PBP1a, *E. coli* PBP1b, *S. aureus* PBP2 and *E. faecalis* PBP2a had limiting chain lengths of approximately 30, 50, 15 and 15 disaccharide units respectively and these values remained unchanged upon varying the enzyme:substrate ratio. Due to the processive nature of the transglycosylases, there must be an unidentified intrinsic mechanism that limits chain length and allows the glycan product to be released once a threshold length is reached (Wang *et al.*, 2008).

4.1.2. The proposed catalytic mechanism

Although the precise details are not fully understood, a combination of structural and biochemical analyses has led to the proposal of the catalytic mechanism for transglycosylation. The recent transglycosylase crystal structures in complex with the inhibitor moenomycin have been fundamental in elucidating whether Lipid II acts as a donor or acceptor during the polymerisation reactions (Heaslet *et al.*, 2009; Lovering *et al.*, 2007; Sung *et al.*, 2009). In the *S. aureus* PBP2 (Lovering *et al.*, 2007) and *E. coli* PBP1b (Sung *et al.*, 2009) moenomycin co-crystal structures, the elongating glycan chain can be modelled onto moenomycin, where moenomycin

rings E and F (Figure 1.11) correspond to the Glc*N*Ac and Mur*N*Ac constituents of the reducing terminal of the glycan polymer. There is also sufficient space in the structure to model Lipid II in an adjacent site (Lovering *et al.*, 2007). Addition of disaccharide units to the reducing end of an extending polymer positions the elongating glycan chain in the donor site and Lipid II in the acceptor site (Lovering *et al.*, 2007) (Figure 4.1).

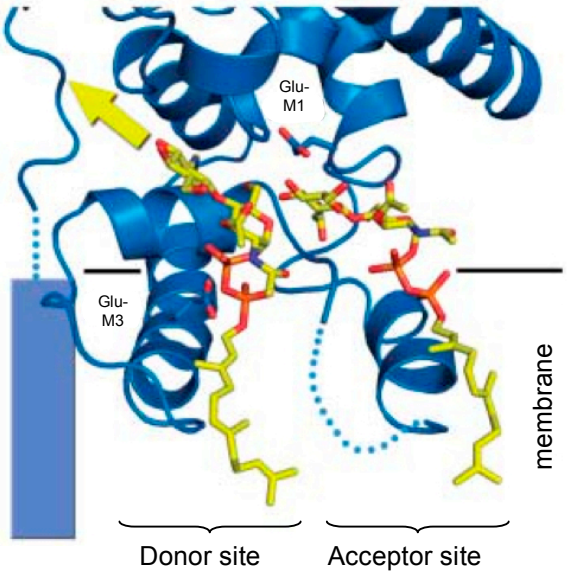

Figure 4.1: Spatial representation of Lipid II analogues modelled into the donor and acceptor sites of *S. aureus* PBP2 transglycosylase domain. The putative catalytic residues Glu-M1 and Glu-M3 (M, conserved motif) are shown in stick forms. The Lipid II analogues (stick forms) are modelled into the donor or acceptor subsites of the catalytic site. The yellow arrow shows the direction of the elongating glycan chain. The membrane interface (black line), the transmembrane domain (blue block) and the missing polypeptide (blue dashed line) are displayed. Modified from Lovering *et al.* (2007).

Based on inferences taken from the lysozyme mechanism of β-1,4-glycosidic bond cleavage between Mur*N*Ac and Glc*N*Ac components of a glycan chain and structural details of the transglycosylase domain, Lovering *et al.* (2008a) and (2007) have proposed a mechanism for transglycosylation. In this model, the placement of substrates positions the C4 hydroxyl group of the accepter Glc*N*Ac for deprotonation by the conserved catalytic glutamate of motif 1, which acts as a base. The resulting nucleophile concomitantly attacks the C1 of the donor Mur*N*Ac acyl-phosphate linkage in an S_N2-like reaction. This causes an inversion of configuration at the C1

anomeric carbon, from an α-linked precursor to a β-1,4-glycosidic bond-linked product. The undecaprenyl pyrophosphate leaving group is then free to diffuse away from the active site.

The conserved Glu of motif 3 could have different roles in the transglycosylation mechanism depending on its undefined protonation state (Figure 4.2). In a protonated state (glutamic acid), it could donate a proton to the departing undecaprenyl pyrophosphate or coordinate the pyrophosphate group via a hydrogen bond (Lovering *et al.*, 2007). Alternatively, in a deprotonated state, the glutamate residue could stabilise the pyrophosphate moiety by an indirect interaction, mediated through the co-ordination of either a divalent cation (Lovering *et al.*, 2007) or an arginine residue (as suggested by the crystal structure of *S. aureus* MGT complexed with moenomycin (Heaslet *et al.*, 2009)).

For subsequent rounds of transglycosylation, the newly synthesised product needs to be translocated into the donor site (according to the processive model (Barrett *et al.*, 2007; Yuan *et al.*, 2007)). It is believed that the pyrophosphate moiety has a higher affinity for the donor site (which contains conserved positively charged residues locating to the pyrophosphate binding region) compared to the acceptor site, thus promoting translocation (Lovering *et al.*, 2007).

The proposed transglycosylase catalytic mechanism (Figure 4.2) will require validation by future work.

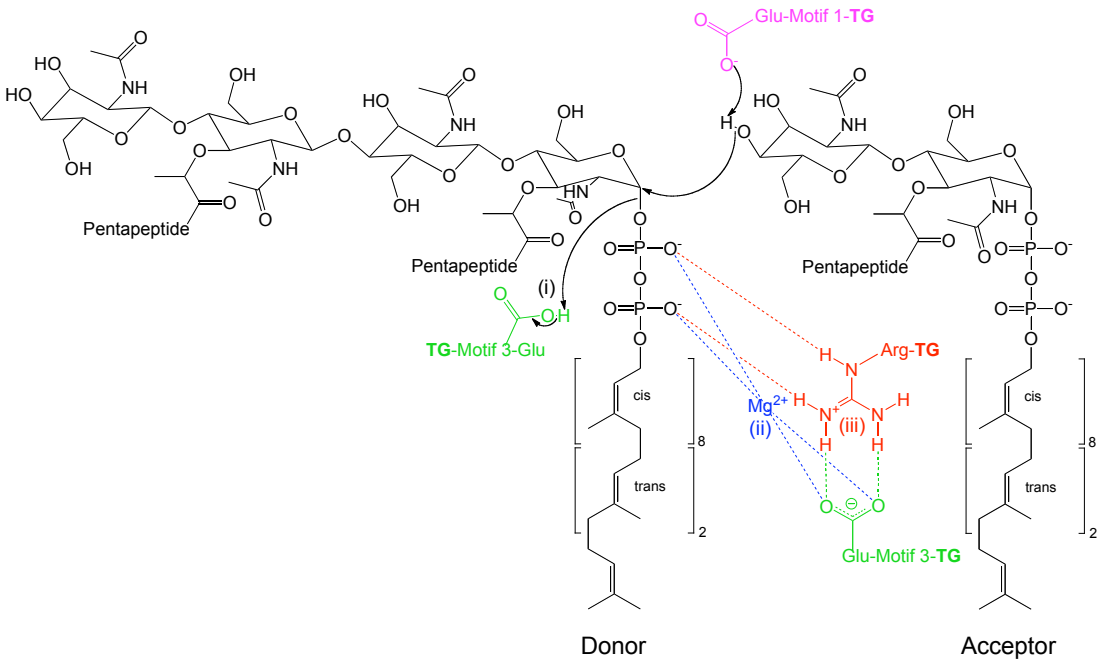

Figure 4.2: Proposed mechanism for transglycosylation. The elongating glycan chain is the donor; the Lipid II monomer is the acceptor. The Glu residues are shown as part of the designated conserved motif of the transglycosylase domain (TG). The conserved Glu of motif 1 (magenta) deprotonates the C4 hydroxyl group of the acceptor, which concomitantly attacks the C1 of the donor, causing an inversion in configuration to form β-linked products. Three potential situations are shown for the role of the conserved Glu of motif 3 (green). (i) It can donate a proton to the leaving undecaprenyl pyrophosphate group, or it can indirectly stabilise the pyrophosphate moiety of the leaving group through the coordination of (ii) a metal ion (blue) or (iii) an arginine residue (red). Adapted from Lovering *et al.* (2007).

4.1.3. Current strategies to analyse transglycosylase activity

4.1.3.1. Substrate and derivatives

The advent of the ability to synthesise lipid-linked intermediates of peptidoglycan has revolutionised the study of the transglycosylase activity. Although the availability of Lipid II remains restrictive, the incorporation of a radioactive or fluorescent group into the substrate enables limiting amounts to be used whilst maintaining a high sensitivity of detection. In many cases, derivatives of Lipid II are used. However, structural modifications of Lipid II can interfere with activity of the enzyme, impeding or elevating it. This poses the question of whether these substrate analogues are appropriate to obtain a realistic representation of the native activity of the enzyme. Ye *et al.* (2001) discovered that transglycosylases in *E. coli* membranes

had a preference for a Lipid II analogue containing a betulaheptaprenyl lipid chain (35 carbon atoms) over the natural substrate. The shorter lipid chain minimises the possibility of aggregation as observed with the 55-carbon chain of the undecaprenyl constituent of Lipid II (Ye *et al.*, 2001).

4.1.3.2. Radioactivity-based assays

There are various radioactivity-dependent assays that have been employed to functionally and kinetically characterise transglycosylase activity. As previously described, gel electrophoresis can be used to separate radiolabelled glycan polymers, allowing chain length and processivity to be addressed (Barrett *et al.*, 2007; Yuan *et al.*, 2007). Paper chromatography can also be employed to separate products of transglycosylation; glycan polymers remain immobile on the chromatogram whilst Lipid II migrates. Given that the Lipid II substrate is labelled either radioactively or with fluorescence, the products of transglycosylation can be detected and quantified. Paper chromatography with radiolabelled substrates was used by Terrak and Nguyen-Distèche (2006) to characterise *S. aureus* MGT.

4.1.3.3. Fluorescence-based assays

High performance liquid chromatography (HPLC) can be used to analyse the polymerisation of Lipid II (labelled with fluorescence before or after a transglycosylation reaction), monitored by the appearance of a peak representing glycan polymers and the disappearance of a Lipid II peak. This technique was applied by Heaslet *et al.* (2009) to determine the effect of different mutations on the activity of *S. aureus* MGT and has been used by Schwartz *et al.* (2002) to kinetically characterise *E. coli* PBP1b. Schwartz *et al.* (2002) have also developed a continuous fluorescence assay to assess transglycosylase activity, where the polymerisation of dansyl-Lipid II is coupled to a muramidase that ultimately results in a decrease in fluorescence signal. Liu and Wong (2006) have employed a nitrophenol Lipid II analogue to characterise *S. pneumoniae* PBP1b spectrophotometrically, where a series of reactions leads to the production of nitrophenol, which can be monitored by absorbance at 405 nm.

4.1.4. The future of transglycosylase assays

The development of a high-throughput assay system to assess transglycosylase activity with the natural unmodified substrate is desirable to allow the rapid characterisation of transglycosylases. Ultimately, this system will enable a vast library of inhibitors to be screened with immediate results, which will have significant implications for the future discovery of antagonists of the transglycosylase antimicrobial target. The design of such an assay system is addressed in this Chapter.

4.2. Experimental aims

- To over-express and purify *S. aureus* Monofunctional Glycosyl Transferase (MGT), an appropriate control enzyme for transglycosylase activity

- To develop a spectrophotometric assay for the detection of transglycosylase activity

- To establish optimal assay conditions and to kinetically characterise the transglycosylase activity of *S. aureus* MGT and *S. pneumoniae* PBP1a using the novel spectrophotometric assay

- To establish an efficient method for the enzymatic synthesis of [^{14}C]-labelled Lys-Lipid II

- To analyse products of MGT and PBP1a-dependent transglycosylation using SDS-PAGE separation with [^{14}C]-labelled Lys-Lipid II and a novel, non-radioactive detection system

4.3. *S. aureus* MGT as a control enzyme for transglycosylase activity

The transglycosylase activity of *S. aureus* MGT, devoid of its membrane anchor, has been characterised, kinetically (Terrak and Nguyen-Distèche, 2006) and structurally (Heaslet *et al.*, 2009). MGT has a single functional domain exhibiting transglycosylase activity, common to Class A PBPs, but concomitantly lacks the penicillin-binding domain. The monofunctionality and established activity of this enzyme make it a suitable control enzyme for the analysis of transglycosylase activity.

4.3.1. Establishment of expression constructs for the wild-type and the active-site mutant of MGT

The expression construct pET46::*mgt*, carrying the truncated *mgt* gene encoding D68-R268 (equivalent in length to the N-terminally truncated MGT characterised by Terrak and Nguyen-Distèche (2006)) in the pET46 Ek/LIC vector, was provided by T. Clarke. Upon expression, *S. aureus* MGT-Δ67 (devoid of the first 67 amino acid residues of the N-terminus) contained a vector-encoded N-terminal hexa-histidine tag, and is referred to as MGT from here onwards.

In future assays, to attribute any activity detected to MGT-dependent transglycosylation, a catalytically inactive form of MGT was required for comparative purposes. A glutamate residue (E100 in the MGT sequence) is present in the first conserved motif of all Class A PBPs and MGTs. Terrak and Nguyen-Distèche (2006) have confirmed that this residue is essential for transglycosylase activity *in vitro*: *S. aureus* MGT-E100Q exhibits a 500-fold reduction in activity compared to the wild-type enzyme. The absence of the conserved glutamate residue essentially renders the transglycosylase inactive, a desirable property for future studies.

Quik-Change site-directed mutagenesis (Section 2.3.10) was used to replace the glutamate-100 residue with glutamine (E100Q). The primers for mutagenesis were

identical to those used by Terrak and Nguyen-Distèche (2006) (Table 4.1). Sequence analysis of the constructs (using primers in Table 2.2) following the mutagenesis identified the presence of the specified mutation; the plasmid containing the desired mutation was termed pET46::*mgt-E100Q* (recombinant protein designated MGT-E100Q).

Primer name	Sequence (5'-3')
E100Q sense	CCTTTATTTCAATG**CAA**GATGAACGATTCATC
E100Q antisense	GTAGAATCGTTCATC**TTG**CATTGAAATAAAGG

Table 4.1: Primers for MGT site-directed mutagenesis of *S. aureus mgt*. The modified codon for the desired mutation is highlighted in bold type.

4.3.2. Expression and purification of wild-type MGT and MGT-E100Q

MGT and MGT-E100Q were expressed in *E. coli* BL21 Star (DE3) cells harbouring the pRosetta plasmid under autoinduction at 25°C (Section 2.4.2.1). The recombinant proteins over-expressed solely in the insoluble fraction of the cells, from which they were extracted (Section 2.4.2.2) and purified by IMAC (Section 2.4.3.1) and size exclusion chromatography (Section 2.4.3.2) in the buffer 50 mM sodium phosphate, 0.5 M NaCl, 20 % glycerol (w/v), pH 7.6. Fractions from different stages of the extraction and purification were analysed by SDS-PAGE (Figure 4.3). The molecular weight of the truncated MGT is 23.4 kDa. MGT was stored in 50 % (v/v) glycerol at -20°C (freezing at -80°C was detrimental to enzyme activity).

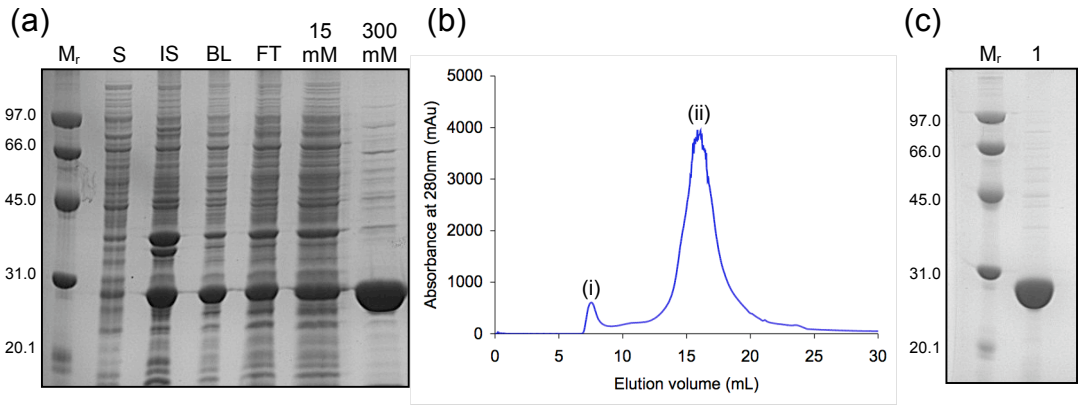

Figure 4.3: Purification of *S. aureus* MGT by immobilised metal chelate affinity chromatography and size exclusion chromatography. (a) 12 % SDS-PAGE Coomassie-stained gel analysis of the extraction of MGT from the insoluble fraction and subsequent IMAC purification. M_r, molecular weight markers (kDa); lane S, soluble cytoplasmic cellular fraction; lane IS, insoluble cellular fraction; lane BL, solubilised proteins from the insoluble fraction before loading onto the IMAC column; lane FT, flow-through; lane 15 mM, buffer with 15 mM imidazole; lane 300 mM, buffer with 300 mM imidazole. (b) The chromatogram of size exclusion chromatography using the Superose 6 10/300 GL column. The peak (i) denotes aggregated material eluting in the column void volume and peak (ii) identifies the elution of MGT. (c) 12 % SDS-PAGE Coomassie-stained gel analysis of the final purity of MGT. M_r, molecular weight markers (kDa); lane 1, purity of MGT following IMAC and size exclusion chromatography.

MGT and MGT-E100Q exhibited similar properties: expressing to comparable levels and requiring a high salt concentration to remain soluble at high protein concentrations.

The MGT recombinant protein was highly similar to that used by Terrak and Nguyen-Distèche (2006), who were able to detect MGT-dependent transglycosylase activity. Therefore, it was anticipated that MGT would also demonstrate glycan chain polymerising activity.

4.4. Discontinuous spectrophotometric assay for the detection of transglycosylase-dependent undecaprenyl pyrophosphate production

The monofunctional transglycosylases and Class A PBPs are responsible for the transglycosylation of the Lipid II substrate (as reviewed by Sauvage *et al.* (2008a)). They catalyse the formation of a β-1,4-glycosidic bond between the Mur*N*Ac unit (at the reducing end of an extending glycan chain) and the Glc*N*Ac unit (of the incoming Lipid II substrate) with the concurrent release of undecaprenyl pyrophosphate (Perlstein *et al.*, 2007). The discontinuous production of undecaprenyl pyrophosphate (indicative of a transglycosylation reaction) can be coupled to a continuous spectrophotometric assay as outlined in Figure 4.4. Dephosphorylation of undecaprenyl pyrophosphate by an undecaprenyl pyrophosphate phosphatase generates undecaprenyl phosphate and inorganic phosphate (P_i). The undecaprenyl-pyrophosphate-phosphatase-dependent P_i release can be linked to the phosphorolysis of a chromogenic nucleoside, 7-methyl-6-thioguanosine. This reaction is catalysed by purine nucleoside phosphorylase (PNP) to form 7-methyl-6-thioguanine, giving a spectrophotometric signal at 360 nm (Webb, 1992).

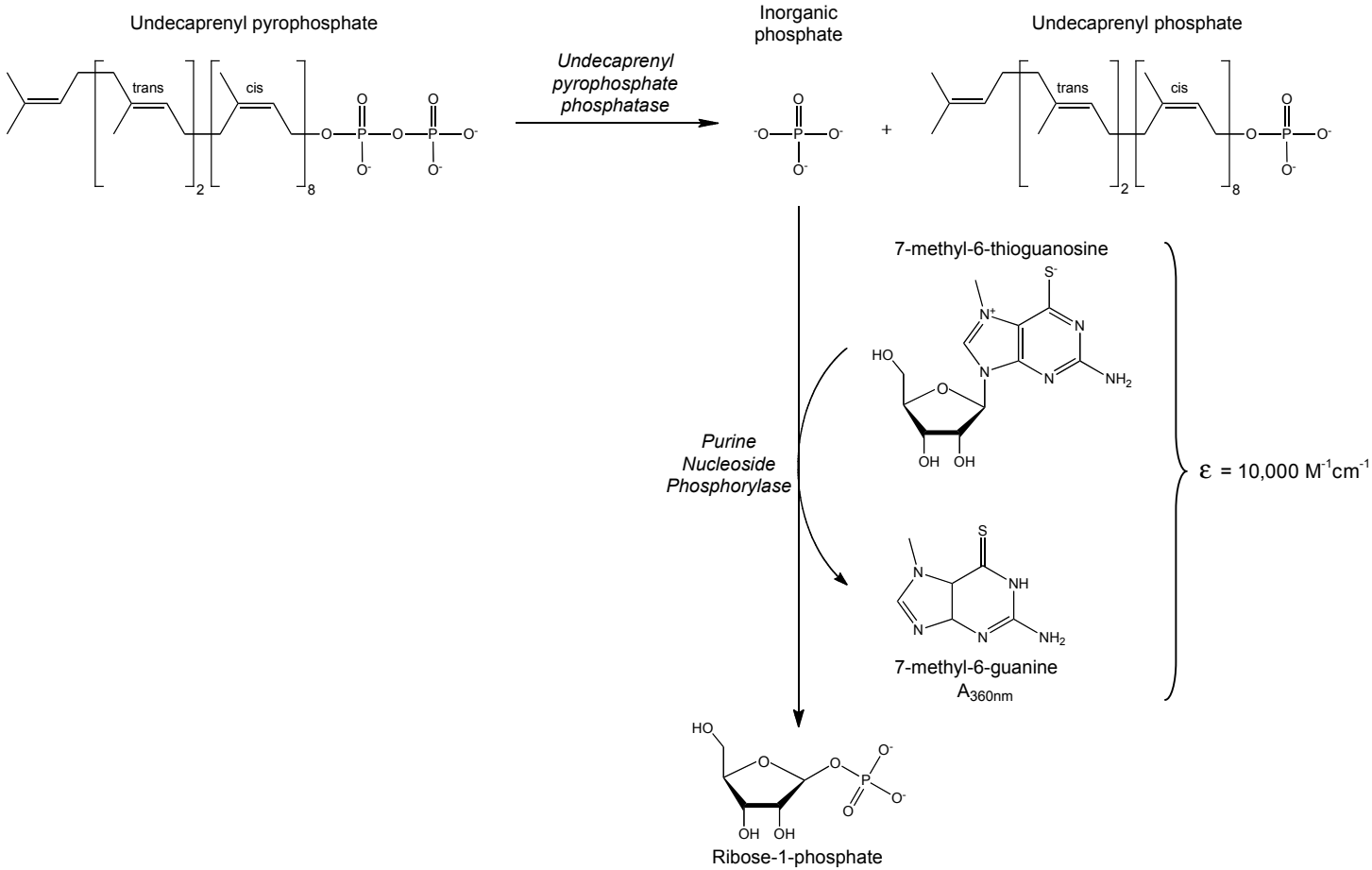

Figure 4.4: A continuous spectrophotometric assay for inorganic phosphate release. A product from the transglycosylation reactions is undecaprenyl pyrophosphate. An undecaprenyl pyrophosphate phosphatase dephosphorylates undecaprenyl pyrophosphate generating undecaprenyl phosphate and P_i. The latter product is involved in the phosphorolysis of 7-methyl-6-thioguanosine, catalysed by purine nucleoside phosphorylase, giving an intense signal at 360 nm.

4.5. The undecaprenyl pyrophosphate phosphatase coupling enzyme for undecaprenyl pyrophosphate production

4.5.1. Selection of the undecaprenyl pyrophosphate phosphatase

A number of undecaprenyl pyrophosphate phosphatases have been identified in *E. coli* including UppP, YbjG, YeiU and PgpB, having the essential role of undecaprenyl phosphate regeneration (Tatar *et al.*, 2007). Touzé *et al*. (2008) have kinetically characterised the phosphatase-specific activity of *E. coli* PgpB *in vitro*. For this reason, *E. coli* PgpB was the employed undecaprenyl pyrophosphate phosphatase in the assays.

4.5.2. Expression and purification of PgpB

The expression construct pTrcHis60::*pgpB* (IPTG-inducible; encoding ampicillin resistance) was a gift from T. Touzé (Université Paris-Sud), which encodes a recombinant protein of wild-type *E. coli* PgpB (an integral membrane protein with six transmembrane-spanning helices) with a C-terminal hexa-histidine tag (denoted PgpB). Following the experimental procedures for protein expression as detailed by Touzé *et al.* (2008), the over-expression of PgpB was not apparent. Therefore, a novel method for PgpB over-expression was developed.

PgpB was expressed in *E. coli* BL21 (DE3) under 0.5 mM IPTG induction (Section 2.4.1.1). Following induction, the cells were cultured at 10°C for 48 h (supplemented with ampicillin after the first 24 h) prior to cell harvesting.

The target protein was extracted from the *E. coli* membranes and purified using the generalised method of IMAC described in Section 2.5.5 with specific alterations. Given the low yield of PgpB over-expression, PgpB was purified from the membranes extracted from 2 L culture (as opposed to 1 L). The protein was purified by IMAC in the buffer: 1 × PBS, 0.1% (w/v) DDM, pH 7.6 supplemented with 0.75 M NaCl (Figure 4.5a).

Following IMAC, the fractions containing PgpB at the highest level of purity were combined and subjected to size exclusion chromatography (Section 2.5.5.3) to further purify PgpB and to remove any aggregated material. The chromatogram and the final purity of PgpB are demonstrated in Figure 4.5b and c. PgpB was stored in 50 % (v/v) glycerol at -20°C; enzymes stored at -80°C were inactive.

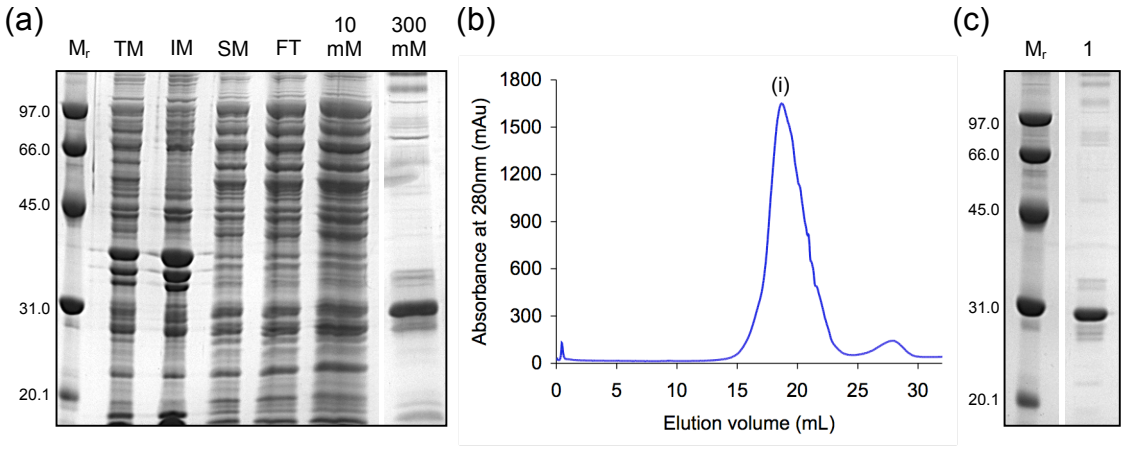

Figure 4.5: Purification of *E. coli* PgpB by immobilised metal chelate affinity chromatography and size exclusion chromatography. (a) 12 % SDS-PAGE Coomassie-stained gel analysis of the extraction of PgpB from the membrane cellular fraction and IMAC purification. M_r, molecular weight markers (kDa); lane TM, total membrane fraction; lane IM, membrane proteins remaining insoluble following detergent treatment; lane SM, detergent-solubilised membrane proteins prior to incubation with IMAC resin; lane FT, flow-through; lanes 10 mM and 300 mM, buffer with 10 mM and 300 mM imidazole respectively. (b) Chromatogram of size exclusion chromatography using the Superose 6 10/300 GL column. The peak (i) identifies the elution of PgpB. (c) 12 % SDS-PAGE Coomassie-stained gel analysis of the purity of the final product of PgpB purification. M_r, molecular weight markers (kDa); lane 1, purity of PgpB following IMAC and size exclusion chromatography with an expected molecular weight of 30.3 kDa.

4.5.3. Preliminary characterisations of *E. coli* PgpB phosphatase activity

A prerequisite to the development of the discontinuous coupled assays for monitoring transglycosylation was to establish the suitability of PgpB as an undecaprenyl pyrophosphate phosphatase *in vitro*. A continuous spectrophotometric assay, outlined in Section 2.8.1.1, was evaluated to ensure P_i release was dependent on the presence of all assay components, specifically PgpB and undecaprenyl

pyrophosphate (the natural substrate of PgpB). Control reactions monitoring the activity of PgpB with undecaprenyl phosphate (product of PgpB activity) and Lys-Lipid II (substrate of the transglycosylases) was also assessed, to confirm that these compounds were not substrates of PgpB and did not interfere with PgpB-catalysed dephosphorylation of undecaprenyl pyrophosphate. To ensure a false positive signal was not produced, P_i was absent from all reaction buffers. Figure 4.6 shows the continuous spectrophotometric time course, displaying the results of these analyses.

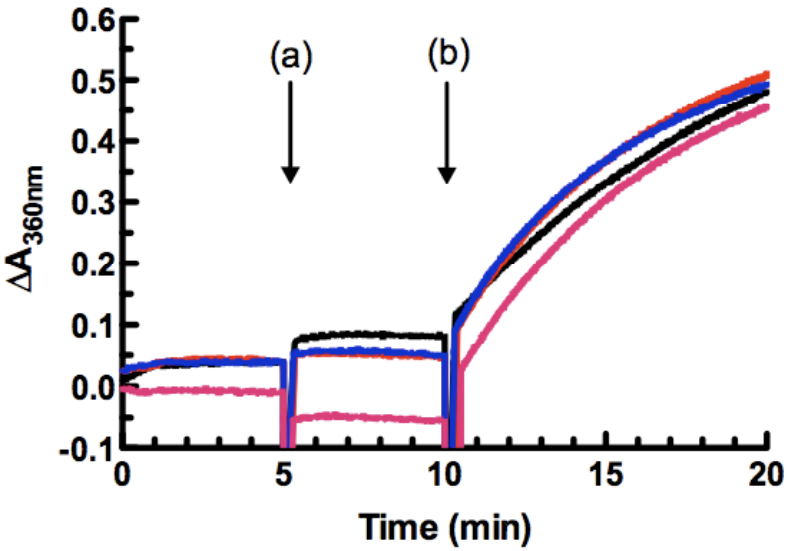

Line	Assay components present at time 0 min	Assay component added at point (a)	Assay component added at point (b)
———	P_i detection reagents	PgpB	Undecaprenyl pyrophosphate
———	P_i detection reagents	Undecaprenyl pyrophosphate	PgpB
———	P_i detection reagents, PgpB	Lys-Lipid II	Undecaprenyl pyrophosphate
———	P_i detection reagents, PgpB	Undecaprenyl phosphate	Undecaprenyl pyrophosphate

Figure 4.6: A continuous spectrophotometric time course for *E. coli* PgpB dependent dephosphorylation of undecaprenyl pyrophosphate measured by P_i release. The table describes the assay components present at time 0 min, and at points of addition (a) and (b). The P_i detection reagents are 1 unit PNP and 400 µM MESG. The final concentration of PgpB in each assay was constantly 1.78 µM. A final concentration of 200 µM of undecaprenyl pyrophosphate, undecaprenyl phosphate or Lys-Lipid II was added to the assays.

Figure 4.6 conclusively demonstrates that P_i release was dependent on the presence of both PgpB and its natural substrate, undecaprenyl pyrophosphate. The presence of Lys-Lipid II or undecaprenyl phosphate had no adverse effect on PgpB activity *in vitro* (e.g. product inhibition). The findings of Touzé *et al.* (2008) were confirmed: undecaprenyl phosphate was not a substrate of PgpB. This signifies that PgpB generates one P_i for every turnover of undecaprenyl pyrophosphate, important information for the calculating kinetic rates from the P_i-dependent changes in absorbance.

4.5.4. Kinetics of dependence of *E. coli* PgpB on undecaprenyl pyrophosphate

The rates of PgpB-specific activity have previously been analysed with a variety of substrates (Touzé *et al.*, 2008). Despite this, the phosphatase activity of PgpB was kinetically characterised with its natural substrate in the assay system described in Section 2.8.1.1, where an alternative P_i detection system was employed compared to that published in literature (see Touzé *et al.* (2008)). Various concentrations of undecaprenyl pyrophosphate were added to the reactions, which were initiated by the addition PgpB to a final concentration of 1.78 μM. Assays were performed in duplicate at each substrate concentration.

The kinetic profile of PgpB with undecaprenyl pyrophosphate is displayed in Figure 4.7. There is a hyperbolic relationship between the initial enzyme velocity (v_0) and the substrate concentration, enabling the data to be fitted to the Michaelis-Menten equation (Equation 1) (Appendix B1) to determine k_{cat} and K_m by non-linear regression.

Equation 1

$$v_0 = \frac{V_{max}[S]}{K_m + [S]}$$

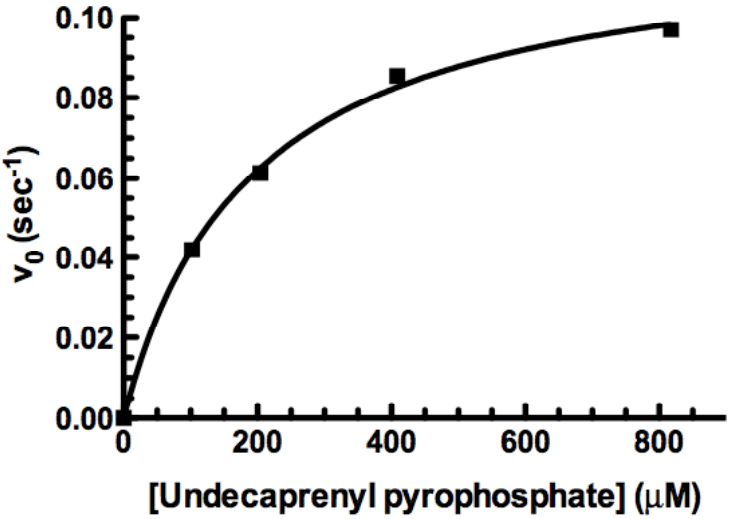

Figure 4.7: Kinetics of dependence of *E. coli* PgpB phosphatase activity with its natural substrate. Average initial velocity (based on two data sets) of PgpB-dependent P_i release is plotted versus [undecaprenyl pyrophosphate]. The R^2 value is 0.99, signifying the data was well-fitted to the Michaelis-Menten equation.

The kinetic parameters of PgpB-dependent P_i release are presented in Table 4.2.

Substrate	Kinetic constants		
	K_m[a] (μM)	k_{cat}[a] (min^{-1})	k_{cat}/K_m ($s^{-1}M^{-1}$)
Undecaprenyl pyrophosphate	191.90±17.23	7.29±0.23	633.14

Table 4.2: Kinetic constants of *E. coli* PgpB catalysed P_i hydrolysis from undecaprenyl pyrophosphate. PgpB-dependent dephosphorylation was monitored by the change in absorbance at 360 nm using the assay described in Section 2.8.1.1. The data was fitted to Equation 1 by non-linear regression, enabling kinetic constants to be derived. [a]Values ± standard error of duplicate reactions.

The activity of PgpB is significantly enhanced in the presence of phospholipids. The phospholipids are proposed to influence the arrangement of undecaprenyl pyrophosphate within a micelle, presenting it as a better substrate, as opposed to directly stimulating the enzyme (Touzé *et al.*, 2008). Reproduction of these findings was trialled with the phospholipids cardiolipin and phosphatidyl glycerol, under the same assay conditions described in Section 2.8.1.1. The presence of 1 mM cardiolipin or 1 mM phosphatidyl glycerol improved the rate by approximately 5-fold, a result similar those published (5.4-fold and 5.2-fold increase respectively) (Touzé *et al.*, 2008). In combination, the effect of cardiolipin and phosphatidyl glycerol was additive. These have future implications for the development of a continuous spectrophotometric assay for transglycosylation (Section 4.13.7).

4.6. Establishing the protocol of the discontinuous spectrophotometric assay for transglycosylation detection

4.6.1. Experimental parameters dictated by the MGT control enzyme

To establish whether the discontinuous PgpB-coupled assay is a plausible method for monitoring transglycosylase activity, the activity of the control enzyme, MGT, was assessed. The assay conditions were designed to maintain MGT in a stable state. MGT relied on a high [NaCl] or [detergent] to remain soluble; 0.1% (w/v) DDM was included in the discontinuous assay. MGT was unstable (signified by precipitation) at temperatures approaching 30°C; the discontinuous assays were performed at 20°C.

4.6.2. Experimental design

The details of the discontinuous-coupled continuous assays are described in Section 2.8.1.2. The basic reaction buffer was comprised of 20 mM Tris, 10 mM $MgCl_2$, 0.1% (w/v) DDM, pH 8.0. Lys-Lipid II (synthesis described in Section 2.7.3), the transglycosylase substrate, was present at concentrations varying between 0-1.47 mM. Addition of the transglycosylase initiated the reactions, which were performed at 20ºC. The reaction was stopped by heat denaturation at 60ºC for 10 min. The insoluble material was pelleted by centrifugation. A fraction of the total reaction volume was added to the continuous spectrophotometric assay components (20 mM Tris, 150 mM NaCl, 0.1 % (w/v) DDM, 1 unit PNP and 400 µM MESG, pH 7.5) where any P_i present in the sample (originating from the Lys-Lipid preparation) would be immediately eliminated. A baseline absorbance was monitored at 360 nm prior to the addition of PgpB to a final concentration of 4.4 µM. The activity of PgpB was recorded until a plateau was reached. The total change in absorbance between the baseline and plateau represented the total PgpB-dependent P_i release from undecaprenyl pyrophosphate, which in turn, signified the total undecaprenyl pyrophosphate produced by MGT-dependent transglycosylation.

4.6.3. Derivation of kinetic constants

In vitro, transglycosylases perform *de novo* synthesis of glycan chains and require two Lipid II substrate molecules to bind into the active site as described by Scheme 2.

Scheme 2

$$[E]+[S] \overset{K_{m1}}{\rightleftharpoons} [ES] \underset{-[S]}{\overset{K_{m2}}{\overset{+[S]}{\rightleftharpoons}}} [ES_2] \xrightarrow{k_{cat}} [E]+[P]$$

A kinetic equation (Equation 2) can be derived from Scheme 2 (Appendix B2) on the assumption that rapid equilibrium kinetics exist and that K_{m1} and K_{m2} are equilibrium constants. It is also assumed that the substrate remains unchanged over the initial rate measurements, which are based on the formation of Lipid IV from two molecules of Lipid II.

Equation 2

$$v_0 = \frac{V_{max}[S]^2}{K_{m1}K_{m2} + K_{m2}[S] + [S]^2}$$

4.7. Characterisation of MGT transglycosylase activity using the discontinuous spectrophotometric assay

4.7.1. Initial trials to determine transglycosylase activity

The assay system outlined in Sections 4.6.2 was used to analyse MGT and MGT-E100Q transglycosylation activity, establishing it as a suitable method for the discontinuous detection of Lipid II polymerisation. Figure 4.8 displays the continuous spectrophotometric time course of PgpB-dependent P_i release in the presence of the discontinued transglycosylation reactions of MGT and MGT-E100Q. The results conclusively show that the reaction of MGT with Lys-Lipid II led to the generation of undecaprenyl pyrophosphate, the substrate for PgpB-dependent P_i release, indicating transglycosylation had occurred. Conversely, MGT-E100Q did not exhibit any transglycosylation activity, signified by the absence of PgpB activity in the continuous assay.

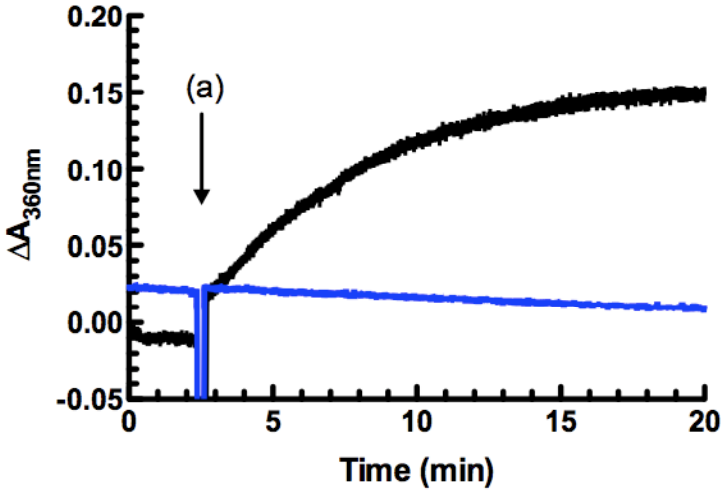

Figure 4.8: A continuous spectrophotometric time course for PgpB-dependent P_i release from MGT-generated undecaprenyl pyrophosphate. At 0 min, all reaction components, including the discontinued transglycosylation reactions of MGT (——) and MGT-E100Q (——), were present, with the exception of PgpB, which initiated the dephosphorylation of undecaprenyl pyrophosphate at point (a). The transglycosylase was present at a final concentration of 155 µM in the discontinuous assays with 0.67 mM Lipid II. The discontinuous assays were performed at 20°C for 6 min.

This initial characterisation of MGT and MGT-E100Q confirmed the findings of Terrak and Nguyen-Distèche (2006): MGT is capable of using a substrate that differentiates from the natural at the pentapeptide stem (*S. aureus* Lipid II has a pentaglycine branch); the glutamate at residue 100 is important for the catalytic activity of MGT.

4.7.2. Generation of a time-dependent profile for MGT transglycosylation.

At a fixed concentration of enzyme and substrate, a time-course of MGT activity was established, displayed in Figure 4.9. Following the protocol outlined in Section 4.6.2, a discontinuous assay of MGT activity was initiated with sampling at discrete time points. The undecaprenyl pyrophosphate generated from the MGT-dependent transglycosylation reactions was quantified using the continuous spectrophotometric assay.

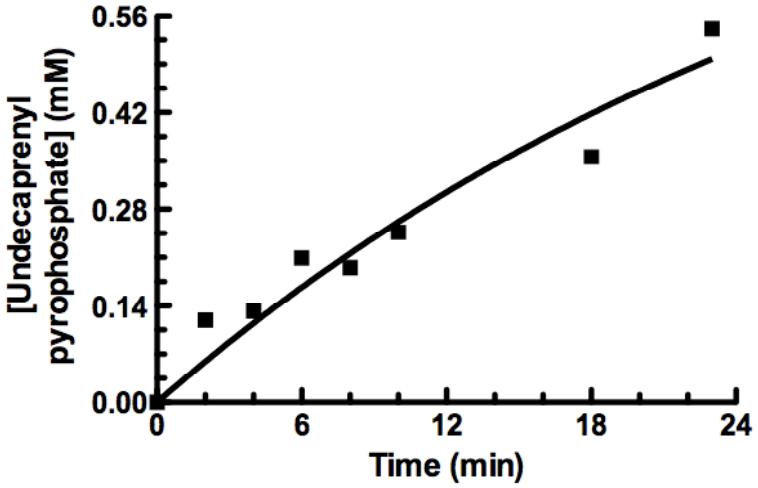

Figure 4.9: Time-dependent undecaprenyl pyrophosphate release reaction profile of MGT-catalysed transglycosylation. Following the defined time point sampling of the transglycosylation reactions, quantification of undecaprenyl pyrophosphate via PgpB-dependent P_i release provided an indirect measurement of MGT activity. MGT and Lipid II concentrations were constant at 155 µM and 0.67 mM respectively in the discontinuous assays. The profile was generated based on duplicated reactions. [Undecaprenyl pyrophosphate] relates to the concentration in the discontinuous assay.

Over the specified time-course, the initial rate of undecaprenyl pyrophosphate production was linear, representing the steady-state phase of the reaction. The reaction was approaching, but did not reach completion, signified by the curvature of the line fitted towards the production of 0.56 mM undecaprenyl pyrophosphate at 24 min.

Determination of the steady-state phase of MGT-dependent undecaprenyl pyrophosphate release was the preliminary stage towards the kinetic characterisation of MGT activity.

4.7.3. Establishing the kinetic profile of MGT using the discontinuous-coupled spectrophotometric assay

The kinetic parameters of MGT-dependent undecaprenyl pyrophosphate generation were investigated. The reactions were performed with different concentrations of the Lys-Lipid II substrate, according to the protocol described in Section 2.8.1.2.1. An end time point of 8 min (situated in the steady-state phase, Figure 4.9) was employed. Figure 4.10a and b display the relationship between MGT activity and Lipid II concentration and the Lineweaver-Burk plot respectively, taken from the

data set of one day. The dependence of MGT velocity on substrate concentration exhibited day-to-day variation but with the same general trend: at low Lipid II concentrations there was a sigmoidal dependence on Lipid II and at high Lipid II concentrations the transglycosylase became inhibited.

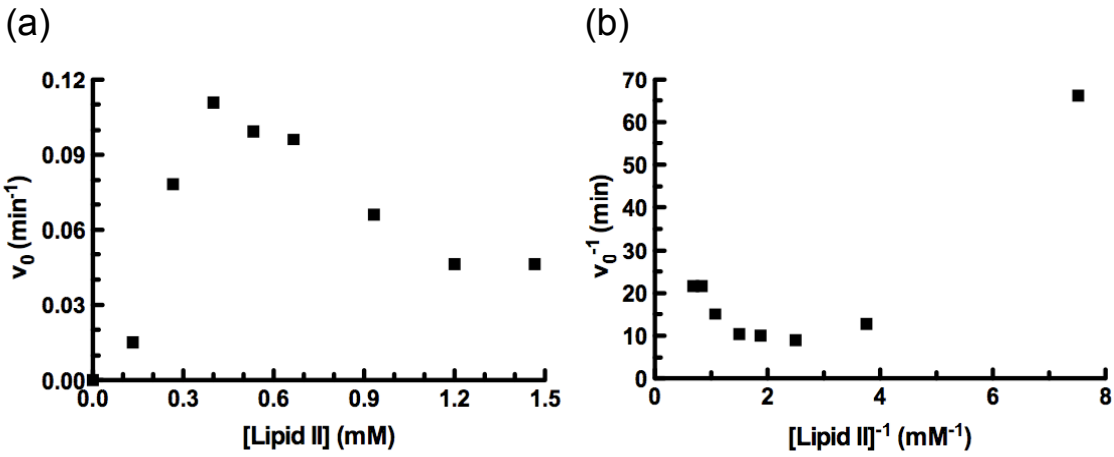

Figure 4.10: Kinetics of Lipid II dependence of *S. aureus* MGT transglycosylase activity. (a) Initial velocity of MGT-dependent undecaprenyl pyrophosphate release (v_0) plotted versus [Lys-Lipid II]. (b) Lineweaver-Burk plot of the data from (a). [MGT] was present at 155 μM. At each substrate concentration, the initial velocity determinations were performed in duplicate.

The data in Figure 4.10 could not be fitted to Equation 2 due to the severe susceptibility to substrate inhibition displayed by MGT, thus kinetic constants could not be determined. A model for MGT activity is described in Section 4.13.2.2 and from this, a kinetic equation has been derived to endeavour to establish the kinetic parameters.

4.7.4. Investigating the effect of Lipid I on MGT activity

MGT is known to catalyse the transglycosylation of Lipid II to form a polymerised glycan chain (Terrak and Nguyen-Distèche, 2006). The stereochemistry of Lipid II indicates that Lipid I, lacking the Glc*N*Ac component of Lipid II, should not be a suitable substrate. This is demonstrated in Figure 4.11, where the formation of a β-1,4-glycosidic bond would enforce a constrained conformation, given the requirement of the lipid chains to be situated in the membrane. However, if Lipid I were to reach the active site of MGT, what would be the consequence of this interaction? This was investigated in a single experiment.

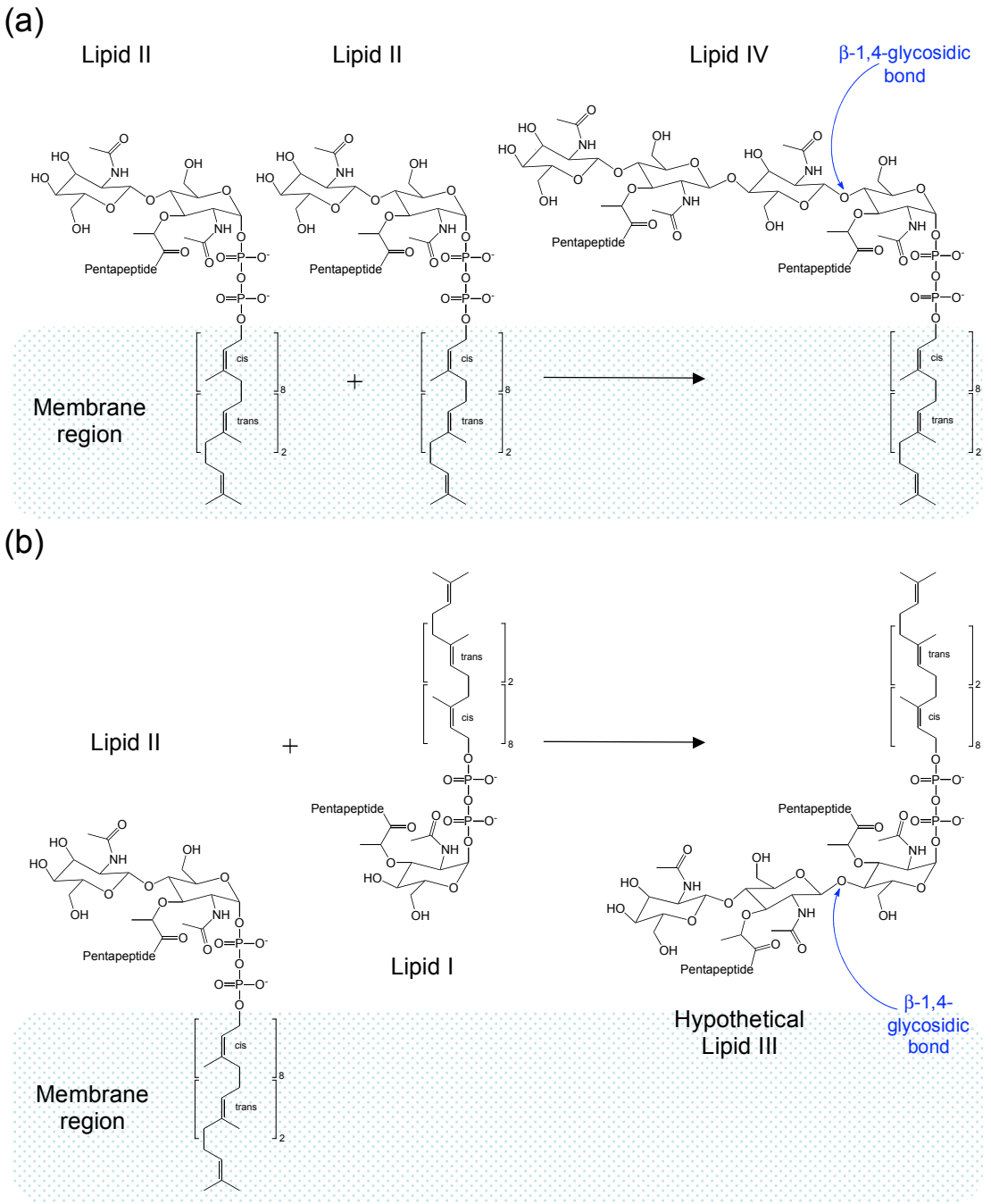

Figure 4.11: The stereochemistry of Lipid I and Lipid II transglycosylation. (a) The formation of a β-1,4-glycosidic bond between the Mur*N*Ac and Glc*N*Ac moieties of adjacent Lipid II molecules. This bond conformation ensures the synthesis of straight glycan chains. (b) The formation of a β-1,4-glycosidic bond between the Mur*N*Ac moiety of adjacent Lipid II and Lipid I molecules. As depicted in the figure, in order for this bond to occur, the lipid anchor of Lipid I would need to be positioned in an opposite plane to the membrane containing Lipid II. The conformational constraints are likely to prevent this reaction from occurring.

In two parallel experiments, 275 µM MGT was incubated for 20 min at 20°C with and without 2.96 mM Lys-Lipid I. Addition of Lys-Lipid II to a final concentration of 0.33 mM initiated the reactions, adjusting the MGT and Lys-Lipid I to final concentrations of 155 µM and 1.67 mM respectively, making the Lipid I concentration 5-fold greater than the Lys-Lipid II concentration. Aliquots were sampled at time points of 0, 10, 20 and 30 min to assess for transglycosylase activity following the protocol established in Section 2.8.1.2. It was previously established that Lys-Lipid I did not impede PgpB activity. Figure 4.12 displays the time course of MGT activity in the presence and absence of Lys-Lipid I.

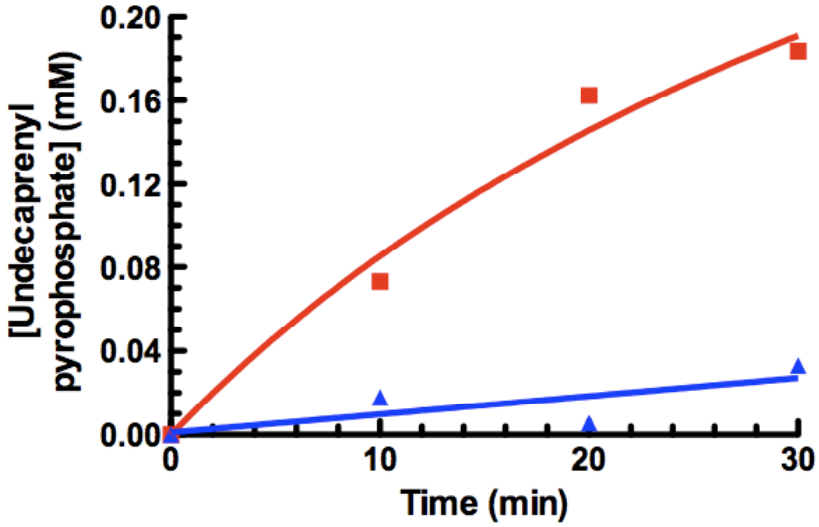

Figure 4.12: The interference of Lys-Lipid I with MGT-catalysed release of undecaprenyl pyrophosphate from Lys-Lipid II. A time-course of MGT activity with 0.33 mM Lys-Lipid II, in the presence (—) and absence (—) of a pre-incubation with Lys-Lipid I (to a final concentration of 1.67 mM in the reaction). Reaction profile generated based on duplicate reactions.

Figure 4.12 clearly demonstrates that in the presence of Lys-Lipid I, MGT transglycosylation was inhibited. This is likely to be a result of competitive inhibition, where the Lipid I and Lipid II would be competing for the same site of MGT, given the similarities in their structures. The results also demonstrate that Lys-Lipid I is not a suitable substrate. If it were, at the point of Lys-Lipid II addition at 0 min, the generation of undecaprenyl pyrophosphate would have been evident.

4.8. The characterisation of the bifunctional *S. pneumoniae* PBP1a transglycosylase activity

The *in vitro* activities of the transglycosylase domains of various Class A PBPs have been well characterised, kinetically and structurally, with and without the N-terminal membrane anchor (*E. coli* PBP1b for example (Schwartz *et al.*, 2002; Sung *et al.*, 2009; Terrak *et al.*, 1999)). However, the characterisation of the Class A *S. pneumoniae* PBP1a has proved a greater challenge. In the following sections, the *in vitro* activity of the full-length PBP1a transglycosylase domain is revealed, and the kinetic parameters are investigated.

4.8.1. Establishment of *S. pneumoniae* PBP1a transglycosylase activity

The assay outlined in Section 2.8.1.2 for the discontinuous-coupled spectrophotometric detection of undecaprenyl pyrophosphate release was applied to assess the activity of PBP1a, PBP1a-Δ30 (devoid of the membrane anchor) and PBP1a-E91Q (mutation of the glutamate in the first conserved transglycosylase motif to glutamine, analogous to the MGT-E100Q mutation). The discontinuous transglycosylase reactions were performed and analysed for the presence of undecaprenyl pyrophosphate in the continuous spectrophotometric assay. The rate of PBP1a-dependent transglycosylation was immediately identified as being extremely slow, where long incubations (on an hour timescale) were necessary for significant levels of undecaprenyl pyrophosphate release. Figure 4.13 displays the continuous time course of PgpB-dependent P_i release from undecaprenyl pyrophosphate, which was generated by transglycosylation reactions of PBP1a variants in the discontinuous assays.

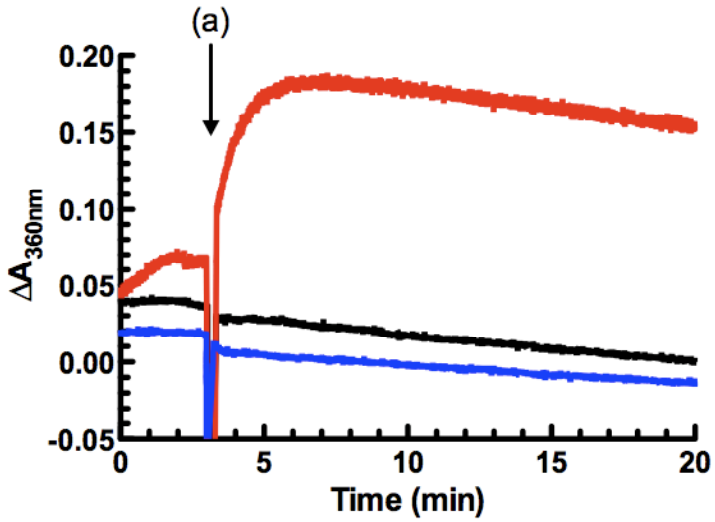

Figure 4.13: Continuous spectrophotometric time course of PgpB-dependent P_i release from PBP1a-generated undecaprenyl pyrophosphate. The discontinuous reactions were performed over a 3 h time period at 20°C in the presence of 77 µM enzyme and 0.56 mM Lys-Lipid II. The transglycosylase activities of PBP1a (—), PBP1a-Δ30 (—) and PBP1a-E91Q (—) were determined, where at time 0 min, all assay components (including the discontinuous transglycosylation reaction) were present with the exception of PgpB, which was added at time (a) to initiate the dephosphorylation of undecaprenyl pyrophosphate, a product of transglycosylase activity.

Figure 4.13 conclusively demonstrates the transglycosylase activity of PBP1a, which was not an artefact of the assay. PBP1a-E91Q did not exhibit any transglycosylase activity, an expected result given the mutation of an essential glutamate residue in the transglycosylase active site. PBP1a-Δ30 did not show evidence of transglycosylase activity, signifying that the removal of 30 amino acid residues from the N-terminal of PBP1a had a detrimental effect on transglycosylase activity.

4.8.2. Establishment of a discontinuous time course for *S. pneumoniae* PBP1a-dependent transglycosylase activity

A time-dependent profile of PBP1a transglycosylase activity was established after ensuring that the generation of undecaprenyl pyrophosphate did not impose product inhibition. The discontinuous assays were performed according to Section 2.8.1.2. The ability of two different detergents to facilitate transglycosylase activity were evaluated in the reaction buffer: 0.5 % (w/v) CHAPS and 0.1% (w/v) DDM. Aliquots of the reaction were sampled on an hourly basis. Figure 4.14 displays the time-course of PBP1a activity in the two different experiments.

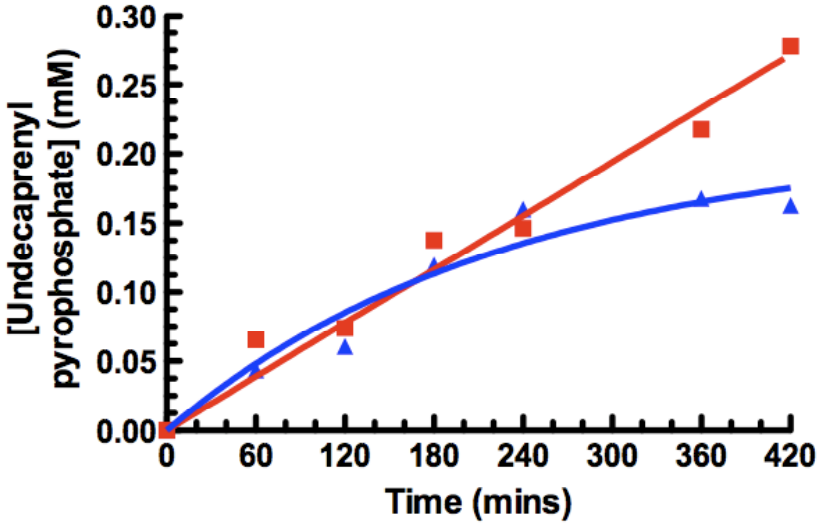

Figure 4.14: A discontinuous time-dependent profile of PBP1a transglycosylase activity. A reaction between Lys-Lipid II (0.56 mM) and PBP1a (77 µM) was sampled at defined time points and the undecaprenyl pyrophosphate produced was quantified. The time courses were determined from duplicate discontinuous assays in buffer that differed by the presence of either 0.5 % (w/v) CHAPS (—) or 0.1 % (w/v) DDM (—).

From the transglycosylase time-course (Figure 4.14), the reaction of PBP1a with Lys-Lipid II (in buffers containing both detergents) did not reach completion (discussed in Section 4.13.3.1). PBP1a was purified in the presence of 0.03 % (w/v) DDM and the detergent used in the reaction buffer was additional. The plateau of transglycosylase activity appearing towards the 6 h incubation in the presence of the CHAPS detergent signified the gradual inactivation of PBP1a, probably a result of detergent-imposed aggregation. PBP1a exhibited a steady state of activity in the presence of DDM over the entire time course. Consequently, DDM was the detergent used in future experiments. The time course conclusively demonstrates that under the specified assay conditions, the rate of PBP1a transglycosylation was extremely slow, which will be addressed in subsequent sections.

4.8.3. Kinetic characterisation of the transglycosylase activity of *S. pneumoniae* PBP1a

The kinetics of PBP1a transglycosylase activity were investigated using the established protocol described in Section 2.8.1.2. The enzyme concentration was held constant at 77 μM, with the Lys-Lipid II concentration ranging from 0-1.11 mM. The discontinuous assays were stopped after a 3 h incubation (time point in the steady state phase, Figure 4.14) and the total undecaprenyl pyrophosphate generated was established. Figure 4.15 shows the kinetic profile of PBP1a.

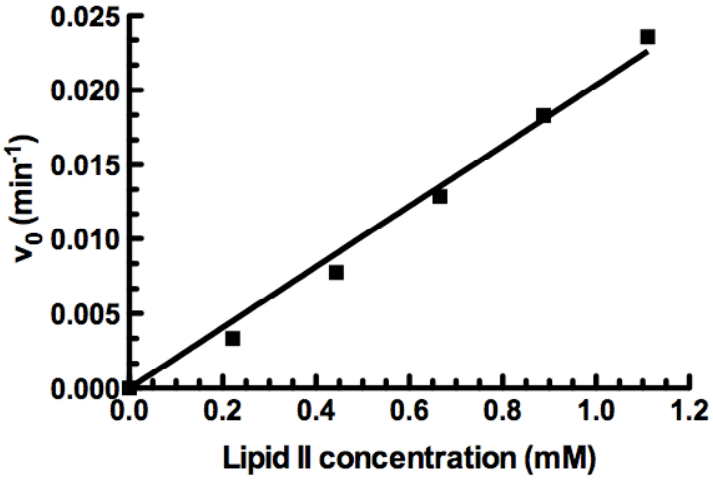

Figure 4.15: Kinetics of Lipid II dependence on *S. pneumoniae* PBP1a transglycosylase activity. Initial velocity of PBP1a-dependent undecaprenyl pyrophosphate release (v_0) plotted versus [Lys-Lipid II]. [PBP1a] was present at 77 μM. At each substrate concentration, the initial velocity determinations were performed in duplicate.

Figure 4.15 clearly demonstrates that the maximum concentration of Lipid II used was insufficient to even begin to saturate the enzyme. This prevented the fitting of Equation 2 to the data. As a consequence, the kinetic parameters, K_{m1}, K_{m2} and k_{cat}, could not be derived.

The relationship between velocity versus substrate concentration shows no significant deviation from linearity. This observation could be rationalised in two ways. The first, it could be assumed that K_{m2} was much greater than K_{m1}, thus the relationship would obey the Michaelis-Menten equation (detailed in Appendix B2). The second, Equation 2 has been derived based on the assumption that initial rates of

transglycosylation were being measured, where two molecules of Lipid II were required to bind to the active site, and that the generation of the transglycosylase product, Lipid IV, was the rate limiting step (Scheme 2). If it were assumed that the rate-limiting step was before the binding of the second Lipid II substrate, the kinetics of transglycosylation would also obey the Michaelis-Menten equation (Appendix B2 for details). Given the apparent linear relationship between velocity and substrate concentration and that there was no evidence for the approach of V_{max}, it can be further assumed that the K_m was much greater than the substrate concentrations tested. Thus, both explanations would obey Equation 3.

Equation 3

$$v_0 = \frac{V_{max}[S]}{K_m}$$

The gradient of the linear region (Figure 4.15) is equal to k_{cat}/K_m, giving a value of 0.34 $s^{-1}M^{-1}$.

4.9. Optimisation of *S. aureus* MGT and *S. pneumoniae* PBP1a transglycosylase assay conditions

The assay conditions for monitoring transglycosylase activity were basic and not optimised to enhance the transglycosylation activity of MGT and PBP1a. Consequently, the rates observed would not be fast enough to be physiologically relevant. Various parameters were therefore investigated to enhance the turnover of substrates.

4.9.1. Establishing the effect of temperature on transglycosylation activity

The temperature selected to perform the assays was based on the denaturation of MGT at temperatures reaching 30°C. PBP1a was stable at higher temperatures and its transglycosylase activity was compared at 20°C and 37°C. At the higher temperature, PBP1a activity was not enhanced.

4.9.2. The effect of metal ions on transglycosylase activity

It has been established that metal ions are essential for transglycosylase activity in PBPs and MGTs: in the presence of EDTA, the transglycosylase activity is abolished (Schwartz *et al.*, 2002; Terrak and Nguyen-Distèche, 2006). Terrak and Nguyen-Distèche (2006) have shown the stimulation of MGT transglycosylase activity with different concentrations of metal ions. Schwartz *et al.* (2002) have demonstrated the effect of various metal ions on the activity of the bifunctional *E. coli* PBP1b, and revealed that the presence of 10 mM $CaCl_2$ enhances *E. coli* PBP1b transglycosylation by 6-fold compared to the $MgCl_2$ standard. The rates of MGT and PBP1a-dependent transglycosylation were analysed (using the assay described in Section 2.8.1.2) in the presence of 10 mM $MgCl_2$ and $CaCl_2$. The observed and relative rates are displayed in Table 4.3.

Enzyme	Metal ion	v_{obs} (nmol/min/mg)	k_{rel}
MGT	Mg^{2+}	3.19	1
	Ca^{2+}	5.65	1.8
PBP1a	Mg^{2+}	7.85×10^{-2}	1
	Ca^{2+}	5.61×10^{-2}	0.7

Table 4.3: Relative rates of MGT and PBP1a catalysed transglycosylation in the presence of different metal ions. MGT and PBP1a transglycosylation reactions were performed for 10 min and 3 h respectively. 10 mM $MgCl_2$ or $CaCl_2$ substituted the metal ion present in the transglycosylase buffer (Section 2.8.1.2.1). Following the incubations, the undecaprenyl pyrophosphate generated was determined using the spectrophotometric assay. The rates observed (v_{obs}) and the relative rate constants (k_{rel}) (with reference to Mg^{2+}) are shown. The rates are based on duplicated discontinuous reactions.

The results show that MGT-dependent transglycosylase activity was enhanced almost 2-fold in the presence of Ca^{2+} compared to Mg^{2+}. Terrak and Nguyen-Distèche (2006) also found that MGT activity was marginally enhanced by the presence of Ca^{2+}. Ca^{2+} has an apparent negative influence on the rate of *S. pneumoniae* PBP1a transglycosylase activity. These results show that different transglycosylases have varying sensitivities to metal ions.

4.9.3. Does native peptidoglycan influence *S. aureus* MGT *and S. pneumoniae* PBP1a activity?

It has been documented that Class A PBP transglycosylases, such as *E. coli* PBP1a (Barrett *et al.*, 2007) and PBP1b (Schwartz *et al.*, 2002), exhibit a lag phase. *In vitro*, upon initiation of a transglycosylase reaction, glycan chains do not exist and the enzyme has to perform *de novo* polymerisation of Lipid II forming a short polymeric glycan strand. *In vivo*, however, transglycosylases are 'primed' by a pre-existing polymerised precursor (Schwartz *et al.*, 2002). Therefore, the transglycosylase activities of PBP1a and MGT were assessed in the presence of 0.1 % (w/v) *E. coli* peptidoglycan (prepared by T. Clarke) (using the assay system described in Section 2.8.1.2) to analyse whether existing glycan chains provide a scaffold for elongation. An increase in undecaprenyl pyrophosphate generation was not observed, signifying the transglycosylase activities were not enhanced.

4.9.4. Do the presence of lipids common to the bacterial inner membrane promote MGT and PBP1a transglycosylation?

Given that cardiolipin and phosphatidyl glycerol greatly improve the dephosphorylation activity of the integral membrane protein PgpB, the transglycosylase activity of MGT and PBP1a was assessed in the presence of these lipids, which provide a more membrane-like environment. The discontinuous assays were performed (as in Section 2.8.1.2) with the addition of 1 mM of either cardiolipin or phosphatidyl glycerol. Neither lipid had a positive effect on the rate of MGT or PBP1a transglycosylase activity.

4.9.5. Modulation of transglycosylase activity by additives that enhance the solubility of enzyme and substrate

It has been well established that the detergent octaethylene glycol monodecyl ether (referred to as Decyl PEG) and dimethyl sulfoxide (DMSO) enhance the transglycosylase activity of MGTs and PBPs in aqueous solution (Offant *et al.*, 2010; Schwartz *et al.*, 2002; Terrak and Nguyen-Distèche, 2006). Under these conditions, a membrane-like environment is created, promoting the solubility of substrate and the fusion of substrate and enzyme micelles (Schwartz *et al.*, 2002). Omission of either Decyl PEG or DMSO has been shown to dramatically reduce the transglycosylase activity of MGT (Terrak and Nguyen-Distèche, 2006), indicating their effects are additive. The influence of Decyl PEG and DMSO on the transglycosylase activities of MGT and PBP1a was therefore investigated.

4.9.5.1. Establishing the effects of Decyl PEG and DMSO on *S. aureus* MGT-dependent transglycosylation

The transglycosylation activity of MGT was analysed (using the assay system in Section 2.8.1.2) in the presence of varying concentrations of either Decyl PEG (0-20 × CMC) or DMSO (0-20 % (v/v)). Decyl PEG had a detrimental effect on MGT transglycosylase activity, with inhibition occurring at high concentrations. A similar effect has been documented for *E. coli* PBP1b (Schwartz *et al.*, 2002). DMSO had a positive effect on transglycosylase activity (Figure 4.16a). As it has been documented that MGT requires the presence of both Decyl PEG and DMSO for optimum activity (Terrak and Nguyen-Distèche, 2006), the combined effect of Decyl PEG and DMSO was established; the DMSO concentration providing the greatest level of transglycosylase activity (20 % (v/v)) was assayed with a range of Decyl PEG concentrations (Figure 4.16b).

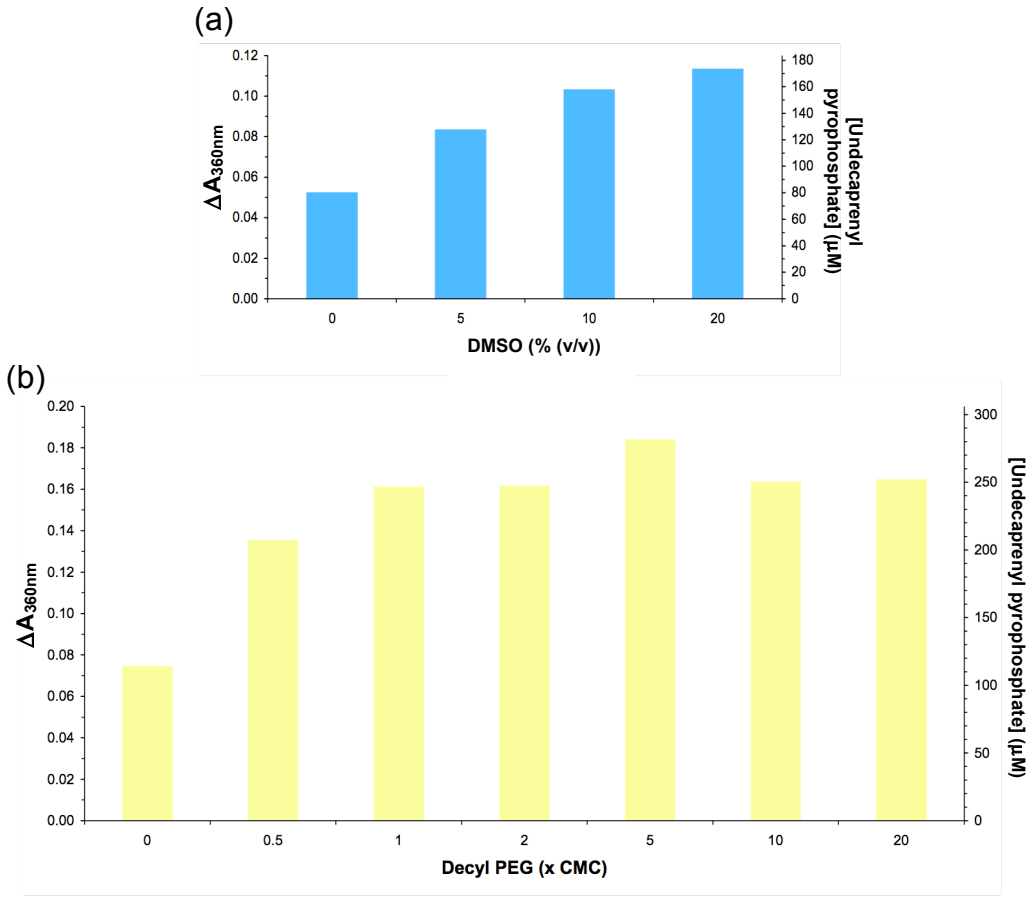

Figure 4.16: Effect of Decyl PEG and DMSO on MGT transglycosylase activity. The discontinuous assay for MGT transglycosylation was performed for 8 min (as in Section 4.7.3) in the presence of the specified concentrations of (a) DMSO (% (v/v)) and (b) Decyl PEG (× CMC) with 20 % (v/v) DMSO. The activities are expressed as the total absorbance change at 360 nm due to P_i release from undecaprenyl pyrophosphate (primary y-axis) and the concentration of undecaprenyl pyrophosphate in the discontinuous assays corresponding to the absorbance change (secondary y-axis). Values represent the mean of duplicate reactions.

Figure 4.16a demonstrates that upon increasing the DMSO concentration in the assays, the rate of MGT activity also increased, signifying that the activity of the enzyme was maintained even at 20 % (v/v) DMSO (the percentage providing optimum activity). Figure 4.16b shows that the transglycosylase activity in assays containing 20 % (v/v) DMSO were further increased by the addition of Decyl PEG, the concentration of which did not significantly influence the transglycosylase rate beyond a concentration of 1 × CMC. The transglycosylation reactions with 20 % (v/v) DMSO (Figure 4.16a) and 20 % (v/v) DMSO with 0 × CMC Decyl PEG (Figure 4.16b) were identical incubations, despite yielding different amounts of undecaprenyl pyrophosphate. This can be attributed to the day-to-day variation in data as previously described (Section 4.7.3), which is discussed in Section 4.13.5.

4.9.5.2. Establishing the effects of Decyl PEG and DMSO on *S. pneumoniae* PBP1a-dependent transglycosylation

The individual effects of Decyl PEG and DMSO on the transglycosylase activity of PBP1a were analysed in a similar manner as described in Section 4.9.5.1 (the effect of Decyl PEG on transglycosylase activity was established in the absence of DMSO). The results are displayed in Figure 4.17.

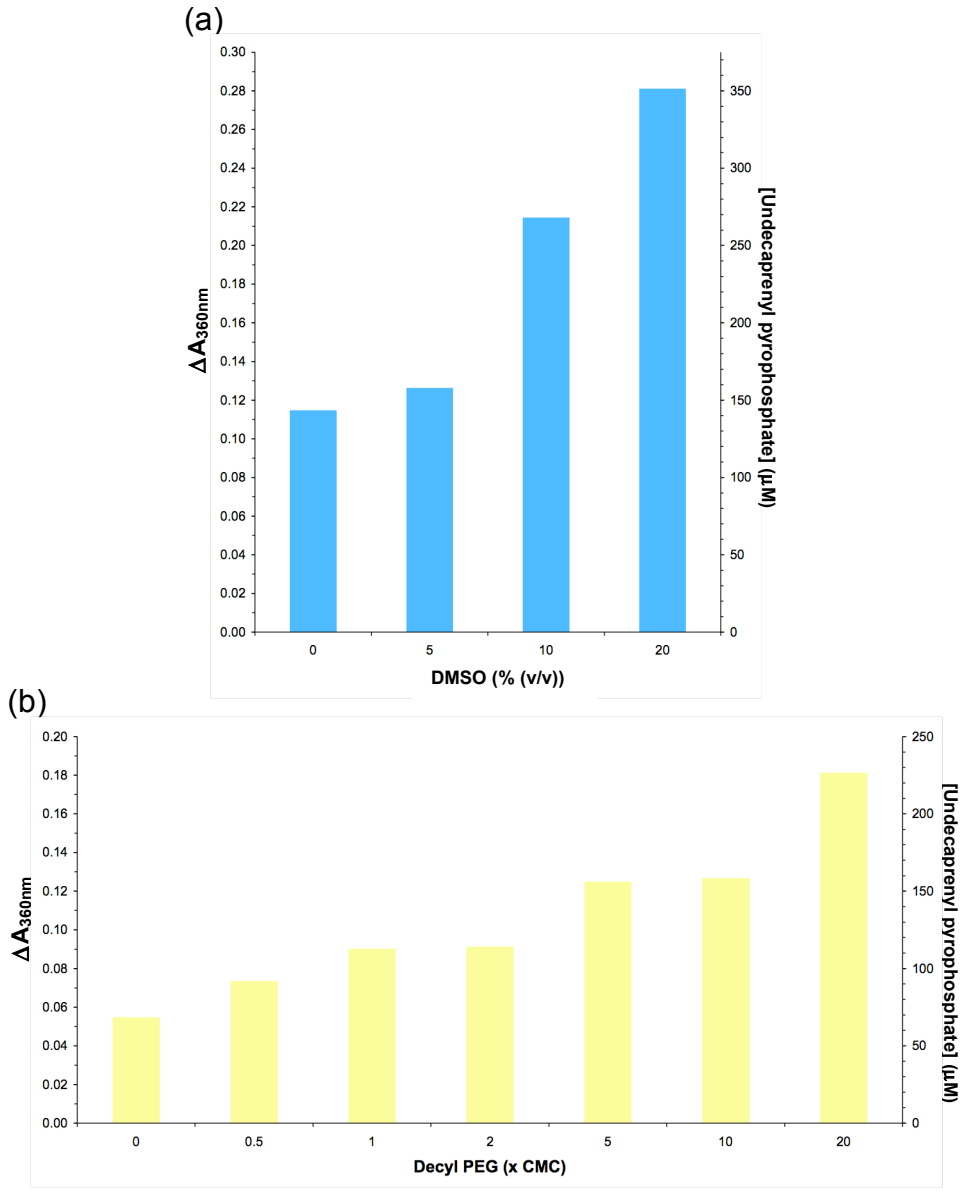

Figure 4.17: Effect of Decyl PEG and DMSO on PBP1a transglycosylase activity. The discontinuous assay for PBP1a transglycosylase activity was performed for 3 h (as in Section 4.8.3) in the presence of the indicated concentrations of (a) DMSO (% (v/v)) and (b) Decyl PEG (× CMC). The primary and secondary y-axes show the total change in absorbance at 360 nm measured using the spectrophotometric assay and the corresponding concentration of undecaprenyl pyrophosphate generated in the discontinuous assays respectively. Values represent the mean of duplicate reactions.

Figure 4.17 demonstrates that with the full-length PBP1a, in contrast to MGT, Decyl PEG (in the absence of DMSO) had a positive effect on the transglycosylase activity, which was optimum at 20 × CMC Decyl PEG (22 mM). This could signify that the detergent enhances the stability of PBP1a via the membrane anchor, a feature that is absent in the MGT construct. PBP1a transglycosylase activity, similar to MGT, concurrently increased with the percentage of DMSO in the assay buffer, with 20 % (v/v) DMSO resulting in maximum activity observed. The cumulated effect of 20 × CMC Decyl PEG and 20 % (v/v) DMSO had a further positive impact on the transglycosylase activity. The amount of DMSO or Decyl PEG required to improve transglycosylase activity appears to be enzyme specific. For example, Offant *et al.* (2010) have found that *Thermotoga maritima* PBP1a-Δ33 transglycosylase activity is optimised in the presence of 2.5-5 × CMC Decyl PEG with 20 % (v/v) DMSO. These concentrations of additives may need further optimisation for the full-length *T. maritima* PBP1a transglycosylase activity.

Based on the parameters varied in the above sections, the optimum assay conditions for *in vitro* PBP1a transglycosylase activity were: 20 mM Tris, 10 mM $MgCl_2$, 0.1 % (w/v) DDM, 22 mM Decyl PEG, 20 % (v/v) DMSO, with a 30 sec sonication upon initiation with enzyme. An identical buffer system can be used for optimum activity of MGT, with the exchange of 10 mM $MgCl_2$ for $CaCl_2$. These conditions can be applied in future analyses to increase the level of transglycosylase activity observed, reducing the amount of limiting enzyme and substrate used and minimising the level of background noise.

4.10. Does the transglycosylase domain of the Class A *S. pneumoniae* PBP1a function independently of the transpeptidase domain?

4.10.1. Transglycosylase activity of PBP1a variants

To investigate the dependency of the transglycosylase activity on a fully functioning transpeptidase domain, the transglycosylase activities of wild-type PBP1a and its corresponding transglycosylase (E91Q) and transpeptidase (S370A) active site mutants were assayed. Discontinuous transglycosylase reactions were performed with the Lys-Lipid II substrate and combinations of enzymes in the optimised buffer system (Section 4.9). The protocol from Section 2.8.1.2 was further modified: total reaction volume, 25 μL; volume of reaction added to the spectrophotometric assay, 20 μL; enzyme concentration, 56 μM; Lys-Lipid II concentration, 0.32 mM. Assays were discontinued after 0 h (to determine background levels) and 2 h. The results are displayed in Figure 4.18, showing the total change in absorbance and the corresponding levels of undecaprenyl pyrophosphate generated.

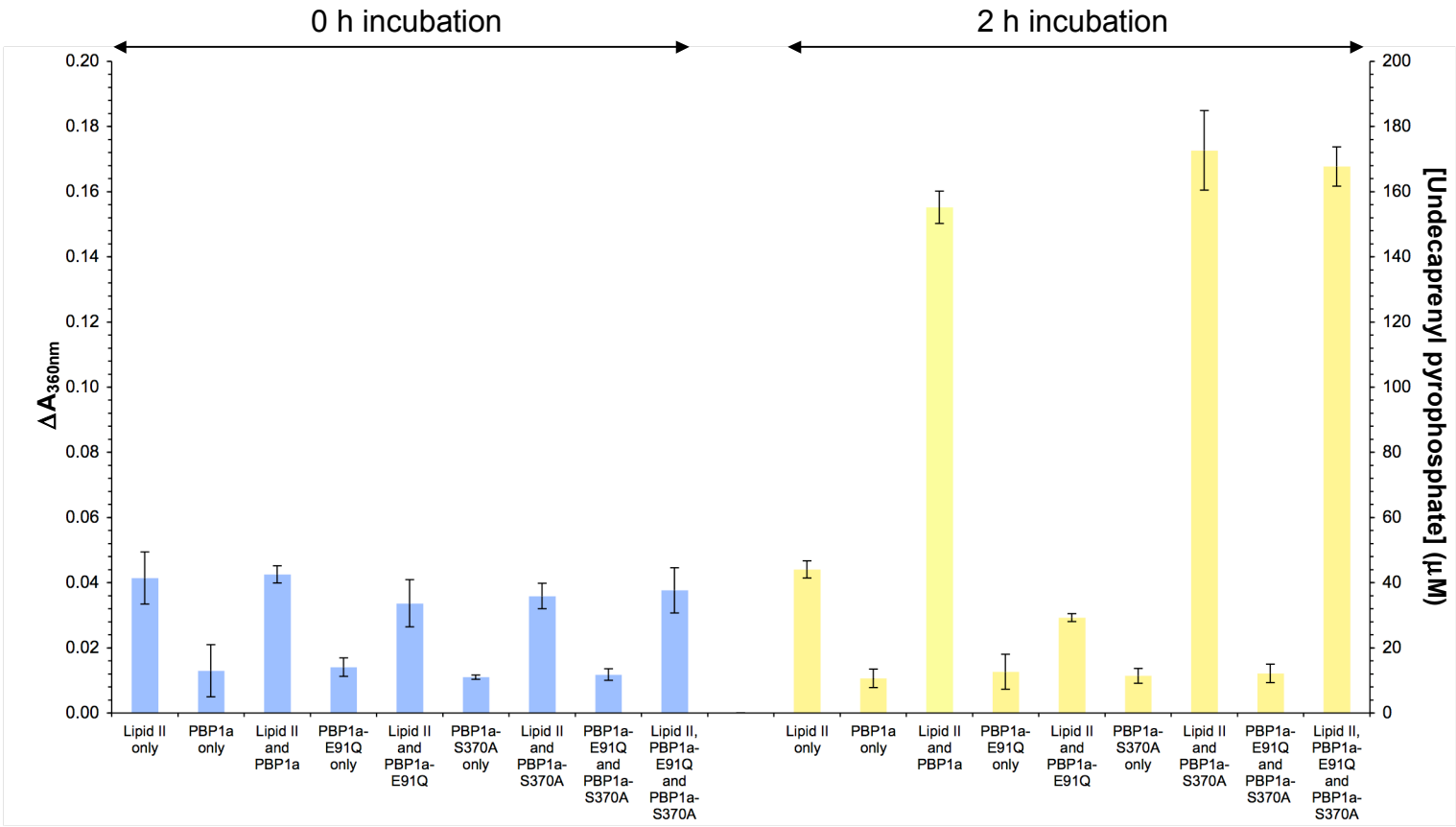

Figure 4.18: The transglycosylase activity of PBP1a variants. The transglycosylase activities of PBP1a, PBP1a-E91Q, PBP1a-S370A and the combined active site mutants were assessed (the reactions are labelled on the x-axis of the Figure, where Lys-Lipid II is abbreviated to Lipid II). The level of undecaprenyl pyrophosphate generated after 0 h (■) and 2 h (■) is displayed in terms of total absorbance change due to PgpB-dependent P_i release following spectrophotometric determinations (primary y-axis) and the corresponding [undecaprenyl pyrophosphate] (μM) in the discontinuous assays (secondary y-axis). Concentrations of each enzyme were equivalent in the reactions. Control reactions comprised of 0 h time points and enzyme only and substrate only incubations. Values represent the mean ± standard deviation of triplicate reactions.

Figure 4.18 clearly identifies that the transglycosylase domain works independently of the transpeptidase domain. The transglycosylase domain of PBP1a-S370A, devoid of an active transpeptidase domain, in the presence or absence of transpeptidation (a product of PBP1a-E91Q activity), exhibited near equivalent levels of activity compared to the wild-type enzyme. At 0 h, the level of activity detected in the enzyme and substrate incubations corresponded to that of the Lipid II only control, where substrate degradation contributed to the presence of undecaprenyl pyrophosphate observed. The enzyme PBP1a-E91Q, with a mutation of an essential transglycosylase active site residue was incapable of transglycosylation as anticipated: the level of undecaprenyl pyrophosphate present was analogous to the Lipid II only control.

4.10.2. Statistical analysis of PBP1a-dependent transglycosylation using Student's two-tailed *t*-test

To determine the statistical significance of the variants of PBP1a-dependent transglycosylation, Student's *t*-test was performed on the data from Section 2.10.1. For clarity of the comparisons, the [undecaprenyl pyrophosphate] produced from the 0 h incubation was subtracted from the level of undecaprenyl pyrophosphate generated after the 2 h incubation, shown in Figure 4.19, where the results from the statistical evaluation are also displayed.

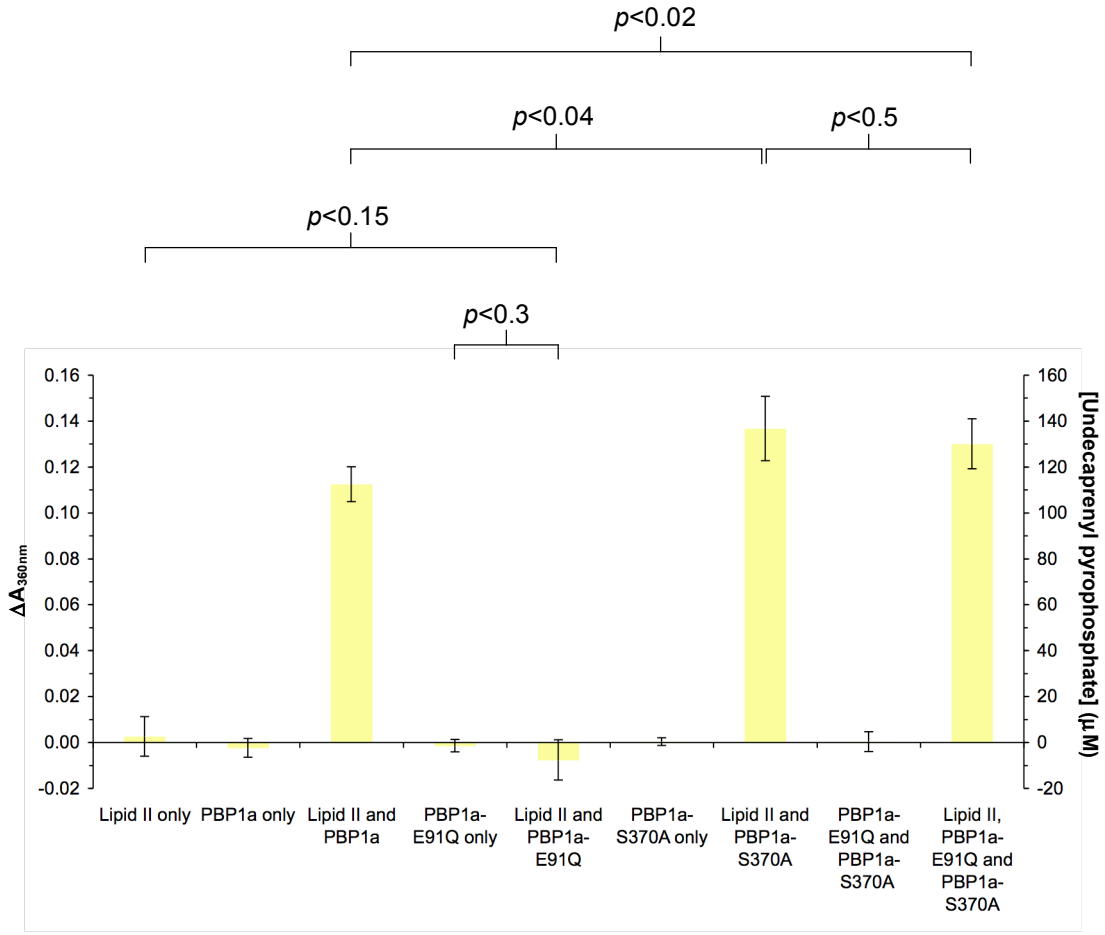

Figure 4.19: Statistical analysis of the transglycosylase activity of PBP1a active site variants. To reveal the [undecaprenyl pyrophosphate] generated specific to transglycosylase activity, the [undecaprenyl pyrophosphate] produced from the 0 h incubations of the controls and PBP1a variants with Lys-Lipid II was subtracted from the [undecaprenyl pyrophosphate] produced after the 2 h incubations of equivalent reactions (Figure 4.18). The primary and secondary y-axes represent the absorbance change at 360 nm due to P_i release from undecaprenyl pyrophosphate and the corresponding concentration of undecaprenyl pyrophosphate respectively. The constituents of each reaction are labelled on the x-axis of the Figure. Values represent the corrected mean ± standard deviation of triplicate reactions. Student's two-tailed *t*-test was performed to determine any statistical relevance between data sets as detailed on the Figure. With the exception of the specified incubations with PBP1a-E91Q (see Figure), all statistical comparisons of either the Lipid II only or enzyme only controls with both Lipid II and enzyme combined, gave *p* values of <0.0001 (not shown on Figure).

The results of the statistical analysis are discussed in Section 4.13.3.4.

4.11. Analysis of transglycosylation products by SDS-PAGE

SDS-PAGE separation of glycan polymer products of transglycosylation can reveal valuable information about the transglycosylase under investigation. Information regarding the product length and distribution, substrate specificity and roles of specific residues in catalysis can be established using this technique (Barrett *et al.*, 2007). Initially developed by Schägger and von Jagow (1987) to separate proteins of low molecular weight, the SDS-PAGE system was modified by Barrett *et al.* (2007) to analyse polymerised transglycosylation products.

4.11.1. Synthesis of [^{14}C]-labelled Lys-Lipid II

A means of the detection of glycan chains on the SDS-PAGE gel involves the incorporation of a radiolabel, and this is achieved via the Lipid II precursor. The protocol for [^{14}C]-Glc*N*Ac-labelled Lys-Lipid II synthesis was based upon the syntheses of [^{14}C]-Glc*N*Ac-labelled Lipid II by Bertsche *et al.* (2005) and non-radiolabelled Lys-Lipid II (reported in Section 2.7.3) . Following the experimental procedure described below and detailed in Section 2.7.7, if every reaction proceeded to completion then the [^{14}C]-Glc*N*Ac-labelled Lys-Lipid II synthesised would have a specific activity of 1940 disintegrations per minute (dpm)/nmol.

4.11.1.1. Experimental details and rational of [^{14}C]-Glc*N*Ac-labelled Lys-Lipid II synthesis

The synthesis of radiolabelled Lipid II took place in a final volume of 3.5 mL and was performed in the reaction buffer: 0.1 M Tris, 5 mM $MgCl_2$, 1 % (v/v) Triton X-100, pH 8.0. 5.67 µmol (1.62 mM) undecaprenyl phosphate was incubated with 3.5 mg/mL *M. flavus* membranes and a total of 6.96 µmol (2 mM) of UDP-Mur*N*Ac-pentapeptide. The undecaprenyl phosphate limited the total Lipid I and Lipid II ultimately synthesised to 5.67 µmol. Addition of 5 µCi [^{14}C]-UDP-Glc*N*Ac (317 mCi/mmol, supplied in 200 µL, with a concentration of 78.88 µM) provided 15.78 nmol of 'hot' UDP-Glc*N*Ac to the reaction. 140 µg *E. coli* MurG (expressed and purified according to Ha *et al.* (1999)) was used to supplement the reaction to

further facilitate the transfer of Glc*N*Ac from UDP to the Mur*N*Ac-C4-hydroxyl of Lipid I. The reaction was incubated for 1 h at 37°C. 'Cold' UDP-Glc*N*Ac was then added to the incubation, making the total concentration of 35 mM 'hot' and 'cold' UDP-Glc*N*Ac. The reaction was incubated for a further 2 h at 37°C with intermittent mixing. The reaction was stopped by the addition of 3.5 mL 6 M pyridinium acetate (pH 4.2) and 7 mL *n*-butanol and the lipids were extracted as for non-radiolabelled Lipid II (Section 2.7.3.1). [^{14}C]-Glc*N*Ac-labelled Lys-Lipid II was purified using a similar approach to non-radiolabelled-Lys-Lipid II as described in Section 2.7.7.2.

On the assumption that 15.78 nmol [^{14}C]-UDP-Glc*N*Ac reacted with 5.67 μmol Lipid I as a result of MurG activity in the first hour of incubation, 5.65 μmol Lipid I would remain, which would be converted to Lipid II by the non-radiolabelled UDP-Glc*N*Ac in the second stage of the incubation. If each reaction went to completion, and any Lipid II synthesised was not polymerised by the PBPs within the *M. flavus* membrane preparation, a total of 5.67 μmol of [^{14}C]-Glc*N*Ac-labelled Lys-Lipid II would be produced containing 5 μCi. This is equivalent to a specific activity of 1940 dpm/nmol. The [^{14}C]-Glc*N*Ac-labelled Lys-Lipid II is referred to as [^{14}C]-Lys-Lipid II from here onwards.

4.11.1.2. Determination of [^{14}C]-Lys-Lipid II purity and concentration

TLC was performed to analyse the purity and concentration of [^{14}C]-Lys-Lipid II (Section 2.7.8). The concentration of [^{14}C]-Lys-Lipid II was established by comparing the intensity of the iodine-stained [^{14}C]-Lys-Lipid II band from a 15 μL sample to standards of non-radiolabelled Lys-Lipid II with known concentrations. Figure 4.20 displays the TLC plate following staining with iodine and the specific band due to [^{14}C]-Lys-Lipid II imaged by autoradiography.

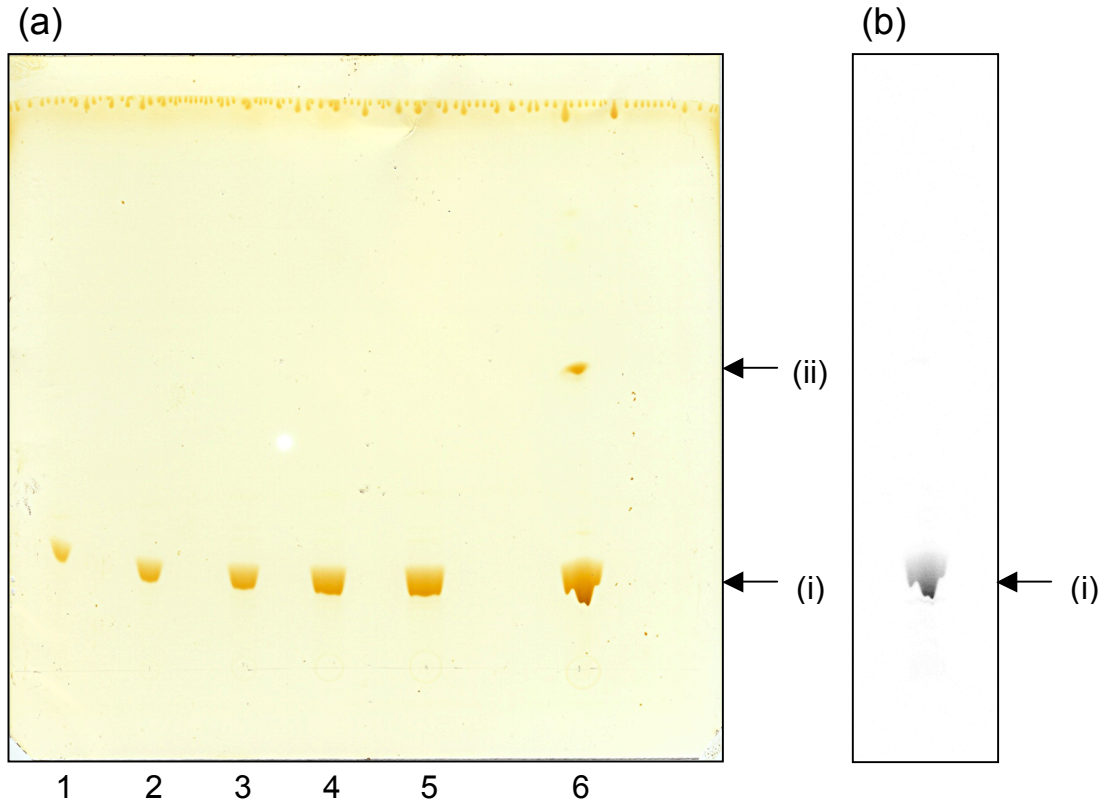

Figure 4.20: TLC plate and the corresponding autoradiograph of [^{14}C]-Lys-Lipid II. (a) An iodine-stained TLC of [^{14}C]-Lys-Lipid II with non-radiolabelled Lys-Lipid II standards. Lanes 1-5, 3.48, 6.96, 10.43, 13.91, 17.39 nmol Lys-Lipid II respectively; lane 6, [^{14}C]-Lys-Lipid II preparation. The bands representing Lipid II (i) and contaminating lipid (ii) are indicated. (b) An autoradiograph of [^{14}C]-Lys-Lipid II from (a) following an exposure time of 48 h, using a tritium storage phosphor screen and imager.

Figure 4.20 clearly demonstrates that [^{14}C]-Lys-Lipid II was synthesised. Undecaprenyl phosphate, a major component involved in Lipid II synthesis represents the lipid contaminating the [^{14}C]-Lys-Lipid II preparation (marked by (i) on the figure). This could be removed by integrating further wash steps during purification. The intensities of the Lipid II standards and the [^{14}C]-Lys-Lipid II band were measured by pixel analysis using ImageJ software (Abràmoff *et al.*, 2004). Figure 4.21 shows the standard curve of different amounts of Lipid II with their corresponding intensities following iodine staining. The mean grey value at 0 nmol Lipid II represents the background pixel intensity.

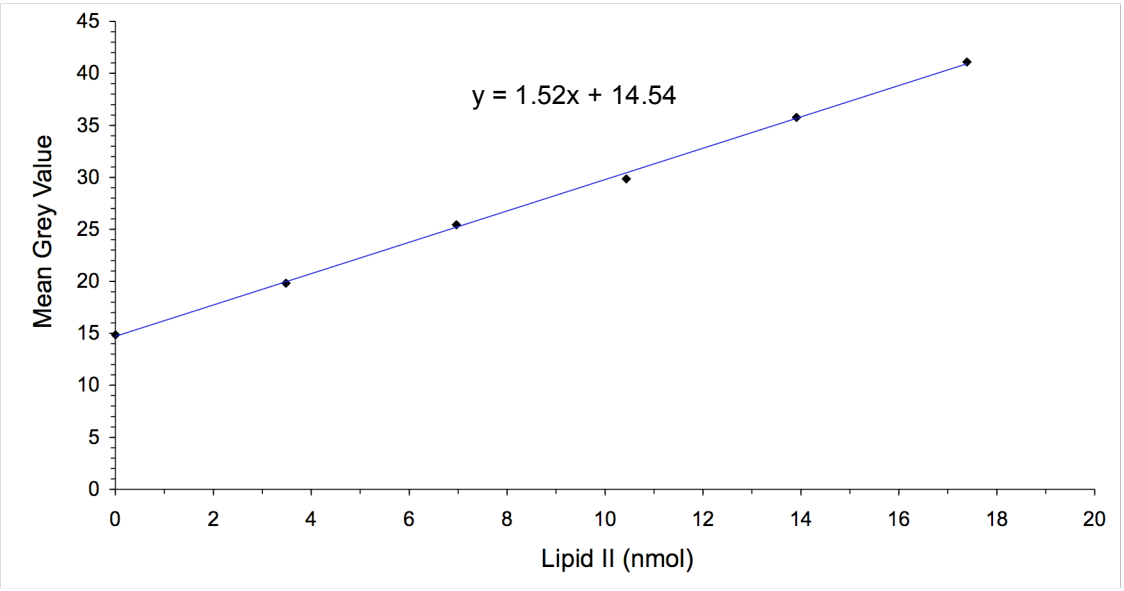

Figure 4.21: Iodine-stained Lipid II pixel analysis. The iodine-stained Lipid II standards from the TLC (Figure 4.20) were subject to ImageJ pixel analysis, where mean grey values were estimated, representing arbitrary units of intensities. The amounts of Lipid II were plotted against the mean grey values. A trend-line has been fitted to the data by linear regression to extrapolate the quantity of [^{14}C]-Lys-Lipid II from the relative intensity of the band on the TLC (equation shown on graph).

From the pixel analysis, the concentration of [^{14}C]-Lys-Lipid II can be calculated. The iodine-stained band had a mean grey value of 49.15, which, according to Figure 4.21, is equivalent to 22.76 nmol [^{14}C]-Lys-Lipid II (resulting from the 15 µL sample). This gives an estimated concentration of 1.52 mM [^{14}C]-Lys-Lipid II. The stock of [^{14}C]-Lys-Lipid II had 152 cpm/µL, resulting in a specific activity of 100 cpm/nmol, a value significantly lower than anticipated (1940 dpm/nmol).

4.11.2. SDS-PAGE analysis of glycan chain polymerisation by the transglycosylase activities of MGT and PBP1a

The SDS-PAGE gel system for visualising glycan chains was prepared according to the method developed by Barrett *et al.* (2007) with minor adjustments as described in Section 2.8.2.

The transglycosylase assays (Section 2.8.2.2.1) of variants of MGT (MGT and MGT-E100Q) and PBP1a (PBP1a, PBP1a-E91Q, PBP1a-Δ30 and PBP1a with ampicillin) were performed with enzyme concentrations of 155 μM and 77 μM respectively. Given the low specific activity of the [^{14}C]-Lys-Lipid II substrate, a concentration of 4.4 mM was used to ensure a signal was detected following autoradiography. Optimised buffer systems were used (Section 4.9), with Decyl PEG omitted because it was shown to cause irregular migration of Lipid II through the SDS-PAGE gel. The reactions were incubated for 4 h at 20°C and stopped by heat denaturation. Following SDS-PAGE, the gels were dried without fixing. Radiolabelled products were visualised with a tritium phosphor screen for an exposure period of 2 weeks. The results from the autoradiograph are shown in Figure 4.22.

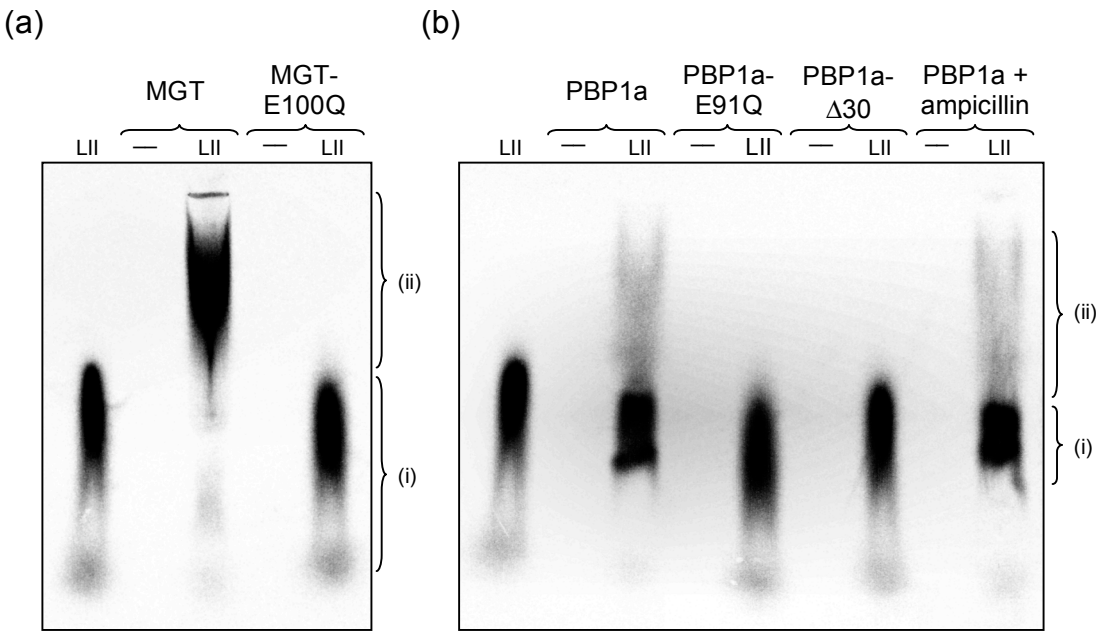

Figure 4.22: SDS-PAGE analysis of [^{14}C]-Lys-Lipid II polymerisation catalysed by MGT and PBP1a variants. Incubations of the various transglycosylases with [^{14}C]-Lys-Lipid II were run on a 9 % T/2.6 % C (T, total percentage concentration of acrylamide and bis-acrylamide; C, percentage of the cross-linker bis-acrylamide) SDS-PAGE gel. The resultant autoradiographs are shown, labelled with the assay constituents. Assays were performed in the presence of (LII) and absence of (—) [^{14}C]-Lys-Lipid II. (a) Transglycosylation by MGT variants. (b) Transglycosylation by PBP1a variants. The controls are represented by the lanes of [^{14}C]-Lys-Lipid II only and enzyme only. Unpolymerised [^{14}C]-Lys-Lipid II and the glycan chains are indicated as (i) and (ii) respectively. Radioactivity was detected using a tritium phosphor screen and imager.

Despite the poor resolution of glycan chain separation displayed in Figure 4.22, conclusions can be drawn. Polymerised glycan chains migrate through the SDS-PAGE gel with dependence on their chain length. [^{14}C]-Lys-Lipid II migrates towards the bromophenol dye front. Figure 4.22a demonstrates the transglycosylase activity of MGT, where [^{14}C]-Lys-Lipid II has been replaced by a high molecular weight species. MGT-E100Q did not catalyse the polymerisation of [^{14}C]-Lys-Lipid II, confirming the results observed in Section 4.7.1.

The transglycosylation activities of the PBP1a variants are shown in Figure 4.22b, which also validate the findings from the discontinuous spectrophotometric assays (Section 4.8.1). PBP1a and PBP1a in the presence of ampicillin (inhibiting the transpeptidase activity) were capable of transglycosylation as demonstrated by the appearance of higher molecular weight species. The activity of PBP1a was clearly slow: the vast majority of [^{14}C]-Lys-Lipid II remained unpolymerised after 4 h. PBP1a-E91Q and PBP1a-Δ30 did not catalyse [^{14}C]-Lys-Lipid II polymerisation as indicated by the sole presence of [^{14}C]-Lys-Lipid II, which was coincident with the [^{14}C]-Lys-Lipid II only control.

4.11.3. Time dependency of MGT and PBP1a transglycosylation

The polymer size distribution profiles of the transglycosylases were analysed in a time dependent manner. MGT and PBP1a were incubated with [^{14}C]-Lys-Lipid II (as described in Section 2.8.2.2.1). Aliquots were sampled at specified time intervals and quenched by heat denaturation. Figure 4.23 shows the time-dependent transglycosylation profile of (a) MGT and (b) PBP1a following SDS-PAGE and autoradiography.

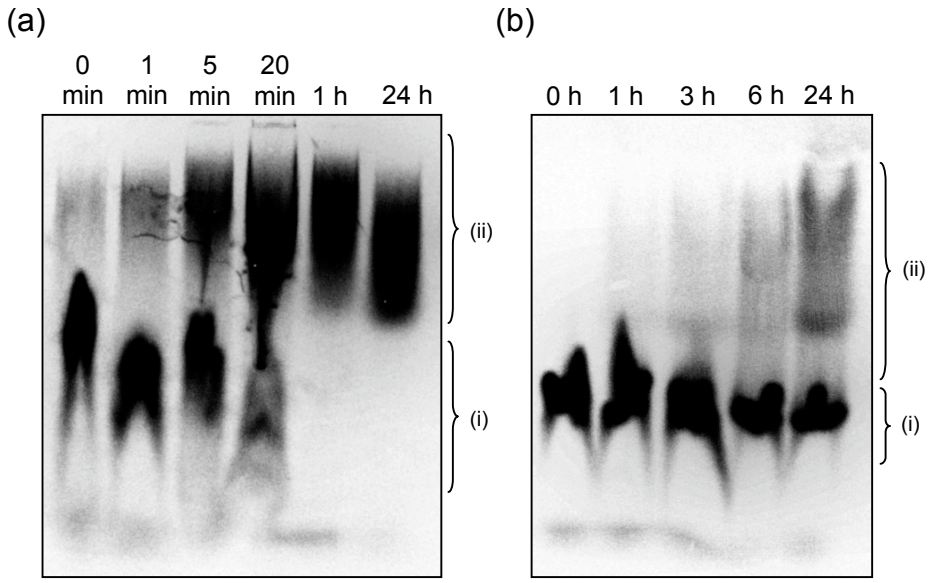

Figure 4.23: SDS-PAGE analysis of transglycosylase product distribution with time. Autoradiographs of SDS-PAGE-separated glycan chains on a 9 % T/2.6 % C gel. (a) Time-dependent transglycosylation by MGT. (b) Time-dependent transglycosylation by PBP1a. Incubation times are displayed on the figure. Unpolymerised [^{14}C]-Lys-Lipid II and the glycan chains are indicated as (i) and (ii) respectively. Radioactivity was detected using a tritium phosphor screen and imager. [MGT], 155 µM; [PBP1a], 77 µM; [[^{14}C]-Lys-Lipid II], 4.4 mM.

A size distribution profile of transglycosylase activity over time was not established because the different length polymers were not discretely resolved. Figure 4.23a shows that the level of [^{14}C]-Lys-Lipid II decreased with time as the amount of MGT-polymerised product increased. At 0 min there appeared to be a slight degree of polymerisation, which probably resulted from a time lapse between initiating the transglycosylation reaction, sampling and MGT-denaturation. By 1 h, all of the [^{14}C]-Lys-Lipid II had been converted into a polymerised product.

Figure 4.23b demonstrates that following an incubation with PBP1a, there was a gradual increase in intensity of the polymerised glycan chains with time, which was absent at 0 h. At the 24 h time point, [^{14}C]-Lys-Lipid II still existed, indicative of extremely slow PBP1a transglycosylase activity. The high molecular weight polymerised glycan chains appeared to increase in relative molecular weight with time. This could signify the production of longer glycan chains or be an artefact of the unresolved polymers.

Separating the different length polymers to a suitable resolution is a prerequisite for further enzymatic characterisations using this technique.

4.12. A novel approach for the visualisation of glycan chains separated by SDS-PAGE

To eliminate the requirement of a radiolabel for the detection of glycan chains on an SDS-PAGE gel, a new approach was developed. Transglycosylated glycan chains exhibit a common feature: pentapeptide side stems. The antibiotic vancomycin can bind to the terminal of the pentapeptide, providing the residues at positions 4 and 5 are D-Ala-D-Ala (Nieto and Perkins, 1971). This attribute can be exploited in a polymer detection system by using a fluorescent analogue of vancomycin: VanFL (a BODIPY FL conjugate of vancomycin). Vancomycin does not bind to a tetrapeptide stem, making it a necessity to eliminate transpeptidase or D,D-carboxypeptidase activity prior to the transglycosylation of Lipid II.

4.12.1. Suitability of VanFL for the detection of pentapeptide side stems

Initial trials were performed to establish whether VanFL was sufficiently sensitive to detect glycan polymers via the pentapeptide side stem. Following SDS-PAGE and fluorescence detection, unbound VanFL was shown to run with the gel front. When pre-incubated with a pentapeptide fragment of L-Ala-γ-D-Glu-L-Lys-D-Ala-D-Ala, VanFL exhibited different migratory properties signifying binding. VanFL-bound Lys-Lipid II ran in an equivalent position to unbound VanFL on the SDS-PAGE, preventing the two from being distinguished. Consequently, VanFL must be used in limiting amounts to prevent a fluorescence signal appearing due to unbound VanFL.

The components of the optimised buffer system (Section 4.9) for MGT and PBP1a activity were assessed to analyse their influence on VanFL migration through the SDS-PAGE gel. In the presence of Decyl-PEG, VanFL migration was retarded, whereas DMSO prevented a discrete band of VanFL fluorescence. As a result, both components were omitted from transglycosylase assays.

4.12.2. SDS-PAGE analysis of glycan chains with VanFL detection

SDS-PAGE gels were prepared as described in Section 2.8.2.1. Transglycosylation reactions of MGT variants (MGT and MGT-E100Q) and PBP1a-S370A were performed with 2 mM Lys-Lipid II (Section 2.8.2.2.1). The transpeptidase activity of PBP1a was eliminated by using the transpeptidase active site mutant of PBP1a, which has near-equivalent levels of transglycosylase activity to the wild-type (Section 4.10). A polymerisation of 4.4 mM [^{14}C]-Lys-Lipid II by MGT was also performed. Following a 4 h incubation at 20°C, the enzymes were removed by heat-denaturation and centrifugation and the glycan chains were incubated with 24 μM VanFL (Section 2.8.2.2.2). The SDS-PAGE separation of VanFL-bound to MGT products of transglycosylation is shown in Figure 4.24.

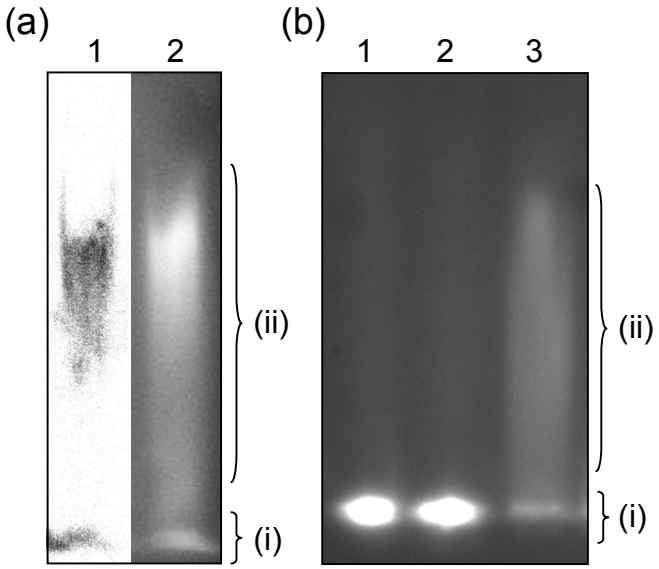

Figure 4.24: VanFL detection of polymerised glycan chains. Products of transglycosylation with bound VanFL were separated on a 9 % T/2.6 % C SDS-PAGE gel. VanFL fluorescence was detected using GeneSnap Gel Doc with a blue light converter and filter for the detection of VanFL fluorescence at 512 nm. Radioactivity was detected using a tritium phosphor screen and imager. (a) An autoradiograph of MGT-polymerised [^{14}C]-Lys-Lipid II (lane 1) and the equivalent VanFL fluorescence (lane 2). VanFL fluorescence was detected prior to gel-drying and autoradiography. (b) Fluorescence of VanFL bound to Lys-Lipid II (lane 1) and to the products of MGT-E100Q (lane 2) and MGT (lane 3) activity. Unpolymerised Lys-Lipid II and the glycan chains are indicated as (i) and (ii) respectively.

Figure 4.24a conclusively shows that binding of VanFL enables the detection of MGT transglycosylation products. VanFL fluorescence was detected at an equivalent position to the [^{14}C]-labelled glycan chains on the autoradiograph. Figure 4.24b coincides with the results obtained using [^{14}C]-Lys-Lipid II, where VanFL-bound high molecular weight species appeared in the incubation of Lys-Lipid II with MGT, but were absent in the incubation with MGT-E100Q. Transglycosylation products of PBP1a-S370A were not detected by VanFL fluorescence. PBP1a-S370A catalysed transglycosylation at a very slow rate. After the 4 h incubation, few transglycosylated products would have been made, especially in the absence of DMSO and Decyl PEG. Therefore, the sensitivity of VanFL is not sufficient to detect the activities of transglycosylases with slow rates of catalysis.

The binding of VanFL to pentapeptide side stems is an effective technique of detecting products of transglycosylation (given sufficient quantities are present). Analysis of glycan chain size and distribution by VanFL was hindered by poor separation on SDS-PAGE gels, a problem previously encountered (Sections 4.11.2 and 4.11.3).

4.13. Discussion and future work

The work presented in this Chapter provides a valuable foundation for the future kinetic characterisations of the transglycosylases. The following section discusses: the biological explanations and implications of the results obtained; strategies to resolve issues encountered; future work.

4.13.1. The discontinuous spectrophotometric assay for the detection of transglycosylase activity

4.13.1.1. The success of the discontinuous spectrophotometric assay

In literature, transglycosylase activity is detected by one of two methods: either with radiolabelled or fluorophore-labelled substrates (examples included in Offant *et al.* (2010), Schwartz *et al.* (2002) and Terrak and Nguyen-Distèche (2006)). The

discontinuous spectrophotometric assay system developed in this Chapter has provided a novel technique for the kinetic characterisation of transglycosylase activity, in a simple, time-efficient manner, with the use of natural substrates. The efficacy of the assay has been proven by the detection of the elusive transglycosylase activity of *S. pneumoniae* PBP1a in addition to that of *S. aureus* MGT. The assay enables rates of transglycosylase activity to be evaluated in a discontinuous fashion, but information regarding the length of polymers produced cannot be extrapolated. Ultimately, it would be desirable to develop the assay from a discontinuous to a continuous spectrophotometric detection system for transglycosylase activity (further discussed in Section 4.13.7).

4.13.1.2. An identified limitation of the assay system

A recognised limitation of the assay is that heat inactivation of the transglycosylases may not have occurred instantaneously. Quenching the reactions with EDTA was evaluated, but the enzymes retained a small degree of activity. Inhibition with the transglycosylase antibiotic, moenomycin, would have been more effective. Flavomycin, a combination of antibiotic compounds including moenomycin, was assessed as a means to quench the transglycosylase reactions but was shown to have no inhibitory effects on the transglycosylase activity. Moenomycin can be extracted from flavomycin with a final yield of 1.92 % (w/w) (Adachi *et al.*, 2006). This apparently low abundance of moenomycin in flavomycin and the obligatory high concentrations of Lipid II required in the transglycosylase assays meant that the competition of moenomycin versus Lipid II was too weak to register an inhibitory effect. The use of ramoplanin as an inhibitor of MGT activity was also evaluated, where it is postulated to bind as a dimer to Lipid II between the membrane and the disaccharide component, sequestering the substrate (Hamburger *et al.*, 2009). In the presence of NaCl, a requirement of the assays, ramoplanin formed a precipitate, documented as the polymerisation of the ramoplanin-Lipid II complex, forming insoluble fibrils (Lo *et al.*, 2000).

4.13.2. Kinetic characteristics of *S. aureus* MGT transglycosylase activity

4.13.2.1. Features of the MGT kinetic profile

The dependence of MGT transglycosylase activity on Lipid II concentration (Figure 4.10) demonstrated a sigmoidal approach to V_{max}, culminating with a reduction of enzyme activity at higher substrate concentrations. MGT has two binding sites: one for the elongating glycan chain (donor site) and one for the incoming Lipid II substrate (acceptor site). At time 0, both binding sites will be free of substrate. Upon the addition of substrate, Lipid II binding to the donor site may induce a conformational change, facilitating the binding of the Lipid II substrate at the acceptor site. This would be advantageous if the binding of the two substrates to the donor and acceptor sites occurred in an ordered manner.

An alternative explanation for the initial sigmoidal dependence of velocity on substrate concentration is that the detergent concentration was inhibitory at low substrate concentrations. At constant detergent concentrations, with a low concentration of Lipid II, there would be an excess of detergent micelles devoid of substrate compared to at high Lipid II concentrations. The crowding caused by 'empty' micelles could interfere with the enzyme activity. High concentrations of detergent have been documented to detrimentally affect the activity of PgpB (Touzé *et al.*, 2008) and *E. coli* PBP1b (Schwartz *et al.*, 2002). The excess detergent is believed to reduce the surface concentration of the substrate as opposed to directly inhibiting the enzyme (Schwartz *et al.*, 2002; Touzé *et al.*, 2008).

Beyond the approach of V_{max} (at approximately 0.5 mM Lys-Lipid II), MGT exhibited severe substrate inhibition. The classical explanation of substrate inhibition is that at high substrate concentrations, the substrate binds in a manner that is catalytically incompetent. Alternatively, if the binding of substrates A and B (to the transglycosylase donor and acceptor sites respectively) occurs in an ordered mechanism (e.g. A then B), the binding of B to the acceptor site first could prevent the binding of substrate A to the donor site and result in inhibition. Given the processive model for transglycosylation (Yuan *et al.*, 2007), newly synthesised

products are not released until a threshold chain length is reached (Wang *et al.*, 2008), indicating that the donor site would generally have substrate A bound (Schwartz *et al.*, 2002).

In the assays subsequent to the discovery of MGT substrate inhibition, the concentration of Lipid II in the discontinuous spectrophotometric assay was lowered to 0.40 mM. Thus, in *S. aureus*, *in vivo*, the concentration of substrate at which the MGT is working at its maximum rate must be finely tuned to avoid the immediate substrate inhibition following the approach of V_{max}.

4.13.2.2. A kinetic model of MGT activity to derive kinetic constants

A kinetic model describing the characteristic kinetic features of MGT is shown in Scheme 3, where Lipid II is the substrate in both donor and acceptor subsites. The enzyme E, combines with the Lipid II substrate, S, in the donor site forming an enzyme substrate complex, ES. A second molecule of Lipid II binds to the acceptor site, forming the reactive enzyme substrate complex, ES_2. This complex has two fates: substrate inhibition with the formation of ES_3, or the formation of product, P, and free enzyme, E. As transglycosylation progresses past the initial formation of Lipid IV, the processive model dictates that the substrate in the donor site will change by the addition of the disaccharide moiety, thus complicating the scenario and is not described by the model in Scheme 3. However, the assumption is made that the constantly polymerising substrate can be ignored as only the initial rates of the reaction are being considered.

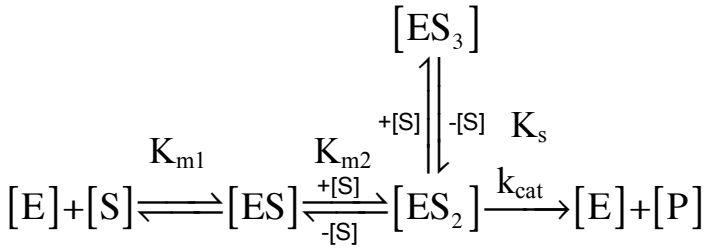

Scheme 3

A kinetic equation (Equation 4) can be derived from the reaction scheme (as described in Appendix B3) based on the assumption that rapid equilibrium kinetics

exist and that K_{m1} and K_{m2} are equilibrium constants. To ensure this mechanism is valid, further analyses need to be performed during pre-steady state kinetics, using stopped flow experiments for example.

$$v_0 = \frac{V_{max}[S]}{K_{m2}\left(\frac{K_{m1}}{[S]}+1\right)+[S]\left(1+\frac{[S]}{K_s}\right)}$$

Equation 4

This equation was applied to fit the MGT kinetic data (of Figure 4.10) to establish the kinetic constants. The outcome is displayed in Figure 4.25.

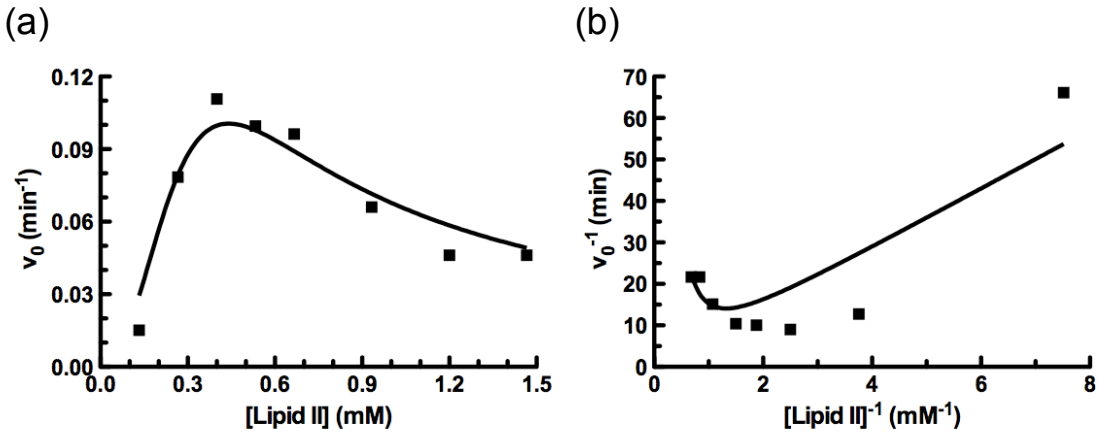

Figure 4.25: The kinetics of Lipid II dependence of MGT-catalysed transglycosylation. (a) A plot of MGT-dependent velocity as a function of substrate concentration. The data was fitted by non-linear regression to Equation 4 using Graph Pad PRISM 5, with constraints that all parameters must be greater than 0 and the initial value of V_{max} equal to 0.594 (estimated by non-linear regression from the Lineweaver-Burk plot of (b)) (R^2=0.93). (b) Lineweaver-Burk plot of Equation 4 (R^2=0.76).

It is evident from the R^2 values that the data does not sufficiently correlate with Equation 4. It is also clear that it is likely that there are insufficient data to allow a reliable fitting of Equation 4 to the data in Figure 4.25a. Approximate rough estimates of the kinetic parameters could be extracted (Table 4.4); however, their validity requires further experimentation as evidenced by the smaller K_s value compared to K_{m2} and the excessively high standard errors that characterise the values of the constants.

Substrate	Kinetic constants				
	K_{m1}^a (mM)	K_{m2}^a (mM)	K_s^a (mM)	k_{cat}^a (s^{-1})	k_{cat}^a/K_m^a ($s^{-1}M^{-1}$)
Lys-Lipid II	9.12×10^{-4} ±4.15	0.44±3.57	9.75×10^{-2} ±0.95	13.16×10^{-3} ±0.12	28.92

Table 4.4: Kinetic parameters of MGT-catalysed transglycosylation. The data was fitted to Equation 4, enabling kinetic constants to be derived. [a]Values ± standard error based on duplicate reactions.

Assuming rapid equilibrium kinetics exist, it may be that the first subsite had a higher affinity for the substrate than the second binding site. This is plausible given that a processive model for transglycosylation exists. However, considering the standard errors of similar values, this speculation requires some considerable further validation.

The kinetic constants of MGT reported here are comparable with the values obtained by Terrak and Nguyen-Distèche (2006). In the presence of different metal ions, k_{cat} was found to vary between 6.3×10^{-3} and 13.0×10^{-3} s^{-1} (Terrak and Nguyen-Distèche, 2006), which is highly similar to that obtained from the spectrophotometric assay (13.2×10^{-3} s^{-1}). There are significant differences between the k_{cat}/K_m, which can be accounted for by the fact that the published data was characterised by Michaelis-Menten kinetics with one substrate binding, whereas the data reported here was characterised by a two substrate binding model with substrate inhibition.

4.13.2.3. Specificity of the MGT substrate

The natural substrate of *S. aureus* MGT is Lys-Lipid II with a penta-glycine branch from L-Lys (Schleifer and Kandler, 1972). In this study, the substrate provided for MGT was Lys-Lipid II, a near-natural substrate. The absence of a penta-glycine branch on Lys-Lipid II could contribute to the observed substrate inhibition of MGT; the branch could sterically prevent the substrate from binding in an aberrant manner. Previous investigations have shown that MGT is capable of catalysing glycan chain polymerisation of Lipid II with varying pentapeptide side chains, for example *meso*-DAP-Lipid II (Terrak and Nguyen-Distèche, 2006). However, studies have not been

performed with the natural substrate of MGT, thus the specificity of MGT for the amino acids residing in the pentapeptide side chain has yet to be evaluated. Future investigation will decipher whether the pentapeptide side chain is involved in recognition by the transglycosylase domain.

4.13.2.4. A structural explanation for Lipid I inhibition of MGT transglycosylation

The competitive inhibition displayed by Lipid I is likely to arise from the obstruction of the natural substrate binding sites of MGT. The transglycosylase domain has two binding sites: one for the donor strand (elongating glycan chain) and one for the incoming acceptor (Lipid II) (Lovering *et al.*, 2007) (Figure 4.26a). Following the incubation of MGT with a vast excess of Lipid I, both binding sites were likely to have bound Lipid I. This situation is displayed in Figure 4.26b. Lipid I in the acceptor site cannot perform a transglycosylation reaction because it lacks a Glc*N*Ac moiety, the C4-hydroxyl group of which forms the linkage to the adjacent muramyl sugar ring of the substrate in the donor site. The minimal activity detected could have resulted from Lipid II accessing the acceptor site (with Lipid I or Lipid II in the donor site), enabling a transglycosylation reaction to occur.

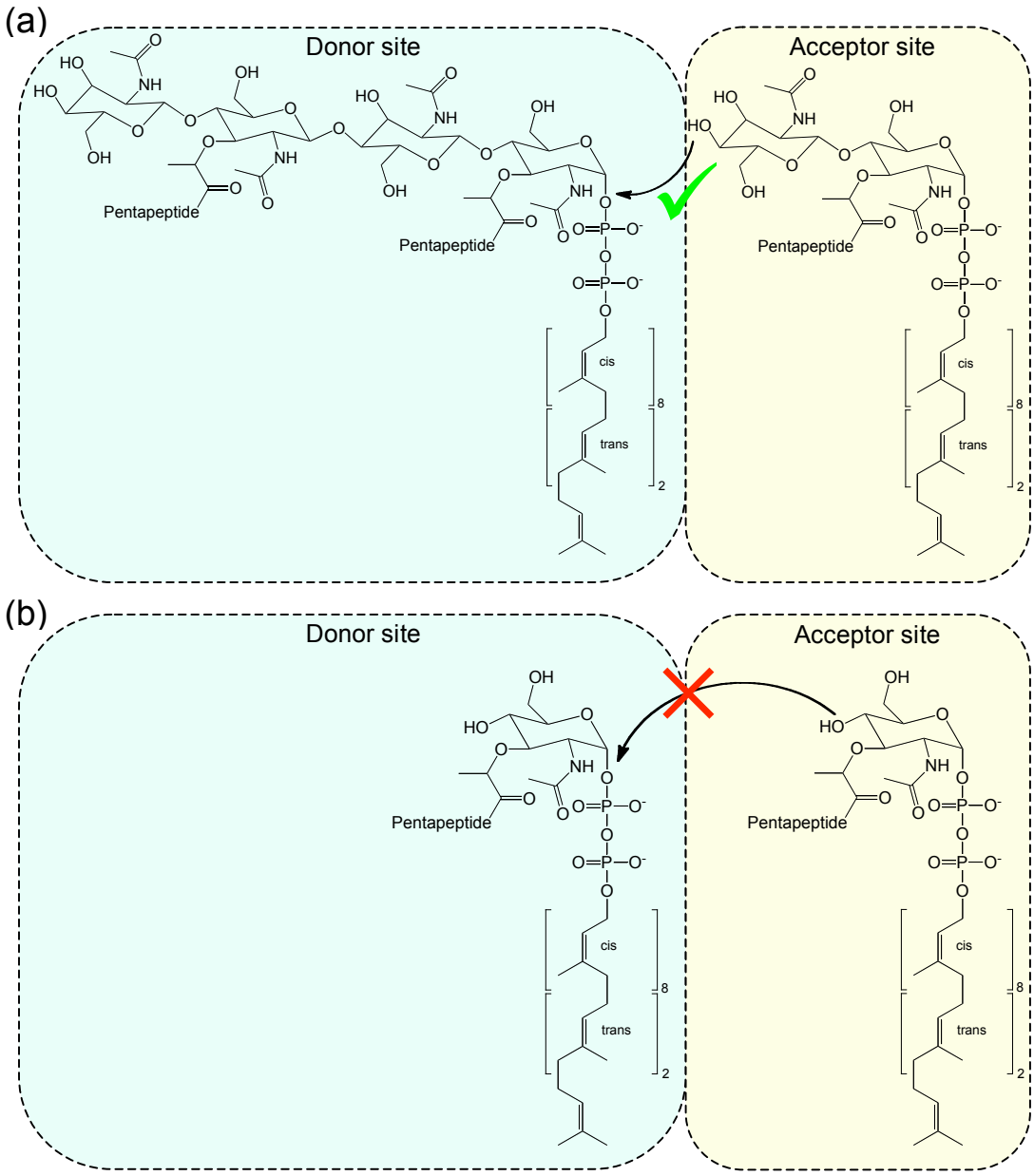

Figure 4.26: The binding of substrates in the donor and acceptor sites of the transglycosylase catalytic cleft. (a) A transglycosylation reaction can occur when an elongating glycan chain is situated in the donor site, with an incoming Lipid II molecule in the acceptor site. (b) Transglycosylation does not occur between Lipid I (shown) or Lipid II in the donor site with Lipid I in the acceptor site. The structural similarities between Lipid I and Lipid II could allow the former molecule to be recognised by residues lining the active site cleft, thus competing with Lipid II for binding.

The similar structural features present in Lipid I and Lipid II enable the former compound to act as an inhibitor, whilst enabling the latter to act as a substrate. This finding has two implications: (a) structure based drug design of the transglycosylases

could be centred on a Lipid I analogue and (b) the specificity of the putative flippase must distinguish between Lipid I and Lipid II to prevent the former reaching the extracellular side of the membrane.

4.13.3. Kinetic characteristics of *S. pneumoniae* PBP1a transglycosylase activity

4.13.3.1. The time-dependent profile of PBP1a transglycosylation

The time course of PBP1a-dependent transglycosylation did not reach completion after 6 h (Figure 4.14). If PBP1a were only capable of catalysing a single transglycosylation reaction between two molecules of Lipid II, Lipid IV would be formed without further extension. As a result one molecule of undecaprenyl pyrophosphate would be generated for every two Lipid II molecules transglycosylated. At maximum, 0.28 mM undecaprenyl pyrophosphate would be produced from 0.56 mM Lys-Lipid II. This is far from the concentration obtained after a 6 h transglycosylation reaction containing CHAPS detergent, where hyperbolic curve signified the reaction was nearing an end point. The use of CHAPS has been documented as a successful solubilising detergent for various PBPs, including *S. pneumoniae* PBP2a devoid of its membrane anchor (Di Guilmi *et al.*, 1999). However, purification of *S. pneumoniae* PBP1a, PBP2b and PBP2x in CHAPS caused aggregation, identified via size exclusion chromatography. A similar observation has been made upon purification of *T. maritima* PBP1a (Offant *et al.*, 2010). Therefore, it is likely that CHAPS promoted enzyme denaturation, preventing the complete transglycosylation of Lipid II by PBP1a. In buffer containing DDM, PBP1a transglycosylation produced approximately 0.28 mM undecaprenyl pyrophosphate after 6 h. At this time point, the enzyme appeared to be catalysing undecaprenyl pyrophosphate production with steady-state kinetics. Therefore, it can be deduced that PBP1a produces glycan chains, which are longer than Lipid IV.

4.13.3.2. The dependence of PBP1a transglycosylation on Lipid II concentration

The Lipid II dependence of PBP1a transglycosylase activity demonstrates that despite the high concentrations of Lys-Lipid II in the assays, V_{max} was not reached. This has implications for the K_m, which would be high under the assay conditions used (speculated to be greater than 1.11 mM), signifying that PBP1a would have a low binding affinity for Lipid II in at least one of the substrate binding sites (assuming rapid equilibrium kinetics exist). This result is unexpected given the low copy number of Lipid II *in vivo* (van Heijenoort *et al*., 1992).

The rate of PBP1a transglycosylase activity measured *in vitro*, far from matches the rate expected *in vivo.* During the log phase, *S. pneumoniae* divide with a rate of (μ) 20-30 min (Tuomanen, 2006). At the highest substrate concentration tested, 1.11 mM Lys-Lipid II, PBP1a transglycosylation proceeded with a turnover value of 1.44 h^{-1}, measured over 3 h. This is equivalent to the turnover of one molecule of substrate per enzyme molecule every 42 min. Di Guilmi *et al.* (2003b) determined that *S. pneumoniae* PBP2a has a k_{cat} value of 1.55×10^{-4} h^{-1}, which corresponds to the turnover of one substrate molecule by one molecule of enzyme approximately every 9 months! The turnover number of PBP1a activity at subsaturating concentrations is over 9,000 fold greater than the k_{cat} of PBP2a, although both rates are vastly insufficient to support bacterial growth. The turnover of enzymes upstream of the transglycosylases must also be considered. For example, Hu *et al.* (2003) established *E. coli* MurG, responsible for the intracellular formation of Lipid II from Lipid I and UDP-Glc*N*Ac, has a k_{cat} value of 837 min^{-1}. This is significantly faster than the turnover of PBP1a (and PBP2a), and would lead to the accumulation of peptidoglycan precursors. Given that there are estimated to be only 1000-2000 Lipid II molecules per bacterial cell (*E. coli*) (van Heijenoort *et al.*, 1992), either Lipid II is synthesised and subsequently degraded (an energetically unfavourable process), or the transglycosylases rapidly polymerise Lipid II. The latter option signifies that either the remaining *S. pneumoniae* Class A PBP (PBP1b) is responsible for the majority of glycan chain formation *in vivo* or the transglycosylase activity of PBP1a (and PBP2a) is substantially greater than estimated from the *in vitro* experiments. Since the presence of either PBP1a or PBP2a is essential for

S. pneumoniae viability (Hoskins *et al.*, 1999), the latter option is probable (discussed in the following section).

The k_{cat}/K_m of PBP1a was determined (based on the assumptions made in Section 4.8.3 and Appendix B2): 0.34 $s^{-1}M^{-1}$. *S. pneumoniae* PBP2a (devoid of cytoplasmic and transmembrane regions) has a catalytic efficiency of 1×10^{-3} $s^{-1}M^{-1}$ (Di Guilmi *et al.*, 2003b), 340 orders of magnitude lower than the value for PBP1a. The N-terminal truncation of PBP2a construct could account for this discrepancy, which may compromise catalytic efficiency.

4.13.3.3. PBP1a-Δ30 transglycosylase activity

PBP1a-Δ30 did not exhibit any transglycosylase activity, which could be explained by the instability of the construct (Section 3.8.1.3). Different levels of truncation would establish the minimum requirement of the transmembrane anchor. Di Guilmi *et al.* (1998) have shown that PBP1a-Δ37 (devoid of the N-terminal 37 amino acid residues encompassing the transmembrane domain) was able to bind the inhibitor moenomycin, indicating that with this degree of truncation (and presumably the Δ30 truncation analysed here), the active site was in at least a near-native conformation. Studies by Sung *et al.* (2009) have established that the transglycosylase activity of full-length *E. coli* PBP1b is greater than its counterpart devoid of the transmembrane anchor and have proposed that the transmembrane helix is essential for protein-protein and protein-lipid interactions (stabilising the enzyme within its natural environment) as opposed to having an involvement in substrate recognition. The role of the transmembrane domain of HMW-PBPs will require further exploration by future work.

4.13.3.4. Statistical analysis of PBP1a transglycosylase activity

The statistical analysis of the transglycosylase activity of PBP1a variants revealed that the undecaprenyl pyrophosphate produced from incubations of either PBP1a or PBP1a-S370A with substrate was substantially significantly different from the corresponding enzyme only and Lys-Lipid II only controls (Figure 4.19). This

demonstrated that undecaprenyl pyrophosphate generation was dependent on the presence of transglycosylase and substrate. The results also demonstrated that the transglycosylase domain was capable of functioning independently of the transpeptidase domain. The transglycosylase activity of PBP1a-E91Q (with substrate) compared to the enzyme only and Lys-Lipid II only controls gave *p* values of <0.3 and <0.15 respectively, indicating that the signal generated by this mutant, attributed to its activity, was not significantly different to that of the controls.

The measurements of product generated after a 2 h incubation of enzyme and substrate demonstrated that PBP1a had similar levels of activity compared to PBP1a-S370A and PBP1a-S370A with PBP1a-E91Q. However, with *p* values of <0.04 and <0.02 respectively, these results indicated that there was a significant difference between the activities, where the wild-type enzyme produced a lower amount of undecaprenyl pyrophosphate. The transglycosylase activity of PBP1a-S370A and PBP1a-S370A with PBP1a-E91Q were highly similar (p<0.5). The results suggest that when the transglycosylase activity acts in concert with the transpeptidase activity present on the same enzyme molecule, the rate of former activity is reduced, compared to if the transglycosylase domain is present in a separate entity devoid of transpeptidase activity (in the presence or absence of transpeptidation). This outcome is not unreasonable: if the model proposed by Sung *et al.* (2009) is correct, the transglycosylase domain feeds the polymerising glycan chain (and thus the pentapeptide stem) to the transpeptidase domain. A transpeptidation reaction with an adjacent pentapeptide stem could momentarily hinder further transglycosylation until the reaction were complete. The functional dependency of the transpeptidase activity on transglycosylation is investigated in Chapter 5.

4.13.3.5. Factors influencing the rate of PBP1a-dependent transpeptidation

Numerous factors could cause the unrealistic rate of PBP1a transglycosylation. The presentation of the Lys-Lipid II substrate within a detergent micelle may not have been suitable, where detergent molecules could mask substrate recognition sites. The composition of the Lipid II pentapeptide side chain could be important in substrate recognition. Lys-Lipid II (substrate containing a pentapeptide chain of L-Ala-γ-D-Glu-L-Lys-D-Ala-D-Ala) was used as a substrate for *S. pneumoniae*

PBP1a. This differentiates from the *S. pneumoniae*-specific pentapeptide chain, which contains an *iso*-Gln in the corresponding position of D-Glu (and the existence of stem branches (Garcia-Bustos and Tomasz, 1990)). X-ray crystal structures of transglycosylases complexed with the Lipid IV mimetic moenomycin (Figure 1.12) reveal that few contacts are made with rings A and D, which are proposed to represent the positions of the pentapeptide side chains (Lovering *et al.*, 2008b). Thus, it is not believed that the transglycosylases distinguish between Lipid II substrates at the peptide stem level. The transglycosylase activity of PBP1a could be analysed with peptide stem variants of Lys-Lipid II to validate this theory.

Optimisations of the assay conditions (discussed in the following sections) enhanced the activity of PBP1a to an extent, by providing a more membrane-like environment. *In vivo*, it is expected that factors present in the membranes (such as activating lipids or proteins) or environmental conditions promote PBP1a activity, which are absent in the *in vitro* assays. These features are discussed in detail with reference to the transpeptidase activity of PBPs in Section 5.12.4.

4.13.4. Optimisation of assay conditions enhance *S. aureus* MGT and *S. pneumoniae* PBP1a transglycosylase activity

In vitro, transglycosylase activity is greatly influenced by the assay conditions, including various additives, metal ions and pH, which are enzyme-specific. MGT and PBP1a exhibited different sensitivities to metal ions: MGT had a preference for Ca^{2+}, whereas PBP1a favoured Mg^{2+}.

In vitro, transglycosylases perform *de novo* polymerisation of Lipid II. This process is believed to be inefficient (Schwartz *et al.*, 2002) and can result in a delay in the formation of glycan chain products as documented in the transglycosylase reactions of *E. coli* PBP1a (Barrett *et al.*, 2007) and PBP1b (Schwartz *et al.*, 2002). It is likely that an extended cleft (identified by crystal structures of transglycosylases with bound moenomycin (Section 1.9.1.4) (Heaslet *et al.*, 2009; Lovering *et al.*, 2007)) for interactions with an elongating glycan chain is not utilised by the initial Lipid II (Schwartz *et al.*, 2002). Upon synthesis of the short oligosaccharide primer, the transglycosylase adds Lipid II units in a processive manner (Barrett *et al.*, 2007) with

steady state kinetics (Schwartz *et al.*, 2002). As a result of these findings, the transglycosylase activities of MGT or PBP1a were evaluated in the presence of *E. coli* peptidoglycan, which was proposed to provide a starting material for transglycosylase extension. The transglycosylase activities of MGT and PBP1a were not enhanced. Born *et al.* (2006) have also demonstrated that *E. coli* PBP1a cannot incorporate radiolabelled-Lipid II into existing sacculi via transglycosylation. The insoluble nature and Gram-negative origin of the peptidoglycan, with its post-transglycosylation modifications was likely to impede its purpose of supplying glycan chains. Pre-polymerisation of Lipid II by MGT could establish the preference of existing glycan chains as a substrate for the donor site of PBP1a or MGT.

The combination of Decyl PEG and DMSO improved the transglycosylase activity of MGT and PBP1a (Section 4.9). Decyl PEG is a detergent and thus its role in the assays could be to increase the solubility and stability of the transmembrane region of Lys-Lipid II and integral membrane proteins. DMSO is a small amphiphilic molecule that is believed to enhance the solubility of Lipid II (Schwartz *et al.*, 2002). It has been demonstrated that DMSO promotes the fluidity and permeability of membranes (Gurtovenko and Anwar, 2007), thus DMSO could also enhance micelle permeability and fusion. MGT activity was reduced in the presence of Decyl PEG alone, where excess detergent micelles devoid of Lipid II could have interfered with the rate at which the enzyme encountered the substrate (Schwartz *et al.*, 2002).

4.13.5. Reducing the day-to-day variation of data

Although the kinetic trends exhibited by MGT and PBP1a transglycosylase activity were replicable on a day-to-day basis, the data was not. This can be explained in one of two ways, both in reference to the lipid substrate. The first, Lys-Lipid II was stored in volatile solvents: chloroform/methanol/water 2:3:1 (v/v). Upon sampling, the solvents could have evaporated from the stock, gradually increasing the concentration of Lys-Lipid II. Alternatively, the variability in data could have arisen from the insufficient redissolution of Lys-Lipid II, following the removal of solvents. Both issues could be resolved by immediately removing the solvents after concentration calculations and solubilising the lipid in a suitable storage buffer.

4.13.6. Analysis of products from transglycosylation by SDS-PAGE

The synthesis of [^{14}C]-Lys-Lipid II was successful, but the specific activity was almost 20-fold less than anticipated. This could have resulted from either the low availability of Lipid I (the precursor to Lipid II) in the synthesis or from the low activity of MurG. A better approach would be to synthesise [^{14}C]-Lys-Lipid II from a known amount of Lipid I provided from a separate synthesis (as performed by Bertsche *et al.* (2005)).

The SDS-PAGE analysis of glycan chain lengths was hindered by the severe smearing of substrate and transglycosylase products through the gel. This occurred regardless of whether or not the samples were heat denatured (to remove protein) prior to loading. The level of purity of the buffers used may have contributed to this issue. Until the glycan chains are efficiently resolved, characterisation of the transglycosylases using this method cannot be achieved. In spite of this, the SDS-PAGE gels did reveal and confirm features of the MGT and PBP1a transglycosylases established by the spectrophotometric assays:

- MGT transglycosylation of 66 nmol Lys-Lipid II was complete before 1 h
- PBP1a transglycosylation of 66 nmol Lys-Lipid II was not complete after an overnight incubation (enzyme denaturation is a likely cause)
- The transglycosylase active site mutants of PBP1a and MGT (E91Q and E100Q respectively) were incapable of transglycosylation
- PBP1a transglycosylation can proceed in the absence of a functioning transpeptidase domain

The use of VanFL to detect SDS-PAGE separated glycan chains by fluorescence was possible provided that sufficient amounts of polymer were present. To improve the sensitivity and specificity of detecting glycan chains by fluorescence, the precursor, Lipid II, could be covalently labelled with a fluorescent molecule (such as dansylated-Lipid II as described by Di Guilmi *et al.* (2003b)). This would ensure that each disaccharide moiety of the glycan chains would be labelled with fluorescence.

4.13.7. Towards a continuous spectrophotometric assay of transglycosylase activity

E. coli PgpB is the undecaprenyl pyrophosphate phosphatase coupling enzyme that forms the link between the discontinuous transglycosylase assay and continuous spectrophotometric assay for P_i generation. Following expression and purification of PgpB, a sufficient quantity of enzyme with a high rate of phosphatase activity was not available to support a continuous assay for transglycosylation. PgpB expression levels would be a primary aspect to improve. Alternatively, a different source of the undecaprenyl pyrophosphate phosphatase activity could be investigated. Analyses of PgpB activity revealed that the phospholipids cardiolipin and phosphatidyl glycerol greatly enhanced the activity of the enzyme. Further optimisations of the conditions for PgpB activity could augment the phosphatase activity, including trials of pH dependence and the presence of DMSO or Decyl PEG.

The level of the coupling enzyme activity is not the only factor to be considered when developing a continuous spectrophotometric assay; the rate of transglycosylation must be fast enough to detect on a suitable timescale. The spectrophotometric assays are performed in 200 µL reactions, over 10 times greater than the volume of the discontinuous assays described here (Section 2.8.1.2). Consequently, the total quantities of enzyme and substrate required would need to be substantially higher, which may not be feasible given their limited availability.

4.13.8. A high-throughput screening technique for the rapid analysis of transglycosylase activity

The initial characterisations of MGT and PBP1a transglycosylase activity presented in this Chapter have provided the basis for future investigations. A number of factors influencing the transglycosylase activity need to be addressed to fully characterise MGT and PBP1a, including:

- Substrate specificity
- Optimal buffer conditions (pH, metal ion, DMSO, Decyl PEG, potentially having a cumulative effect)
- Roles of essential active site residues
- Effect of reconstitution into liposomes (a more membrane-like environment)
- Significance of the mutations T103S and A124T on PBP1a transglycosylase activity. These two mutations are the only sequence differences in the transglycosylase domains of the penicillin-sensitive *S. pneumoniae* D39 PBP1a and the penicillin-resistant *S. pneumoniae* 5204 PBP1a

Development of a 96-well plate spectrophotometric assay for undecaprenyl pyrophosphate generation would enable the parallel screening of a variety of parameters in a time-efficient manner. Manually, the assays could be set-up in a 96-well PCR plate with a total reaction volume of 15 µL in each well, comparable to the transglycosylase assays described in this Chapter. The PCR plate could be incubated in a PCR machine at a specified temperature (even with a gradient across the plate) for a specified amount of time. Following heat denaturation, the plate could be centrifuged to pellet any precipitated protein. A multi-channel pipette could then be used to transfer 13 µL of the supernatant to a P_i-detection-spectrophotometric assay in a 96-well plate. A plate reader could monitor the absorbance over the course of the assay. Generation of P_i following the addition of an undecaprenyl pyrophosphate phosphatase would signify the presence of undecaprenyl pyrophosphate and thus transglycosylase activity.

This high-throughput system could ultimately be applied to screen for transglycosylase inhibitors, a preliminary step in the discovery of new antibiotics.

4.14. Conclusion

A novel spectrophotometric assay for transglycosylase activity has been developed, contributing to the preliminary characterisations of *S. aureus* MGT and *S. pneumoniae* PBP1a. The assay system will facilitate the elucidation of kinetic parameters of all transglycosylases. It also provides an excellent basis for future work to establish the precise mechanism of transglycosylation in terms of substrate recognition and catalysis.

Chapter 5. Enzymology of transpeptidation: assay development towards the kinetic characterisations of the penicillin-binding domain of *Streptococcus pneumoniae* PBP1a, PBP2b and PBP2x

5.1. Introduction

For almost half a century, since the inhibition by penicillin led to their discovery, the PBP transpeptidases have been recognised as essential enzymes involved in maintaining the integrity of the bacterial cell wall (Tipper and Strominger, 1965). The penicillin-binding domain of the PBPs is an established target for antimicrobial inhibition by β-lactam antibiotics (Ghuysen, 1991). Consequently, much effort has been implemented to biochemically characterise the PBPs, to further the understanding of this important group of antimicrobial targets in terms of their enzymology and from the perspective of antibiotic development. The following sections discuss the existing knowledge of the PBP catalytic mechanism and the current strategies to analyse transpeptidase activity.

5.1.1. Transpeptidation and D,D-carboxypeptidation

The penicillin-binding domain of HMW-PBPs and LMW-PBPs is responsible for transpeptidation and D,D-carboxypeptidation (or endopeptidation) respectively (Ghuysen, 1991). Not aforementioned is the potential ability of these enzymes to also perform activities of each other to varying extents. This is plausible given the analogous catalytic residues and conserved sequence motifs of the penicillin-binding domains of different PBP classes. Examples include *Streptomyces* R61 D,D-peptidase, capable of transpeptidation and D,D-carboxypeptidation (Kumar and Pratt, 2005), and *E. coli* PBP4, capable of D,D-carboxypeptidation and endopeptidation (Clarke *et al.*, 2009). It is likely that substrate specificity, e.g. the ability to bind an acceptor peptide strand, defines the predominant role of each PBP *in vivo*.

The present understanding of the mechanistic enzymology of the three-state model for transpeptidation and D,D-carboxypeptidation is illustrated in Figures 5.1 and 5.2 respectively. The residues involved in substrate binding and catalysis remain controversial. During the formation of the acyl enzyme intermediate, it is believed that the conserved Lys of the first motif and the conserved Ser (Tyr in *Streptomyces* R61 D,D-peptidase) of the second motif are involved in a proton relay system (Lee *et al.*, 2001; Rhazi *et al.*, 2003). The ε-amino group of Lys (motif 1) is poised in a deprotonated state to abstract a proton from the active site serine γOH (motif 1), which concomitantly performs a nucleophilic attack of the donor carbonyl carbon (Macheboeuf *et al.*, 2006; Nicola *et al.*, 2005; Sauvage *et al.*, 2007). The γOH of Ser (motif 2) could participate in the protonation of the leaving group nitrogen (Rhazi *et al.*, 2003). The subsequent Ser γO could recover a proton from the protonated Lys ε-amino group (Rhazi *et al.*, 2003). Alternatively, in the deacylation step, Ser/Tyr γO (motif 2) (or a deprotonated Lys of motif 3 (Nicola *et al.*, 2005)) could abstract a proton from the acceptor (either an amino group or water), activating it for the attack of the acyl enzyme intermediate (Lee *et al.*, 2001; Nicola *et al.*, 2005). Eventually, a proton would be back donated to the active site serine (Rhazi *et al.*, 2003). Clearly, further experiments are required to decipher the precise mechanistic details and assign roles of the residues in this complex reaction.

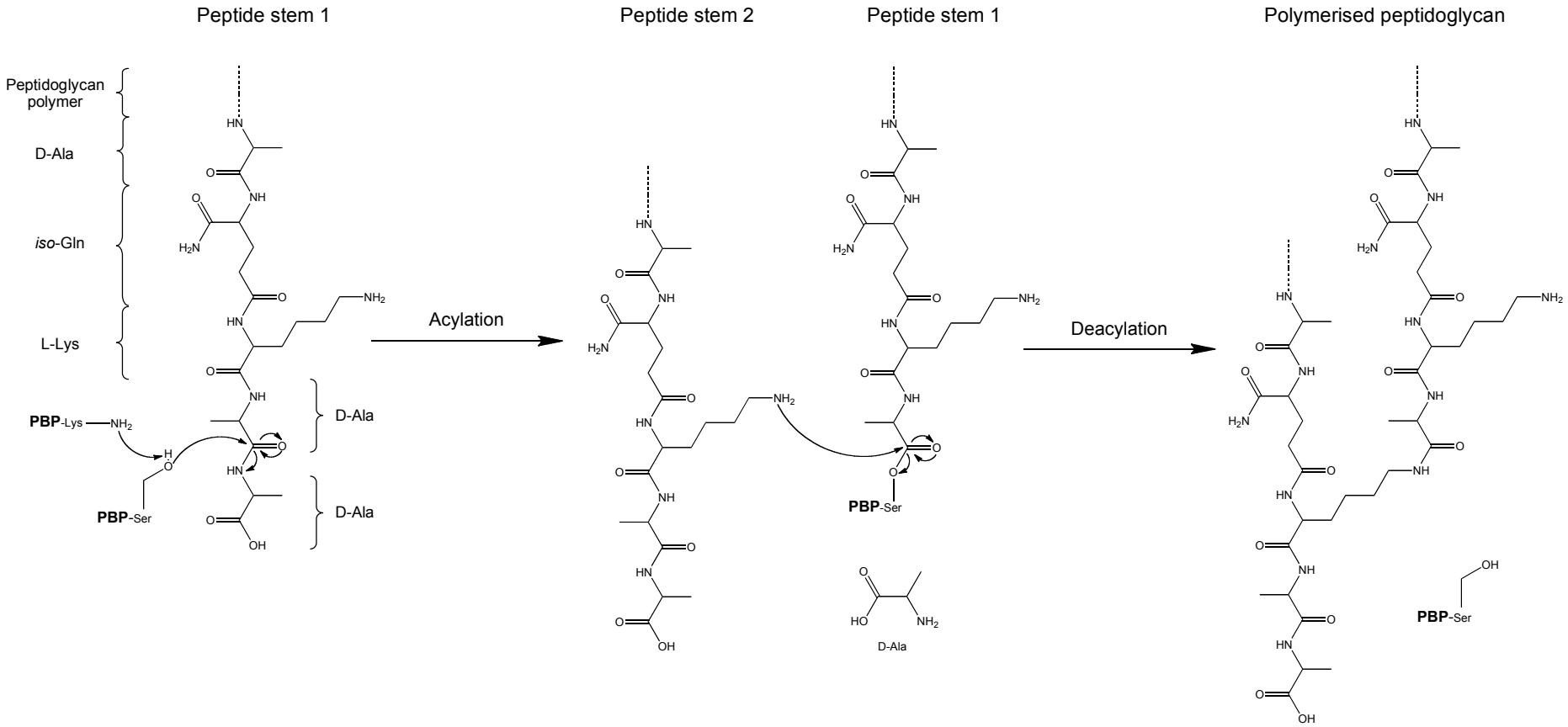

Figure 5.1: Proposed mechanism for transpeptidation. The pentapeptide stem of the peptidoglycan is displayed. During acylation, Lys (motif 1) abstracts a proton from the catalytic Ser (motif 1), which concomitantly attacks the donor carbonyl carbon of the penultimate D-Ala (Stem peptide 1), forming an acyl-enzyme intermediate and releasing the terminal D-Ala. In the deacylation step, the acceptor ε-amino group of the third position L-Lys (Stem peptide 2) (or the amino group of a branching enzyme from L-Lys) cleaves the acyl-enzyme intermediate by forming a cross-link with Stem peptide 1, concurrently regenerating the active site Ser.

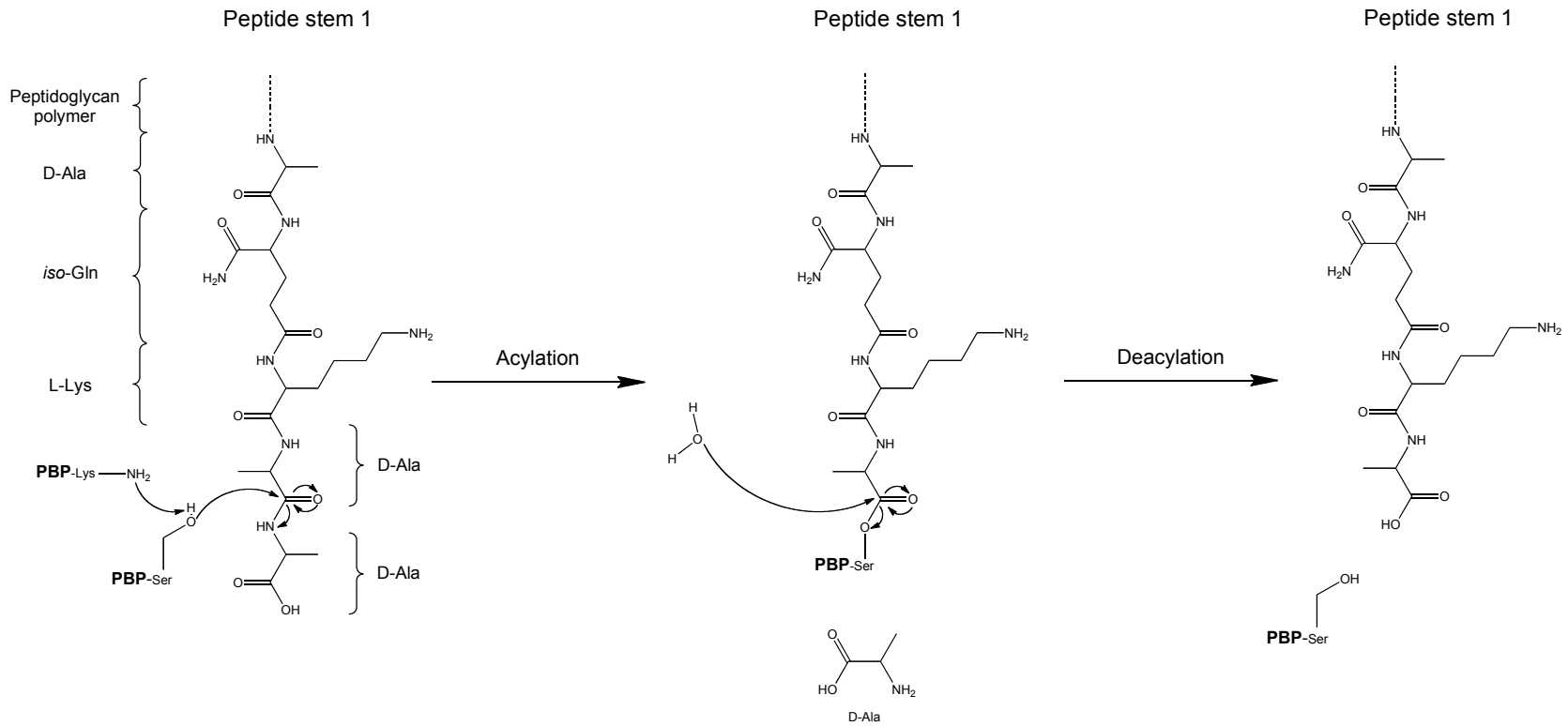

Figure 5.2: Proposed mechanism for D,D-carboxypeptidation. The pentapeptide stem of the peptidoglycan is shown. The acylation step proceeds as for transpeptidation (Figure 5.1). During deacylation, the acyl-enzyme intermediate is hydrolysed by the attack of a water molecule (instead of the amino group of an adjacent peptide stem), regenerating the active site serine and releasing a tetrapeptide stem, without the formation of a peptide bond.

5.1.2. Existing strategies to monitor transpeptidation or D,D-carboxypeptidation

The development of appropriate and sensitive techniques to detect transpeptidase activity is paramount to gain a comprehensive insight into the kinetic properties of the PBPs, information from which could contribute towards the design of novel drugs against these antimicrobial targets. The following sections discuss the current kinetic assays for the analysis of transpeptidase or D,D-carboxypeptidase activity.

5.1.2.1. D-ala release assays

Transpeptidase or D,D-carboxypeptidase reactions result in the release of the terminal D-Ala from the peptidoglycan pentapeptide stem. From as early as 1972, the detection of D-Ala has been a means of monitoring these activities. This technique is limited by its simplicity; D-Ala released from transpeptidation or D,D-carboxypeptidation cannot be distinguished. There are numerous methods to detect D-Ala release. Preliminary experiments performed by Mirelman *et al.* (1972) followed the incorporation of UDP-Mur*N*Ac-L-Ala-D-*iso*-Glu-L-Lys-D-Ala-[^{14}C]-D-Ala into crude membrane preparations of *Micrococcus luteus* and the PBP-dependent release of [^{14}C]-D-Ala was monitored. An alternative method to monitor D-Ala release is to couple the amino acid to a chromogenic assay, such as the one described later in this Chapter.

5.1.2.2. Peptide thioester pseudosubstrates

PBPs can exhibit thioesterase activity, where the hydrolysis of peptide thioester substrates can be monitored spectrophotometrically by a decrease in absorbance at 250 nm, which can be further sensitised by reacting the free thiol groups with 4,4'-dithiodipyridine (detected at 324 nm) (Wilkin *et al.*, 1993). The hydrolysis of the thioester substrates (donors) can be coupled concomitantly with transpeptidation reactions using amino acid substrates (acceptors) (Jamin *et al.*, 1993; Wilkin *et al.*, 1993). This approach can be used to monitor the effect of inhibitors, where the thioester acts as a reporter substrate. The inhibition of *S. pneumoniae* PBP2x by arylalkylidene rhodanine derivatives has been examined using this technique (Zervosen *et al.*, 2004).

5.1.2.3. Substrate analogue and inhibitor binding assays

Substrate analogue and inhibitor binding studies are common techniques to measure acylation and deacylation rates of PBPs. For example, the formation of an acyl-enzyme intermediate with a substrate analogue or inhibitor can be determined by measuring the decrease of the intrinsic protein fluorescence (due to quenching) using stopped-flow apparatus (Jamin *et al.*, 1993; Josephine *et al.*, 2006). Deacylation rates can be determined by labelling a PBP with [^{3}H]-benzylpenicillin, followed by an analysis of the amount of radioactivity retained by the protein over time (Pagliero *et al.*, 2004). A rapid technique to calculate binding constants has been developed by Stefanova *et al.* (2010). This approach involves the immobilisation of PBPs to a surface and subsequent labelling with a biotin-ampicillin conjugate. Treatment with a streptavidin-horseradish peroxide conjugate followed by a reaction with a fluorogenic substrate enables the detection of the PBPs. This provides the basis of a competition-binding assay where inhibitors compete with biotin-ampicillin for interactions with the PBP.

5.1.2.4. High Performance Liquid Chromatography (HPLC) analysis of transpeptidase products

HPLC analysis is the single technique that is able to distinguish between transpeptidase and D,D-carboxypeptidase products, which have different retention times depending on their retardation in the column material. The quantities of transpeptidation and hydrolysis products separated by HPLC can be measured by integration of the peak area, thus providing ratios for transpeptidase and D,D-carboxypeptidase activity (Wilkin *et al.*, 1993). Vinatier *et al.* (2009) have described a method where products of D,D-peptidation and transglycosylation can be detected by fluorescence during HPLC separation. D-Cys is incorporated into the pentapeptide chain of the peptidoglycan precursor, replacing the penultimate D-Ala. Following an incubation with a PBP, the products are treated with fluorescein maleimide, fluorescently labelling D-Cys.

Vollmer and colleagues (Bertsche *et al.*, 2005; Born *et al.*, 2006) have used HPLC to separate radiolabelled products of transglycosylase and transpeptidase activities.

Using this technique, the specificities of *E. coli* PBP1a (Born *et al.*, 2006) and PBP1b (Bertsche *et al.*, 2005) catalysed reactions were analysed using different acceptor strands for transpeptidation.

5.1.3. The future of transpeptidase assays

The assays described above aim to elucidate the complex transpeptidation reactions. However, kinetic information regarding the transpeptidase activity of many HMW-PBPs remains scarce. The recent, highly sensitive HPLC assays designed by Vollmer and co-workers (Bertsche *et al.*, 2005; Born *et al.*, 2006) to simultaneously analyse transglycosylation and transpeptidation reactions should have stimulated substantial progress in the analysis of HMW-PBPs. However, this has not transpired. A key explanation for this is that activity from isolated HMW-PBPs is often undetectable or weak *in vitro* owing to a lack of understanding of the preferred substrates (Pratt, 2008) and the absence of a membrane environment. Thus, establishing the optimum conditions for transpeptidation to occur remains challenging but is fundamental for advances in this area of research.

The work presented in this Chapter aims to investigate the transpeptidase activities of the *S. pneumoniae* β-lactam resistance determinants. These enzymes are of particular interest as they are the target of antimicrobial activity but are also the source of the β-lactam resistance mechanism. Different assays have been designed to analyse transpeptidase activity and rely on the ability to detect the hydrolysis of the terminal D-Ala from the peptidoglycan pentapeptide stem as summarised in Figure 5.3.

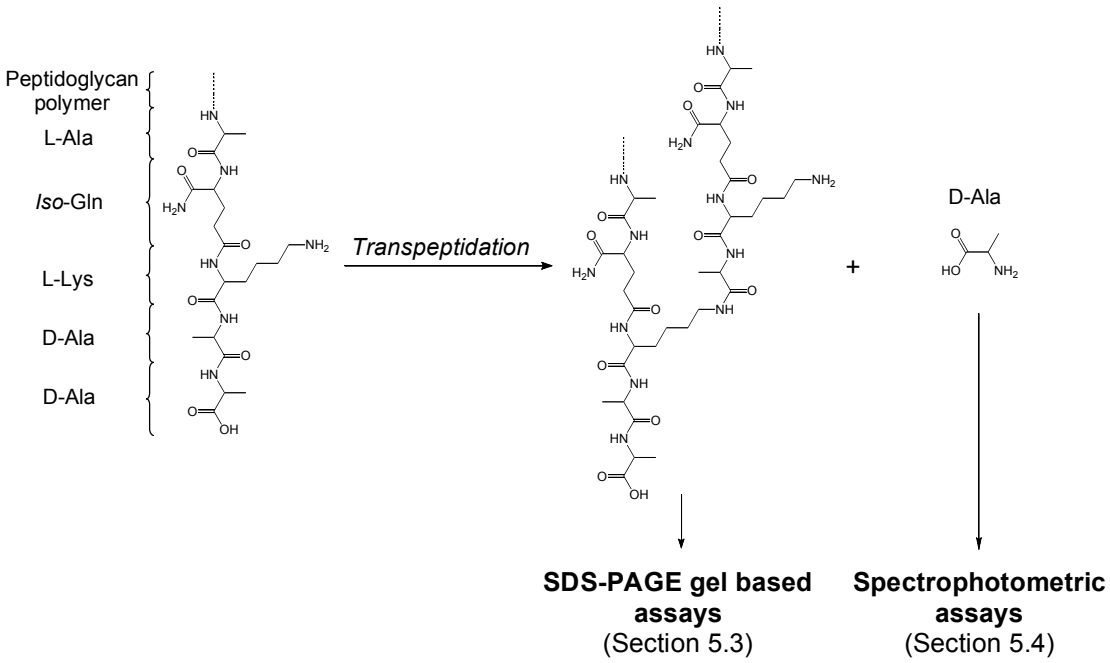

Figure 5.3: Features of transpeptidation exploited to monitor transpeptidase activity in this Chapter. The generation of a tetrapeptide stem or D-Ala was used to analyse transpeptidase (or D,D-carboxypeptidase) activity by two different techniques labelled on the Figure.

5.2. Experimental aims

- To detect the transpeptidase or D,D-carboxypeptidase activities of *S. pneumoniae* PBP1a, PBP2b and PBP2x by SDS-PAGE analysis

- To design a continuous spectrophotometric assay for the kinetic characterisation of the transpeptidase or D,D-carboxypeptidase activities of PBPs

- To kinetically characterise *Actinomadura* R39 D,D-peptidase using the developed continuous spectrophotometric assay

- To establish transpeptidase activity assays of *S. pneumoniae* PBP1a, PBP2b and PBP2x so to investigate their preferred substrates

5.3. Detection of transpeptidase or D,D-carboxypeptidase activity using SDS-PAGE

The penicillin-binding domains of *S. pneumoniae* PBP1a, PBP2b and PBP2x catalyse transpeptidation (forming a cross-link between two adjacent peptide side chains) and potentially D,D-carboxypeptidation (hydrolysing the terminal peptide bond of the peptide side chains) to undefined extents (see Section 5.1.1) (reactions reviewed by Sauvage *et al.* (2008a)). In both situations, the resulting peptidoglycan will consist of either penta- or tetrapeptide side chains and it is this aspect that can be exploited to identify transpeptidase or D,D-carboxypeptidase activity.

The SDS-PAGE technique of analysing the products from transglycosylation using VanFL, the fluorescent derivative of vancomycin (as described in Section 4.12), can be further developed to detect transpeptidation or D,D-carboxypeptidation. The vancomycin constituent of VanFL binds to the penultimate and ultimate D-Ala residues of the peptidoglycan pentapeptide stem (Nieto and Perkins, 1971), enabling the fluorescence detection of polymerised glycan chains separated by SDS-PAGE. VanFL is incapable of binding to the tetrapeptide stem. Therefore, in situations where the terminal D-Ala residue of a glycan chain peptide stem has been hydrolysed, either by transpeptidation or D,D-carboxypeptidation, the fluorescence signal resulting from VanFL binding would be reduced and a discrete fluorescence band that runs at the gel front would signify the presence of unbound VanFL. A drawback to this detection technique is that VanFL-bound Lipid II runs at the same position as unbound VanFL on the SDS-PAGE gel. This prevents analysis of transpeptidation or D,D-carboxypeptidation on the Lipid II monomer.

S. aureus MGT was utilised to provide the glycan chain substrate, which can be separated by SDS-PAGE (established in Section 4.12.2). The full-length PBP1a, PBP2b and PBP2x and their equivalent membrane-spanning truncates were incubated with polymerised substrate at 20°C for 3 hours (experimental details in Section 2.9.3). The glycan chain products were incubated with VanFL and separated by SDS-PAGE for the analysis of transpeptidase or D,D-carboxypeptidase activity. Figure 5.4 summarises the VanFL fluorescence signal detected following the various

incubations. VanFL was used in limiting amounts, ensuring that all VanFL bound to the pentapeptide side chains. Any unbound VanFL resulted from its inability to bind to the tetrapeptide side chain.

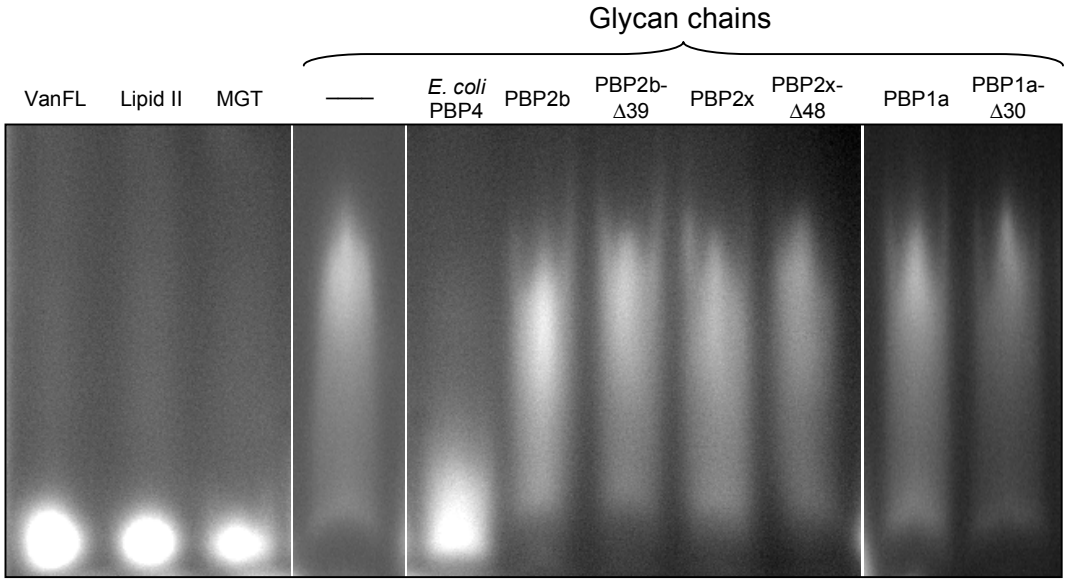

Figure 5.4: SDS-PAGE analysis of PBP-dependent transpeptidation or D,D-carboxypeptidation. Polymerised glycan chains were provided by MGT transglycosylation of Lys-Lipid II, prior to incubation with the transpeptidase variants. Following enzyme inactivation and removal, VanFL was added to each reaction, the products were separated by SDS-PAGE and VanFL-specific fluorescence was detected using GeneSnap Gel Doc with a blue light converter and filter (Section 2.9.3). VanFL is present in each lane in addition to the stated components; the reactions containing both Lipid II and MGT refer to the product of transglycosylation, glycan chains; the PBPs originate from *S. pneumoniae* unless otherwise stated.

The results from the fluorescence based SDS-PAGE gel analyses are inconclusive: the lanes containing the *S. pneumoniae* PBPs show little deviation in fluorescence from the glycan chain only control. Transpeptidase or D,D-carboxypeptidase activity of the *S. pneumoniae* PBPs was not apparent, but the activity could be present at considerably low levels. The control enzyme *E. coli* PBP4, a highly active D,D-carboxypeptidase (and endopeptidase) (Clarke *et al.*, 2009), clearly demonstrated D-Ala hydrolysis from the pentapeptide stem of the glycan chains; there is a substantial loss of fluorescence signal in the glycan chain expected region of the gel, and there is an intense fluorescent band at the gel front signifying unbound VanFL. The PBP4 control exemplifies that this technique is valid for demonstrating the hydrolysis of the terminal D-Ala from a pentapeptide stem of a polymerised glycan chain, but relies on an enzyme with extensive D-Ala hydrolysis activity.

5.4. Continuous spectrophotometric assay for PBP transpeptidase or D,D-carboxypeptidase-dependent D-Ala release

The penicillin-binding domains of PBPs are capable of hydrolysing the terminal D-Ala from the peptidoglycan pentapeptide side chain through either transpeptidase or D,D-carboxypeptidase activity. The generation of D-Ala could be followed by two continuous spectrophotometric assays outlined in Figure 5.5.

Assay (a) couples the esterification of D-Ala with D-Lac via the D-Ala-D-Lac ligase, VanA, with the concomitant conversion of the ATP cofactor to ADP and P_i. The production of ADP (assay ai), a substrate of pyruvate kinase, is then coupled to the dephosphorylation of phosphoenolpyruvate to pyruvate (yielding ATP). Pyruvate, in turn, is reduced to lactate by lactate dehydrogenase using the NADH cofactor, which is oxidised to NAD^+, monitored by a change in absorbance at 340 nm. Alternatively, the released P_i (assay aii) can be linked to the phosphorolysis of the chromogenic nucleoside MESG by PNP (as described in Section 4.4) releasing ribose-1-phosphate and 7-methyl-6-thioguanine giving a spectrophotometric signal at 360 nm.

Assay (b) is a recognised method of detecting D-Ala release from D,D-carboxypeptidases (Gutheil *et al.*, 2000). It relies on the oxidative deamination of D-Ala catalysed by D-amino acid oxidase (DAAO) with the formation of pyruvate, NH_3 and H_2O_2. Horseradish peroxidase (HRP) oxidises H_2O_2 to O_2 with the simultaneous breakdown of Amplex Red to resorufin giving a change in absorbance at 555 nm. Assay (a) was designed to combat issues with false positive signals produced from the breakdown of Amplex Red in assay (b) under long incubation times in the buffer system used.

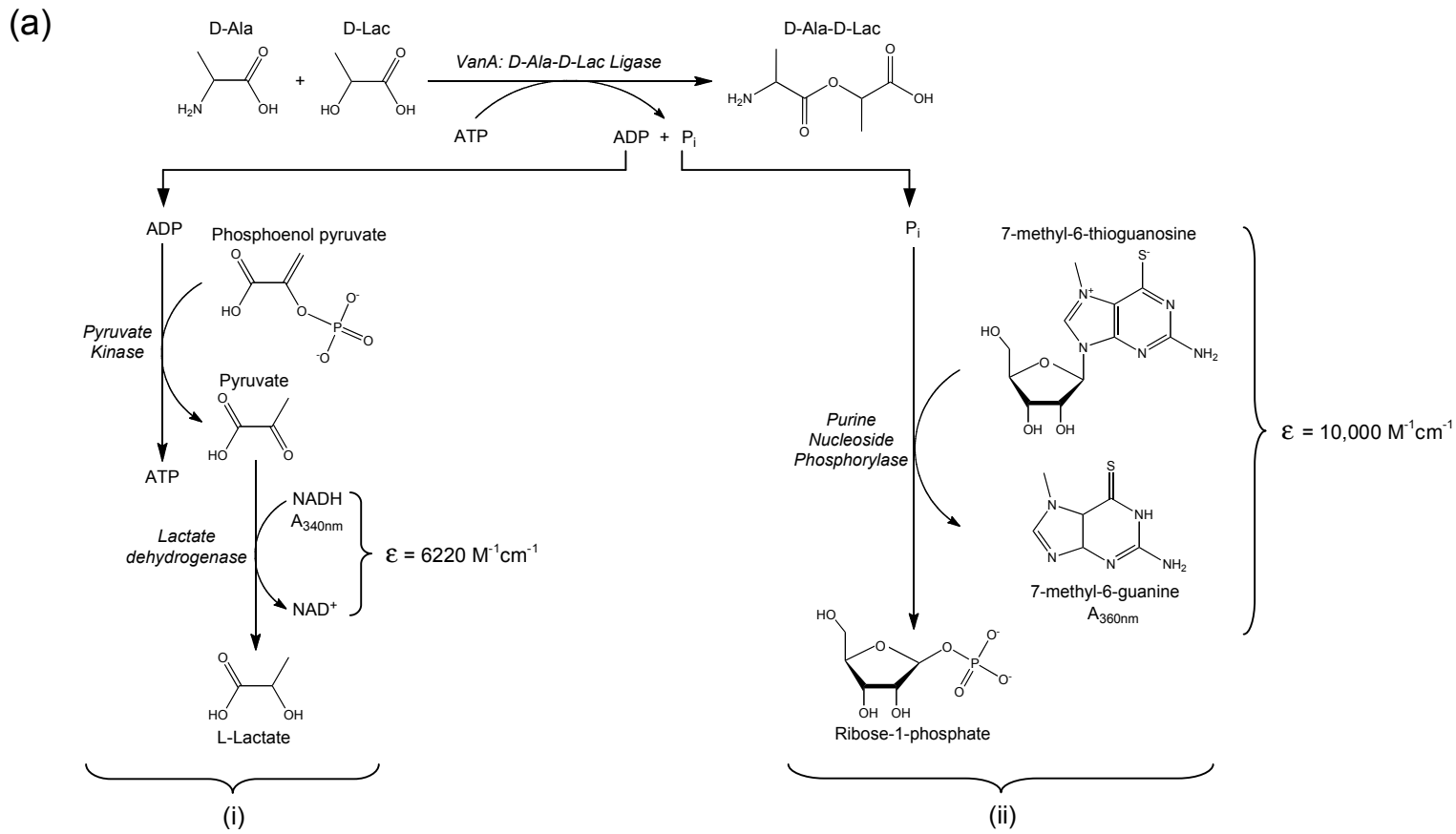

Figure 5.5: Continuous spectrophotometric assays for D-Ala release. (a) VanA catalyses the ligation of D-Ala and D-Lac, with the concomitant use of ATP, which is the source of spectrophotometric analysis. (i) Pyruvate kinase utilises ADP, converting phosphoenol pyruvate to pyruvate, and generating ATP. Pyruvate is reduced to lactate, catalysed by lactate dehydrogenase with the concurrent oxidation of NADH to NAD^+, detected by a change in absorbance at 340 nm. (ii) P_i is involved in the phosphorolysis of 7-methyl-6-thioguanosine catalysed by purine nucleoside phosphorylase, generating 7-methyl-6-thioguanine, which can be monitored by absorbance at 360 nm.

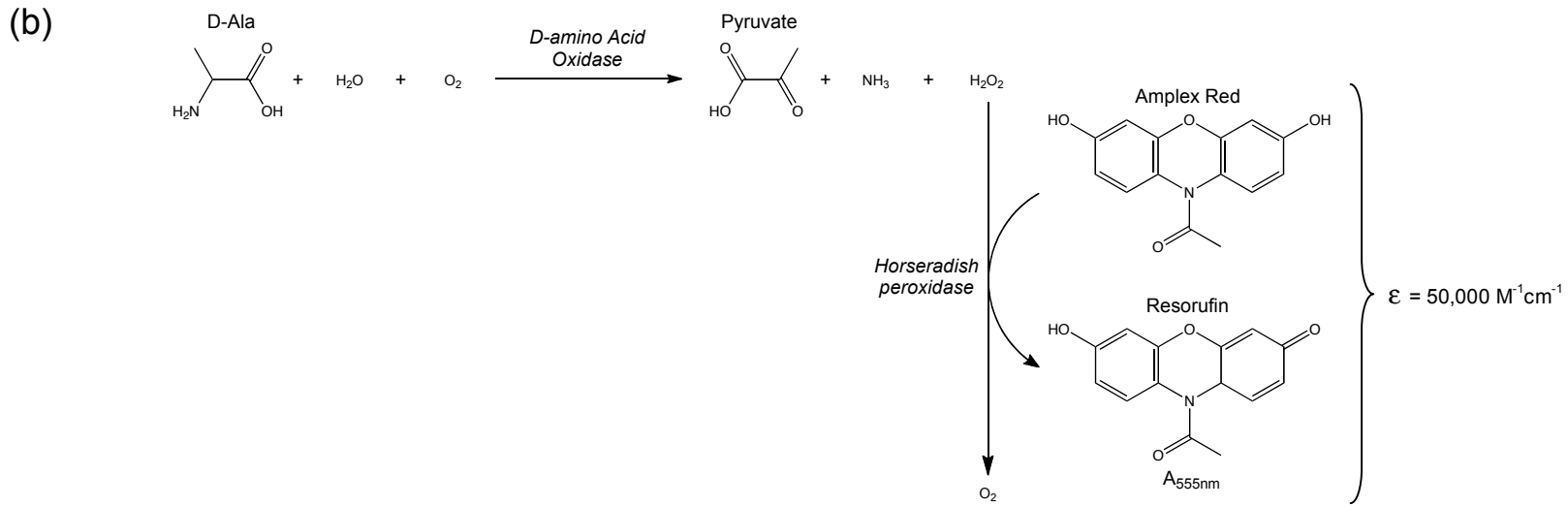

Figure 5.5 (continued): Continuous spectrophotometric assays for D-Ala release. (b) D-amino acid oxidase catalyses the oxidation of D-Ala to pyruvate, producing hydrogen peroxide. Horseradish peroxidase uses hydrogen peroxide to catalyse the breakdown of Amplex Red to resorufin, which absorbs strongly at 555 nm.

The assays outlined above are specific for D-Ala release only and do not provide a means of distinguishing between transpeptidation and D,D-carboxypeptidation.

5.5. The D-Ala-D-Lac ligase coupling enzyme for D-Ala detection

The kinetic characteristics of VanA (Appendix C1), having a minimal preference for D-Ala in its second substrate binding site, make it a suitable D-Ala-D-Lac ligase for use in the coupled assays for D-Ala release.

5.5.1. Expression and purification of VanA

The vector pET28d::*vanA* (*E. faecalis vanA* cloned into the pET28d vector) was provided by S. Batson. VanA was expressed and purified according to Batson (2010) (described and illustrated in Appendix C2).

5.5.2. Characterisation of the VanA-coupled assay for D-Ala hydrolysis by P_i release

To establish that the VanA-coupled assay was capable of monitoring D-Ala release in a continuous manner, a control enzyme known to hydrolyse D-Ala from the peptidoglycan peptide stem was required. This role was fulfilled by the *Actinomadura* sp. R39 D,D-peptidase (kindly provided by J-M. Frère, Univeristy of Liège), a well-characterised water-soluble (loosely membrane associated) Class C PBP that exhibits D,D-carboxypeptidation and transpeptidation *in vitro* (Granier *et al.*, 1992). The dependence on all assay components for the detection of D-Ala was confirmed by the continuous spectrophotometric assay time course (Figure 5.6) (experimental details in Section 2.9.1.1). Reactions initiated in the absence of a single assay constituent (Figure 5.6, point (a)) did not show a change in absorbance at the specified wavelength until the omitted component was introduced (Figure 5.6 point (b)). D-Ala release was reliant on the presence of D,D-peptidase and the peptidoglycan fragment substrate. The antibiotic ampicillin, demonstrated the β-lactam-sensitivity of the PBP. The *S. pneumoniae* PBPs of future interest require the presence of detergent to remain soluble. Consequently, 0.1 % (w/v) DDM was assessed in the coupled assay and confirmed not to influence the coupling enzymes.

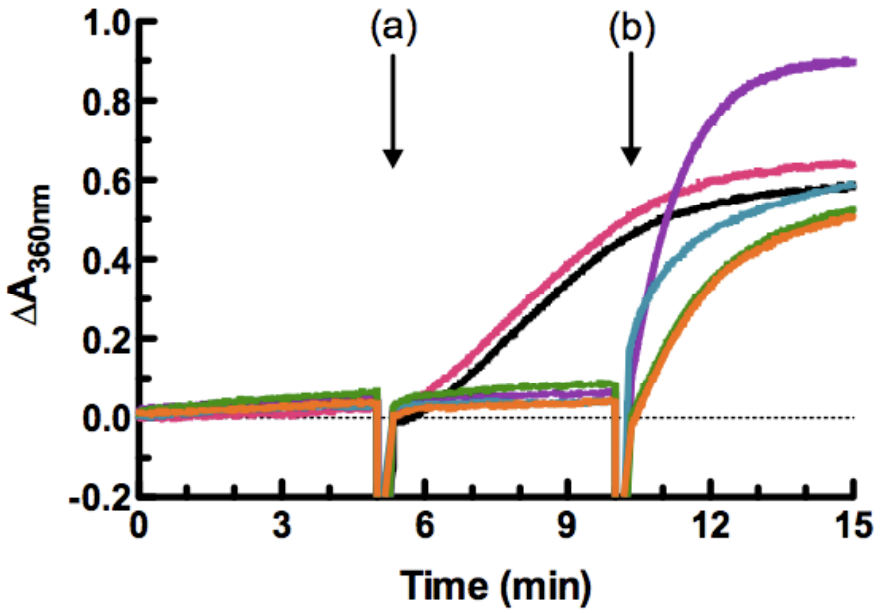

Line	Assay components present at time 0 min	Assay component added at point (a)	Assay component added at point (b)
———	P_i detection reagents, VanA, D-Lac, ATP, D,D-peptidase	UDP-Mur*N*Ac-*meso*-DAP-pentapeptide	n/a
———	P_i detection reagents, VanA, D-Lac, ATP, UDP-Mur*N*Ac-*meso*-DAP-pentapeptide	D,D-peptidase	n/a
———	P_i detection reagents, ampicillin, VanA, D-Lac, ATP, D,D-peptidase	UDP-Mur*N*Ac-*meso*-DAP-pentapeptide	D-Ala
———	P_i detection reagents, VanA, D-Lac, D,D-peptidase	UDP-Mur*N*Ac-*meso*-DAP-pentapeptide	ATP
———	P_i detection reagents, D-Lac, ATP, D,D-peptidase	UDP-Mur*N*Ac-*meso*-DAP-pentapeptide	VanA
———	P_i detection reagents, VanA, ATP, D,D-peptidase	UDP-Mur*N*Ac-*meso*-DAP-pentapeptide	D-Lac

Figure 5.6: Continuous spectrophotometric time course demonstrating the dependence on assay components for the detection of *Actinomadura* R39 D,D-peptidase activity. The embedded table describes the assay components present at time 0 min, and at points of addition (a) and (b). P_i detection agents: 1 unit PNP, 400 µM MESG. [UDP-*N*-acetylmuramyl-L-Ala-γ-D-Glu-*meso*-DAP-D-Ala-D-Ala] (abbreviated to UDP-Mur*N*Ac-*meso*-DAP-pentapeptide) was 100 µM and [*Actinomadura* R39 D,D-peptidase] was 35 nM in each reaction.

The VanA-coupled assay exhibited a lag phase prior to the steady state velocity, where the substrate of VanA, D-Ala, from the initial reaction of the coupled sequence, was accumulating. This is a feature occasionally observed in enzyme-coupled assays and is caused by coupling enzyme insufficiency. The lag phase (dependent on the coupling enzymes, not the initial enzyme (Easterby, 1973)) could be minimised by additional VanA. The length of the linear, steady state velocity period (determined by the initial enzyme) was sufficient to allow rate measurements to be calculated. It was ensured that the D,D-peptidase reaction remained rate-limiting at the highest substrate concentrations and further addition of VanA did not enhance the rate of D-Ala production.

5.6. Kinetic characterisation and substrate specificity of *Actinomadura* R39 D,D-peptidase using the VanA-coupled assay system for detection of D-Ala release

The suitability of the VanA-coupled assay system for the kinetic characterisation of PBP-mediated transpeptidase and D,D-carboxypeptidase activity was established using *Actinomadura* R39 D,D-peptidase. This enzyme has been characterised in detail, both kinetically (Anderson *et al.*, 2003) and structurally (Sauvage *et al.*, 2005). Anderson *et al.* (2003) have examined the activity of the enzyme with various synthetic peptidoglycan mimetic substrates by monitoring the hydrolysis of the peptide bond spectrophotometrically. Two of the synthetic peptide substrates used were: D-α-Aminopimelyl-ε-D-Alanyl-D-Ala and ε-Aminohexanoyl-D-Alanyl-D-Ala. Both represent peptide analogues of the three amino acids at the terminal of the peptidoglycan stem peptide. The former is a mimetic analogue of *Actinomadura* peptidoglycan (i.e. *meso*-DAP-D-Ala-D-Ala positions 3-5 of the stem peptide), whereas the latter is a peptide analogue of Gram-positive peptidoglycan (i.e. L-Lys-D-Ala-D-Ala positions 3-5 of the stem peptide). Although the D,D-peptidase rapidly hydrolyses both substrates, the *Actinomadura* R39 D,D-peptidase shows specificity towards the amino acid at position 3 of the peptidoglycan peptide side chain, suggesting recognition of *meso*-DAP is key to the reaction catalysed (Anderson *et al.*, 2003).

Similar to the peptidoglycan analogues utilised by Anderson *et al.* (2003), two UDP-linked peptidoglycan precursors were used as substrates for the kinetic characterisation of *Actinomadura* R39 D,D-peptidase: UDP-*N*-acetylmuramyl-L-Ala-γ-D-Glu-*meso*-DAP-D-Ala-D-Ala and UDP-*N*-acetylmuramyl-L-Ala-γ-D-Glu-L-Lys-D-Ala-D-Ala (provided by A. Catherwood). The structures of these substrates vary only at position 3 of the pentapeptide side chain, where the former substrate has a carboxyl group present on the ε-carbon atom in addition to the ε-amino group of the third position L-Lys in the latter substrate, generating a *meso*-DAP residue.

The kinetic characterisation of *Actinomadura* R39 D,D-peptidase with UDP-*N*-acetylmuramyl-L-Ala-γ-D-Glu-*meso*-DAP-D-Ala-D-Ala was completed using the assay outlined in Figure 5.5aii (experimental details in Section 2.9.1.1.2), and the equivalent characterisation with the near identical substrate UDP-*N*-acetylmuramyl-L-Ala-γ-D-Glu-L-Lys-D-Ala-D-Ala was performed using the assay depicted in Figure 5.5ai (experimental details in Section 2.9.1.1.1). Extreme phosphate contamination present in the latter substrate (resulting from co-elution during purification) dictated that D-Ala release was detected by monitoring ADP release.

A hyperbolic relationship was displayed between the D,D-peptidase initial velocity and the substrate concentration of both UDP-linked-*N*-acetylmuramyl pentapeptide substrates (Figure 5.7). Consequently, the kinetic data was fitted to the Michaelis-Menten equation by non-linear regression (Equation 1) to solve k_{cat} and K_m.

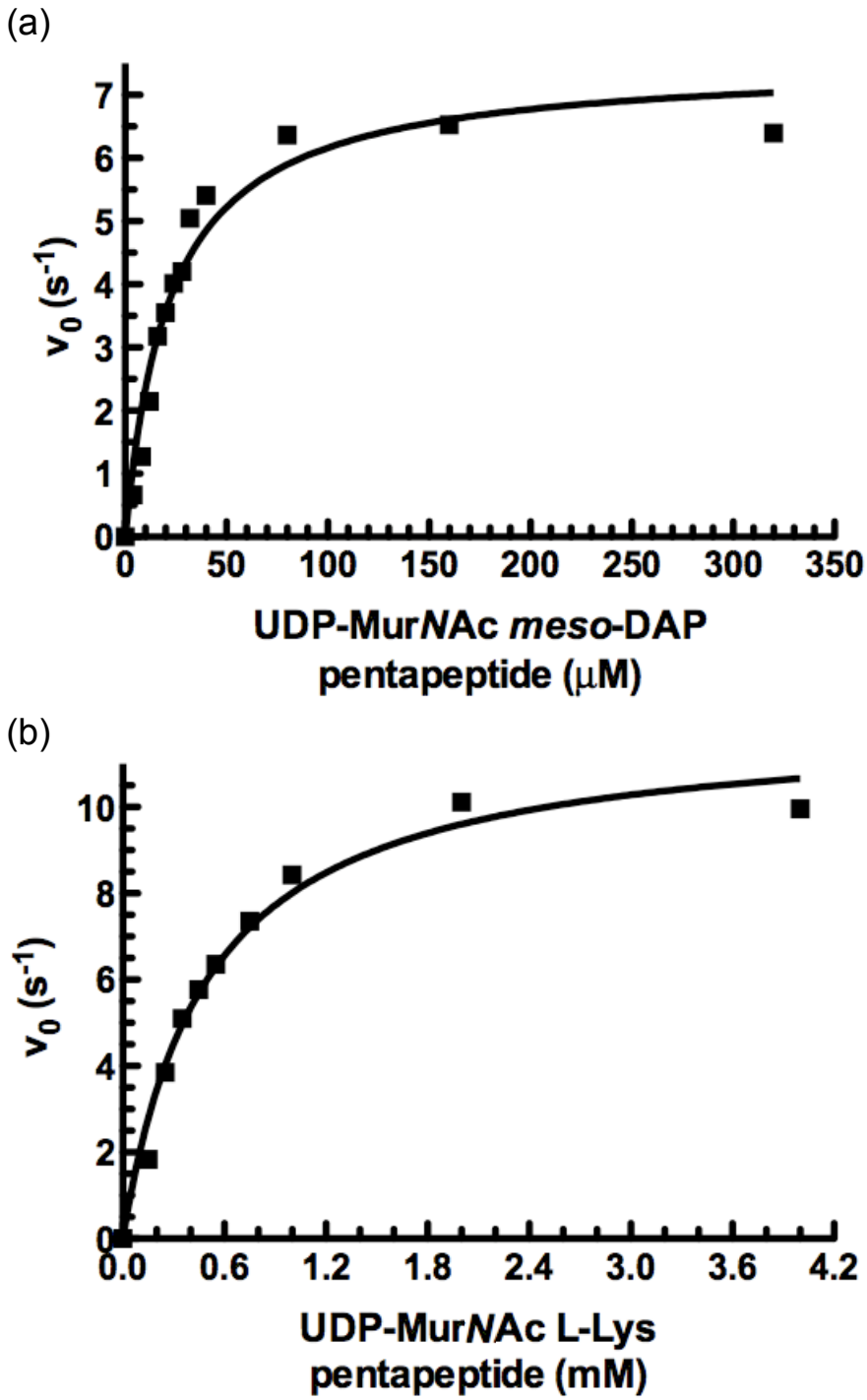

Figure 5.7: Kinetics of dependence of *Actinomadura* R39 D,D-peptidase on UDP-linked-*N*-acetylmuramyl pentapeptide substrates. Velocity of *Actinomadura* R39 D,D-peptidase-dependent D-Ala release (established by the VanA-coupled assay system) at different substrate concentrations. (a) Initial velocity plotted versus [UDP-*N*-acetylmuramyl-L-Ala-γ-D-Glu-*meso*-DAP-D-Ala-D-Ala] (referred to as UDP-Mur*N*Ac *meso*-DAP pentapeptide). (b) Initial velocity plotted versus [UDP-*N*-acetylmuramyl-L-Ala-γ-D-Glu-L-Lys-D-Ala-D-Ala] (referred to as UDP-Mur*N*Ac L-Lys pentapeptide). [*Actinomadura* R39 D,D-peptidase] was constant at 35 nM. Data were fitted by non-linear regression to Equation 1.

The kinetic parameters of *Actinomadura* R39 D,D-peptidase with the UDP-linked peptidoglycan fragments are presented in Table 5.1.

Substrate	Assay	Kinetic constants		
		K_m[a] (μM)	k_{cat}[a] (s^{-1})	k_{cat}[a]/K_m[a] ($s^{-1}M^{-1}$)
UDP-*N*-acetylmuramyl-L-Ala-γ-D-Glu-*meso*-DAP-D-Ala-D-Ala	D-Ala release by P_i detection (Figure 5.5aii)	22.04±3.40	7.52±0.40	3.41×10^5
UDP-*N*-acetylmuramyl-L-Ala-γ-D-Glu-L-Lys-D-Ala-D-Ala	D-Ala release by ADP detection (Figure 5.5ai)	495.80±64.15	11.98±0.56	2.41×10^4

Table 5.1: Kinetic parameters of D-Ala hydrolysis catalysed by *Actinomadura* R39 D,D-peptidase. The D-Ala hydrolysis was monitored by the assay system stated, referring to the reaction pathway displayed in Figure 5.5a. The kinetic constants were derived according to Equation 1, following fitting of the data by non-linear regression (using Graph Pad PRISM 5) with R^2 values of 0.96 and 0.98 for the substrates UDP-*N*-acetylmuramyl-L-Ala-γ-D-Glu-*meso*-DAP-D-Ala-D-Ala and UDP-*N*-acetylmuramyl-L-Ala-γ-D-Glu-L-Lys-D-Ala-D-Ala respectively. [a]Values ± standard error.

In support of the kinetic data collected by Anderson *et al.* (2003), the data presented in Table 5.1 demonstrates that *Actinomadura* R39 D,D-peptidase has a selective specificity for a *meso*-DAP residue residing at position 3 in the pentapeptide chain of the UDP-linked peptidoglycan precursor. D-Ala is hydrolysed from the UDP-linked peptidoglycan fragment with a k_{cat}/K_m of 15× greater magnitude when the ε-carbon atom is supplemented with a carboxyl group in addition to the ε-amino group. The higher k_{cat}/K_m arises from the lower K_m, with a minimal difference between the two values of k_{cat} for the different substrates. This suggests that the third position of the pentapeptide side chain is subject to a specific recognition by the enzyme. Structural analyses of *Actinomadura* R39 D,D-peptidase by Sauvage *et al.* (2005) and Dzhekieva *et al.* (2010) have confirmed the presence of a suspected binding pocket specific for the D-α-aminopimelyl side chain (discussed in Section 6.1.3.1, Figure 6.1), which features a hydrophobic cleft for the short carbon chain and strong hydrogen binding for the polar terminus of the amino acid residue (Sauvage *et al.*,

2008b). The latter attribute could significantly contribute to the difference in K_m of D,D-peptidase with the two substrates used in this study, where the additional carboxyl group of the *meso*-DAP side chain could promote stronger hydrogen bonding to the PBP-active site in comparison to that of L-Lys.

5.7. Spectrophotometric assays for the detection of D-Ala release by *S. pneumoniae* Class A and B PBPs

5.7.1. Substrate selection

To maximise the probability of observing activity from the penicillin-binding domain of Class A and B PBPs (a rare experience *in vitro*), a substrate most resembling the natural substrate was essential. In reference to *S. pneumoniae* PBPs, monomeric or polymerised Lys-Lipid II fulfilled this role (D-Glu replaced the *S. pneumoniae*-specific *iso*-Gln (Garcia-Bustos and Tomasz, 1990) at position 2 of the Lys-Lipid II pentapeptide side chain as the latter form was unavailable). Soluble peptidoglycan fragments (such as a UDP-Mur*N*Ac pentapeptide) were not employed to examine the full-length PBP activity because they may have lacked a component vital for substrate recognition by these enzymes.

5.7.2. The Amplex Red assay: a sensitive system for D-Ala detection

The continuous spectrophotometric VanA coupled assay can be used to characterise PBPs with high rates of catalysis. Enzymes exhibiting low rates of catalysis could be monitored using the VanA-coupled assay system in a discontinous manner. Difficulties arise when the enzyme of interest has a slow rate of catalysis, and uses a substrate of high expense in limited supply (i.e. Lipid II).

The Amplex Red assay (Figure 5.5b) was employed to monitor D-Ala release by the transpeptidase activities of the *S. pneumoniae* Class A and B PBPs. This assay is five times more sensitive for D-Ala detection than the VanA-coupled assay (compare the molar extinction coefficients of the absorbing molecules in the assays shown in Figure 5.5). The increased sensitivity of the Amplex Red assay was crucial to

optimise the detection of the PBP D-Ala hydrolysis activity, which was anticipated to be low *in vitro*.

The Amplex Red assay is well-established and has been used to characterise the D,D-carboxypeptidase activity of various PBPs including *E. coli* PBP5 (Stefanova *et al.*, 2002), *E. coli* PBP4 (Clarke *et al.*, 2009) and *N. gonorrhoeae* PBP3 (Peddi *et al.*, 2009). The assay has been fully characterised and factors such as the production of H_2O_2 have been confirmed not to interfere with the functioning of the assay constituents (Clarke *et al.* (2009) and Clark (2008) for details). For the purposes of this study, the presence of 0.1 % (w/v) DDM in the assay, essential for maintaining lipid and membrane protein solubility, was investigated and shown to have no effect on the coupling system.

5.8. Development of a discontinous spectrophotometric assay for the D-Ala release activity of *S. pneumoniae* PBP1a, PBP2b and PBP2x

5.8.1. Production of polymerised Lipid II substrates

To establish whether the D-Ala hydrolysis activities of *S. pneumoniae* PBP1a, PBP2b and PBP2x have a substrate preference for a polymerised glycan chain (reminiscent of the peptidoglycan structure) over the monomeric Lipid II subunit, synthesis of the former substrate was required. This was achieved by incubating MGT or PBP1a-S370A with Lys-Lipid II; both enzymes have validated active transglycosylase domains (Chapter 4).

5.8.1.1. Discovery of a contaminating enzyme with D-Ala hydrolysis activity

The Amplex Red assay was used to confirm the anticipated minimal background levels of D-Ala contamination following transglycosylation. Unexpectedly, both MGT and PBP1a-S370A demonstrated significant D-Ala hydrolysis activity (despite lacking active transpeptidase domains), which was not an artefact of the assay or D-Ala contamination in the enzyme or Lipid II preparations. Incubation of the transglycosylases with a 10-fold excess concentration of ampicillin prior to the addition of Lys-Lipid II dramatically reduced the production of D-Ala in the MGT and PBP1a-S370A reactions. Inhibition by a β-lactam is a specific property of the penicillin-binding proteins, signifying that the contaminating protein was a PBP, the sole source of which would have been from the *E. coli* host upon target protein expression. The inability to totally eliminate the D-Ala hydrolysis activity in the MGT preparation indicated that more than one contaminating PBP could have been present with different β-lactam sensitivities.

5.8.1.2. Investigating the identity of the contaminating D-Ala hydrolysing enzyme

In an attempt to identify the contaminating *E. coli* PBP by its molecular weight, the preparations of MGT and PBP1a-S370A were pre-incubated with BOCILLIN FL (see Section 3.7) and analysed by SDS-PAGE. The SDS-PAGE gel failed to highlight any contaminating protein with BOCILLIN FL-dependent fluorescence. In a comparative assay to that involving ampicillin (Section 5.8.1.1), it was found that BOCILLIN FL was incapable of reducing or eliminating the D-Ala hydrolysis activity. The large fluorescent constituent of BOCILLIN FL could have sterically prevented the reaction with the active site serine of the contaminating PBP.

5.8.1.3. Removal of the contaminating D-Ala hydrolysis activity

Despite the identity of the enzyme responsible for the contaminating D-Ala hydrolysis activity remaining elusive, it needed to be eradicated so as not to interfere with future PBP characterisation studies. Developing a purification method that ensured the elimination of the contaminating enzyme from the MGT and PBP1a-S370A preparations would imply its absence from the other PBP protein preparations.

MGT and PBP1a-S370A were purified using IMAC under denaturing conditions (2M urea), but this resulted in protein aggregation and precipitation. MGT was also purified in the presence of ampicillin to inactivate the D-Ala hydrolysis activity. This successfully reduced the level of the contaminating D-Ala hydrolysis activity, although a significant level remained, comparable to that contaminating the PBP1a-S370A enzyme preparation. There are many other possible solutions to eliminate the contaminating activity, which are discussed later in this Chapter.

Regardless of the persistent contaminating D-Ala hydrolysis activity in the enzyme preparations required to make the glycan chain substrates, the transpeptidase/D,D-carboxypeptidase activities of *S. pneumoniae* PBP1a, PBP2b and PBP2x were analysed. Appropriate control experiments eliminated the impact of the contaminating D-Ala hydrolysis activity, ensuring that any activity detected was specific to the PBP under investigation.

5.8.2. Duration of enzyme incubations with substrate

Long incubation times of the *S. pneumoniae* PBP1a, PBP2b and PBP2x with the Lys-Lipid II substrate were essential to allow the maximum opportunity to detect D-Ala hydrolysis. 6 h and 18 h incubations were completed at 20°C and D-Ala hydrolysis was detected using the Amplex Red assay (Section 2.9.2.1 for experimental details). The 6 h incubations gave changes in absorbance that could not be reliably distinguished from background levels, whereas a significant increase in absorbance was detected following the 18 h incubations.

5.8.3. Experimental design

A detailed account of the experimental procedures for measuring the D-Ala production by *S. pneumoniae* PBP1a, PBP2b and PBP2x, including their equivalent active site mutants (PBP1a-S370A, PBP1a-E91Q, PBP2b-S391A, PBP2x-S337A) is described in Section 2.9.2.1. Briefly, 45 μM of each PBP (or 120 μM MGT) was incubated for 18 h at 20°C with the specified substrate (either Lys-Lipid II or a polymerised form obtained through a pre-incubation of Lys-Lipid II with MGT or PBP1a-S370A). Lys-Lipid II was present at a final concentration of 0.33 mM (prior to any enzymatic processing i.e. transglycosylation), ensuring the concentration of available pentapeptide chains was identical in each reaction. The buffer used was that optimised for PBP1a transglycosylation (Section 4.9): 20 mM Tris, 1 mM $MgCl_2$, 0.1 % (w/v) DDM, 22 mM Decyl PEG, 20 % (v/v) DMSO, pH 8.0. Following the overnight incubation, the protein was inactivated by heat denaturation. This method was chosen over β-lactam inactivation because the protein needed to be removed prior to D-Ala analysis by the Amplex Red assay. The precipitated material was pelleted by centrifugation and the presence of D-Ala in the supernatant was determined using the Amplex Red assay.

5.9. Analysis of PBP1a-dependent transpeptidation or D,D-carboxypeptidation.

5.9.1. D-Ala release activity of PBP1a

PBP1a is a bifunctional enzyme, capable of transglycosylation (established in Chapter 4) and transpeptidation. Under the assay conditions described above, the ability of the penicillin-binding domain to hydrolyse D-Ala, either from a monomeric or polymeric Lys-Lipid II substrate, was assessed. The results are presented in Figure 5.8, displaying the raw experimental data, and the corrected data (revealing the level of activity specific to the enzyme of interest, irrespective of background signals).

Figure 5.8 (following page): *S. pneumoniae* PBP1a-dependent D-Ala release. Variants of PBP1a were incubated with Lys-Lipid II and MGT-polymerised Lys-Lipid II for 18 h. The Amplex Red assay determined the level of D-Ala release resulting from either transpeptidation or D,D-carboxypeptidation. The primary y-axis shows the absorbance change at 555 nm due to the presence of D-Ala and the secondary y-axis shows the corresponding [D-Ala] in the discontinuous assay. The lanes are labelled with the reaction components and have been designated a number. The raw experimental data (■) (a) and the corrected data (■) (b) are shown. The corrected data was established by subtracting the raw value of the controls (enzyme only and Lipid II only) away from the raw value of the combined enzyme with Lipid II incubations, giving a true estimation of D-Ala release activity. Enzyme only and Lys-Lipid II only controls are represented in lanes 1-8. The reactions of MGT with Lipid II (lane 9), and PBP1a-S370A with Lipid II (lane 13), enzymes only capable of transglycosylation, show significant levels of contaminating D-Ala hydrolysis activity present in the enzyme preparations. To correct for this, the raw value of [D-Ala] generated upon incubation with Lipid II and MGT or PBP1a-S370A (lanes 9a and 13a respectively) was subtracted from the raw data of reactions incubated with an additional PBP (lanes 12a, 14a and 15a) (further to the subtraction of the value for the enzyme only control). The black-dashed line on lane 10b signifies the level of PBP1a-dependent D-Ala release allowing for an equivalent level of contaminating D-Ala hydrolysis activity as in the PBP1a-E91Q preparation (if the activity observed in the presence of glycan chains is a result of the contaminant, lane 12b; see text). Values represent the mean ± standard deviation of the raw (a) and corrected (b) data, based on triplicate reactions.

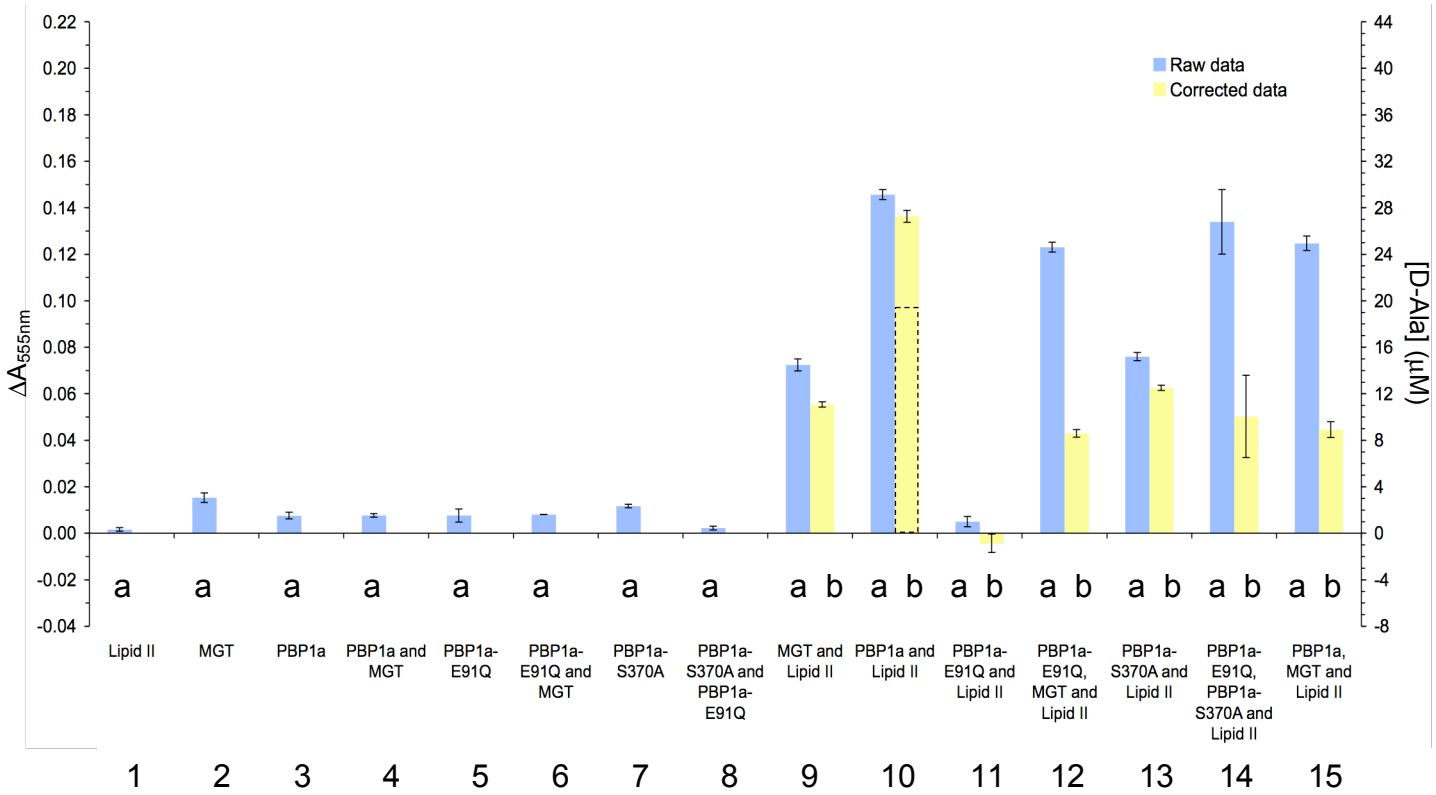

Figure 5.8: *S. pneumoniae* PBP1a-dependent D-Ala release. Legend on previous page.

The known contaminating D-Ala hydrolysis activity present in the MGT and PBP1a-S370A preparations (lanes 9 and 13 respectively) leads to difficulties in interpreting the D-Ala hydrolysis activity of PBP1a variants. The contaminant appeared to be absent in the PBP1a-E91Q preparation; D-Ala production was not detected in the incubation of PBP1a-E91Q with Lipid II (lane 11b). The existence of the contaminant in the PBP1a preparation was evaluated by addressing the theory that in the sole presence of glycan chains (and absence of Lipid II monomers), PBP1a and PBP1a-E91Q should have equivalent D-Ala release activities because only the transpeptidase domains would be functional. Therefore, any additional activity observed in the PBP1a incubations would be a consequence of a contaminating activity. MGT was used to polymerise Lys-Lipid II to completion prior to incubation with PBP1a (lane 15) or PBP1a-E91Q (lane 12). The levels of D-Ala release in the incubations are comparable, suggesting that the contaminant was absent in the PBP1a preparation.

A point to note is that the contaminating D-Ala activity was evident in incubations where glycan chains were generated (MGT, lane 9; PBP1a-S370A, lane 14), but was not apparent in incubations where glycan chains were absent (PBP1a-E91Q with Lipid II, lane 11). The contaminant, therefore, could have had a substrate preference for glycan chains. Thus, the D-Ala release activities presumed to be attributed to the transpeptidase domain of PBP1a-E91Q when in the presence of glycan chains (lanes 12 and 14) (discussed below) could in fact have been a result of the contaminating activity. The incubation of PBP1a with MGT-polymerised glycan chains (lane 15b) yielded ~9 μM D-Ala. On the assumption that the 9 μM D-Ala produced was a product of the contaminating activity in the PBP1a preparation, the incubation of PBP1a with Lys-Lipid II still produced a further 19 μM (lane 10b, black-dashed line), thus implying D-Ala hydrolysis specific to PBP1a activity.

In order to evaluate the results further, the assumption is made that the contaminating activity was not present in the PBP1a-E91Q and PBP1a preparations. This is based on the absence of contaminating activity in the PBP1a-E91Q incubation (with Lipid II, lane 11) and the comparison of D-Ala release activities of PBP1a-E91Q and PBP1a in the presence of glycan chains (lanes 12 and 15 respectively).

5.9.2. Investigating the substrate preference of the transpeptidase domain of PBP1a

The preferential substrate of PBP1a was determined using active site mutants of the enzyme: PBP1a-E91Q (capable of transpeptidase/D,D-carboxypeptidation only) and PBP1a-S370A (capable of transglycosylation only). No D-Ala hydrolysis activity was detected upon incubation of PBP1a-E91Q with Lys-Lipid II (lane 11), signifying the lipid monomer alone was not a suitable substrate.

To assess whether PBP1a-E91Q could perform transpeptidation/D,D-carboxypeptidation using a polymerised glycan chain, the enzyme was incubated in two separate reactions, each having a different source of the polymerised Lys-Lipid II (derived from either MGT or PBP1a-S370A activities, lanes 12 and 14 respectively). The results from both incubations are clear: the presence of both PBP1a-E91Q and polymerised glycan chains significantly increased the level of D-Ala detected, indicative of transpeptidase/D,D-carboxypeptidase activity. Thus, the penicillin-binding domain of PBP1a required the presence of glycan chains, to either act as a substrate or to stimulate the transpeptidase activity. A similar result has been found for *E. coli* PBP1a; transpeptidation by this enzyme was delayed until a glycan chain substrate was provided (Born *et al.*, 2006). It is important to note that the rate of MGT-mediated Lys-Lipid II transglycosylation was much greater than the equivalent activity performed by PBP1a-S370A (exemplified by Figure 4.23). Therefore, unlike incubations with MGT, Lys-Lipid II polymerisation by PBP1a-S370A would not have reached completion prior to the addition of the transpeptidase/D,D-carboxypeptidase. Consequently, fewer glycan chains would be present and monomeric Lys-Lipid II would remain. In spite of this, there was little difference between the total D-Ala produced when PBP1a-E91Q was incubated with either MGT (lane 12) or PBP1a-S370A (lane 14) derived glycan chains. There are three potential explanations for this:

- PBP1a-E91Q has a higher preference for PBP1a-S370A derived glycan chains over those produced from MGT, which may be of a different length.

- The glycan chain concentration may be high enough in both reactions so as not to limit the rate of D-Ala hydrolysis activity of PBP1a-E91Q.

- Transpeptidation could occur between two adjacent glycan chains, or between a glycan chain and monomeric Lys-Lipid II. The transpeptidase may require the glycan chain for substrate recognition and transient reaction with the active site serine, but it may have less selectivity for the attacking nucleophile, (either Lys-Lipid II or a polymerised form) or vice versa. Born *et al.* (2006) have found that *E. coli* PBP1a is capable of performing transpeptidation reactions between glycan chains and sacculi or peptidoglycan precursors (UDP-Mur*N*Ac-tri/tetra/penta-peptides). The use of Lys-Lipid II as a transpeptidase acceptor substrate could be determined by monitoring the incorporation of [^{14}C]-labelled Lipid II by PBP1a-E91Q into a polymerised glycan chain, which could be analysed by SDS-PAGE.

5.9.3. Evaluation of the transglycosylase dependency of PBP1a transpeptidation

It has been established that the transglycosylase domain of PBP1a can function in the absence of transpeptidase activity (Section 4.10). However, are the two activities linked? To address this question, the D-Ala release activity of PBP1a was compared to the D-Ala release activity of PBP1a-E91Q in the presence of PBP1a-S370A. Lys-Lipid II was used as the substrate in both incubations, which would be polymerised by the transglycosylase activity of the enzymes; PBP1a and PBP1a-S370A have near equivalent levels of transglycosylase activity (Section 4.10), thus the substrate compositions would be equivalent (a mixture of glycan chains and monomeric Lys-Lipid II). The level of D-Ala produced by PBP1a (lane 10b) was significantly greater (by ~19 μM D-Ala) than that produced by PBP1a-E91Q (lane 12b) (despite these enzymes having equivalent activities in the presence of MGT-polymerised substrate, lanes 12b and 15b). Additionally, PBP1a in the sole presence of glycan chains (produced by MGT) (lane 15b) generated less D-Ala compared to PBP1a with Lipid II (lane 10b). This last finding is comparable to the observation made by Bertsche *et al.* (2005): in the presence of pre-formed glycan chains (and absence of Lipid II), *E. coli* PBP1b-catalysed transpeptidation proceeded with a 12-fold lower

rate compared to the simultaneous transglycosylation and transpeptidation of Lipid II by the same enzyme. These results cumulatively imply that the D-Ala hydrolysis activity of PBP1a is enhanced when functioning in concert with the transglycosylase activity on the same enzyme molecule.

If the D-Ala activity observed upon incubation of PBP1a-E91Q with a glycan polymer (lanes 12b and 14b) was solely due to the contaminating activity, this would indicate that the transpeptidase domain of PBP1a-E91Q was not functional in the absence of an active transglycosylase domain on the same enzyme entity. This result would be comparable to that found by Born *et al.* (2006): *E. coli* PBP1a with an inactive transglycosylase domain was unable to catalyse transpeptidation.

The crystal structure of *E. coli* PBP1b has lead to the proposal that the transglycosylase domain feeds the newly polymerised glycan chain to the transpeptidase domain (Sung *et al.*, 2009). The results concur with this hypothesis, where the rate of D-Ala hydrolysis activity is likely to be enhanced if the donor substrate is being directed to the transpeptidase active site. Given that the transpeptidase activity of *S. pneumoniae* PBP1a (data shown here), *E. coli* PBP1a (Born *et al.*, 2006) or *E. coli* PBP1b (Bertsche *et al.*, 2005) was either reduced or absent when concomitant transglycosylation was not possible, this could suggest that the primary role of these bifunctional PBPs in a cell is to form nascent cross-linked peptidoglycan from Lipid II. Their secondary role could be to integrate the newly formed peptidoglycan into the existing sacculi (an activity that would not require transglycosylation), which could be the main responsibility of the monofunctional transpeptidases, allowing for cell elongation and division.

To conclude, the results clearly demonstrate that the penicillin-binding domain of PBP1a performs D-Ala hydrolysis activity in the presence of ongoing transglycosylation by the same enzyme molecule. Intervening factors, such as the contaminating D-Ala hydrolysis activity present in some enzyme preparations, complicate the interpretation of results and prevent further conclusions being drawn.

5.10. Analysis of PBP2b-dependent transpeptidation or D,D-carboxypeptidation.

PBP2b is a high molecular weight Class B penicillin-binding protein (Sauvage *et al.*, 2008a), performing the role of transpeptidation (and potentially D,D-carboxypeptidation to a lesser extent (discussed in Section 5.1.1)) in *S. pneumoniae* peptidoglycan. The D-Ala hydrolysis activity of PBP2b was analysed with two different substrates: Lys-Lipid II and MGT-polymerised Lipid II (prepared as in Section 2.9.2.1). Figure 5.9 presents the results of PBP2b-dependent D-Ala hydrolysis activity.

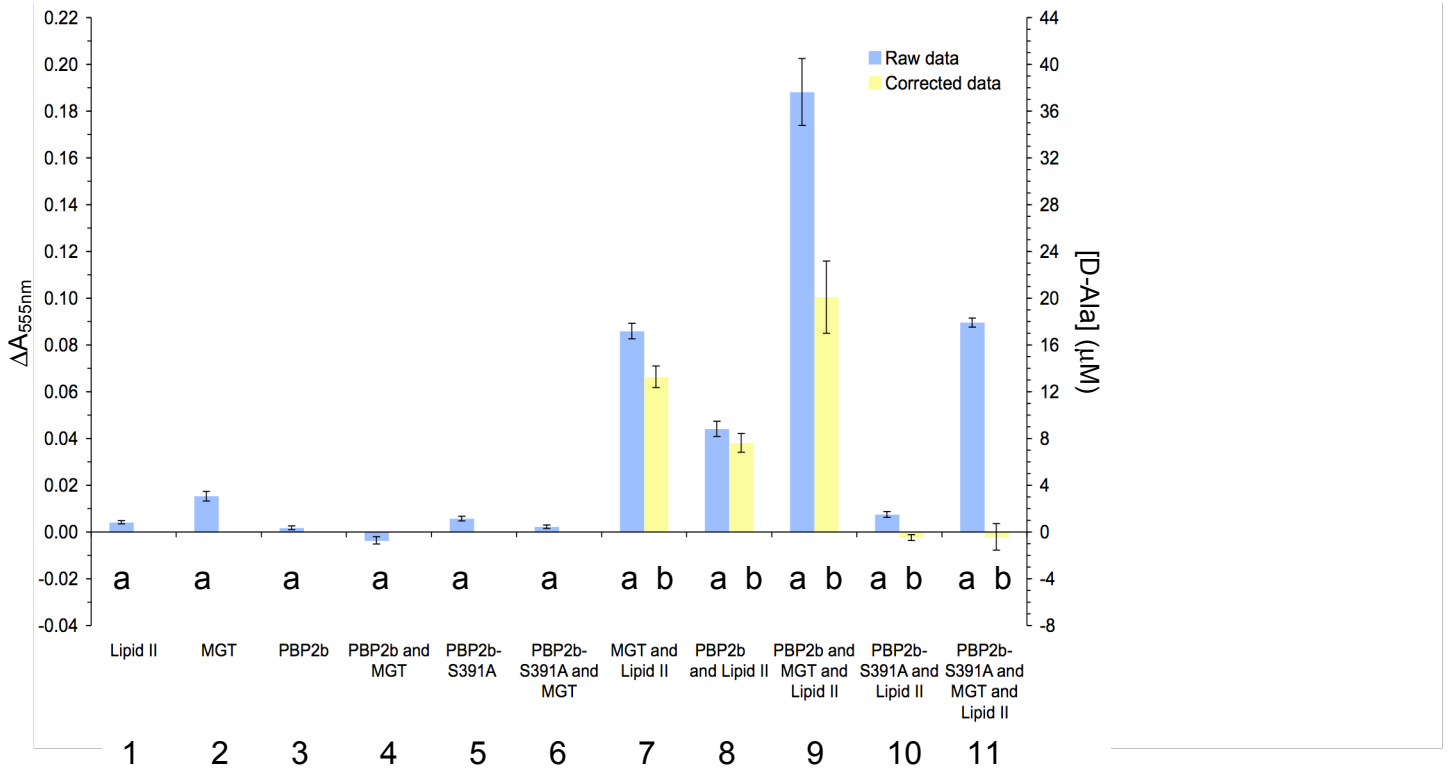

Figure 5.9: *S. pneumoniae* PBP2b-dependent D-Ala release. Variants of PBP2b were incubated with Lys-Lipid II and MGT-polymerised Lys-Lipid II for 18 h. Refer to Figure legend 5.8 for a detailed description of the Figure. Enzyme only and Lys-Lipid II only controls are represented in lanes 1-6. Lanes 9a and 11a were corrected by lane 7a to account for the contaminating D-Ala hydrolysis activity in the MGT preparation (see Figure legend 5.8). Values represent the mean ± standard deviation of the raw (a) and corrected (b) data, based on triplicate reactions.

With the knowledge that there was variability in the enzyme preparations with regards to a contaminating D-Ala hydrolysis activity, caution must be applied when analysing the results. The contaminating D-Ala hydrolysis activity was evidently absent from the PBP2b-S391A enzyme preparation; no D-Ala activity was detected following the incubation of PBP2b-S391A with Lipid II (lane 10b) or glycan chains (lane 11b). Therefore, it can be assumed that the contaminant was absent from the PBP2b preparation.

The PBP2b-S391A mutant clearly demonstrated its incapability of D-Ala hydrolysis in the presence of Lys-Lipid II or a polymerised glycan chain (lanes 10b and 11b respectively). This was anticipated because the active site serine, an essential residue in the transpeptidase/D,D-carboxypeptidase activity, had been replaced by an inert residue, alanine (Section 3.3.6). On the contrary, the wild-type PBP2b exhibited D-Ala release activity with both Lys-Lipid II (lane 8b) and the MGT-produced glycan chains (lane 9b) with a greater than 2-fold preference for polymerised glycan chains over the monomeric counterpart.

5.11. Analysis of PBP2x-dependent transpeptidation or D,D-carboxypeptidation.

S. pneumoniae PBP2x is a high molecular weight Class B, monofunctional PBP, sharing a similar role to PBP2b (Sauvage *et al.*, 2008a). Under the assay conditions described in Section 2.9.2.1, the D-Ala release activity of PBP2x was analysed. The results are displayed in Figure 5.10.

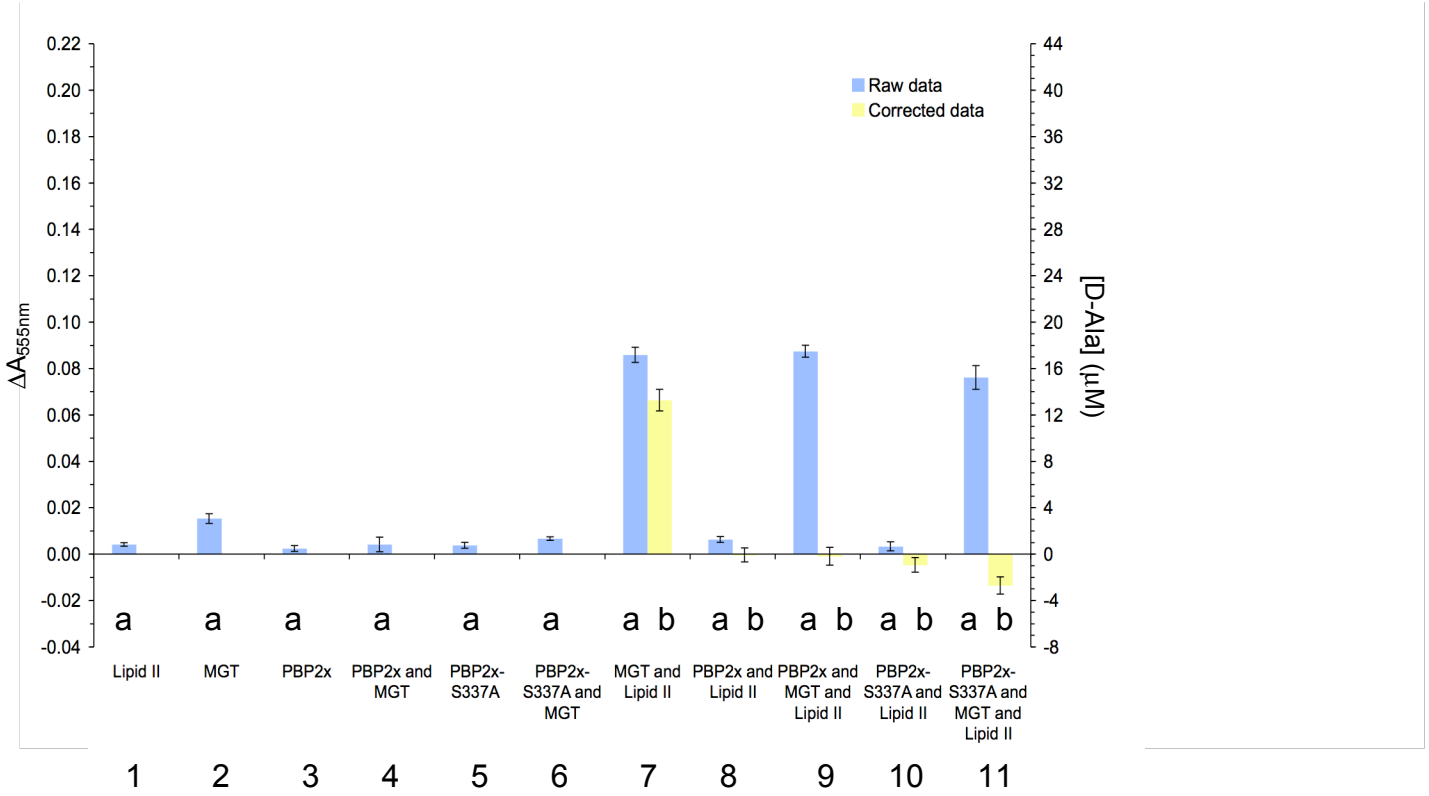

Figure 5.10: *S. pneumoniae* PBP2x-dependent D-Ala release. Variants of PBP2x were incubated with Lys-Lipid II and MGT-polymerised Lys-Lipid II for 18 h. Refer to Figure legend 5.8 for a detailed description of the Figure. Enzyme only and Lys-Lipid II only controls are represented in lanes 1-6. Lanes 9a and 11a were corrected by lane 7a to account for the contaminating D-Ala hydrolysis activity in the MGT preparation (see Figure legend 5.8). Values represent the mean ± standard deviation of the raw (a) and corrected (b) data, based on triplicate reactions.

PBP2x did not exhibit transpeptidase/D,D-carboxypeptidase-dependent D-Ala hydrolysis when either Lys-Lipid II (lane 8) or a polymerised glycan chain (lane 9) were tested as the potential substrates. It is worthy to note that no contaminating D-Ala hydrolysis activity was present in the enzyme preparations of PBP2x (lanes 8 and 9) or PBP2x-S337A (lanes 10 and 11).

Factors that could explain the apparent inactivity of PBP2x (and the low activities of PBP1a and PBP2b) are described later in the Chapter.

5.12. Discussion

For clarity, the experimental results obtained have been discussed throughout this Chapter. The following section discusses the transpeptidation/D,D-carboxypeptidation detection systems developed in this Chapter in terms of: the *in vivo* relevance of the activity rates obtained, the suitability of the detection techniques and the strategies to overcome problems encountered.

5.12.1. Establishment of transpeptidation/D,D-carboxypeptidation by two novel detection methods

Two novel techniques were developed for the identification of the transpeptidase/D,D-carboxypeptidase activity of PBPs. The first was fluorescence analysis of VanFL-bound glycan chains following treatment with a transpeptidase/D,D-carboxypeptidase and SDS-PAGE separation. The activity was detected by a reduction of VanFL binding (and hence fluorescence), which relied upon the absence of the terminal D-Ala of a pentapeptide side chain within the glycan chain. The second was a continuous spectrophotometric assay that used a VanA coupling system to monitor D-Ala hydrolysis, a consequence of transpeptidation/D,D-carboxypeptidation. Both techniques are valid approaches for establishing and monitoring transpeptidation/D,D-carboxypeptidation, but have two significant limitations: the rate of PBP-catalysis needs to be high enough to detect activity and the techniques cannot distinguish between D,D-carboxypeptidation and transpeptidation. The high sensitivity of the Amplex Red assay enabled

S. pneumoniae PBP transpeptidation/D,D-carboxypeptidation to be detected and additionally identified the presence of a D-Ala hydrolysing enzyme contaminating various protein preparations.

5.12.2. The *E. coli* D-Ala hydrolysing contaminant

The contaminating enzyme, believed to be a PBP originating from the *E. coli* expression system, could have caused an underestimation of the true *S. pneumoniae* PBP D-Ala hydrolysis activity observed (by reducing the availability of the substrate) and will impede all future transpeptidase analyses of the PBPs (using the detection systems described) by causing ambiguity in the results. Therefore, its elimination becomes a priority.

5.12.2.1. Properties of the contaminating enzyme

Substantial contaminating D-Ala hydrolysis activity was identified in two protein preparations: MGT and PBP1a-S370A. Two factors ensured that these enzymes were not responsible for the activity observed. The first, sequence analysis validated the absence of a penicillin-binding domain or an active site serine residue within the penicillin-binding domain of MGT and PBP1a-S370A respectively. The second factor was that the enzymes could not bind BOCILLIN FL (where wild-type PBP1a could). Inclusion of ampicillin in the reactions of Lys-Lipid II with these enzymes caused virtually total elimination of the contaminating activity, identifying the contaminant as a probable PBP.

It is likely that the contaminating PBP was a D,D-carboxypeptidase and not a transpeptidase. Mengin-Lecreulx *et al.* (1999) have demonstrated that the over-expression of *S. aureus* MurE (responsible for the incorporation of L-Lys onto the third position of Lipid II peptide stem) in *E. coli* resulted in the replacement of 50 % *meso*-DAP-containing peptidoglycan stem peptides with L-Lys. Transpeptidation was still detected. However, the acceptor in the cross-linking reaction was found to be exclusively *meso*-DAP, suggesting that the *E. coli* transpeptidases could not use L-Lys in an equivalent manner (although the stem peptide containing L-Lys could act as a donor) (Mengin-Lecreulx *et al.*, 1999). The incubations with the PBPs

described here employed Lys-Lipid II as a substrate. Therefore, from the findings of Mengin-Lecreulx *et al.* (1999), *E. coli* transpeptidases would not be able to use the L-Lys-containing stem peptides as acceptor substrates. Thus, only D,D-carboxypeptidase activity would have been possible.

5.12.2.2. Identification of the contaminant

The primary step in the total elimination of the contaminating D-Ala hydrolysis activity would be the identification of the responsible enzyme. This could be achieved by mass spectrometry: proteins separated by SDS-PAGE could be excised from the gel, subjected to a tryptic digest, and the products analysed by electrospray ionisation tandem mass spectrometry (ESI-MS/MS). This procedure could be performed in duplicate, with and without pre-treatment of the protein sample with ampicillin (this antibiotic has been shown to inhibit the activity of the contaminant, presumably by covalently interacting with the catalytic Serine residue). Following ESI-MS/MS analysis, detection of an ion that differs by the molecular weight of ampicillin between the two protein samples could lead to the identification of the *E. coli* PBP contaminant.

5.12.2.3. Potential strategies for the removal of the contaminant

Further purification strategies could be undertaken to remove the contaminant including affinity, ion exchange, and hydrophobic interaction chromatography. For example, it has been well documented that PBPs have varying affinities for different textile dyes, and this property has been exploited in the successful purification of many PBPs including *E. coli* PBP5 (van der Linden *et al.*, 1992) and a soluble form of *S. pneumoniae* PBP2x (Laible *et al.*, 1992) by dye-affinity chromatography. Experimental conditions (such as ionic strength and pH) could influence the affinity of the PBP for a particular dye, and thus a purification procedure could be established. This technique could be developed for the removal of the contaminating enzyme in the MGT or PBP1a-S370A preparations.

The elimination of the contaminating *E. coli* PBP from the MGT and PBP1a-S370A preparations by purification is hindered by a single factor for each enzyme: MGT requires detergent or a high concentration of NaCl to remain stable, enhancing hydrophobic interactions and thus the potential association with the PBP; PBP1a-S370A is situated in a detergent micelle to remain soluble, where the surrounding detergent would promote any protein-protein interactions (ionic detergents could be used to disrupt this interaction, but are often denaturants).

5.12.3. Do the levels of D-Ala hydrolysis detected represent the true activity of the PBPs *in vivo*?

In vivo, the rate of transpeptidation must be substantial to support bacterial growth, although the extent of the cross-linking is species specific (Bugg, 1999). In the absence of cross-linking activity, the peptidoglycan becomes weak and susceptible to rupture, a property caused by β-lactam antibiotics (Macheboeuf *et al.*, 2006). *In vitro*, detection of activity from the penicillin-binding domain is a rare event; in this study, minimal levels of activity have been detected from the transpeptidase domain of PBP1a and PBP2b, with PBP2x demonstrating no activity under the conditions provided following an 18 h incubation. PBP1a, for example, after an 18 h incubation with 10 nmol Lys-Lipid II, turned over one molecule of D-Ala every 1.23 days. Evidently, after 18 h, the enzymes are likely to have lost activity *in vitro*, but this rate would still be vastly insufficient to sustain bacterial growth. This signifies there were underlying factors preventing the native rate of PBP activity *in vitro*. Minimal knowledge of the optimal activity conditions and preferential substrates has hindered progress in the kinetic characterisation of the transpeptidase activity. The following section provides explanations for the low rates of *S. pneumoniae* PBP1a, PBP2b and PBP2x transpeptidase/D,D-carboxypeptidase activities detected in these experiments, which must be considered in future analyses.

5.12.4. Factors contributing to the sub-physiological rate of the transpeptidase activities of *S. pneumoniae* PBP1a, PBP2b and PBP2x

Kinetic characterisation of *S. pneumoniae* PBP1a, PBP2b and PBP2x transpeptidation was thwarted by the inability to detect sufficient levels of D-Ala release activity. Numerous factors could be responsible for the absence of significant enzyme activity and are discussed below.

5.12.4.1. Purification renders the protein inactive

The isolation and subsequent purification of the PBP from the membrane could disrupt its native-like conformation, where the distortion in structure could prevent the enzyme functioning with optimal activity.

PBP2x appeared totally inactive upon incubation with potential substrates; the same was not true for PBP1a and PBP2b. Given that PBP1a, PBP2b and PBP2x were prepared in identical ways (Chapter 3), it seems unlikely that the purification method would cause the complete inactivation of the latter enzyme and not the former enzymes. BOCILLIN FL was able to covalently modify the active site serine of the PBP2x transpeptidase domain (Figure 3.14), where the active site must resemble a native-like structure for this to occur. This suggests that the enzyme had at least a vague resemblance to the native conformation.

The detergents used in the purification of PBP1a, PBP2b and PBP2x, sodium deoxycholate and DDM, are renowned for their ability to extract and purify membrane-bound enzymes in a functional form (Seddon *et al.*, 2004). Therefore, it seems unlikely that they would severely disrupt the performance of the enzymes; different detergents could be used to address this.

5.12.4.2. Purification removes a component of the bacterial membrane essential for activity.

In their natural environment, the membrane proteins are surrounded by lipids and proteins, some of which are known to enhance enzyme activity. For example, a combination of cardiolipin and phosphatidyl glycerol has a positive impact on the catalysis rate of PgpB (Touzé *et al.*, 2008). The PBPs may have an essential lipid requirement, which is diminished upon purification.

5.12.4.3. An element responsible for enhancing the PBP activity *in vivo* is absent *in vitro*

Peptidoglycan synthesis is a highly organised process, controlled by a myriad of enzymes acting in complexes at different points during the cell cycle. Examples include: the recruitment of PBPs to the divisome complex enabling nascent peptidoglycan expansion (Vicente *et al.*, 2006) and the enhancement of *E. coli* PBP2 activity in the presence of RodA (Ishino *et al.*, 1986). Other elements have been found to boost PBP activity. For example, the outer membrane lipoproteins, LpoA and LpoB, residing in the periplasmic space, are essential for stimulating the transpeptidase activities of *E. coli* PBP1a and PBP1b respectively (Paradis-Bleau *et al.*, 2010; Typas *et al.*, 2010). An equivalent element has not yet been identified in Gram-positive bacteria. It is therefore highly plausible that a PBP-associating component essential for the transpeptidase activities of *S. pneumoniae* PBP1a, PBP2b and PBP2x exists but was absent in the *in vitro* assays. *E. coli* PBP1b has elevated activity when functioning as a dimer *in vitro* (Bertsche *et al.*, 2005). The high concentrations of enzymes used in the assays are likely to have permitted homodimerisation. However, PBP1a, PBP2b or PBP2x may form heterodimers *in vivo*.

5.12.4.4. Substrates tested were not suitable for optimum PBP1a, PBP2b or PBP2x activity

In the experiments conducted, Lipid II (with a pentapeptide side chain of L-Ala-γ-D-Glu-L-Lys-D-Ala-D-Ala) was trialled as a substrate in its monomeric and

polymerised form. An equivalent Lipid II molecule is the precursor to *S. pneumoniae* peptidoglycan, but has a single difference: the D-Glu at the second amino acid residue position of the pentapeptide chain is replaced by *iso*-Gln in *S. pneumoniae* (Garcia-Bustos and Tomasz, 1990). This variation could reduce the substrate recognition of the *S. pneumoniae* PBPs. Additionally, tripeptide and branched peptide stems are significant constituents of *S. pneumoniae* peptidoglycan (Garcia-Bustos and Tomasz, 1990); the preference of these acceptor substrates during transpeptidation has yet to be determined.

The results indicate that the PBPs have different substrate specificities. Both PBP1a and PBP2b were capable of utilising polymerised glycan chains as substrates, whereas only PBP2b could perform D-Ala hydrolysis using Lipid II as a substrate. These differences could arise through distinct substrate recognition mechanisms. It has been proposed that the transglycosylase domain of PBP1a directs the polymerising glycan chain to the transpeptidase domain. PBP2b does not have a transglycosylase domain, thus would require a different mechanism of substrate recognition.

5.12.4.5. The assay conditions were not optimal for transpeptidase activity

The assay conditions employed corresponded to the optimised conditions for the transglycosylase activity of PBP1a. The optimum temperature and buffer system for activity is likely to vary between the different transpeptidases, which can now be established for PBP1a and PBP2b following the detection of activity.

The presence of the detergent, although essential for the membrane protein and lipid solubility, could interfere with the PBP activity by obscuring sites on the substrate or enzyme, essential for recognition purposes. The assays could be performed in the presence of different detergents to address this factor.

The factors described above detail potential explanations for the minimal PBP activity observed, which must be taken into consideration before future analyses.

5.13. Future work

The work presented in this Chapter has provided the foundation towards the future kinetic characterisations of the transpeptidase activities of the *S. pneumoniae* PBPs and those from other bacterial species. The following section describes methods to further develop an understanding of how the transpeptidase domains of *S. pneumoniae* PBP1a, PBP2b and PBP2x function *in vivo*.

5.13.1. Distinguishing between the transpeptidase and D,D-carboxypeptidase activities of the penicillin-binding domains of Class A and B PBPs.

The techniques described in this Chapter enable the detection of activity from the penicillin-binding domain of the PBPs via D-Ala hydrolysis from the pentapeptide stem of a peptidoglycan precursor. However, these methods do not differentiate between D-Ala hydrolysis resulting from transpeptidation or D,D-carboxypeptidation, limiting the full characterisation of these enzymes.

5.13.1.1. In-gel strategies to distinguish between transpeptidation and D,D-carboxypeptidation

At the current separation resolution of the glycan chains following SDS-PAGE, it is impossible to differentiate between products of transpeptidation or D,D-carboxypeptidation upon VanFL detection (Section 5.3). Discrete separation of the glycan chains would enable the two activities to be distinguished. Polymerised glycan chains treated with a D,D-carboxypeptidase would simply show a reduction of fluorescence signal in relation to the untreated glycan chains. Glycan chains treated with a transpeptidase would show a different separation pattern following SDS-PAGE due to the formation of cross-links between chains. This latter factor would be sensitised by the use of [^{14}C]-labelled Lipid II, although D,D-carboxypeptidation could not be detected in this way.

5.13.1.2. Development of a fluorescence or absorbance based assay to distinguish between levels of transpeptidation and D,D-carboxypeptidation

Transpeptidation reactions form cross-links between the fourth position D-Ala and the third position L-Lys/*meso*-DAP of adjacent pentapeptide side chains in peptidoglycan (Figure 5.1). This eliminates the free ε-amino group of the third position amino acid residue. Quantification of the free ε-amino group could be achieved by labelling with a fluorescent or chromogenic molecule, thus establishing the level of transpeptidation. Figure 5.11 displays the outline of this proposed assay system. The reaction of free amino groups with 2,4,6-trinitrobenzene sulphonic acid (TNBS) leads to an increase in absorbance at 345 nm, which can be followed spectrophotometrically. Following a transpeptidation reaction, it is important to eliminate the D-Ala hydrolysed from these experiments, where the free amino-group of D-Ala could be labelled. D-Ala could be converted to pyruvate by DAAO, releasing NH_3 and H_2O_2. Freeze-drying the reaction would remove NH_3, which also has the potential to react with TNBS. The reaction could be reconstituted into an appropriate buffer system (excluding buffers with an amino group e.g. Tris) and the reaction with TNBS monitored.

The level of transpeptidation and D,D-carboxypeptidation could be quantified using putative natural substrates (following a reaction with and without a transpeptidase) by comparing the amount of free ε-amino groups with the total concentration of D-Ala released (established by the Amplex Red assay in a parallel reaction).

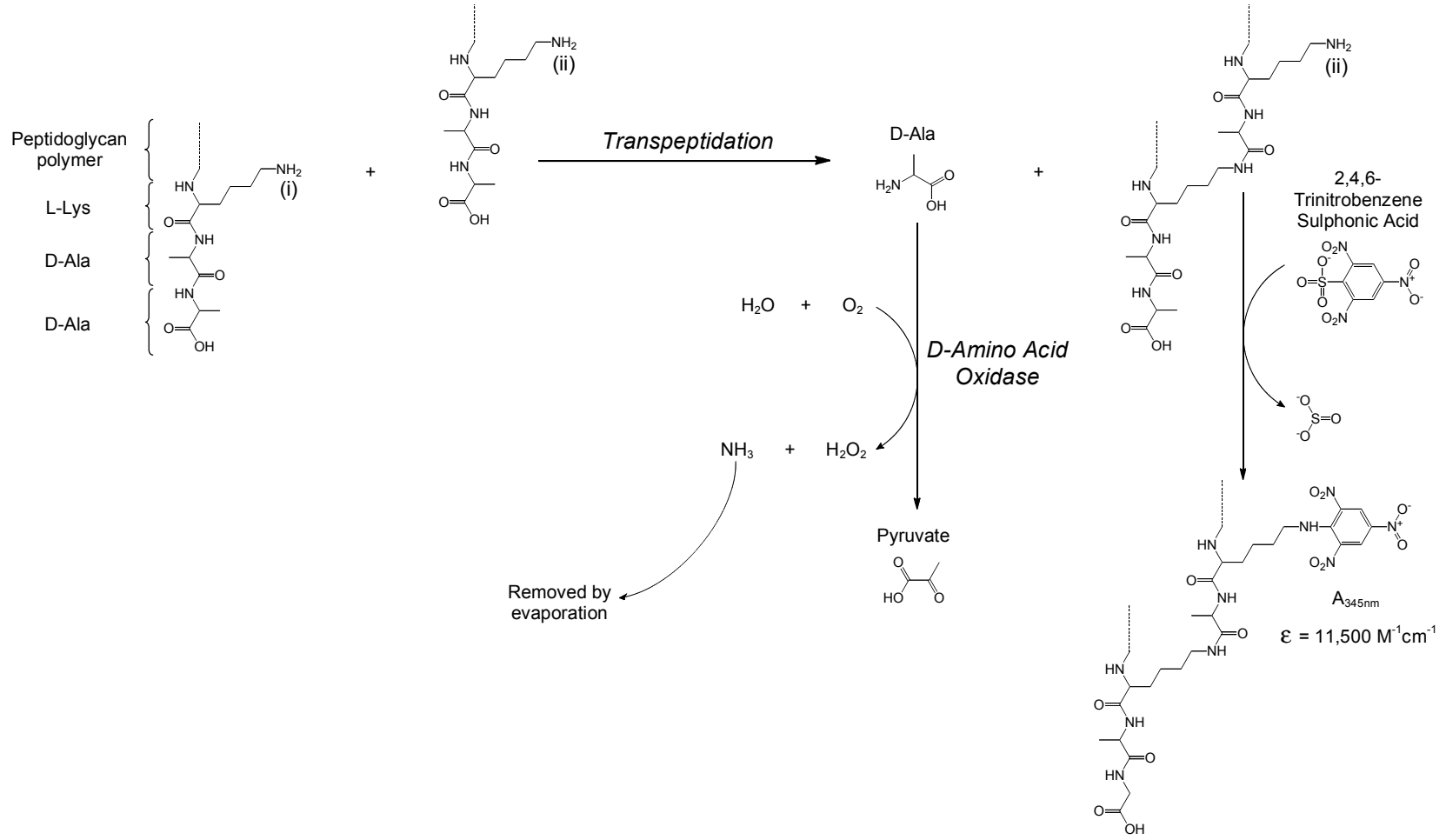

Figure 5.11: An approach to distinguish between transpeptidation and D,D-carboxypeptidation. The terminal tripeptide of the peptidoglycan pentapeptide stem is shown. Following a transpeptidation or D,D-carboxypeptidation reaction, the terminal D-Ala is liberated, the amine group of which can be eliminated by D-amino acid oxidase. A transpeptidation reaction eliminates the amine group (i), whilst amine (ii) is free to react with TNBS, which can be monitored by an absorbance change at 345 nm.

5.13.2. A high-throughput screening process for the rapid analysis of transpeptidase/D,D-carboxypeptidase activity.

The transpeptidase activities of *S. pneumoniae* PBP1a, PBP2b and PBP2x are poorly understood. Various factors need to be addressed to fully characterise the enzymes including:

- Optimal assay conditions (e.g. temperature, pH, metal ions, detergent, membrane-like environment)
- Minimal structural requirements of enzyme (e.g. analyse the activity of membrane truncated PBPs)
- Minimal structural requirements of the substrate (e.g. use diverse peptidoglycan fragments as substrates)
- Substrate specifications of β-lactam resistant PBPs (e.g. analyse 5204 PBPs with branched or unbranched pentapeptide side chain substrates)

The establishment of D-Ala hydrolysis activities by *S. pneumoniae* PBP1a and PBP2b provides the initial step towards their full characterisation. To address the factors discussed above using the assay set-up described would be extremely time-consuming. Development of the assays into a 96-well plate format (described in Section 4.13.8) would allow high throughput screening of activity (by D-Ala release) under various parameters in a time-efficient manner.

5.14. Conclusion

In summary, two techniques for the detection of PBP-dependent transpeptidation/D,D-carboxypeptidation have been developed, adaptations of which will enable the differentiation between these two activities. The continuous spectrophotometric assay designed to monitor D-Ala release has been used to kinetically characterise *Actinomadura* R39 D,D-peptidase with findings comparable to those in literature. Initial studies have revealed the elusive activities of the penicillin-binding domains of PBP1a and PBP2b, thus providing a foundation for future investigations into this complex area of research.

Chapter 6. Preliminary crystallisation studies of *Staphylococcus aureus* MGT and *Streptococcus pneumoniae* PBP1a, PBP2b and PBP2x

6.1. Introduction

6.1.1. X-ray crystallography

The three-dimensional structure of proteins can provide valuable insights into how the macromolecule functions and interacts with its surroundings. There are three techniques in modern biophysics that can determine the 3D-architecture of proteins to at least a near atomic resolution: nuclear magnetic resonance spectroscopy (NMR), electron microscopy (EM) and X-ray crystallography. The RCSB Protein Data Bank (PDB: www.rcsb.org) is an online database documenting the 3D-structures of proteins and nucleic acids. To date, the PDB statistics reveal that there are just over 68,000 protein structures deposited in this database, approximately 60,000 of which were determined by X-ray crystallography. Therefore, since the 1946 Nobel Prize for Chemistry (awarded to Sumner, Northrup and Stanley) recognised the importance of the discovery that enzymes can be crystallised, X-ray crystallography has developed into a profound biophysical technique of choice for the establishment of protein structure.

X-ray crystallography relies on the target protein associating in a periodic array forming a crystal lattice (Sawyer and Turner, 1999). Exposure of the crystal to intense X-rays causes the incident beam to scatter in different directions with different intensities. This can be recorded as an X-ray diffraction pattern, which holds the information regarding the protein 3D-structure (Sawyer and Turner, 1999). There is one major limitation of this technique concerning the structural information obtained: the *in vitro* crystal lattice of the target protein represents a single static structure sampled by the protein, which does not necessarily reflect the native state of the protein *in vivo* (Acharya and Lloyd, 2005).

6.1.2. Crystallisation of membrane proteins: the challenge

This Chapter focuses towards obtaining crystal structures of the full-length integral membrane proteins of *S. pneumoniae* PBP1a, PBP2b and PBP2x. Structural characterisations of membrane proteins remain to be an appreciable challenge. They represent approximately one-third of the proteins encoded in the genome (Krogh *et al.*, 2001), yet only 1.1 % of the structures in the PDB correspond to membrane proteins (www.rcsb.org). Since the first crystal structure of an integral membrane protein, a photosynthetic bacterial reaction centre in 1984 (Deisenhofer *et al.*, 1984), merely 764 membrane protein structures have been solved, only 266 of which are unique (at the time of writing) (Membrane Proteins of Known 3D Structure: http://blanco.biomol.uci.edu/Membrane_Proteins_xtal.html). The discrepancy between the numbers of crystal structures of soluble and membrane proteins arises from the complexity of the latter. This imbalance must be surmounted to enable a full understanding of the membrane proteome (Loll, 2003).

6.1.3. Current X-ray crystal structures of PBPs

Until recently, PBP crystal structures were based on the enzymes devoid of their membrane anchor, and not on the full-length counterparts, and because of this, the role of the transmembrane domain has not been appreciated. In 2009, the structure of the first full-length Class A PBP, *E. coli* PBP1b, was established (Sung *et al.*, 2009). It is anticipated that the recent advances in membrane protein crystallography, including specifically designed high-throughput screens, will facilitate the elucidation of further full-length PBP structures.

The crystal structures of apo- and ligand-bound forms of various membrane truncated HMW and LMW-PBPs and MGTs reveal: the positioning of the conserved motifs; an insight into residues involved in substrate binding; residues proposed to catalyse the enzyme-specific reactions; an explanation for different properties displayed between the same enzyme of two different bacterial strains (i.e. penicillin-resistant and non-penicillin resistant). These findings are illustrated in the following section using appropriate examples.

6.1.3.1. Substrate-binding pocket

The crystal structure of *Actinomadura* R39 D,D-peptidase (Sauvage *et al.*, 2005) (the activity of which is discussed in Section 5.6) has revealed a distinctive pocket located at the bottom of the active site. The pocket is defined by residues W139, D142, Y147, R351 and M414 as shown in Figure 6.1. The former 3 residues belong to a unique domain of Class C PBPs, and the latter two belong to the penicillin-binding domain. It has been proposed that these residues are involved in substrate specificity, favouring the binding of *meso*-DAP (a natural constituent of *Actinomadura* R39 peptidoglycan) instead of L-Lys at the third position of the pentapeptide stem of a peptidoglycan fragment (Sauvage *et al.*, 2005). The substrate preference is supported with kinetic data (Section 5.6).

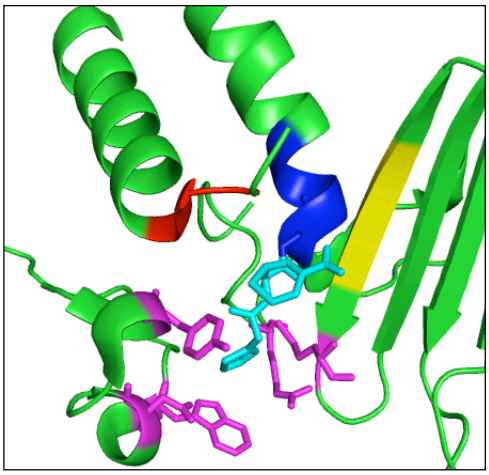

Figure 6.1: *Actinomadura* R39 D,D-peptidase substrate-binding pocket. The catalytic serine is acylated with the β-lactam nitrocefin (cyan). The conserved motifs 1-3 are blue, red and yellow respectively. The hydrophobic residues constituting the substrate-binding pocket are magenta. Adapted from Sauvage *et al.* (2005).

6.1.3.2. Residues involved in substrate binding and catalysis

The crystal structures of transglycosylases (in apoenzyme and moenomycin-bound forms) and the transpeptidases and D,D-carboxypeptidases (in apoenzyme, inhibitor and substrate-mimetic bound forms) have revealed residues potentially involved in substrate recognition and catalysis of transglycosylation (Sections 1.9.1 and 4.1.2), transpeptidation and D,D-carboxypeptidation (Sections 1.9.2 and 5.1).

6.1.3.3. Structural discrepancies between an enzyme of two different bacterial strains

S. pneumoniae R6 and 5204 are penicillin-sensitive and resistant strains respectively (Section 3.1). The absence of a β-lactamase in *S. pneumoniae* infers that the penicillin-binding domains must remodel and modify the transpeptidase active site to confer β-lactam resistance (Hakenbeck *et al.*, 1999). Figure 6.2 shows the crystal structure of the PBP2b active site from the R6 and 5204 strains. In the R6 PBP2b structure, two small β-strands (β3a and β3b) connect the β-strands β3 and β4. In 5204 PBP2b, four mutations locate to this interconnecting region, involving the amino acid conversion of Asp or Ala to Gly. In the 5204 PBP2b structure, β3a and β3b are untraceable on the electron density map, signifying a considerable increase in flexibility due to these mutations. This degree of flexibility surrounding the active site, in addition to mutations affecting the charge and polarity of the catalytic cleft, impose that the enzymes must employ differential means of substrate and antibiotic recognition (Contreras-Martel *et al.*, 2009).

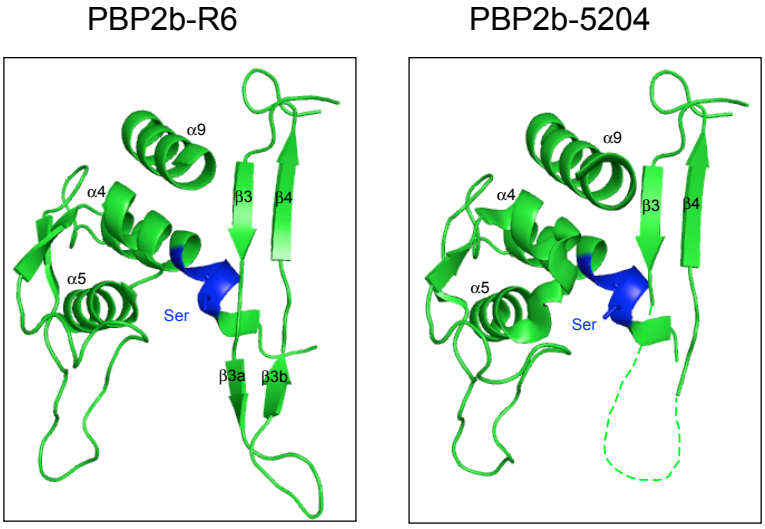

Figure 6.2: The active site of PBP2b from a penicillin sensitive (R6) and resistant (5204) strain of *S. pneumoniae*. The catalytic serine of the first conserved motif (blue) is shown in stick form. The green dashed lines indicate the residues with a high level of flexibility, which were not traceable on the electron density map. Adapted from Contreras-Martel *et al.* (2009).

These examples demonstrate the important role of X-ray crystallography in the structural and mechanistic characterisations of the PBPs.

6.2. Experimental aims

- To crystallise *S. pneumoniae* PBP1a-Δ30, PBP2b-Δ39, PBP2x-Δ48 and *S. aureus* MGT-Δ67

- To crystallise the native *S. pneumoniae* PBP1a, PBP2b and PBP2x and the corresponding transpeptidase active site serine mutants

- To crystallise liganded *S. pneumoniae* PBP variants

6.3. Crystallisation of *S. pneumoniae* PBP1a-Δ30, PBP2b-Δ39, PBP2x-Δ48 and *S. aureus* MGT

The crystal structures of *S. pneumoniae* PBP1a, PBP2b, PBP2x and *S. aureus* MGT devoid of membrane anchors, in apoenzyme and ligand bound forms, exist in literature. Crystallisation of these enzymes was attempted to gain a higher resolution of structural data and to establish possible conditions for future co-crystallisation experiments. Although others exist, examples of the known crystallisation conditions for the enzymes under investigation are displayed in Table 6.1.

Enzyme	Protein concentration (mg/mL)	Ligand	Crystallisation conditions	Structural resolution (Å)	Reference
S. pneumoniae PBP1a-Δ36	5	Tebipenam	50mM MES, 4-6mM zinc sulphate, pH 6.8, 20°C	2.7	Yamada *et al.* (2008)
S. pneumoniae PBP2b-Δ34	Not stated	Apoenzyme	1.4 M ammonium sulphate, 20°C	3.29	Contreras-Martel *et al.* (2009)
S. pneumoniae PBP2x-Δ48	20	Apoenzyme	0.1 M sodium acetate, 1.0-1.3 M ammonium sulphate, pH 4.6, 25°C	2.4	Gordon *et al.* (2000)
S. aureus MGT-Δ67-E100Q	10	Moenomycin	0.1M sodium acetate, 0.2M NaCl, 30% 2-methyl-2,4-pentanediol, pH 4.6, 22°C	2.1	Heaslet *et al.* (2009)

Table 6.1: Successful crystallisation conditions yielding crystal structures of the enzymes under investigation. The crystal structure of *S. pneumoniae* PBP1a-Δ36 was based only on the transpeptidase domain.

6.3.1. Investigating new crystallisation conditions

To improve the resolution of the existing crystal structures, new crystallisation conditions were explored. Protein crystallisation is often referred to as a 'black art', where conditions for nucleation and crystal growth are highly protein-specific and the change in a single variable can prevent crystal formation (Chayen, 2004). In spite of this, sparse matrix screens are often employed, which consist of conditions that are tailored towards those that have successfully generated crystals. There are numerous commercially available sparse matrix screens for soluble proteins, four of which were used to establish crystallisation conditions of *S. pneumoniae* PBP1a-Δ30, PBP2b-Δ39, PBP2x-Δ48 and *S. aureus* MGT-Δ67 (referred to as MGT from here onwards): Wizard I screen (Emerald Biosciences); Newcastle I screen (University of Newcastle); Clear Strategy I screen (Molecular Dimensions); Index screen (Hampton Research). Two additional screens were trialled to crystallise MGT: JCSG-*plus* (Molecular Dimensions) and PACT-premier (Molecular Dimensions). The Honeybee *963* crystallisation robot was used as an automated facility to set up the crystallisation screens in a 96-well plate format. Initial screenings were prepared using the sitting drop vapour diffusion method (Section 2.10.1). The buffer and the concentration of the individual enzymes are shown in Table 6.2.

Enzyme	Enzyme concentration (mg/mL)	Enzyme buffer
S. pneumoniae PBP1a-Δ30	10	20 mM HEPES, pH 7.5
S. pneumoniae PBP2b-Δ39	10, 40	20 mM HEPES, pH 7.5
S. pneumoniae PBP2x-Δ48	10, 40	20 mM HEPES, pH 7.5
S. aureus MGT	10, 30	20 mM HEPES, 250 mM NaCl, pH 7.5

Table 6.2: Enzyme buffer and concentration in the crystallisation trials. PBP1a-Δ30, PBP2b-Δ39 and PBP2x-Δ48 were purified as described in Chapter 3. MGT was purified as described in Chapter 4. In the absence of detergent PBP1a-Δ30 was not stable at high protein concentrations and MGT required a minimal of 250 mM NaCl to prevent protein precipitation.

The crystallisation screens were incubated at 18°C and periodically monitored every 24 h for 1 week and every 48 h during the following month. The initial screens gave an indication of successful precipitants for the crystallisation of the enzymes, with the exception of PBP1a-Δ30. It was likely that this enzyme was unstable (Section 3.8.1.3), preventing associations in an ordered array, and therefore was excluded from future crystallisation trials. Figure 6.3 shows the spherulites and microcrystals of PBP2b-Δ39, PBP2x-Δ48 and MGT that developed in the conditions stated.

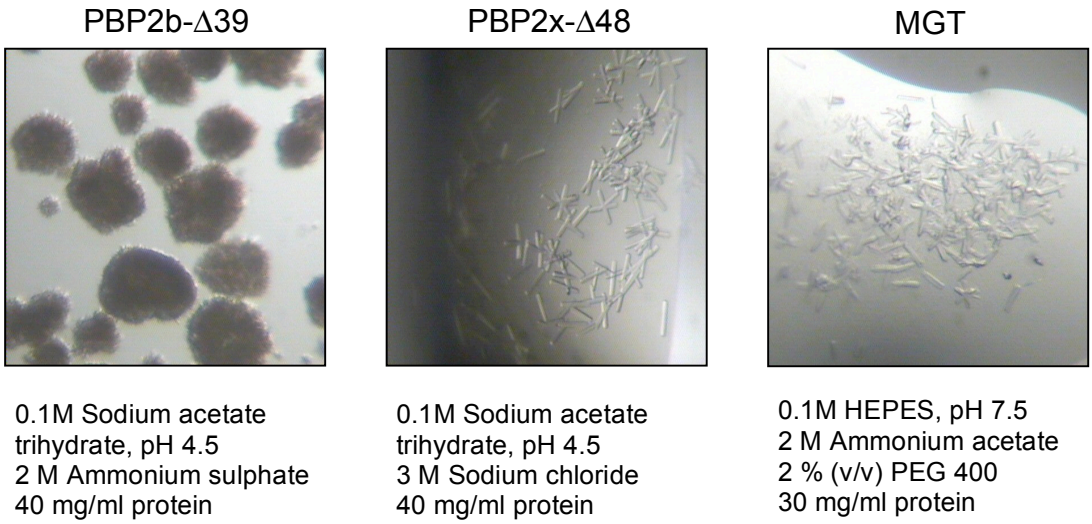

Figure 6.3: Spherulite and microcrystal formation of *S. pneumoniae* PBP2b-Δ39, *S. pneumoniae* PBP2x-Δ48 and *S. aureus* MGT. The sitting drop method of vapour diffusion was used with commercial sparse matrix screens. The precipitant composition is stated.

6.3.2. Fine-screening of crystallisation conditions to improve crystal size and morphology

The spherulites of PBP2b-Δ39, the needle-like crystals of PBP2x-Δ48 and the microcrystals of MGT were unsuitable for diffraction. In-house screens (Section 2.10.3.1) were designed to induce crystallisation (PBP2b-Δ39) and to reduce the level of nucleation (PBP2x-Δ48 and MGT) concurrently with improving crystal size and morphology. The crystal screen promoting spherulite or crystal formation was adjusted by a maximum of 0.6 M precipitant concentration and 1 pH unit above and below the original value, whilst the protein concentration and temperature remained constant. Screening was performed using the hanging drop vapour diffusion method

in a 24-well plate format. Three different ratios of enzyme to precipitate were used: 1:1, 2:1, and 1:2. The crystal screens were monitored as before.

The improvement of crystal size and morphology was achieved for PBP2x-Δ48 only. A precipitate formed instantly in every condition of the MGT trials. Crystallisation of a new protein batch of MGT was trialled in the conditions that provided the initial microcrystals, with no reproducibility. Globular clusters of microcrystalline fibres of PBP2b-Δ39 appeared, showing no deviation from the original spherulites obtained.

The PBP2x-Δ48 crystals were observed after 1 month. At the higher pH and precipitant concentration, a significant degree of nucleation was observed with a tendency to form long thin crystals. However, under certain conditions, crystals of a suitable thickness for diffraction studies were produced, shown in Figure 6.4.

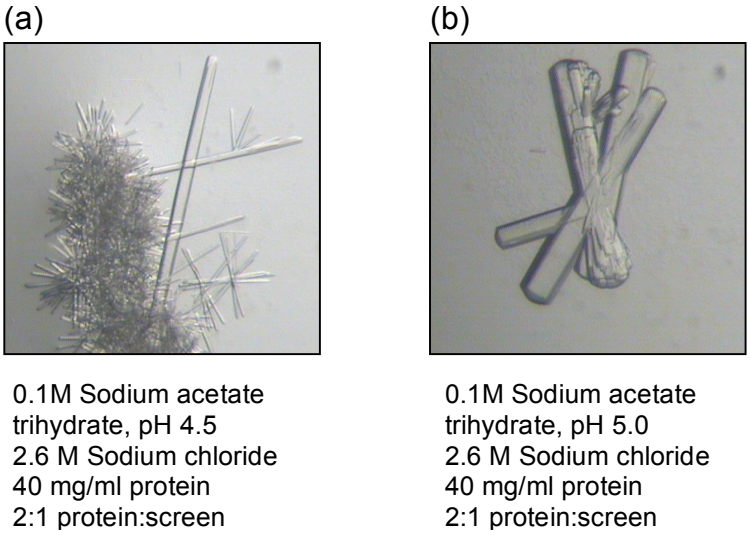

Figure 6.4: Crystal formation of *S. pneumoniae* PBP2x-Δ48. Crystals were obtained using the hanging drop method with in-house screens. The precipitant composition is stated.

A single protein crystal (from Figure 6.4a) was disrupted from the cluster, transferred to a cryoprotectant (mother liquor with 30 % glycerol), and mounted in a nylon loop. The crystals were flash frozen in liquid nitrogen and transported to the Diamond synchrotron radiation facility (Oxford). A complete data set was collected (600 images), and due to the time constraints of this project, the data was processed by Professor Vilmos Fülöp. All data were indexed and integrated with MOSFLM

(Leslie, 1992) and scaled using the SCALA (Evans, 2006). The data collection and processing statistics are shown in Table 6.3. The structure of PBP2x-Δ48 was solved by molecular replacement using the PHASER program (McCoy *et* al., 2007) with the coordinates of the previously established structure of PBP2x-Δ48 (PDB code: 1QME) (space group $P4_12_12$) (Gordon *et al.*, 2000). The crystals belonged to the space group $P3_121$ with one molecule in the crystallographic asymmetric unit, which gave a solvent content of 66 %. Although the crystal form established here was different from the deposited structure in the PDB, the resolution was poorer. Therefore, no further analysis was pursued.

Data collection	**PBP2x-Δ48**
Synchrotron radiation,	Diamond, beamline I24
Detector	Pilatus 6M
Wavelength (Å)	0.9778
Space group	$P3_121$
Unit cell parameters	
$a = b$ (Å)	100.17
c (Å)	187.33
Molecule per asymmetric unit	1
Matthews coefficient (Å^3 Da^{-1})	3.6
Solvent content by (%)	66
Resolution range (Å)	79-2.8 (2.95-2.80)
Total observations	154316 (20024)
Unique reflections	26590 (3763)
Average $I/\sigma(I)$	5.0 (1.5)
R_{sym} (%)[a]	0.222 (1.028)
Completeness (%)	97.4 (96.1)

Table 6.3: Data collection and refinement statistics for PBP2x-Δ-48. Values in parentheses refer to the highest resolution shell. I, Intensity unit; σ; standard deviation. [a]$R_{sym} = \Sigma_j\Sigma_h|I_{h,j} - \langle I_h\rangle|/\Sigma_j\Sigma_h\langle I_h\rangle$ where $I_{h,j}$ is the jth observation of reflection h, and $\langle I_h\rangle$ is the mean intensity of that reflection.

The PBP2x-Δ48 structure is shown in Figure 6.5.

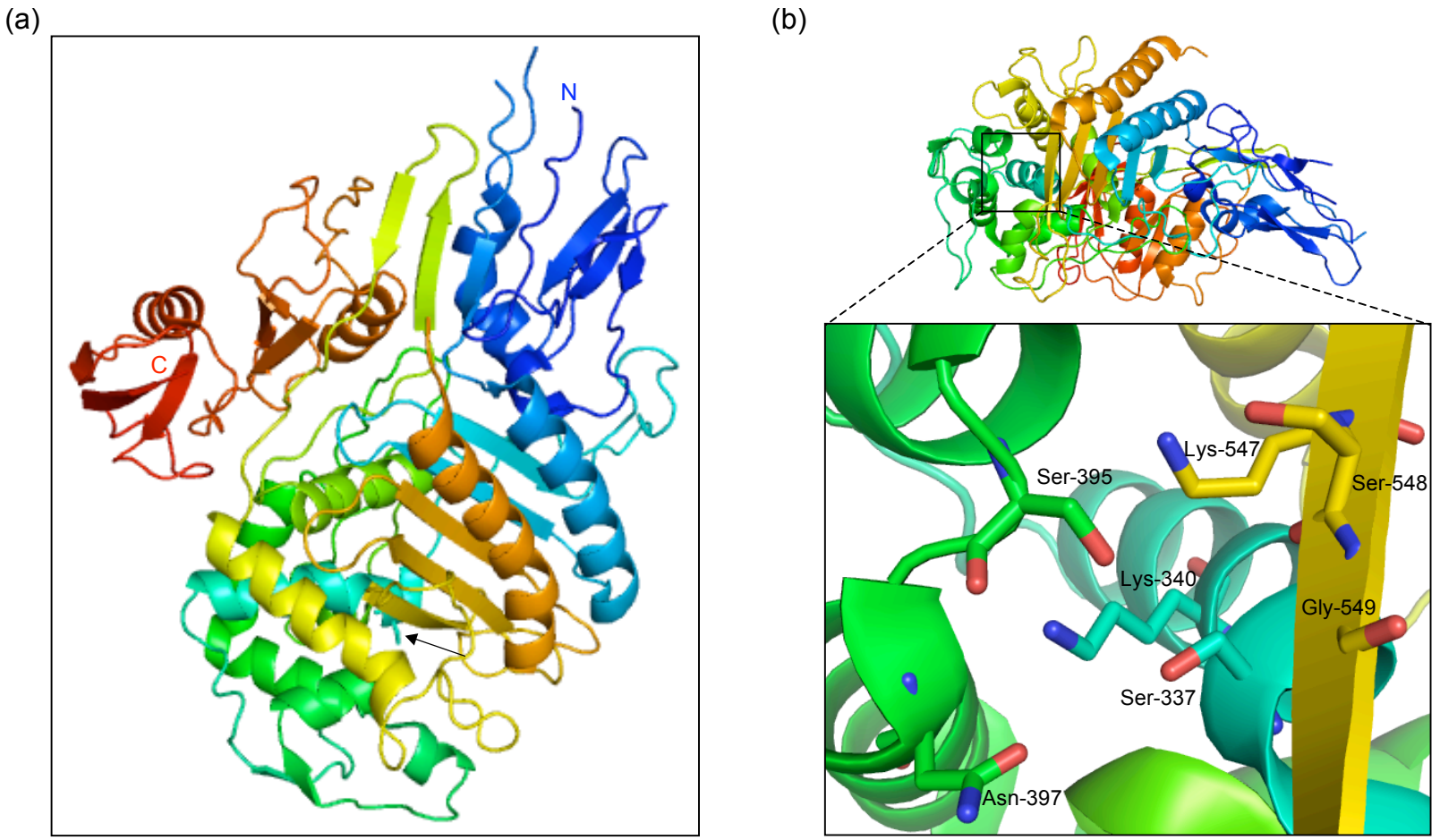

Figure 6.5: Crystal structure of *S. pneumoniae* PBP2x-Δ48. (Gordon *et al.*, 2000). (a) Structure of PBP2x-Δ48. The arrow marks the position of the catalytic Ser. (b) Close up of the active site. The penicillin-binding domain conserved residues are shown in a stick format and are labelled accordingly.

6.3.3. Refinement of the crystallisation conditions of PBP2b-Δ39

It was anticipated that further refinement of the crystallisation conditions that yielded the predominant PBP2b-Δ39 spherulites would ultimately generate single crystals. The Additive Screen and the Silver Bullet Screen (Hampton Research) were employed to introduce small molecules that have been shown to promote crystal lattice formation by stabilising and altering the solubility properties of the protein and by manipulating the protein-protein and protein-solvent interactions. Two mother liquors were trialled in conjunction with the screens (as stated in Figure 6.6). The sitting drop vapour diffusion method was performed and the different screens were applied according to the manufacturer's instructions (Section 2.10.3). 1 µL of 40 mg/mL PBP2b-Δ39 in a total drop size of 2 µL was used.

Two conditions of the Additive Screen promoted the formation of crystals, displayed in Figure 6.6. The large crystal (indicated with an arrow) was divided for analyses. One part was washed in mother liquor (of the remaining solution in the reservoir from the well the crystal originated from) and subjected to SDS-PAGE analysis. The results of the SDS-PAGE are shown in Figure 6.6b, where a Coomassie-stained protein band at the molecular weight of PBP2b-Δ39 signified the crystal was protein and not a salt artefact. The remaining part of the crystal was frozen in cryoprotectant (mother liquor with 30 % (v/v) glycerol) and mounted onto the in-house X-ray facility for diffraction studies. A diffraction pattern was produced (again proving the crystal was of protein origin), but the resolution was insufficient to extract any detailed structural information. Neither crystallisation conditions were reproducible.

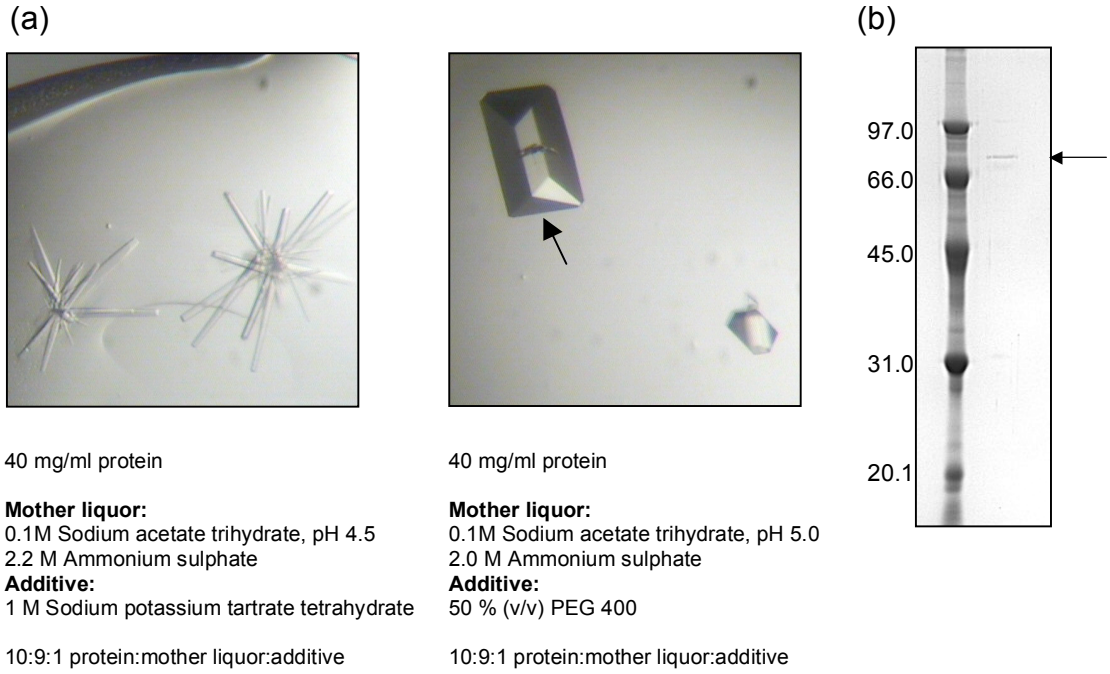

Figure 6.6: Successful *S. pneumoniae* PBP2b-Δ39 crystal formation using the Additive Screen. (a) PBP2b-Δ48 crystals obtained in two different crystallisation conditions (stated). (b) SDS-PAGE analysis of a portion of the crystal (identified with an arrow) from (a).

6.4. Crystallisation of *S. pneumoniae* PBP1a, PBP2b and PBP2x

Crystallisation of integral membrane proteins is notoriously difficult. To date, full-length crystal structures of *S. pneumoniae* PBP1a, PBP2b and PBP2x do not exist. The following sections discuss attempts to rectify this situation.

6.4.1. Sparse matrix screens for membrane proteins

The sparse matrix screens available for soluble proteins present conditions that are often not suitable for membrane protein crystallisation. The Iwata group of the Membrane Protein Laboratory at the Diamond Light Source (Oxford) have designed crystallisation screens, which are targeted towards membrane protein crystallisation: MemStart (48 conditions), MemSys (48 conditions) and MemGold (96 conditions) (Molecular Dimensions).

6.4.2. Initial crystallisation trials

In an analogous system to the soluble counterparts, crystallisations of PBP1a, PBP2b and PBP2x (in DDM or LDAO) (purified as described in Chapter 3) were trialled using the sitting drop vapour diffusion method (Section 2.10.1) in a 96-well plate format using the three membrane protein crystallisation screens, with incubation at 18°C and 4°C. Initial trials were performed with protein concentrated to 20 mg/mL using centrifugal protein concentrators with a molecular weight cut-off of 100 kDa, to limit the coincident concentration of detergent (DDM micelle M_r, ~40-75 kDa (Anatrace-Affymetrix); protein M_r, ~80 kDa; protein-micelle complex M_r, ~140 kDa). Following periodic monitoring of the crystal screens, no condition provided evidence of protein crystallisation.

6.4.3. An adaptation in protein preparation favours crystal formation

Two major influences on membrane protein crystallisation are homogeneity of the protein preparation and the detergent (size, concentration, properties) (as reviewed by Loll (2003) and Privé (2007)). The crystallisation trials were repeated as before with a single modification: following size exclusion chromatography, the protein fraction corresponding to the peak of absorbance maxima at 280 nm (representing the highest protein purity in an unaggregated state) on the chromatogram, was selected and submitted to the crystallisation trial, without prior concentration of the protein. The protein concentrations of the peak fractions were: PBP1a, 1 mg/mL; PBP2b, 2 mg/mL; PBP2x, 1 mg/mL. The detergent was present just above the CMC. This alteration proved to be successful, leading to the formation of PBP1a and PBP2b crystals (Figure 6.7).

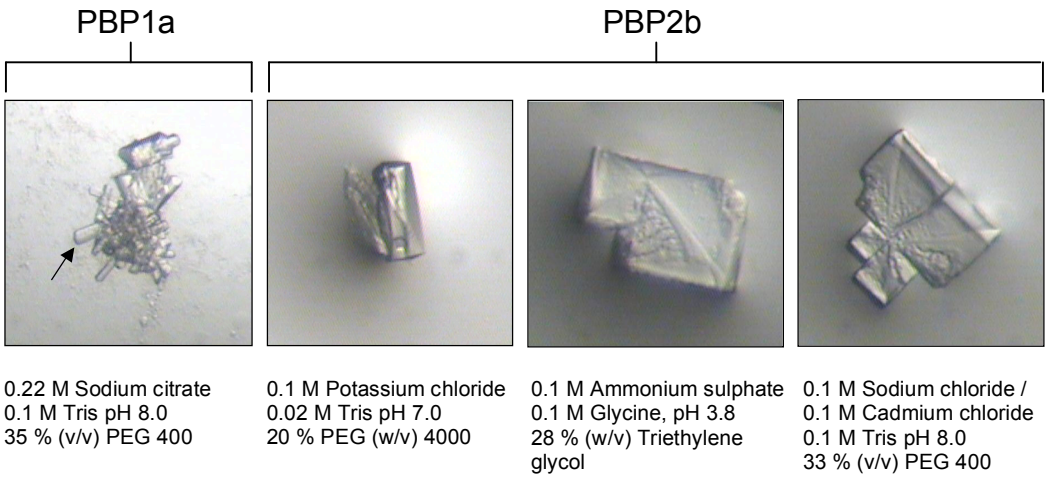

Figure 6.7: Crystals of *S. pneumoniae* PBP1a and PBP2b. Crystals were obtained using the sitting drop method with sparse matrix screens. The arrow indicates the protruding PBP1a crystal that was isolated and frozen. The precipitant composition is stated. Protein buffer solution; 20 mM Tris, 0.15 M NaCl, 0.03 % (w/v) DDM.

PBP2b crystals were analysed during the course of consecutive days. Towards the end of each day, the crystals began to disappear, although the subsequent day, they would reappear with an improved size. Following a weekend, the crystals had completely dissolved. It is believed that temperature fluctuations in the 18°C room were responsible.

The crystal protruding from the PBP1a cluster (indicated by the arrow on Figure 6.7) was sequestered and frozen in cryoprotectant. Unfortunately, the crystal did not survive the freezing process.

Efforts to reproduce the crystal formation in identical conditions were unsuccessful, owing to the potential variability in a myriad of parameters.

6.4.4. Crystallisation of PBP1a, PBP2b and PBP2x variants in the presence of ligands

Crystallisation trials of PBP1a, PBP2b and PBP2x and the corresponding transpeptidase active site serine mutants were performed in the presence and absence of a 10-fold molar excess of the ligands ampicillin and Lys-Lipid II (solubilised in the equivalent buffer to the protein) respectively. The protein-ligand solutions were

incubated at 20°C for 1 h prior to preparing the crystallisation screens. Crystallisation conditions were screened in an analogous method to the native apoenzymes. Crystal nucleation and growth were not apparent.

6.5. Discussion and future work

The purpose of this Chapter was to establish optimal crystallisation conditions for *S. aureus* MGT and the variants of *S. pneumoniae* PBP1a, PBP2b and PBP2x, with the ultimate aim of obtaining structural information to relate to the catalytic mechanism. The following sections discuss the results, parameters that influence membrane protein crystallisation and future work.

6.5.1. *S. pneumoniae* PBP1a-Δ30, PBP2b-Δ39, PBP2x-Δ48 and *S. aureus* MGT crystallisations

The crystallisation of the soluble enzymes had mixed results. PBP1a-Δ30 did not provide any indication of nucleating. This enzyme is predicted to be unstable due to the location of the truncation and its poor expression levels. Additionally, detergent monomers may not have been eliminated from the protein preparation (following extraction from the membranes), which would not be compatible with the crystal screens for soluble proteins. A single condition, out of 576 sparse matrices at two protein concentrations, provided protein crystals of MGT. The difficulty of MGT crystallisation was comparable to the studies by Heaslet *et al.* (2009), where crystals of MGT-E100Q only were of a suitable quality for diffraction. The stability of MGT is problematic, where a high salt content is essential to prevent the protein precipitating out of solution.

It was evident that the conditions required for PBP2b-Δ39 to crystallise were almost suitable given the spherulite formation under variations of the same crystal screen. The additives 1.0 M Potassium sodium tartrate tetrahydrate or 50 % (v/v) PEG 400 promoted crystallisation, and analysis of the crystal proved it was comprised of protein. The insufficient resolution of the diffraction data possibly resulted from the disruption of the crystal lattice upon freezing in an inappropriate cryoprotection

condition. Screening of alternative cryoprotectants could solve this problem, enabling high-resolution data to be obtained.

PBP2x-Δ48 reproducibly crystallised under the conditions described, which were similar to those in literature. Fine screening of the crystallisation conditions by subtly varying the pH and precipitant concentration enabled the growth of crystals with size and morphology suitable for diffraction studies. A single protein crystal in the space group $P3_121$ diffracted to 2.8 Å. Further optimisations could improve on this resolution. In spite of a higher resolution crystal structure in literature, the established crystallisation conditions are important for future work. Ligands could be co-crystallised with the protein, or alternatively, soaked into a pre-formed crystal lattice of the protein to provide valuable structural and binding information.

6.5.2. The challenges of membrane protein crystallisation

Membrane proteins crystals are notoriously difficult to grow, reproduce and generate a crystal structure for a number of reasons. Following expression and purification, the yield and purity of membrane proteins is often not sufficient for crystallisations, where a high concentration of monodisperse protein of near homogeneity is required (Caffrey, 2003). The amphiphilic nature of membrane proteins dictates the requirement for detergents. The choice of detergent, in terms of size, concentration and properties, is empirical to ensure the structural integrity of the protein is maintained in an unaggregated state, suitable for crystallisation (Loll, 2003). The phase behaviour of detergents can impede crystal development, which is affected by environmental conditions including temperature and the presence of precipitants (Reiss-Husson and Picot, 1999). In a vapour diffusion experiment, the protein and detergent concentration will rise in parallel (Caffrey, 2003), where the detergent will be in a transition between monomeric and micellar solution (Loll, 2003). Phase separation commonly occurs where the micellar solution spontaneous separates into two liquid phases: detergent rich and detergent depleted, which is defined at the consolution boundary (Loll, 2003; Reiss-Husson and Picot, 1999). Generally, integral membrane proteins locate to the detergent rich phase, which can cause denaturation (Loll, 2003; Reiss-Husson and Picot, 1999).

Upon obtaining membrane protein crystals, difficulties in generating a structure are encountered. The packing of the detergent molecules in a crystal lattice is commonly disordered and infers that the membrane protein crystals are highly solvated (Carpenter *et al.*, 2008). Consequently, the crystals are fragile, diffract to low resolution and are subject to radiation damage during the diffraction experiment (Carpenter *et al.*, 2008).

6.5.3. Choice of detergent during membrane protein crystallisation

The crystallisations of the full-length membrane proteins were trialled in the presence of two different detergents, DDM and LDAO, at concentrations just above the CMC. Both detergents have a C12 alkyl chain (from structural comparisons), but produce micelles of substantially different sizes. LDAO and DDM have an aggregation number of ~76 and ~78-149, with a micelle size of ~17 kDa and ~40-75 kDa, respectively (information from Anatrace, Affymetrix). The small micelle size of LDAO confers a smaller belt around the hydrophobic regions of the membrane protein. Potentially, this could allow for more interprotein interactions within a crystal lattice and ultimately crystals could be produced that provide a better diffraction pattern (Privé, 2007). The large micelle size of DDM would be expected to mask large areas of the exposed polar surfaces of the protein. In spite of this, DDM was employed in these trials due to its ability to maintain the proteins in a stable, native conformational state in addition to its proven success in the crystallisation of a myriad of membrane proteins. Membrane protein crystals were only generated in the presence of DDM (Figure 6.7), where the properties of LDAO probably inferred gradual protein denaturation, a common attribute of this detergent (Privé, 2007). Upon reproducibility of the membrane protein crystals, detergents of similar properties could be trialled to improve protein contacts within the crystal lattice (Privé, 2007).

6.5.4. *S. pneumoniae* PBP1a, PBP2b and PBP2x crystallisations

Crystals of *S. pneumoniae* PBP1a and PBP2b were obtained when the detergent concentration was just above the CMC (DDM, 0.03% (w/v)), irrespective of the low protein concentration. The cryoprotectant conditions for PBP1a were not suitable to protect the crystal during the freezing process, thus further conditions should be screened prior to freezing to ensure ice crystals do not materialise.

The crystal formation of PBP2b was interfered by subtle temperature fluctuations that ultimately inhibited crystal growth. Temperature has a greater impact on membrane protein crystals compared to soluble protein crystals, due to the dependence of temperature on the detergent CMC. The high detergent content in the crystal lattice of membrane protein crystals dictates that fluctuations in the effective detergent concentration can impact the growing crystals (Barnard *et al.*, 2007).

Crystallisation experiments of the wild-type PBPs and the corresponding transpeptidase active site serine mutants were trialled in the presence of ligands (ampicillin and Lys-Lipid II respectively) with no success. The ligands were employed to stabilise the inherent flexibility of the membrane proteins and to provide information on substrate binding. Crystal formation of PBP1a-S370A in the presence of Lys-Lipid II could have been hindered due to the active transglycosylase domain, which potentially could have polymerised the substrate. A double mutant consisting of active site transpeptidase and transglycosylase mutations should be used in future co-crystallisation experiments.

6.5.5. The reproducibility of crystal nucleation and growth

Both soluble and membrane protein crystals obtained in the vapour diffusion experiments, with the exception of PBP2x-Δ48, were not reproducible. There are a number of explanations for this phenomenon including variations in: protein preparation; protein concentration; temperature; detergent concentration; detergent impurities; precipitant concentration. Additionally, the dodeca-histidine tag on all the *S. pneumoniae* PBP variants would have introduced a further degree of disorder, potentially affecting crystal contacts. Only six of the twelve histidine residues could

be cleaved from the protein (Figure 3.1). Therefore, new constructs need to be made to enable the removal of the full twelve histidine residues.

The precise conditions of the labile supersaturated state determining crystal nucleation are often very sensitive and difficult to reproduce. Microseeding could be used to bypass the crystal nucleation stage. In this technique, small crystals or 'seeds' are introduced into a pre-equilibrated hanging drop in the metastable zone of supersaturation (Bergfors, 2003). Growth from the seeds produces crystals that follow the same lattice symmetry as the original seed.

6.5.6. Crystallisation of proteins with large soluble tags

The crystallisation of membrane proteins could exploit soluble fusion tags integrated onto the protein for purification purposes; examples include maltose-binding protein (MBP) and green fluorescent protein (GFP) tags. Permitting that conformational heterogeneity is not introduced, the readily crystallising soluble tag could act as a scaffold, inducing crystallisation of the membrane protein. This approach has been documented for the co-crystallisation of MBP with *S. aureus* SarR (Liu *et al.*, 2001), *Saccharomyces cerevisiae* MATa1 homodomain (Ke and Wolberger, 2003) and the ectodomain of the human T-cell leukaemia virus I envelope protein gp21 (Kobe *et al.*, 1999). The attachment of scaffold proteins to the full-length (or truncated) PBPs could promote crystallisation of these recombinant membrane proteins allowing co-crystal structures to be solved.

6.5.7. A novel technique to eliminate the requirement of detergent in membrane protein crystallography

SMALP technology (Section 3.8.2.1) provides a new route to the solubilisation and purification of membrane proteins in a stable, monodisperse state in a detergent-free environment. The homogenous discoidal structure of the SMALP could promote protein interactions in an ordered array, which could lead to the formation of crystal nuclei.

6.6. Conclusion

The initial stage in the determination of a crystallographic structure is the growth of crystals suitable for diffraction, which is regarded as the rate-limiting step from protein to structure for both soluble and integral membrane proteins. Conditions were identified that were conducive to the crystallisation of the *S. pneumoniae* PBPs (full-length and devoid of the membrane anchor) and *S. aureus* MGT, which should be pursued to reproduce the crystal nucleation and growth conditions. The recent advances in crystallisation methods and high-throughput screening procedures are anticipated to rapidly expand the number of solved membrane protein structures, enhancing the understanding of the membrane proteome and providing information for structure-based drug design.

Chapter 7. General discussion and conclusions

This Chapter addresses the principal findings of this project with reference to the main objectives outlined in Section 1.11, and highlights areas where further investigation is necessary.

7.1. Production of *S. pneumoniae* β-lactam resistance determinants

The primary focus of this work was to investigate the kinetic and structural characteristics of *S. pneumoniae* PBP1a, PBP2b and PBP2x. These enzymes are highly clinically relevant, being the target of β-lactam antibiotics and mediating the resistance to this important class of antibiotics. Thus, the initial objective was to establish protocols that enabled the expression, solubilisation and purification of these full-length membrane proteins (and variants thereof) in suitable quantities for forthcoming analyses. The PBPs, *S. pneumoniae* D39 and 5204, full-length and devoid of the membrane anchor, and transglycosylase and transpeptidase active site mutants, expressed to high levels in *E. coli* BL21 Star (DE3) pRosetta cells. The exception was PBP1a-Δ30; the expression levels were low probably owing to the instability of the construct. Sodium deoxycholate was found to be the ideal detergent to extract the full-length membrane proteins from the membranes. Each variant of the β-lactam resistance determinants was purified by IMAC and size exclusion chromatography (PBP2b-Δ39 and PBP2x-Δ48 were further purified by anion exchange) with enzyme-specific adaptations to optimise the purity. Each PBP, except the transpeptidase catalytic mutants, was able to bind BOCILLIN FL, indicating that the transpeptidase active site was in a sufficiently native conformation to react with the substrate analogue. Accordingly, it was anticipated that the enzymes had been prepared in a catalytically active form.

7.2. The enzymology of transglycosylation

7.2.1. The development of a spectrophotometric assay for transglycosylase activity

Lipid II is the final monomeric intermediate in the peptidoglycan synthetic pathway, and is the substrate of the PBPs and MGTs. Recently established protocols have enabled suitable quantities of Lipid II to be synthesised, facilitating the study of the final stages of peptidoglycan biosynthesis, which has been hindered in part due to the limited substrate availability.

Chapter 4 details the development of a novel spectrophotometric assay to rapidly analyse the transglycosylation activities of Class A HMW-PBPs and MGTs with their natural substrate, Lipid II. Transglycosylation results in the formation of a β-1,4-glycosidic bond between the Mur*N*Ac moiety of an elongating glycan chain and the Glc*N*Ac moiety of Lipid II, with the concomitant release of undecaprenyl pyrophosphate (Lovering *et al.*, 2007). The generation of this latter product was exploited in the measurement of transglycosylase activity; it was coupled to an undecaprenyl pyrophosphate phosphatase (*E. coli* PgpB), which dephosphorylates undecaprenyl pyrophosphate. The liberated terminal P_i was monitored by the phosphorolysis of a chromogenic substrate, MESG. This assay was used in a discontinuous manner to successfully establish transglycosylase activity from *S. aureus* MGT and *S. pneumoniae* PBP1a.

Given the transglycosylases exhibit substantial activity and that PgpB can be prepared in sufficient quantities, this assay has the potential to measure transglycosylation continuously. Further development of this spectrophotometric assay for use in a plate reader with a 96-well plate would enable a myriad of parameters to be assessed promptly with regards to transglycosylase activity (examples include pH and metal ion dependency, substrate specificity, effects of inhibitors, protein complexes), which could significantly contribute to the understanding of this complex stage of peptidoglycan biosynthesis.

7.2.2. Characterisation of *S. aureus* MGT catalysed transglycosylation

MGT was employed as a control enzyme for transglycosylation; the construct devoid of the membrane anchor has proven activity (Terrak and Nguyen-Distèche, 2006). Using the designed spectrophotometric assay for transglycosylation, kinetic characteristics of MGT were investigated. It was revealed that at low substrate concentrations, the velocity of MGT transglycosylase activity exhibited a sigmoidal dependence on substrate concentration, and at high substrate concentrations, MGT was subjected to severe substrate inhibition. A model was designed to describe these characteristics, to which the kinetic data was applied in an attempt to extract kinetic constants. Further data points are needed to improve the fit of the data to the model.

7.2.3. Characterisation of *S. pneumoniae* PBP1a catalysed transglycosylation

Transglycosylation activities of the full-length integral membrane protein, *S. pneumoniae* PBP1a and the corresponding active site mutants, were explored using the spectrophotometric assay. It was immediately recognised that under the experimental conditions trialled, the rate of transglycosylation was extremely slow and the generation of a velocity versus substrate plot revealed that V_{max} was not reached despite using Lipid II concentrations that caused inhibition of MGT activity. The rates were vastly insufficient to support bacterial growth; the *in vitro* conditions did not suitably recreate the required conditions for transglycosylation. Many factors could influence the transglycosylation activity of PBP1a including the formation of protein and lipid complexes, which could stabilise and activate the enzyme in its natural environment.

Transglycosylation by the transglycosylase putative catalytic mutant was undetectable, validating the importance of this residue. PBP1a transglycosylation was not dependent on transpeptidase activity, although in the absence or uncoupling of the transpeptidation reaction, the rate of transglycosylation was augmented, which was found to be statistically significant *in vitro*. It is plausible that transpeptidation and transglycosylation reactions of the bifunctional enzyme do not occur concomitantly, thus the catalysis of a reaction in one domain could momentarily hinder the activity of the other domain.

7.2.4. Optimisation of *S. aureus* MGT and *S. pneumoniae* PBP1a transglycosylase activity

In an attempt to recreate the *in vivo* conditions and to optimise the rates of transglycosylation by MGT and PBP1a, various experimental parameters were considered including: temperature; metal ion specificity; presence of lipids; presence of Decyl PEG and DMSO. These factors influenced the transglycosylase activity of MGT and PBP1a to varying degrees. Further conditions should be trialled to augment the activity of MGT and PBP1a *in vitro*.

7.3. The enzymology of transpeptidation

7.3.1. The development of a spectrophotometric assay for D-Ala release

Transpeptidation results in the formation of a cross-link between the fourth position D-Ala of a donor stem peptide and either the amino acid at the third position of an adjacent acceptor stem peptide (direct) or by a branching peptide appendage from this third position residue (indirect) (as reviewed by Vollmer *et al.* (2008a)). The terminal D-Ala of the donor stem peptide is released concomitantly, and can be used to follow transpeptidation in a novel continuous spectrophotometric assay as detailed in Chapter 5. The generation of D-Ala can be coupled to the ligation of D-Ala with D-Lac, catalysed by VanA, in an ATP-dependent reaction. The release of ADP or P_i can be measured spectrophotometrically. This assay was successfully employed to characterise *Actinomadura* R39 D,D-peptidase, which demonstrated a substrate preference for peptidoglycan fragments with *meso*-DAP residing at the third position of the peptide stem as opposed to L-Lys, coincident with published literature (Anderson *et al*., 2003). The main limitation of this assay is that the D-Ala released from transpeptidation or D,D-carboxypeptidation cannot be distinguished. This could be solved by the quantification of free peptide stem amino groups; an experimental strategy is discussed in Chapter 5.

7.3.2. Detection of transpeptidation by *S. pneumoniae* primary resistance determinants

The interactions of β-lactam antibiotics with HMW-PBPs have been well studied, but presently, there are few experimental protocols that can analyse transpeptidation by HMW-PBPs with the natural substrate. Consequently, the specificities of the interactions involved are poorly understood. The sensitive Amplex Red assay was used to detect D-Ala release from PBP1a, PBP2b and PBP2x catalysed reactions. The discontinuous assays described in Chapter 5 attempted to produce an environment conducive to transpeptidation *in vitro* using the established optimal conditions for PBP1a-catalysed transglycosylation. The current hypothesis for the ultimate stages of peptidoglycan biosynthesis is that transglycosylation precedes transpeptidation (Born *et al*., 2006). This was investigated using monomeric Lipid II and polymeric forms (produced through MGT or PBP1a-S370A dependent transglycosylation reactions). D-Ala release (representative of transpeptidation or D,D-carboxypeptidation) was detected in incubations with PBP1a and PBP2b; both enzymes exhibited a substrate preference for polymerised glycan strands over the monomeric Lipid II. The results also suggested that transpeptidation catalysed by PBP1a (similar to *E. coli* PBP1a (Born *et al.*, 2006) and *E. coli* PBP1b (Bertsche *et al.*, 2005)) demonstrated a dependency for concomitant transglycosylation reactions catalysed by the same enzyme molecule. This coincides with the model proposed by Sung *et al.* (2009): the nascent transglycosylation product is directed to the transpeptidase domain. Failure to detect D-Ala release by PBP2x was interesting; it raises questions regarding the difference in substrate specificity of the HMW-PBPs, which may relate to their defined roles during different stages of the cell cycle i.e. PBP2b is involved in the biosynthesis of peptidoglycan during elongation and PBP1a and PBP2x are involved in division (Morlot *et al.*, 2003). These enzymes are recruited to multiprotein complexes (Scheffers and Pinho, 2005) and this association with auxiliary proteins may be required to promote the activity of the PBPs as documented for *E. coli* transpeptidases (Paradis-Bleau *et al*., 2010; Typas *et al*., 2010).

In *S. pneumoniae*, it has been estimated that ~50 % peptidoglycan stem peptides are involved in cross-linking (Garcia-Bustos and Tomasz, 1990). The D-Ala released by PBP1a and PBP2b over the 18 h incubation did not coincide with or approach this value. Thus, the level of transpeptidation detected would be substantially inadequate to support the integrity of the cell wall. PBP1a and PBP2b had a preference for peptidoglycan polymers that were not characterised definitively. It is possible that the enzymes required defined polymer lengths, which were present as only a small fraction of the total substrate preparation. Additionally, *S. pneumoniae* PBPs may have an acceptor substrate preference for peptidoglycan tripeptide stems as these constitute up to 30 % of the peptidoglycan composition (Garcia-Bustos and Tomasz, 1990). These points highlight the gaps in the understanding of how the PBPs recognise their substrates.

Chapter 5 describes the preliminary results towards the full kinetic characterisation of the transpeptidase activity of *S. pneumoniae* β-lactam resistance determinants. Future work is required to establish *in vitro* conditions that will enable the PBPs to exhibit substantial activity. This will facilitate further characterisations that could contribute to an elevated understanding of the enzymology of PBP1a, PBP2b and PBP2x and the resistance mechanisms that they employ.

7.4. Towards the structural characterisations of *S. pneumoniae* PBP1a, PBP2b and PBP2x

To fully understand the mechanisms of substrate recognition and catalysis of HMW-PBP-mediated transglycosylation and transpeptidation, structural information of these enzymes in complex with peptidoglycan fragments is required. Recent progress has been made in the area of membrane protein crystallisation and the first PBP structure with a transmembrane domain has been solved (*E. coli* PBP1b (Sung *et al*., 2009)). This structure and others of truncated PBPs (e.g. *S. aureus* PBP2 (Lovering *et al*., 2007)) have been essential in shedding light on the transglycosylase catalytic mechanism. Chapter 6 details attempts to crystallise full-length PBPs and equivalent enzymes devoid of the membrane-spanning domain in apo and liganded forms to various levels of success. The apoenzyme PBP2x-Δ48 formed crystals,

which diffracted to 2.8 Å. Full-length membrane protein crystals were obtained for PBP1a and PBP2b. However, the conditions conducive to crystallisation were not reproducible, a common problem encountered. Further screening of crystallisation and cryoprotectant conditions for the PBPs is required for the pursuit of valuable structural information.

7.5. Conclusion

The recalcitrant nature of *S. pneumoniae* PBPs *in vitro* has thwarted appreciable efforts to biochemically characterise these enzymes. The work presented in this thesis has provided successful strategies to detect transglycosylase and transpeptidase activities of the PBPs, providing an excellent foundation for further work to unravel the mysteries of this complex family of antimicrobial targets.

Bibliography

Abraham, E. P. and Chain, E. (1988). An enzyme from bacteria able to destroy penicillin. 1940. *Rev Infect Dis* **10**, 677-678

Abràmoff, M. D., Magelhaes, P. J. and Ram, S. J. (2004). Image processing with ImageJ. *Biophotonics International* **11**, 36-42

Acharya, K. R. and Lloyd, M. D. (2005). The advantages and limitations of protein crystal structures. *Trends Pharmacol Sci* **26**, 10-14

Adachi, H., Ohta, T. and Matsuzawa, H. (1991). Site-directed mutants, at position 166, of RTEM-1 beta-lactamase that form a stable acyl-enzyme intermediate with penicillin. *J Biol Chem* **266**, 3186-3191

Adachi, M., Zhang, Y., Leimkuhler, C., Sun, B., LaTour, J. V. and Kahne, D. E. (2006). Degradation and reconstruction of moenomycin A and derivatives: dissecting the function of the isoprenoid chain. *J Am Chem Soc* **128**, 14012-14013

Agarwal, A. K. and Fishwick, C. W. (2010). Structure-based design of anti-infectives. *Ann N Y Acad Sci* **1213**, 20-45

Alekshun, M. N. and Levy, S. B. (2007). Molecular mechanisms of antibacterial multidrug resistance. *Cell* **128**, 1037-1050

Alpuche, C., Garau, J. and Lim, V. (2007). Global and local variations in antimicrobial susceptibilities and resistance development in the major respiratory pathogens. *Int J Antimicrob Agents* **30 Suppl 2**, S135-138

Altschul, S. F., Gish, W., Miller, W., Myers, E. W. and Lipman, D. J. (1990). Basic local alignment search tool. *J Mol Biol* **215**, 403-410

Anderson, J. W., Adediran, S. A., Charlier, P., Nguyen-Disteche, M., Frere, J. M., Nicholas, R. A. and Pratt, R. F. (2003). On the substrate specificity of bacterial DD-peptidases: evidence from two series of peptidoglycan-mimetic peptides. *Biochem J* **373**, 949-955

Andersson, D. I. and Hughes, D. (2010). Antibiotic resistance and its cost: is it possible to reverse resistance? *Nat Rev Microbiol* **8**, 260-271

Aslanidis, C. and de Jong, P. J. (1990). Ligation-independent cloning of PCR products (LIC-PCR). *Nucleic Acids Res* **18**, 6069-6074

Baltz, R. H. (2008). Renaissance in antibacterial discovery from actinomycetes. *Curr Opin Pharmacol* **8**, 557-563

Barnard, T. J., Wally, J. L. and Buchanan, S. K. (2007). UNIT 17.9 Crystallization of integral membrane proteins. *Current Protocols in Protein Science*, 17.19.11-17.19.15

Barreteau, H., Kovac, A., Boniface, A., Sova, M., Gobec, S. and Blanot, D. (2008). Cytoplasmic steps of peptidoglycan biosynthesis. *FEMS Microbiol Rev* **32**, 168-207

Barrett, D., Wang, T. S., Yuan, Y., Zhang, Y., Kahne, D. and Walker, S. (2007). Analysis of glycan polymers produced by peptidoglycan glycosyltransferases. *J Biol Chem* **282**, 31964-31971

Batson, S. (2010). Structural enzymology of peptidoglycan biosynthetic D-amino acid dipeptide ligases. Unpublished Ph.D., University of Warwick.

Bebear, C. M. and Pereyre, S. (2005). Mechanisms of drug resistance in *Mycoplasma pneumoniae*. *Curr Drug Targets Infect Disord* **5**, 263-271

Bergfors, T. (2003). Seeds to crystals. *J Struct Biol* **142**, 66-76

Bertani, G. (1951). Studies on lysogenesis. I. The mode of phage liberation by lysogenic *Escherichia coli*. *J Bacteriol* **62**, 293-300

Bertsche, U., Breukink, E., Kast, T. and Vollmer, W. (2005). *In vitro* murein peptidoglycan synthesis by dimers of the bifunctional transglycosylase-transpeptidase PBP1B from *Escherichia coli*. *J Biol Chem* **280**, 38096-38101

Besong, G. E., Bostock, J. M., Stubbings, W., Chopra, I., Roper, D. I., Lloyd, A. J., Fishwick, C. W. and Johnson, A. P. (2005). A *de novo* designed inhibitor of D-Ala-D-Ala ligase from *E. coli*. *Angew Chem Int Ed Engl* **44**, 6403-6406

Beveridge, T. J. and Davies, J. A. (1983). Cellular responses of *Bacillus subtilis* and *Escherichia coli* to the Gram stain. *J Bacteriol* **156**, 846-858

Born, P., Breukink, E. and Vollmer, W. (2006). *In vitro* synthesis of cross-linked murein and its attachment to sacculi by PBP1A from *Escherichia coli*. *J Biol Chem* **281**, 26985-26993

Bouhss, A., Crouvoisier, M., Blanot, D. and Mengin-Lecreulx, D. (2004). Purification and characterization of the bacterial MraY translocase catalyzing the first membrane step of peptidoglycan biosynthesis. *J Biol Chem* **279**, 29974-29980

Bouhss, A., Dementin, S., van Heijenoort, J., Parquet, C. and Blanot, D. (1999). Formation of adenosine 5'-tetraphosphate from the acyl phosphate intermediate: a difference between the MurC and MurD synthetases of *Escherichia coli*. *FEBS Lett* **453**, 15-19

Bradford, M. M. (1976). A rapid and sensitive method for the quantitation of microgram quantities of protein utilizing the principle of protein-dye binding. *Anal Biochem* **72**, 248-254

Breukink, E., van Heusden, H. E., Vollmerhaus, P. J., Swiezewska, E., Brunner, L., Walker, S., Heck, A. J. and de Kruijff, B. (2003). Lipid II is an intrinsic component of the pore induced by nisin in bacterial membranes. *J Biol Chem* **278**, 19898-19903

Bugg, T. D. (1999). Bacterial peptidoglycan biosynthesis and its inhibition. In *Comprehensive Natural Products Chemistry*, 1st edn, vol 3, pp. 241-294. Edited by B. M. Pinto. Oxford: Elsevier Science Ltd.

Bugg, T. D. and Walsh, C. T. (1992). Intracellular steps of bacterial cell wall peptidoglycan biosynthesis: enzymology, antibiotics, and antibiotic resistance. *Nat Prod Rep* **9**, 199-215

Cabeen, M. T. and Jacobs-Wagner, C. (2005). Bacterial cell shape. *Nat Rev Microbiol* **3**, 601-610

Caffrey, M. (2003). Membrane protein crystallization. *J Struct Biol* **142**, 108-132

Carapito, R., Chesnel, L., Vernet, T. and Zapun, A. (2006). Pneumococcal beta-lactam resistance due to a conformational change in penicillin-binding protein 2x. *J Biol Chem* **281**, 1771-1777

Carpenter, E. P., Beis, K., Cameron, A. D. and Iwata, S. (2008). Overcoming the challenges of membrane protein crystallography. *Curr Opin Struct Biol* **18**, 581-586

Centres for Disease Control and Prevention. (1997) Prevention of pneumococcal disease: recommendations of the Advisory Committee on Immunization Practices (ACIP). *MMWR Recomm. Rep.* **46**, 1–24.

Champoux, J. J. (2001). DNA topoisomerases: structure, function, and mechanism. *Annu Rev Biochem* **70**, 369-413

Chayen, N. E. (2004). Turning protein crystallisation from an art into a science. *Curr Opin Struct Biol* **14**, 577-583

Cheng, T. J., Sung, M. T., Liao, H. Y., Chang, Y. F., Chen, C. W., Huang, C. Y., Chou, L. Y., Wu, Y. D., Chen, Y. H., Cheng, Y. S., Wong, C. H., Ma, C. and Cheng, W. C. (2008). Domain requirement of moenomycin binding to bifunctional transglycosylases and development of high-throughput discovery of antibiotics. *Proc Natl Acad Sci U S A* **105**, 431-436

Chesnel, L., Carapito, R., Croize, J., Dideberg, O., Vernet, T. and Zapun, A. (2005). Identical penicillin-binding domains in penicillin-binding proteins of *Streptococcus pneumoniae* clinical isolates with different levels of beta-lactam resistance. *Antimicrob Agents Chemother* **49**, 2895-2902

Chesnel, L., Pernot, L., Lemaire, D., Champelovier, D., Croize, J., Dideberg, O., Vernet, T. and Zapun, A. (2003). The structural modifications induced by the M339F substitution in PBP2x from *Streptococcus pneumoniae* further decreases the susceptibility to beta-lactams of resistant strains. *J Biol Chem* **278**, 44448-44456

Clarke, T. B. (2008). The biochemistry of the latter stages of peptidoglycan biosynthesis and modification. Unpublished Ph. D., University of Warwick.

Clarke, T. B., Kawai, F., Park, S. Y., Tame, J. R., Dowson, C. G. and Roper, D. I. (2009). Mutational analysis of the substrate specificity of *Escherichia coli* penicillin binding protein 4. *Biochemistry* **48**, 2675-2683

Coffey, T. J., Dowson, C. G., Daniels, M. and Spratt, B. G. (1993). Horizontal spread of an altered penicillin-binding protein 2B gene between *Streptococcus pneumoniae* and *Streptococcus oralis*. *FEMS Microbiol Lett* **110**, 335-339

Contreras-Martel, C., Dahout-Gonzalez, C., Martins Ados, S., Kotnik, M. and Dessen, A. (2009). PBP active site flexibility as the key mechanism for beta-lactam resistance in pneumococci. *J Mol Biol* **387**, 899-909

Contreras-Martel, C., Job, V., Di Guilmi, A. M., Vernet, T., Dideberg, O. and Dessen, A. (2006). Crystal structure of penicillin-binding protein 1a (PBP1a) reveals a mutational hotspot implicated in beta-lactam resistance in *Streptococcus pneumoniae*. *J Mol Biol* **355**, 684-696

Cramer, P. (2002). Multisubunit RNA polymerases. *Curr Opin Struct Biol* **12**, 89-97

Davies, J. (2011). How to discover new antibiotics: harvesting the parvome. *Curr Opin Chem Biol* **15**, 5-10

Deisenhofer, J., Epp, O., Miki, K., Huber, R. and Michel, H. (1984). X-ray structure analysis of a membrane protein complex. Electron density map at 3 Å resolution and a model of the chromophores of the photosynthetic reaction center from *Rhodopseudomonas viridis*. *J Mol Biol* **180**, 385-398

Denome, S. A., Elf, P. K., Henderson, T. A., Nelson, D. E. and Young, K. D. (1999). *Escherichia coli* mutants lacking all possible combinations of eight penicillin binding proteins: viability, characteristics, and implications for peptidoglycan synthesis. *J Bacteriol* **181**, 3981-3993

Di Berardino, M., Dijkstra, A., Stuber, D., Keck, W. and Gubler, M. (1996). The monofunctional glycosyltransferase of *Escherichia coli* is a member of a new class of peptidoglycan-synthesising enzymes. *FEBS Lett* **392**, 184-188

Di Guilmi, A. M., Dessen, A., Dideberg, O. and Vernet, T. (2002). Bifunctional penicillin-binding proteins: focus on the glycosyltransferase domain and its specific inhibitor moenomycin. *Curr Pharm Biotechnol* **3**, 63-75

Di Guilmi, A. M., Dessen, A., Dideberg, O. and Vernet, T. (2003a). Functional characterization of penicillin-binding protein 1b from *Streptococcus pneumoniae*. *J Bacteriol* **185**, 1650-1658

Di Guilmi, A. M., Dessen, A., Dideberg, O. and Vernet, T. (2003b). The glycosyltransferase domain of penicillin-binding protein 2a from *Streptococcus pneumoniae* catalyzes the polymerization of murein glycan chains. *J Bacteriol* **185**, 4418-4423

Di Guilmi, A. M., Mouz, N., Andrieu, J. P., Hoskins, J., Jaskunas, S. R., Gagnon, J., Dideberg, O. and Vernet, T. (1998). Identification, purification, and characterization of transpeptidase and glycosyltransferase domains of *Streptococcus pneumoniae* penicillin-binding protein 1a. *J Bacteriol* **180**, 5652-5659

Di Guilmi, A. M., Mouz, N., Martin, L., Hoskins, J., Jaskunas, S. R., Dideberg, O. and Vernet, T. (1999). Glycosyltransferase domain of penicillin-binding protein 2a from *Streptococcus pneumoniae* is membrane associated. *J Bacteriol* **181**, 2773-2781

Dowson, C. G., Hutchison, A., Brannigan, J. A., George, R. C., Hansman, D., Linares, J., Tomasz, A., Smith, J. M. and Spratt, B. G. (1989). Horizontal transfer of penicillin-binding protein genes in penicillin-resistant clinical isolates of *Streptococcus pneumoniae*. *Proc Natl Acad Sci U S A* **86**, 8842-8846

Dowson, C. G., Hutchison, A., Woodford, N., Johnson, A. P., George, R. C. and Spratt, B. G. (1990). Penicillin-resistant viridans streptococci have obtained altered penicillin-binding protein genes from penicillin-resistant strains of *Streptococcus pneumoniae*. *Proc Natl Acad Sci U S A* **87**, 5858-5862

Dzhekieva, L., Rocaboy, M., Kerff, F., Charlier, P., Sauvage, E. and Pratt, R. F. (2010). Crystal structure of a complex between the *Actinomadura* R39 DD-peptidase and a peptidoglycan-mimetic boronate inhibitor: interpretation of a transition state analogue in terms of catalytic mechanism. *Biochemistry* **49**, 6411-6419

Easterby, J. S. (1973). Coupled enzyme assays: a general expression for the transient. *Biochim Biophys Acta* **293**, 552-558

Evans, P. R. (2006). Scaling and assessment of data quality. *Acta Crystallogr D Biol Crystallogr* **62**, 72-82.

Fleischmann, R. D., Adams, M. D., White, O., Clayton, R. A., Kirkness, E. F., Kerlavage, A. R., Bult, C. J., Tomb, J. F., Dougherty, B. A., Merrick, J. M. and et al. (1995). Whole-genome random sequencing and assembly of *Haemophilus influenzae* Rd. *Science* **269**, 496-512

Fluit, A. C. and Schmitz, F. J. (2004). Resistance integrons and super-integrons. *Clin Microbiol Infect* **10**, 272-288

Fonzé, E., Vermeire, M., Nguyen-Disteche, M., Brasseur, R. and Charlier, P. (1999). The crystal structure of a penicilloyl-serine transferase of intermediate penicillin sensitivity. The DD-transpeptidase of streptomyces K15. *J Biol Chem* **274**, 21853-21860

Frère, J. M., Duez, C., Ghuysen, J. M. and Vandekerkhove, J. (1976). Occurrence of a serine residue in the penicillin-binding site of the exocellular DD-carboxy-peptidase-transpeptidase from *Streptomyces* R61. *FEBS Lett* **70**, 257-260

Garcia-Bustos, J. and Tomasz, A. (1990). A biological price of antibiotic resistance: major changes in the peptidoglycan structure of penicillin-resistant pneumococci. *Proc Natl Acad Sci U S A* **87**, 5415-5419

Gardner, A. D. (1940). Morphological effects of penicillin on bacteria. *Nature* **146**, 837-838

Garman, E. F. and Doublié, S. (2003). Cryocooling of macromolecular crystals: optimization methods. *Methods Enzymol* **368**, 188-216

Georgopapadakou, N. H. (1993). Penicillin-binding proteins and bacterial resistance to beta-lactams. *Antimicrob Agents Chemother* **37**, 2045-2053

Ghuysen, J. M. (1991). Serine beta-lactamases and penicillin-binding proteins. *Annu Rev Microbiol* **45**, 37-67

Ghuysen, J. M. (1994). Molecular structures of penicillin-binding proteins and beta-lactamases. *Trends Microbiol* **2**, 372-380

Gillet, V., Johnson, A. P., Mata, P., Sike, S. and Williams, P. (1993). SPROUT: a program for structure generation. *J Comput Aided Mol Des* **7**, 127-153

Glauner, B., Holtje, J. V. and Schwarz, U. (1988). The composition of the murein of *Escherichia coli*. *J Biol Chem* **263**, 10088-10095

Goffin, C. and Ghuysen, J. M. (1998). Multimodular penicillin-binding proteins: an enigmatic family of orthologs and paralogs. *Microbiol Mol Biol Rev* **62**, 1079-1093

Goffin, C. and Ghuysen, J. M. (2002). Biochemistry and comparative genomics of SxxK superfamily acyltransferases offer a clue to the mycobacterial paradox: presence of penicillin-susceptible target proteins versus lack of efficiency of penicillin as therapeutic agent. *Microbiol Mol Biol Rev* **66**, 702-738

Gong, X., Fan, S., Bilderbeck, A., Li M., Pang, H. and Tao, S. (2008). Comparative analysis of essential genes and non-essential genes in *Escherichia coli* K12. *Mol Genet Genomics* **279**, 87-94

Goodell, E. W. (1985). Recycling of murein by *Escherichia coli*. *J Bacteriol* **163**, 305-310

Goodell, E. W. and Schwarz, U. (1985). Release of cell wall peptides into culture medium by exponentially growing *Escherichia coli*. *J Bacteriol* **162**, 391-397

Gordon, E., Mouz, N., Duee, E. and Dideberg, O. (2000). The crystal structure of the penicillin-binding protein 2x from *Streptococcus pneumoniae* and its acyl-enzyme form: implication in drug resistance. *J Mol Biol* **299**, 477-485

Gram, H. (1884). Über die isolierte Färbung der Schizomyceten in Schnitt- und Trockenpräparaten. *Fortschritte der Medizin* **2**, 185-189

Granier, B., Duez, C., Lepage, S., Englebert, S., Dusart, J., Dideberg, O., Van Beeumen, J., Frere, J. M. and Ghuysen, J. M. (1992). Primary and predicted secondary structures of the *Actinomadura* R39 extracellular DD-peptidase, a penicillin-binding protein (PBP) related to the *Escherichia coli* PBP4. *Biochem J* **282 (Pt 3)**, 781-788

Grant, S. G., Jessee, J., Bloom, F. R. and Hanahan, D. (1990). Differential plasmid rescue from transgenic mouse DNAs into *Escherichia coli* methylation-restriction mutants. *Proc Natl Acad Sci U S A* **87**, 4645-4649

Grebe, T. and Hakenbeck, R. (1996). Penicillin-binding proteins 2b and 2x of *Streptococcus pneumoniae* are primary resistance determinants for different classes of beta-lactam antibiotics. *Antimicrob Agents Chemother* **40**, 829-834

Gurtovenko, A. A. and Anwar, J. (2007). Modulating the structure and properties of cell membranes: the molecular mechanism of action of dimethyl sulfoxide. *J Phys Chem B* **111**, 10453-10460

Gutheil, W. G., Stefanova, M. E. and Nicholas, R. A. (2000). Fluorescent coupled enzyme assays for D-alanine: application to penicillin-binding protein and vancomycin activity assays. *Anal Biochem* **287**, 196-202

Ha, S., Chang, E., Lo, M., Men, H., Park, P., Ge, M. and Walker, S. (1999). The Kinetic Characterization of *Escherichia coli* MurG Using Synthetic Substrate Analogues. *J Am Chem Soc* **121**, 8415-8426

Hakenbeck, R., Grebe, T., Zahner, D. and Stock, J. B. (1999). β-lactam resistance in *Streptococcus pneumoniae*: penicillin-binding proteins and non-penicillin-binding proteins. *Mol Microbiol* **33**, 673-678

Hamburger, J. B., Hoertz, A. J., Lee, A., Senturia, R. J., McCafferty, D. G. and Loll, P. J. (2009). A crystal structure of a dimer of the antibiotic ramoplanin illustrates membrane positioning and a potential Lipid II docking interface. *Proc Natl Acad Sci U S A* **106**, 13759-13764

Hartley, M. D., Larkin, A. and Imperiali, B. (2008). Chemoenzymatic synthesis of polyprenyl phosphates. *Bioorg Med Chem* **16**, 5149-5156

Harwell, J. I. and Brown, R. B. (2000). The drug-resistant pneumococcus: clinical relevance, therapy, and prevention. *Chest* **117**, 530-541

Healy, V. L., Lessard, I. A., Roper, D. I., Knox, J. R. and Walsh, C. T. (2000). Vancomycin resistance in enterococci: reprogramming of the D-ala-D-Ala ligases in bacterial peptidoglycan biosynthesis. *Chem Biol* **7**, R109-119

Heaslet, H., Shaw, B., Mistry, A. and Miller, A. A. (2009). Characterization of the active site of *S. aureus* monofunctional glycosyltransferase (Mtg) by site-directed mutation and structural analysis of the protein complexed with moenomycin. *J Struct Biol* **167**, 129-135

Henderson, P. J., Hoyle, C. K. and Ward, A. (2000). Expression, purification and properties of multidrug efflux proteins. *Biochem Soc Trans* **28**, 513-517

Higgins, M. L. and Shockman, G. D. (1970). Model for cell wall growth of *Streptococcus faecalis*. *J Bacteriol* **101**, 643-648

Höltje, J. V. (1998). Growth of the stress-bearing and shape-maintaining murein sacculus of *Escherichia coli*. *Microbiol Mol Biol Rev* **62**, 181-203

Horton, J. R., Bostock, J. M., Chopra, I., Hesse, L., Phillips, S. E., Adams, D. J., Johnson, A. P. and Fishwick, C. W. (2003). Macrocyclic inhibitors of the bacterial cell wall biosynthesis enzyme MurD. *Bioorg Med Chem Lett* **13**, 1557-1560

Hoskins, J., Matsushima, P., Mullen, D. L., Tang, J., Zhao, G., Meier, T. I., Nicas, T. I. and Jaskunas, S. R. (1999). Gene disruption studies of penicillin-binding proteins 1a, 1b, and 2a in *Streptococcus pneumoniae*. *J Bacteriol* **181**, 6552-6555

Hu, Y., Chen, L., Ha, S., Gross, B., Falcone, B., Walker, D., Mokhtarzadeh, M. and Walker, S. (2003). Crystal structure of the MurG:UDP-GlcNAc complex reveals common structural principles of a superfamily of glycosyltransferases. *Proc Natl Acad Sci U S A* **100**, 845-849

Huber, G. and Nesemann, G. (1968). Moenomycin, an inhibitor of cell wall synthesis. *Biochem Biophys Res Commun* **30**, 7-13

Ikeda, M., Wachi, M., Jung, H. K., Ishino, F. and Matsuhashi, M. (1991). The *Escherichia coli* mraY gene encoding UDP-N-acetylmuramoyl-pentapeptide: undecaprenyl-phosphate phospho-N-acetylmuramoyl-pentapeptide transferase. *J Bacteriol* **173**, 1021-1026

Ishino, F., Park, W., Tomioka, S., Tamaki, S., Takase, I., Kunugita, K., Matsuzawa, H., Asoh, S., Ohta, T., Spratt, B. G. and et al. (1986). Peptidoglycan synthetic activities in membranes of *Escherichia coli* caused by overproduction of penicillin-binding protein 2 and rodA protein. *J Biol Chem* **261**, 7024-7031

Jamin, M., Damblon, C., Millier, S., Hakenbeck, R. and Frere, J. M. (1993). Penicillin-binding protein 2x of *Streptococcus pneumoniae*: enzymic activities and interactions with beta-lactams. *Biochem J* **292 (Pt 3)**, 735-741

Job, V., Carapito, R., Vernet, T., Dessen, A. and Zapun, A. (2008). Common alterations in PBP1a from resistant *Streptococcus pneumoniae* decrease its reactivity toward beta-lactams: structural insights. *J Biol Chem* **283**, 4886-4894

Johnson, A. P., Uttley, A. H., Woodford, N. and George, R. C. (1990). Resistance to vancomycin and teicoplanin: an emerging clinical problem. *Clin Microbiol Rev* **3**, 280-291

Josephine, H. R., Charlier, P., Davies, C., Nicholas, R. A. and Pratt, R. F. (2006). Reactivity of penicillin-binding proteins with peptidoglycan-mimetic beta-lactams: what's wrong with these enzymes? *Biochemistry* **45**, 15873-15883

Ke, A. and Wolberger, C. (2003). Insights into binding cooperativity of MATa1/MATalpha2 from the crystal structure of a MATa1 homeodomain-maltose binding protein chimera. *Protein Sci* **12**, 306-312

Kell, C. M., Sharma, U. K., Dowson, C. G., Town, C., Balganesh, T. S. and Spratt, B. G. (1993). Deletion analysis of the essentiality of penicillin-binding proteins 1A, 2B and 2X of *Streptococcus pneumoniae*. *FEMS Microbiol Lett* **106**, 171-175

Kelly, J. A., Kuzin, A. P., Charlier, P. and Fonzé, E. (1998). X-ray studies of enzymes that interact with penicillins. *Cell Mol Life Sci* **54**, 353-358

Knowles, T. J., Finka, R., Smith, C., Lin, Y. P., Dafforn, T. and Overduin, M. (2009). Membrane proteins solubilized intact in lipid containing nanoparticles bounded by styrene maleic acid copolymer. *J Am Chem Soc* **131**, 7484-7485

Kobe, B., Center, R. J., Kemp, B. E. and Poumbourios, P. (1999). Crystal structure of human T cell leukemia virus type 1 gp21 ectodomain crystallized as a maltose-binding protein chimera reveals structural evolution of retroviral transmembrane proteins. *Proc Natl Acad Sci U S A* **96**, 4319-4324

Koch, A. L. (2000). Penicillin binding proteins, beta-lactams, and lactamases: offensives, attacks, and defensive countermeasures. *Crit Rev Microbiol* **26**, 205-220

Koch, A. L. and Doyle, R. J. (1985). Inside-to-outside growth and turnover of the wall of gram-positive rods. *J Theor Biol* **117**, 137-157

Krogh, A., Larsson, B., von Heijne, G. and Sonnhammer, E. L. (2001). Predicting transmembrane protein topology with a hidden Markov model: application to complete genomes. *J Mol Biol* **305**, 567-580

Kumar, I. and Pratt, R. F. (2005). Transpeptidation reactions of a specific substrate catalyzed by the *Streptomyces* R61 DD-peptidase: the structural basis of acyl acceptor specificity. *Biochemistry* **44**, 9961-9970

Laemmli, U. K. (1970). Cleavage of structural proteins during the assembly of the head of bacteriophage T4. *Nature* **227**, 680-685

Laible, G., Keck, W., Lurz, R., Mottl, H., Frere, J. M., Jamin, M. and Hakenbeck, R. (1992). Penicillin-binding protein 2x of *Streptococcus pneumoniae*. Expression in *Escherichia coli* and purification of a soluble enzymatically active derivative. *Eur J Biochem* **207**, 943-949

Laible, G., Spratt, B. G. and Hakenbeck, R. (1991). Interspecies recombinational events during the evolution of altered PBP 2x genes in penicillin-resistant clinical isolates of *Streptococcus pneumoniae*. *Mol Microbiol* **5**, 1993-2002

Lambert, P. A. (2002). Mechanisms of antibiotic resistance in *Pseudomonas aeruginosa*. *J R Soc Med* **95 Suppl 41**, 22-26

Larkin, M. A., Blackshields, G., Brown, N. P., Chenna, R., McGettigan, P. A., McWilliam, H., Valentin, F., Wallace, I. M., Wilm, A., Lopez, R., Thompson, J. D., Gibson, T. J. and Higgins, D. G. (2007). Clustal W and Clustal X version 2.0. *Bioinformatics* **23**, 2947-2948

Lavollay, M., Arthur, M., Fourgeaud, M., Dubost, L., Marie, A., Veziris, N., Blanot, D., Gutmann, L. and Mainardi, J. L. (2008). The peptidoglycan of stationary-phase *Mycobacterium tuberculosis* predominantly contains cross-links generated by L,D-transpeptidation. *J Bacteriol* **190**, 4360-4366

Lazar, K. and Walker, S. (2002). Substrate analogues to study cell-wall biosynthesis and its inhibition. *Curr Opin Chem Biol* **6**, 786-793

le Maire, M., Champeil, P. and Moller, J. V. (2000). Interaction of membrane proteins and lipids with solubilizing detergents. *Biochim Biophys Acta* **1508**, 86-111

Lee, W., McDonough, M. A., Kotra, L., Li, Z. H., Silvaggi, N. R., Takeda, Y., Kelly, J. A. and Mobashery, S. (2001). A 1.2-Å snapshot of the final step of bacterial cell wall biosynthesis. *Proc Natl Acad Sci U S A* **98**, 1427-1431

Leslie, A. G. W. (1992). Recent changes to the MOSFLM package for processing film and image plate data. *In Joint CCP4 + ESF-EAMCB Newsletter on Protein Crystallography*, No. 26.

Levy, S. B. and Marshall, B. (2004). Antibacterial resistance worldwide: causes, challenges and responses. *Nat Med* **10**, S122-129

Liu, H. and Wong, C. H. (2006). Characterization of a transglycosylase domain of *Streptococcus pneumoniae* PBP1b. *Bioorg Med Chem* **14**, 7187-7195

Liu, Y., Manna, A., Li, R., Martin, W. E., Murphy, R. C., Cheung, A. L. and Zhang, G. (2001). Crystal structure of the SarR protein from *Staphylococcus aureus*. *Proc Natl Acad Sci U S A* **98**, 6877-6882

Lloyd, A. J., Brandish, P. E., Gilbey, A. M. and Bugg, T. D. (2004). Phospho-N-acetyl-muramyl-pentapeptide translocase from *Escherichia coli*: catalytic role of conserved aspartic acid residues. *J Bacteriol* **186**, 1747-1757

Lloyd, A. J., Gilbey, A. M., Blewett, A. M., De Pascale, G., El Zoeiby, A., Levesque, R. C., Catherwood, A. C., Tomasz, A., Bugg, T. D., Roper, D. I. and Dowson, C. G. (2008). Characterization of tRNA-dependent peptide bond formation by MurM in the synthesis of *Streptococcus pneumoniae* peptidoglycan. *J Biol Chem* **283**, 6402-6417

Lo, M.-C., Men, H., Branstrom, A., Helm, J., Yao, N., Goldman, R. and Walker, S. (2000). A new mechanism of action proposed for Ramoplanin. *J Am Chem Soc* **122**, 3540-3541

Lodish, H., Berk, A., Matsudaira, P., Kaiser, C. A., Krieger, M., Scott, M. P., Zipursky, L., Darnell, J. (2004). *Molecular Cell Biology*, 5th edn, p. 124. New York: W. H. Freeman and Company.

Loll, P. J. (2003). Membrane protein structural biology: the high throughput challenge. *J Struct Biol* **142**, 144-153

Lopez, P. J., Marchand, I., Joyce, S. A. and Dreyfus, M. (1999). The C-terminal half of RNase E, which organizes the *Escherichia coli* degradosome, participates in mRNA degradation but not rRNA processing *in vivo*. *Mol Microbiol* **33**, 188-199

Lovering, A. L., de Castro, L., Lim, D. and Strynadka, N. C. (2007). Structural insight into the transglycosylation step of bacterial cell-wall biosynthesis. *Science* **315**, 1402-1405

Lovering, A. L., de Castro, L. and Strynadka, N. C. (2008a). Identification of dynamic structural motifs involved in peptidoglycan glycosyltransfer. *J Mol Biol* **383**, 167-177

Lovering, A. L., Gretes, M. and Strynadka, N. C. (2008b). Structural details of the glycosyltransferase step of peptidoglycan assembly. *Curr Opin Struct Biol* **18**, 534-543

Macheboeuf, P., Contreras-Martel, C., Job, V., Dideberg, O. and Dessen, A. (2006). Penicillin binding proteins: key players in bacterial cell cycle and drug resistance processes. *FEMS Microbiol Rev* **30**, 673-691

Macheboeuf, P., Di Guilmi, A. M., Job, V., Vernet, T., Dideberg, O. and Dessen, A. (2005). Active site restructuring regulates ligand recognition in class A penicillin-binding proteins. *Proc Natl Acad Sci U S A* **102**, 577-582

Mainardi, J. L., Legrand, R., Arthur, M., Schoot, B., van Heijenoort, J. and Gutmann, L. (2000). Novel mechanism of beta-lactam resistance due to bypass of DD-transpeptidation in *Enterococcus faecium*. *J Biol Chem* **275**, 16490-16496

Martin, C., Sibold, C. and Hakenbeck, R. (1992). Relatedness of penicillin-binding protein 1a genes from different clones of penicillin-resistant *Streptococcus pneumoniae* isolated in South Africa and Spain. *Embo J* **11**, 3831-3836

Martin, H. H. (1964). Composition of the mucopolymer in cell walls of the unstable and stable L-form of *Proteus mirabilis*. *J Gen Microbiol* **36**, 441-450

Masterton, R. (2008). The importance and future of antimicrobial surveillance studies. *Clin Infect Dis* **47 Suppl 1**, S21-31

Matias, V. R., Al-Amoudi, A., Dubochet, J. and Beveridge, T. J. (2003). Cryo-transmission electron microscopy of frozen-hydrated sections of *Escherichia coli* and *Pseudomonas aeruginosa*. *J Bacteriol* **185**, 6112-6118

Mazel, D. (2006). Integrons: agents of bacterial evolution. *Nat Rev Microbiol* **4**, 608-620

Mazmanian, S. K., Liu, G., Ton-That, H. and Schneewind, O. (1999). *Staphylococcus aureus* sortase, an enzyme that anchors surface proteins to the cell wall. *Science* **285**, 760-763

Mazodier, P., Cossart, P., Giraud, E. and Gasser, F. (1985). Completion of the nucleotide sequence of the central region of Tn5 confirms the presence of three resistance genes. *Nucleic Acids Res* **13**, 195-205

McComas, C. C., Crowley, B. M. and Boger, D. L. (2003). Partitioning the loss in vancomycin binding affinity for D-Ala-D-Lac into lost H-bond and repulsive lone pair contributions. *J Am Chem Soc* **125**, 9314-9315

McCoy, A. J., Grosse-Kunstleve, R. W., Adams, P. D., Winn, M. D., Storoni, L. C. & Read, R. J. (2007). Phaser crystallographic software. *J Appl Crystallogr* **40**, 658-674.

McCoy, A. J. and Maurelli, A. T. (2006). Building the invisible wall: updating the chlamydial peptidoglycan anomaly. *Trends Microbiol* **14**, 70-77

McDevitt, D. and Rosenberg, M. (2001). Exploiting genomics to discover new antibiotics. *Trends Microbiol* **9**, 611-617

McDonough, M. A., Anderson, J. W., Silvaggi, N. R., Pratt, R. F., Knox, J. R. and Kelly, J. A. (2002). Structures of two kinetic intermediates reveal species specificity of penicillin-binding proteins. *J Mol Biol* **322**, 111-122

Mengin-Lecreulx, D., Falla, T., Blanot, D., van Heijenoort, J., Adams, D. J. and Chopra, I. (1999). Expression of the *Staphylococcus aureus* UDP-N-acetylmuramoyl- L-alanyl-D-glutamate:L-lysine ligase in *Escherichia coli* and effects on peptidoglycan biosynthesis and cell growth. *J Bacteriol* **181**, 5909-5914

Meroueh, S. O., Minasov, G., Lee, W., Shoichet, B. K. and Mobashery, S. (2003). Structural aspects for evolution of beta-lactamases from penicillin-binding proteins. *J Am Chem Soc* **125**, 9612-9618

Mirelman, D., Bracha, R. and Sharon, N. (1972). Role of the penicillin-sensitive transpeptidation reaction in attachment of newly synthesized peptidoglycan to cell walls of *Micrococcus luteus*. *Proc Natl Acad Sci U S A* **69**, 3355-3359

Miroux, B. and Walker, J. E. (1996). Over-production of proteins in *Escherichia coli*: mutant hosts that allow synthesis of some membrane proteins and globular proteins at high levels. *J Mol Biol* **260**, 289-298

Mohammadi, T., van Dam, V., Sijbrandi, R., Vernet, T., Zapun, A., Bouhss, A., Diepeveen-de Bruin, M., Nguyen-Disteche, M., de Kruijff, B. and Breukink, E. (2011). Identification of FtsW as a transporter of lipid-linked cell wall precursors across the membrane. *Embo J* **30**, 1425-1432

Morlot, C., Noirclerc-Savoye, M., Zapun, A., Dideberg, O. and Vernet, T. (2004). The D,D-carboxypeptidase PBP3 organizes the division process of *Streptococcus pneumoniae*. *Mol Microbiol* **51**, 1641-1648

Morlot, C., Pernot, L., Le Gouellec, A., Di Guilmi, A. M., Vernet, T., Dideberg, O. and Dessen, A. (2005). Crystal structure of a peptidoglycan synthesis regulatory factor (PBP3) from *Streptococcus pneumoniae*. *J Biol Chem* **280**, 15984-15991

Morlot, C., Zapun, A., Dideberg, O. and Vernet, T. (2003). Growth and division of *Streptococcus pneumoniae*: localization of the high molecular weight penicillin-binding proteins during the cell cycle. *Mol Microbiol* **50**, 845-855

Mouz, N., Di Guilmi, A. M., Gordon, E., Hakenbeck, R., Dideberg, O. and Vernet, T. (1999). Mutations in the active site of penicillin-binding protein PBP2x from *Streptococcus pneumoniae*. Role in the specificity for beta-lactam antibiotics. *J Biol Chem* **274**, 19175-19180

Mouz, N., Gordon, E., Di Guilmi, A. M., Petit, I., Petillot, Y., Dupont, Y., Hakenbeck, R., Vernet, T. and Dideberg, O. (1998). Identification of a structural determinant for resistance to beta-lactam antibiotics in Gram-positive bacteria. *Proc Natl Acad Sci U S A* **95**, 13403-13406

Murata, Y., Sugihara, G., Fukushima, K., Tanaka, M. and Matsushita, K. (1982). Study of the micelle formation of sodium deoxycholate. Concentration dependence of Carbon-13 nuclear magnetic resonance chemical shift. *J Phys Chem* **86**, 4690-4694

National Audit Office. (2009). Reducing healthcare associated infections in hospitals in England. London: The Stationary Office

Newman, D. J., Cragg, G. M. and Snader, K. M. (2003). Natural products as sources of new drugs over the period 1981-2002. *J Nat Prod* **66**, 1022-1037

Nicola, G., Peddi, S., Stefanova, M., Nicholas, R. A., Gutheil, W. G. and Davies, C. (2005). Crystal structure of *Escherichia coli* penicillin-binding protein 5 bound to a tripeptide boronic acid inhibitor: a role for Ser-110 in deacylation. *Biochemistry* **44**, 8207-8217

Nieto, M. and Perkins, H. R. (1971). Modifications of the acyl-D-alanyl-D-alanine terminus affecting complex-formation with vancomycin. *Biochem J* **123**, 789-803

Normark, B. H. and Normark, S. (2002). Evolution and spread of antibiotic resistance. *J Intern Med* **252**, 91-106

Offant, J., Terrak, M., Derouaux, A., Breukink, E., Nguyen-Disteche, M., Zapun, A. and Vernet, T. (2010). Optimization of conditions for the glycosyltransferase activity of penicillin-binding protein 1a from *Thermotoga maritima*. *Febs J* **277**, 4290-4298

Ostash, B. and Walker, S. (2010). Moenomycin family antibiotics: chemical synthesis, biosynthesis, and biological activity. *Nat Prod Rep* **27**, 1594-1617

Pagliero, E., Chesnel, L., Hopkins, J., Croize, J., Dideberg, O., Vernet, T. and Di Guilmi, A. M. (2004). Biochemical characterization of *Streptococcus pneumoniae* penicillin-binding protein 2b and its implication in beta-lactam resistance. *Antimicrob Agents Chemother* **48**, 1848-1855

Paradis-Bleau, C., Markovski, M., Uehara, T., Lupoli, T. J., Walker, S., Kahne, D. E. and Bernhardt, T. G. (2010). Lipoprotein cofactors located in the outer membrane activate bacterial cell wall polymerases. *Cell* **143**, 1110-1120

Park, J. T. and Uehara, T. (2008). How bacteria consume their own exoskeletons (turnover and recycling of cell wall peptidoglycan). *Microbiol Mol Biol Rev* **72**, 211-227

Payne, D. J., Gwynn, M. N., Holmes, D. J. and Pompliano, D. L. (2007). Drugs for bad bugs: confronting the challenges of antibacterial discovery. *Nat Rev Drug Discov* **6**, 29-40

Peddi, S., Nicholas, R. A. and Gutheil, W. G. (2009). *Neisseria gonorrhoeae* penicillin-binding protein 3 demonstrates a pronounced preference for N^{ε}-acylated substrates. *Biochemistry* **48**, 5731-5737

Perlstein, D. L., Zhang, Y., Wang, T. S., Kahne, D. E. and Walker, S. (2007). The direction of glycan chain elongation by peptidoglycan glycosyltransferases. *J Am Chem Soc* **129**, 12674-12675

Potluri, L., Karczmarek, A., Verheul, J., Piette, A., Wilkin, J. M., Werth, N., Banzhaf, M., Vollmer, W., Young, K. D., Nguyen-Disteche, M. and den Blaauwen, T. (2010). Septal and lateral wall localization of PBP5, the major D,D-carboxypeptidase of *Escherichia coli*, requires substrate recognition and membrane attachment. *Mol Microbiol* **77**, 300-323

Pratt, R. F. (2008). Substrate specificity of bacterial DD-peptidases (penicillin-binding proteins). *Cell Mol Life Sci* **65**, 2138-2155

Privé, G. G. (2007). Detergents for the stabilization and crystallization of membrane proteins. *Methods* **41**, 388-397

Reading, C. and Cole, M. (1977). Clavulanic acid: a beta-lactamase-inhiting beta-lactam from *Streptomyces clavuligerus*. *Antimicrob Agents Chemother* **11**, 852-857

Regev-Yochay, G., Raz, M., Dagan, R., Porat, N., Shainberg, B., Pinco, E., Keller, N. and Rubinstein, E. (2004). Nasopharyngeal carriage of *Streptococcus pneumoniae* by adults and children in community and family settings. *Clin Infect Dis* **38**, 632-639

Reiss-Husson, F. and Picot, D. (1999). Crystallization of membrane proteins. In *Crystallisation of Nucleic Acids and Proteins – A Practical Approach*, 2nd edn, pp. 245-268. Edited by A. Ducruix and R. Giegé. Oxford: Oxford University Press.

Rhazi, N., Charlier, P., Dehareng, D., Engher, D., Vermeire, M., Frere, J. M., Nguyen-Disteche, M. and Fonzé, E. (2003). Catalytic mechanism of the *Streptomyces* K15 DD-transpeptidase/penicillin-binding protein probed by site-directed mutagenesis and structural analysis. *Biochemistry* **42**, 2895-2906

Ruiz, N. (2008). Bioinformatics identification of MurJ (MviN) as the peptidoglycan lipid II flippase in *Escherichia coli*. *Proc Natl Acad Sci U S A* **105**, 15553-15557

Sanbongi, Y., Ida, T., Ishikawa, M., Osaki, Y., Kataoka, H., Suzuki, T., Kondo, K., Ohsawa, F. and Yonezawa, M. (2004). Complete sequences of six penicillin-binding protein genes from 40 *Streptococcus pneumoniae* clinical isolates collected in Japan. *Antimicrob Agents Chemother* **48**, 2244-2250

Sanyal, S. and Menon, A. K. (2009). Flipping lipids: why an' what's the reason for? *ACS Chem Biol* **4**, 895-909

Sauvage, E., Duez, C., Herman, R., Kerff, F., Petrella, S., Anderson, J. W., Adediran, S. A., Pratt, R. F., Frere, J. M. and Charlier, P. (2007). Crystal structure of the *Bacillus subtilis* penicillin-binding protein 4a, and its complex with a peptidoglycan mimetic peptide. *J Mol Biol* **371**, 528-539

Sauvage, E., Herman, R., Petrella, S., Duez, C., Bouillenne, F., Frere, J. M. and Charlier, P. (2005). Crystal structure of the *Actinomadura* R39 DD-peptidase reveals new domains in penicillin-binding proteins. *J Biol Chem* **280**, 31249-31256

Sauvage, E., Kerff, F., Terrak, M., Ayala, J. A. and Charlier, P. (2008a). The penicillin-binding proteins: structure and role in peptidoglycan biosynthesis. *FEMS Microbiol Rev* **32**, 234-258

Sauvage, E., Powell, A. J., Heilemann, J., Josephine, H. R., Charlier, P., Davies, C. and Pratt, R. F. (2008b). Crystal structures of complexes of bacterial DD-peptidases with peptidoglycan-mimetic ligands: the substrate specificity puzzle. *J Mol Biol* **381**, 383-393

Sawyer, L. and Turner, M.A. (1999). X-ray analysis. In *Crystallisation of Nucleic Acids and Proteins – A Practical Approach*, 2nd edn, pp. 391-419. Edited by A. Ducruix and R. Giegé. Oxford: Oxford University Press.

Schägger, H. and von Jagow, G. (1987). Tricine-sodium dodecyl sulfate-polyacrylamide gel electrophoresis for the separation of proteins in the range from 1 to 100 kDa. *Anal Biochem* **166**, 368-379

Scheffers, D. J. and Pinho, M. G. (2005). Bacterial cell wall synthesis: new insights from localization studies. *Microbiol Mol Biol Rev* **69**, 585-607

Schleifer, K. H. and Kandler, O. (1972). Peptidoglycan types of bacterial cell walls and their taxonomic implications. *Bacteriol Rev* **36**, 407-477

Schwartz, B., Markwalder, J. A., Seitz, S. P., Wang, Y. and Stein, R. L. (2002). A kinetic characterization of the glycosyltransferase activity of *Escherichia coli* PBP1b and development of a continuous fluorescence assay. *Biochemistry* **41**, 12552-12561

Seddon, A. M., Curnow, P. and Booth, P. J. (2004). Membrane proteins, lipids and detergents: not just a soap opera. *Biochim Biophys Acta* **1666**, 105-117

Severin, A., Schuster, C., Hakenbeck, R. and Tomasz, A. (1992). Altered murein composition in a D,D-carboxypeptidase mutant of *Streptococcus pneumoniae*. *J Bacteriol* **174**, 5152-5155

Smith, A. M. and Klugman, K. P. (1998). Alterations in PBP 1A essential-for high-level penicillin resistance in *Streptococcus pneumoniae*. *Antimicrob Agents Chemother* **42**, 1329-1333

Smith, P. K., Krohn, R. I., Hermanson, G. T., Mallia, A. K., Gartner, F. H., Provenzano, M. D., Fujimoto, E. K., Goeke, N. M., Olson, B. J. and Klenk, D. C. (1985). Measurement of protein using bicinchoninic acid. *Anal Biochem* **150**, 76-85

Sova, M., Cadez, G., Turk, S., Majce, V., Polanc, S., Batson, S., Lloyd, A. J., Roper, D. I., Fishwick, C. W. and Gobec, S. (2009). Design and synthesis of new hydroxyethylamines as inhibitors of D-alanyl-D-lactate ligase (VanA) and D-alanyl-D-alanine ligase (DdlB). *Bioorg Med Chem Lett* **19**, 1376-1379

Spratt, B. G., Zhou, J., Taylor, M. and Merrick, M. J. (1996). Monofunctional biosynthetic peptidoglycan transglycosylases. *Mol Microbiol* **19**, 639-640

Stefanova, M., Bobba, S. and Gutheil, W. G. (2010). A microtiter plate-based beta-lactam binding assay for inhibitors of high-molecular-mass penicillin-binding proteins. *Anal Biochem* **396**, 164-166

Stefanova, M. E., Davies, C., Nicholas, R. A. and Gutheil, W. G. (2002). pH, inhibitor, and substrate specificity studies on *Escherichia coli* penicillin-binding protein 5. *Biochim Biophys Acta* **1597**, 292-300

Steitz, T. A. (2010). From the structure and function of the ribosome to new antibiotics (Nobel Lecture). *Angew Chem Int Ed Engl* **49**, 4381-4398

Strancar, K., Boniface, A., Blanot, D. and Gobec, S. (2007). Phosphinate inhibitors of UDP-N-acetylmuramoyl-L-alanyl-D-glutamate: L-lysine ligase (MurE). *Arch Pharm (Weinheim)* **340**, 127-134

Studier, F. W. (2005). Protein production by auto-induction in high density shaking cultures. *Protein Expr Purif* **41**, 207-234

Studier, F. W. and Moffatt, B. A. (1986). Use of bacteriophage T7 RNA polymerase to direct selective high-level expression of cloned genes. *J Mol Biol* **189**, 113-130

Sung, M. T., Lai, Y. T., Huang, C. Y., Chou, L. Y., Shih, H. W., Cheng, W. C., Wong, C. H. and Ma, C. (2009). Crystal structure of the membrane-bound bifunctional transglycosylase PBP1b from *Escherichia coli*. *Proc Natl Acad Sci U S A* **106**, 8824-8829

Takiff, H. E., Salazar, L., Guerrero, C., Philipp, W., Huang, W. M., Kreiswirth, B., Cole, S. T., Jacobs, W. R., Jr. and Telenti, A. (1994). Cloning and nucleotide sequence of Mycobacterium tuberculosis gyrA and gyrB genes and detection of quinolone resistance mutations. *Antimicrob Agents Chemother* **38**, 773-780

Tatar, L. D., Marolda, C. L., Polischuk, A. N., van Leeuwen, D. and Valvano, M. A. (2007). An *Escherichia coli* undecaprenyl-pyrophosphate phosphatase implicated in undecaprenyl phosphate recycling. *Microbiology* **153**, 2518-2529

Taylor, P. L. and Wright, G. D. (2008). Novel approaches to discovery of antibacterial agents. *Anim Health Res Rev* **9**, 237-246

Terrak, M., Ghosh, T. K., van Heijenoort, J., Van Beeumen, J., Lampilas, M., Aszodi, J., Ayala, J. A., Ghuysen, J. M. and Nguyen-Disteche, M. (1999). The catalytic, glycosyl transferase and acyl transferase modules of the cell wall peptidoglycan-polymerizing penicillin-binding protein 1b of *Escherichia coli*. *Mol Microbiol* **34**, 350-364

Terrak, M. and Nguyen-Distèche, M. (2006). Kinetic characterization of the monofunctional glycosyltransferase from *Staphylococcus aureus*. *J Bacteriol* **188**, 2528-2532

Terrak, M., Sauvage, E., Derouaux, A., Dehareng, D., Bouhss, A., Breukink, E., Jeanjean, S. and Nguyen-Disteche, M. (2008). Importance of the conserved residues in the peptidoglycan glycosyltransferase module of the class A penicillin-binding protein 1b of *Escherichia coli*. *J Biol Chem* **283**, 28464-28470

Tipper, D. J. and Strominger, J. L. (1965). Mechanism of action of penicillins: a proposal based on their structural similarity to acyl-D-alanyl-D-alanine. *Proc Natl Acad Sci U S A* **54**, 1133-1141

Ton-That, H., Liu, G., Mazmanian, S. K., Faull, K. F. and Schneewind, O. (1999). Purification and characterization of sortase, the transpeptidase that cleaves surface proteins of *Staphylococcus aureus* at the LPXTG motif. *Proc Natl Acad Sci U S A* **96**, 12424-12429

Tonge, S. R. and Tighe, B. J. (2001). Responsive hydrophobically associating polymers: a review of structure and properties. *Adv Drug Deliv Rev* **53**, 109-122

Touzé, T., Blanot, D. and Mengin-Lecreulx, D. (2008). Substrate specificity and membrane topology of *Escherichia coli* PgpB, an undecaprenyl pyrophosphate phosphatase. *J Biol Chem* **283**, 16573-16583

Triboulet, S., Arthur, M., Mainardi, J. L., Veckerle, C., Dubee, V., Nguekam-Nouri, A., Gutmann, L., Rice, L. B. and Hugonnet, J. E. (2011) Inactivation kinetics of a new target of β-lactam antibiotics. *J Biol Chem* **286**, 22777-22784

Tuomanen, E. (2006). *Streptococcus pneumoniae*. In *The Prokaryotes. A Handbook on the Biology of Bacteria*, 3rd edn, vol 4, p 151. Edited by M. Dworkin, S. Falkow, E. Rosenberg, K-H. Schleifer and E. Stackebrandt. New York: Springer Science+Business Media, LLC.

Typas, A., Banzhaf, M., van den Berg van Saparoea, B., Verheul, J., Biboy, J., Nichols, R. J., Zietek, M., Beilharz, K., Kannenberg, K., von Rechenberg, M., Breukink, E., den Blaauwen, T., Gross, C. A. and Vollmer, W. (2010). Regulation of peptidoglycan synthesis by outer-membrane proteins. *Cell* **143**, 1097-1109

van der Linden, M. P., Mottl, H. and Keck, W. (1992). Cytoplasmic high-level expression of a soluble, enzymatically active form of the *Escherichia coli* penicillin-binding protein 5 and purification by dye chromatography. *Eur J Biochem* **204**, 197-202

van Heijenoort, Y., Derrien, M. and van Heijenoort, J. (1978). Polymerization by transglycosylation in the biosynthesis of the peptidoglycan of *Escherichia coli* K 12 and its inhibition by antibiotics. *FEBS Lett* **89**, 141-144

van Heijenoort, Y., Gomez, M., Derrien, M., Ayala, J. and van Heijenoort, J. (1992). Membrane intermediates in the peptidoglycan metabolism of *Escherichia coli*: possible roles of PBP 1b and PBP 3. *J Bacteriol* **174**, 3549-3557

Vicente, M., Rico, A. I., Martinez-Arteaga, R. and Mingorance, J. (2006). Septum enlightenment: assembly of bacterial division proteins. *J Bacteriol* **188**, 19-27

Vinatier, V., Blakey, C. B., Braddick, D., Johnson, B. R., Evans, S. D. and Bugg, T. D. (2009). *In vitro* biosynthesis of bacterial peptidoglycan using D-Cys-containing precursors: fluorescent detection of transglycosylation and transpeptidation. *Chem Commun (Camb)*, 4037-4039

Vollmer, W. (2008). Structural variation in the glycan strands of bacterial peptidoglycan. *FEMS Microbiol Rev* **32**, 287-306

Vollmer, W., Blanot, D. and de Pedro, M. A. (2008a). Peptidoglycan structure and architecture. *FEMS Microbiol Rev* **32**, 149-167

Vollmer, W., Joris, B., Charlier, P. and Foster, S. (2008b). Bacterial peptidoglycan (murein) hydrolases. *FEMS Microbiol Rev* **32**, 259-286

von Nussbaum, F., Brands, M., Hinzen, B., Weigand, S. and Habich, D. (2006). Antibacterial natural products in medicinal chemistry-exodus or revival? *Angew Chem Int Ed Engl* **45**, 5072-5129

Wainwright, M. and Kristiansen, J. (2011). On the 75th anniversary of Prontosil. *Dyes and Pigments* **88**, 231-234

Waksman, S. A. (1944). Antibiotic Substances, Production by Microorganisms-Nature and Mode of Action. *Am J Public Health Nations Health* **34**, 358-364

Waldrop, G. L. (2009). Smaller is better for antibiotic discovery. *ACS Chem Biol* **4**, 397-399

Walsh, C. (2000). Molecular mechanisms that confer antibacterial drug resistance. *Nature* **406**, 775-781

Walsh, C. (2003). Where will new antibiotics come from? *Nat Rev Microbiol* **1**, 65-70

Walsh, C., Fisher, S. L., Park, I. S., Prahalad, M. and Wu, Z. (1996). Bacterial resistance to vancomycin: five genes and one missing hydrogen bond tell the story. *Chem Biol* **3**, 21-28

Walsh, C. and Wright, G. (2005). Introduction: antibiotic resistance. *Chem Rev* **105**, 391-394

Wampler, D. E. and Westhead, E. W. (1968). Two aspartokinases from *Escherichia coli*. Nature of the inhibition and molecular changes accompanying reversible inactivation. *Biochemistry* **7**, 1661-1671

Wang, T. S., Manning, S. A., Walker, S. and Kahne, D. (2008). Isolated peptidoglycan glycosyltransferases from different organisms produce different glycan chain lengths. *J Am Chem Soc* **130**, 14068-14069

Ward, A., Sanderson, N. M., O'Reilly, J., Rutherford, N. G., Poolman, B., Henderson, P.J.F. (2000). The amplified expression, identification, purification, assay and properties of hexahistidine-tagged bacterial membrane transport proteins. In *Membrane Transport – A Practical Approach*, 1st edn, pp. 141-166. Edited by S. A. Baldwin. Oxford: Oxford University Press.

Ward, J. B. (1984). Biosynthesis of peptidoglycan: points of attack by wall inhibitors. *Pharmacol Ther* **25**, 327-369

Waxman, D. J. and Strominger, J. L. (1983). Penicillin-binding proteins and the mechanism of action of beta-lactam antibiotics. *Annu Rev Biochem* **52**, 825-869

Webb, M. R. (1992). A continuous spectrophotometric assay for inorganic phosphate and for measuring phosphate release kinetics in biological systems. *Proc Natl Acad Sci U S A* **89**, 4884-4887

Webber, M. A. and Piddock, L. J. (2003). The importance of efflux pumps in bacterial antibiotic resistance. *J Antimicrob Chemother* **51**, 9-11

Welzel, P., Kunisch, F., Kruggel, F., Stein, H., Scherkenbeck, J., Hiltmann, A., Duddeck, H., Müller, D., Maggio, J. E., Fehlhaber, H.-W., Seibert, G., van Heijenoort, Y. and van Heijenoort, J. (1987). Moenomycin A: Minimum structural requirements for biological activity. *Tetrahedron* **43**, 585-598

Wennerström, H. and Lindman, B. (1979). Micelles. Physical chemistry of surfactant association. *Physics Reports* **52**, 1-86

Wilkin, J. M., Jamin, M., Damblon, C., Zhao, G. H., Joris, B., Duez, C. and Frere, J. M. (1993). The mechanism of action of DD-peptidases: the role of tyrosine-159 in the *Streptomyces* R61 DD-peptidase. *Biochem J* **291 (Pt 2)**, 537-544

Williams, S. P., Tait-Kamradt, A. G., Norton, J. E., Albert, T. J. and Dougherty, T. J. (2007). Nucleotide sequence changes between *Streptococcus pneumoniae* R6 and D39 strains determined by an oligonucleotide hybridization DNA sequencing technology. *J Microbiol Methods* **70**, 65-74

World Health Organisation (2007). Pneumococcal conjugate vaccine for childhood immunization--WHO position paper. *Wkly Epidemiol Rec* **82**, 93-104

Yamada, M., Watanabe, T., Baba, N., Takeuchi, Y., Ohsawa, F. and Gomi, S. (2008). Crystal structures of biapenem and tebipenem complexed with penicillin-binding proteins 2X and 1A from *Streptococcus pneumoniae*. *Antimicrob Agents Chemother* **52**, 2053-2060

Yang, Y., Rasmussen, B. A. and Shlaes, D. M. (1999). Class A beta-lactamases--enzyme-inhibitor interactions and resistance. *Pharmacol Ther* **83**, 141-151

Yang, Y., Severin, A., Chopra, R., Krishnamurthy, G., Singh, G., Hu, W., Keeney, D., Svenson, K., Petersen, P. J., Labthavikul, P., Shlaes, D. M., Rasmussen, B. A., Failli, A. A., Shumsky, J. S., Kutterer, K. M., Gilbert, A. and Mansour, T. S. (2006). 3,5-dioxopyrazolidines, novel inhibitors of UDP-N-acetylenolpyruvylglucosamine reductase (MurB) with activity against gram-positive bacteria. *Antimicrob Agents Chemother* **50**, 556-564

Yang, Z. R., Thomson, R., McNeil, P. and Esnouf, R. M. (2005). RONN: the bio-basis function neural network technique applied to the detection of natively disordered regions in proteins. *Bioinformatics* **21**, 3369-3376

Ye, X. Y., Lo, M. C., Brunner, L., Walker, D., Kahne, D. and Walker, S. (2001). Better substrates for bacterial transglycosylases. *J Am Chem Soc* **123**, 3155-3156

Yocum, R. R., Waxman, D. J., Rasmussen, J. R. and Strominger, J. L. (1979). Mechanism of penicillin action: penicillin and substrate bind covalently to the same active site serine in two bacterial D-alanine carboxypeptidases. *Proc Natl Acad Sci U S A* **76**, 2730-2734

Young, K. D. (2003). Bacterial shape. *Mol Microbiol* **49**, 571-580

Yuan, Y., Barrett, D., Zhang, Y., Kahne, D., Sliz, P. and Walker, S. (2007). Crystal structure of a peptidoglycan glycosyltransferase suggests a model for processive glycan chain synthesis. *Proc Natl Acad Sci U S A* **104**, 5348-5353

Zapun, A., Contreras-Martel, C. and Vernet, T. (2008). Penicillin-binding proteins and beta-lactam resistance. *FEMS Microbiol Rev* **32**, 361-385

Zervosen, A., Lu, W. P., Chen, Z., White, R. E., Demuth, T. P., Jr. and Frere, J. M. (2004). Interactions between penicillin-binding proteins (PBPs) and two novel classes of PBP inhibitors, arylalkylidene rhodanines and arylalkylidene iminothiazolidin-4-ones. *Antimicrob Agents Chemother* **48**, 961-969

Zhao, G., Meier, T. I., Kahl, S. D., Gee, K. R. and Blaszczak, L. C. (1999). BOCILLIN FL, a sensitive and commercially available reagent for detection of penicillin-binding proteins. *Antimicrob Agents Chemother* **43**, 1124-1128

Appendix A

Lys-Lipid II purification

Lys-Lipid II was synthesised and purified as described in the Materials and Methods. The TLC of Lys-Lipid II purification is displayed in Figure A1.

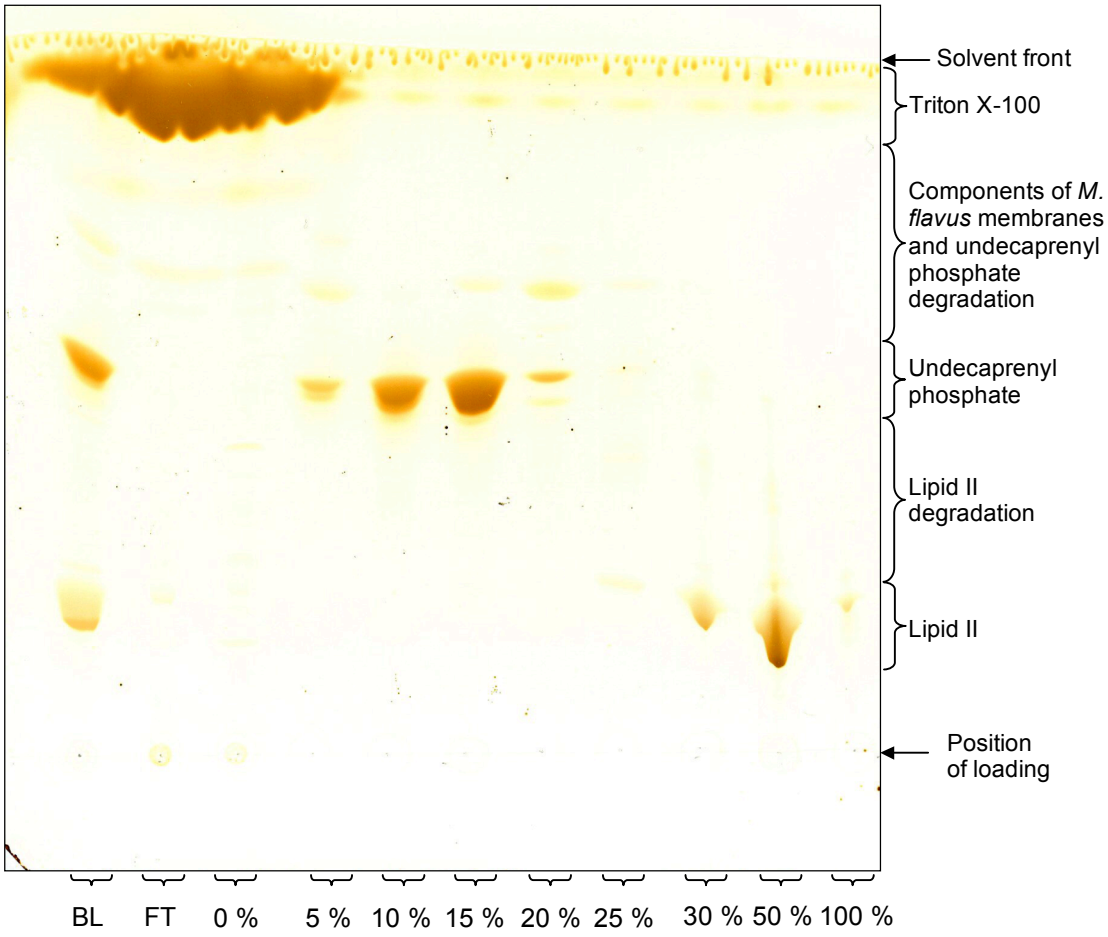

Figure A1: TLC of fractions from anion exchange purification of Lys-Lipid II. Lys-Lipid II was synthesised and purified as described in Section 2.7.3. Samples were loaded on to the silica plate in chloroform/methanol/water 2:3:1 (v/v). Chromatography was performed in chloroform/methanol/water/0.88 ammonia 88:48:10:1 (v/v) and the resulting silica plate was stained with iodine vapour (Section 2.7.4). BL, total lipid before loading on to the DEAE column; FT, flow through; %, % (v/v) solvent B (chloroform/methanol/1 M ammonium bicarbonate 2:3:1 (v/v)). Each lane was loaded with the equivalent of a 500 µL sample from the fraction collected, with the exception of BL, where 50 µL was sampled. Separated components from the synthesis are labelled on the diagram. Arrows mark the position of sample loading on the silica plate and the solvent front.

Appendix B1

Derivation of the Michaelis-Menten equation to determine kinetic constants

The Michaelis-Menten model states that an enzyme, E, combines with substrate, S, forming an enzyme-substrate complex, ES. ES has two possible fates: it can dissociate to E and S or proceed to form product, P. The initial rate depends on [S], which is in large excess over [E]. Upon measuring initial reaction rates, it can be assumed that the product does not revert back to the initial substrate as it has not has not accumulated to an appreciable concentration. This is described in the model:

$$[E]+[S]\underset{k_{-1}}{\overset{k_1}{\rightleftharpoons}}[ES]\xrightarrow{k_2}[E]+[P]$$

The initial rate, v_0, can be determined by the linear region of a curve at the beginning of the reaction (product formation over time):

$$\frac{dp}{dt} = v_0 = k_2[ES] \quad (1)$$

At V_{max} (on a initial velocity over [substrate] profile), the enzyme catalytic sites are saturated with substrate:

$$V_{max} = k_2[E_T] \quad (2)$$

The kinetic constant k_2 can be referred to as k_{cat}.

Using the assumption that steady state kinetics exist, the concentration of ES stays constant and the rates of formation and dissociation of ES are equal:

$$k_1[E][S] = k_2[ES] + k_{-1}[ES] \quad (3)$$

(4) $$\frac{k_2+k_{-1}}{k_1}=\frac{[E][S]}{[ES]}$$

The Michaelis constant, K_m, can be defined as:

(5) $$K_m=\frac{k_2+k_{-1}}{k_1}$$, thus:

(6) $$K_m=\frac{[E][S]}{[ES]}$$

(7) $$[E]=\frac{K_m[ES]}{[S]}$$

The total enzyme concentration is equal to unbound and substrate-bound enzyme:

(8) $$[E_T]=[E]+[ES]$$

Substituting the expression for [E] (equation 7) into equation 8:

(9) $$[E_T]=\frac{K_m[ES]}{[S]}+[ES]$$

(10) $$[E_T]=[ES]\left(\frac{K_m}{[S]}+1\right)$$

Multiplying everything by the rate constant k_2:

(11) $$k_2[E_T]=k_2[ES]\left(\frac{K_m}{[S]}+1\right)$$

Substituting v_0 (1) and V_{max} (2) into equation 11 gives the Michaelis-Menten equation:

$$V_{max} = v_0\left(\frac{K_m}{[S]} + 1\right) \quad (12)$$

$$v_0 = \frac{V_{max}}{\left(\frac{K_m}{[S]} + 1\right)} \quad (13)$$

$$v_0 = \frac{V_{max}[S]}{K_m + [S]} \quad (14)$$

Determination of kinetic constants

K_m is equal to the substrate concentration at which v_0 is half its maximal rate (V_{max}).

At [S] much lower than K_m, the rate is directly proportional to [S], given by:

$$v_0 = \frac{V_{max}[S]}{K_m} \quad (15)$$

At [S] much greater than K_m, the rate is maximal and independent of [S]:

$$v_0 = V_{max} \quad (16)$$

The kinetic constants were determined by plotting a velocity substrate profile. Given that Michaelis-Menten kinetics were obeyed (equation 14), a hyperbolic curve was fitted to the data by non-linear regression using a statistical program, GraphPad PRISM 5. PRISM was used to derive the values of K_m and k_{cat} from the data.

Appendix B2

Derivation of Michaelis-Menten kinetic constants from an enzyme reaction involving two substrates

Initial velocity measurements of transglycosylase reactions involves the binding of two Lipid II molecules *in vitro*, as described by the reaction scheme below:

Scheme A $$[E]+[S] \overset{K_{m1}}{\rightleftharpoons} [ES] \underset{-[S]}{\overset{K_{m2}}{\overset{+[S]}{\rightleftharpoons}}} [ES_2] \xrightarrow{k_{cat}} [E]+[P]$$

The initial rate can be defined by:

(1) $$\frac{dp}{dt} = v_0 = k_{cat}[ES_2]$$

At V_{max}, the enzyme catalytic sites are saturated with substrate:

(2) $$V_{max} = k_{cat}[E_T]$$

A kinetic equation can be derived from Scheme A on the assumption that the substrate of the reaction remains unchanged over the initial rates measured, and that rapid equilibrium kinetics exist.

The kinetic constants from the model can be derived:

(3) (a) $$K_{m1} = \frac{[E][S]}{[ES]}$$ (b) $$K_{m2} = \frac{[ES][S]}{[ES_2]}$$

The total enzyme concentration is equal to the concentration of enzyme in unbound and substrate bound forms:

(4) $$[E_T]=[E]+[ES]+[ES_2]$$

Each term of equation 4 was written in terms of $[ES_2]$, using equations 3ab as follows:

$[ES_2]$: $[ES_2]$

$[ES]$:

$$[ES]=\frac{K_{m2}[ES_2]}{[S]}$$

$[E]$:

$$[E]=\frac{K_{m1}[ES]}{[S]}$$

Substituting in the term for $[ES]$:

$$[E]=\frac{K_{m1}\frac{(K_{m2}[ES_2])}{[S]}}{[S]}$$

$$[E]=\frac{K_{m1}K_{m2}[ES_2]}{[S]^2}$$

Therefore, substituting the above equations for $[E]$, $[ES]$ and $[ES_2]$ into equation 4, $[ET]$ can be described in terms of kinetic constants, $[S]$ and $[ES_2]$:

(5) $$E_T=\frac{K_{m1}K_{m2}[ES_2]}{[S]^2}+\frac{K_{m2}[ES_2]}{[S]}+[ES_2]$$

$$[E_T]=[ES_2]\left(\frac{K_{m1}K_{m2}}{[S]^2}+\frac{K_{m2}}{[S]}+1\right) \quad (6)$$

Multiplying both sides of the equation by k_{cat}:

$$k_{cat}[E_T]=k_{cat}[ES_2]\left(\frac{K_{m1}K_{m2}}{[S]^2}+\frac{K_{m2}}{[S]}+1\right) \quad (7)$$

Substituting v_0 (1) and V_{max} (2) into equation 7:

$$V_{max}=v_0\left(\frac{K_{m1}K_{m2}}{[S]^2}+\frac{K_{m2}}{[S]}+1\right) \quad (8)$$

Rearranging equation 8:

$$v_0=\frac{V_{max}}{\left(\frac{K_{m1}K_{m2}}{[S]^2}+\frac{K_{m2}}{[S]}+1\right)} \quad (9)$$

Multiplying both sides of the equation by $[S]^2/[S]^2$:

$$v_0=\frac{V_{max}[S]^2}{K_{m1}K_{m2}+K_{m2}[S]+[S]^2} \quad (10)$$

Determination of kinetic constants for transglycosylation by PBP1a

It could be interpreted that a linear relationship existed between PBP1a catalysed transglycosylation with the substrate concentrations tested (as described in Figure 4.15). Based on the assumption that K_{m1} was substantially smaller than K_{m2}, the product of these two constants would approximate to 0 mM. Therefore, Equation 10 essentially reduces down to the Michaelis-Menten equation (Equation 11abc).

(11)(a) $$v_0 = \frac{V_{max}[S]^2}{K_{m2}[S]+[S]^2}$$ (b) $$v_0 = \frac{V_{max}[S]^2}{(K_{m2}+[S])[S]}$$ (c) $$v_0 = \frac{V_{max}[S]}{K_{m2}+[S]}$$

The linear trend indicated that the rate was directly proportional to the substrate concentration. As the approach of V_{max} was far from evident on the velocity versus substrate plot (Figure 4.15), it can be assumed that the substrate concentrations trialled were much less than K_{m2} (Equation 12).

(12) $$v_0 = \frac{V_{max}[S]}{K_{m2}}$$

Scheme A describes the binding of two substrates to the enzyme followed by the conversion of the substrate into product, which is considered to be the rate-determining step. This scheme was used to derive Equation 10. However, the rate-determining step could be before the binding of the second substrate as described by Scheme B.

Scheme B $$[E]+[S] \overset{K_m}{\rightleftharpoons} [ES] \underset{-[S]}{\overset{k_{cat}}{\underset{+[S]}{\rightleftharpoons}}} [ES_2] \longrightarrow [E]+[P]$$

In this situation, the generation of product is faster than the rate-determining step, thus the initial rate can be defined by:

(13) $$\frac{dp}{dt} = v_0 = k_{cat}[ES]$$

Equation 13 can be used to derive the Michaelis-Menten equation (as described in Appendix B1):

$$v_0 = \frac{V_{max}[S]}{K_m + [S]} \quad (14)$$

At [S] much lower than K_m, the rate is directly proportional to [S], given by:

$$v_0 = \frac{V_{max}[S]}{K_m} \quad (15)$$

Appendix B3

Determining kinetic constants for a proposed model of two substrate binding with substrate inhibition

The kinetics of MGT (Section 4.7.3) did not satisfy the Michaelis-Menten model for two substrate binding, thus the kinetic properties were described by the proposed model:

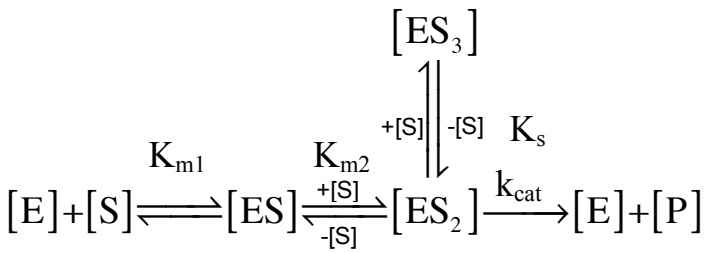

The initial rate can be defined by:

$$\frac{dp}{dt} = v_0 = k_{cat}[ES_2] \quad (1)$$

At V_{max}, the enzyme catalytic sites are saturated with substrate:

$$V_{max} = k_{cat}[E_T] \quad (2)$$

A kinetic equation can be derived from the model above on the assumption that the substrate of the reaction remains unchanged over the initial rates measured, and that rapid equilibrium kinetics exist.

The kinetic constants from the model can be derived:

$$K_{m1} = \frac{[E][S]}{[ES]} \quad (3a) \qquad K_{m2} = \frac{[ES][S]}{[ES_2]} \quad (3b) \qquad K_s = \frac{[ES_2][S]}{[ES_3]} \quad (3c)$$

The total enzyme concentration is equal to the concentration of enzyme in unbound and substrate bound forms:

(4) $$[E_T]=[E]+[ES]+[ES_2]+[ES_3]$$

Each term of equation 4 was written in terms of $[ES_2]$, using equations 3abc as follows:

$[ES_2]$: $[ES_2]$

$[ES]$:

$$[ES]=\frac{K_{m2}[ES_2]}{[S]}$$

$[E]$:

$$[E]=\frac{K_{m1}[ES]}{[S]}$$

Substituting in the term for $[ES]$:

$$[E]=\frac{K_{m1}\frac{(K_{m2}[ES_2])}{[S]}}{[S]}$$

$$[E]=\frac{K_{m1}K_{m2}[ES_2]}{[S]^2}$$

$[ES_3]$:

$$[ES_3]=\frac{[ES_2][S]}{K_s}$$

Therefore, substituting the above equations for $[E]$, $[ES]$, $[ES_2]$ and $[ES_3]$ into equation 4, $[E_T]$ can be described in terms of kinetic constants, $[S]$ and $[ES_2]$:

(5) $$[E_T]=\frac{K_{m1}K_{m2}[ES_2]}{[S]^2}+\frac{K_{m2}[ES_2]}{[S]}+[ES_2]+\frac{[ES_2][S]}{K_s}$$

Rearranged to give:

$$[E_T]=[ES_2]\left(\frac{K_{m1}K_{m2}}{[S]^2}+\frac{K_{m2}}{[S]}+1+\frac{[S]}{K_s}\right) \quad (6)$$

Multiplying both sides of the equation by k_{cat}:

$$k_{cat}[E_T]=k_{cat}[ES_2]\left(\frac{K_{m1}K_{m2}}{[S]^2}+\frac{K_{m2}}{[S]}+1+\frac{[S]}{K_s}\right) \quad (7)$$

Substituting v_0 (1) and V_{max} (2) into equation 7:

$$V_{max}=v_0\left(\frac{K_{m1}K_{m2}}{[S]^2}+\frac{K_{m2}}{[S]}+1+\frac{[S]}{K_s}\right) \quad (8)$$

Rearranging equation 8:

$$v_0=\frac{V_{max}}{\left(\frac{K_{m1}K_{m2}}{[S]^2}+\frac{K_{m2}}{[S]}+1+\frac{[S]}{K_s}\right)} \quad (9)$$

$$v_0=\frac{V_{max}[S]}{\left(\frac{K_{m1}K_{m2}}{[S]}+K_{m2}+[S]+\frac{[S]^2}{K_s}\right)} \quad (10)$$

$$v_0=\frac{V_{max}[S]}{K_{m2}\left(\frac{K_{m1}}{[S]}+1\right)+[S]\left(1+\frac{[S]}{K_s}\right)} \quad (11)$$

The kinetic parameters were determined by plotting the assay data as a velocity-substrate profile. The statistical program GraphPad PRISM 5 was used to fit the data to equation 11 and to extract values for the kinetic constants.

Appendix C1

Kinetic parameters of VanA (Batson, 2010)

(a)

Substrate at subsite 1	**VanA**
	K_{m1}[a] (mM)
D-Ala	1.40±0.23

(b)

Substrate at subsite 2	**VanA**		
	K_{m2}[a] (mM)	**k_{cat} (min^{-1})**	**k_{cat}/K_m[a] ($mM^{-1}min^{-1}$)**
D-Ala	194.30±29.90	118.52	0.16±0.005
D-Lac	1.76±0.19	16.76	9.52±0.03

Table C1: Kinetics of VanA. (a) The kinetic constraints of the exclusive binding of D-Ala in the first subsite. (b) The kinetic constraints of binding D-Ala or D-Lac into the second subsite. Data taken from Batson, (2010), calculated by using data obtained from ADP-coupled release assays.

[a]Values ± standard error

Appendix C2

The expression and purification of *E. faecalis* VanA

E. faecalis VanA was expressed and purified according to Batson, (2010). The vector pET28d::*vanA* (*E. faecalis vanA* cloned into the pET28d vector conferring kanamycin resistance) (supplied by S. Batson) was used to express VanA in *E. coli* BL21 Star (DE3) pRosetta by induction with 1 mM IPTG for 3 hours following a growth at 37°C that had reached an OD of 0.5.

Crude lysates containing the expressed VanA were prepared and were applied to a chelating Ni^{2+} sepharose column (Ni Sepharose High Performance, GE Healthcare) (equilibrated in 50 mM HEPES, 300 mM NaCl, 10 mM imidazole, 10 % (v/v) glycerol, pH 7.5) and enabled the purification of VanA on the basis of its vector-encoded histidine tag by elution with 125-250 mM imidazole. The eluate containing partially purified VanA was applied to a size exclusion column (Superdex 75 26/60) equilibrated in 50 mM HEPES, 150 mM KCl, pH 7.5 in the final purification procedure. Figure C2 demonstrates the purification of VanA to complete homogeneity.

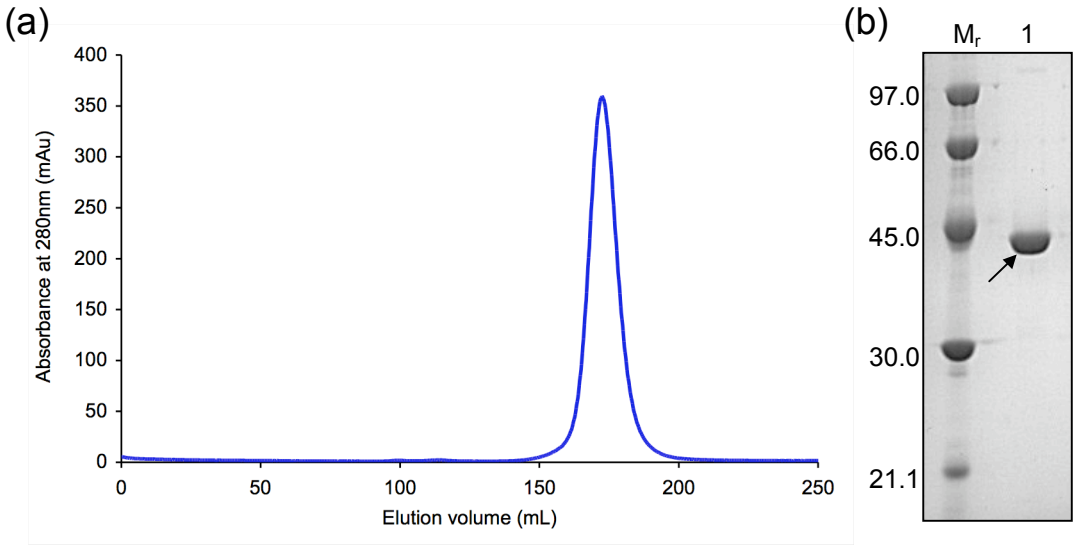

Figure C2: Chromatogram of size exclusion chromatography and a 12 % SDS-PAGE analysis of VanA purification. (a) The pre-equilibrated Superdex 75 26/60 column was injected with partially purified VanA following IMAC, at elution volume 0 mL. (b) SDS-PAGE Coomassie-stained gel analysis of the eluted fraction from size exclusion chromatography representing absorbance maxima at 280 nm. M_r, molecular weight markers (kDa); lane 1, final level of VanA purity following the two purification techniques. The arrow shows the position of VanA (38.4 kDa).